A GEOLOGICAL, GEOCHEMICAL AND STRUCTURAL ANALYSIS OF THE LOWER ORDOVICIAN TULKS HILL Cu-Zn (pb) VOLCANOGENIC MASSIVE SULPHIDE DEPOSIT, CENTRAL NEWFOUNDLAND, CANADA

CHRISTOPHER MORETON

CENTRE FOR NFLD. STUDIES
MAR 16 1988
MEMORIAL UNIVERSITY
OF NEWFOUNDLAND

A GEOLOGICAL, GEOCHEMICAL AND STRUCTURAL ANALYSIS OF THE LOWER ORDOVICIAN TULKS HILL Cu-Zn-(Pb) VOLCANOGENIC MASSIVE SULPHIDE DEPOSIT, CENTRAL NEWFOUNDLAND, CANADA

by

(C) Christopher Moreton B.Sc (Hons.)

A Thesis submitted in partial fulfillment of the requirements for the degree of Master of Science

Department of Earth Sciences,
Memorial University of Newfoundland

July, 1984

St. John's Newfoundland

ISBN 0-315-31037-5

ABSTRACT

The Tulks Hill Cu-Zn-(Pb) prospect is a volcanogenic massive sulphide deposit located in central Newfoundland. Four sulphide lenses, with a total tonnage of less than 1 million tons, are hosted by felsic pyroclastic and volcanic rocks of the pre-Caradoc Victoria Lake Group. A relative abundance of both felsic rocks and Zn and Pb, distinguishes this deposit from the stratigraphically equivalent ones of Notre Dame Bay.

Hydrothermally altered rhyolitic-dacitic pyroclastic and volcanic rocks outcrop in the footwall, whereas a tuffaceous chert and iron formation occur in the hangingwall. Chequerboard albite, Fe/Mg-chlorite, sericite and quartz overgrowths on primary quartz phenocrysts, are characteristic alteration features in the footwall. The immediate stratigraphic base of the deposit has K- and Mg(Fe)-rich zones; these zones are thought to have formed at the locus of hydrothermal fluid exhalation. A subvolcanic intrusion, called the Raven rhyolite, is comagmatic with the footwall rocks. It contains secondary microcline (K-enrichment) and sulphide-rich veinlets, suggesting that it played a part in the mineralising process.

Banded sphalerite-chalcopyrite-galena mineralisation generally overlies massive pyritite; the former two minerals are also common in the siliceous stockwork.

Galena and tennantite become more common towards the hangingwall, apparently at the expense of chalcopyrite, while arsenopyrite is sporadically distributed. Covellite, bornite, digenite, electrum, magnetite, ilmenite and marcasite are minor components.

Dolomite - sericite and siderite - Fe-chlorite are characteristic mineral assemblages of the tuffaceous chert and the iron formation, respectively. Pyrite is the dominant sulphide in these chert-rich chemical sediments.

Tight to isoclinal folding, with faulting parallel to the axial planes, is the best developed phase (D1) of the three documented deformation episodes. Recumbent folding is inferred to pre-date D1 since the stratigraphy is inverted. Mobilisation of the more plastically deformed sulphides accompanied the development of the S1 schistosity. D1 is thought to have occurred in a brittle-ductile regime since annealed pyrite, with distinct pressure shadows, both oriented subparallel to S1, typically lie adjacent to zones of granulated pyrite (fault zones?).

ACKNOWLEDGEMENTS

I would like to acknowledge and thank the following people for their help during the course of my studies:

-- My supervisor, Dr. D. F. Strong, for advice, guidence and the patience to review earlier drafts of this manuscript;

-- Drs. B. J. Fryer and R. P. Taylor who acted as temporary co-supervisors;

-- Dr. J. G. Thurlow, Mr. D. M. Barbour, and the remaining staff of Abitibi-Price Mineral Resources Ltd., Buchans, for discussions and logistical help;

-- Abitibi-Price Mineral Resources Ltd. for giving me the opportunity to study the Tulks Hill prospect;

-- D. Press, P. Finn, G. Andrews and H. Longerich for their assistance in obtaining geochemical and electron microprobe analyses;

-- W. Marsh for photographic help and F. Thornhill, L. Warford and G. Ford for thin and polished section preparation. Also, W. Howell for improving my draughting techniques;

-- The faculty and graduate students in the Department of Earth Sciences, for discussions and mental stimulation;

-- Jeannie Hiscock, Annie Reid and Alva Johnson for typing most of the data tables in this thesis;

-- The cooks and loggers at the Roebucks woods camp for their good food and good humour, respectively. In

particular, I would like to thank the camp foreman, John Paul, for his unlimited co-operation and for giving me the chance to see truly awful B movies.

Financial assistance was in the form of a Memorial University of Newfoundland Graduate Fellowship (1981-83) and a NSERC operating grant to Dr. D. F. Strong. Abitibi-Price Mineral Resources Ltd. gave a grant for logistical and academic support. All sources of funding are appreciated.

Finally, I would like to thank Linda J. Chafe for her encouragement and friendship during my three year stay in Newfoundland.

TABLE OF CONTENTS

CHAPTER 3

VICTORIA LAKE GROUP

CHAPTER 4

THE GEOLOGY AND PETROGRAPHY OF THE TULKS HILL ROCKS

CHAPTER 5

SULPHIDE MINERALOGY

CHAPTER 6

PETROCHEMISTRY

CHAPTER 7

RARE EARTH ELEMENTS

CHAPTER 10

GENETIC MODEL

LIST OF TABLES

LIST OF FIGURES

LIST OF PLATES

CHAPTER 1

INTRODUCTION

1.1 LOCATION AND ACCESS

Tulks Hill is located in central Newfoundland (NTS map sheet 12A/11) at the northern extremity of the Annieopsquotch Mountains, between longitudes 57° 10' 75" and 57° 13' 25"west and latitudes 48° 31' 20" and 48° 25' 00"north (Fig. 1.1). Access is by a recently constructed logging road from a woods camp ("Roebucks") owned and operated by Abitibi-Price Paper and Pulp Incorporated. The camp is serviced by good logging roads from Millertown, a small settlement on the shores of Red Indian Lake, located at the southern end of highway 370.

Road access from the woods camp to the study area may be restricted during times of heavy rainfall due to wash-outs, so that either walking, muskeg tractor or helicopter is the only viable means of access. Alternatively, access may be had by float plane, landing either at the mouth of Tulks River or on the numerous lakes surrounding the study area (eg. Costigan Lake), and thence walking to the study area.

1.2 SIZE OF THE STUDY AREA AND METHOD OF INVESTIGATION

The area of study is roughly rectangular in shape measuring approximately 960m by 2640m (Map 1).

Outcrop is moderate on top of Tulks Hill but generally

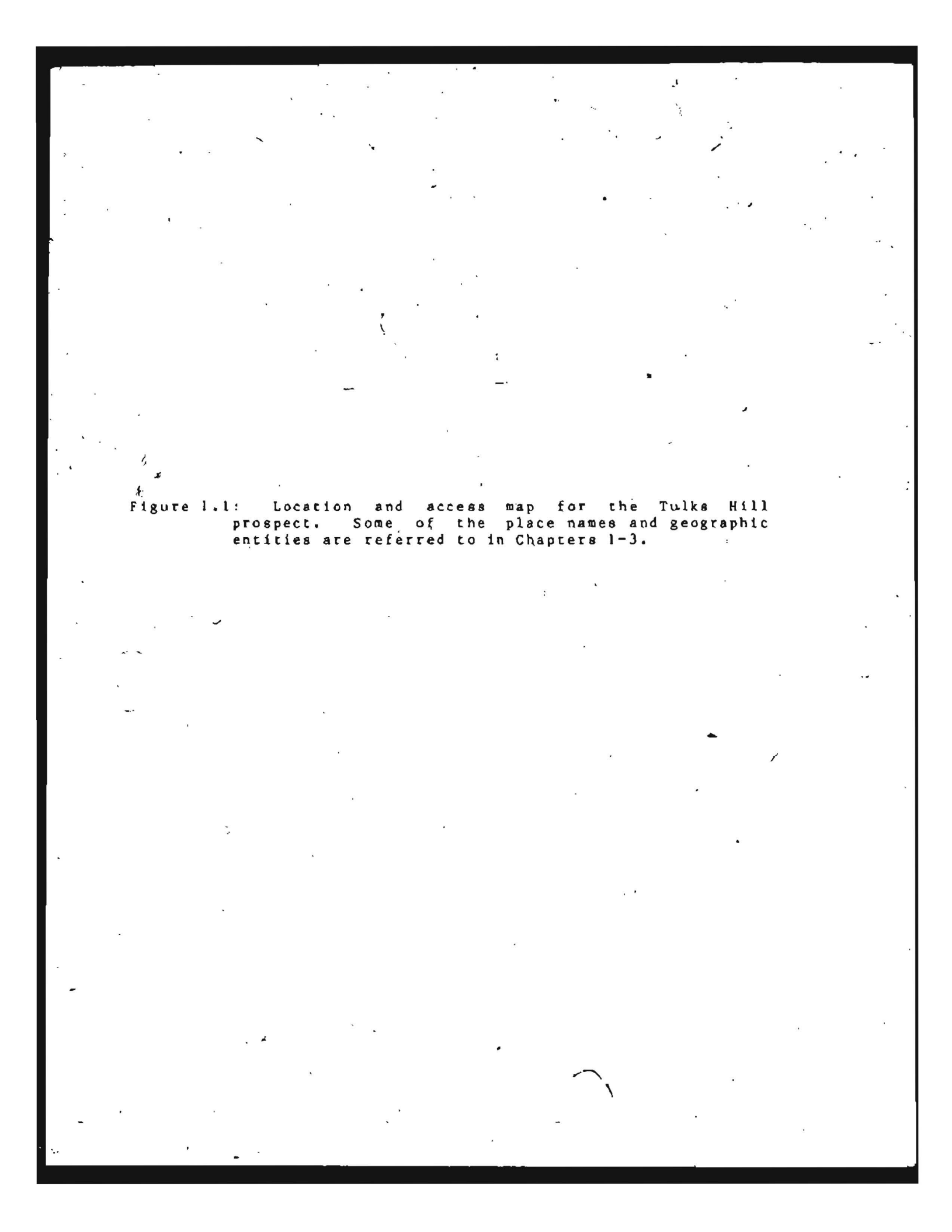

Figure 1.1: Location and access map for the Tulks Hill prospect. Some of the place names and geographic entities are referred to in Chapters 1-3.

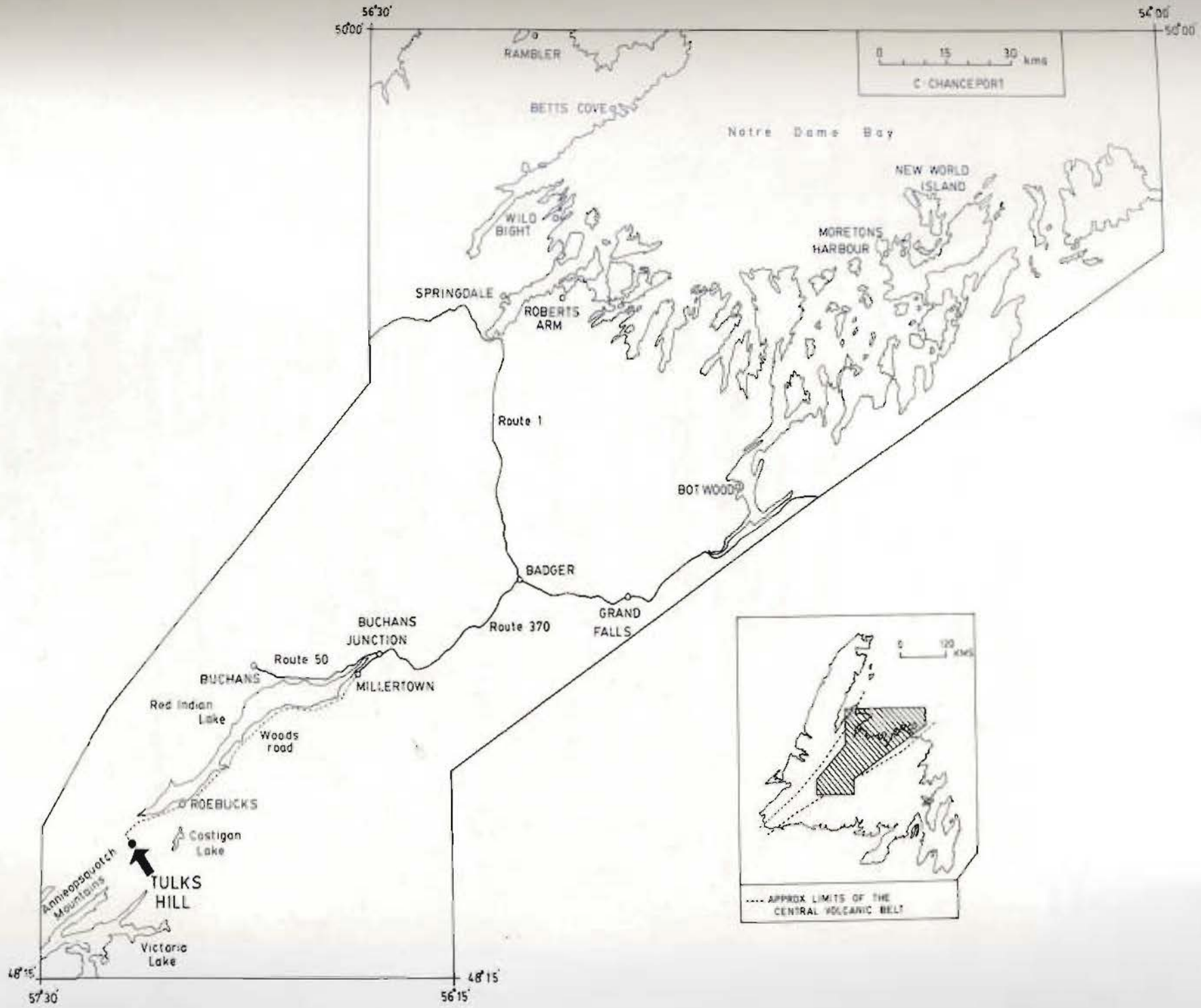
56°30'
50°00'
54°00'
50°00'
RAMBLER
0 15 30 kms
C CHANCEPORT
BETTS COVE
Notre Dame Bay
NEW WORLD ISLAND
WILD BIGHT
MORETONS HARBOUR
SPRINGDALE
ROBERTS ARM
Route 1
BOTWOOD
BADGER
GRAND FALLS
BUCHANS JUNCTION
Route 370
Route 50
BUCHANS
MILLERTOWN
Red Indian Lake
Woods road
ROEBUCKS
Costigan Lake
TULKS HILL
Annieopsquotch Mountains
Victoria Lake
48°15'
57°30'
56°15'
48°15'
0 120 kms
---- APPROX LIMITS OF THE CENTRAL VOLCANIC BELT

very poor in the heavily-wooded areas on the northern slopes and southwest part of the map area. Drill core is available, housed in a core shed at Buchans, some of which was used to construct a cross-section of the T3 sulphide lens (Map 3). Further access to this lens is via an adit, driven in 1980, which exposes a section of host rock from the footwall, through the mineralised horizon into the hangingwall. Most samples were taken from the adit (which was mapped in detail; Map 2) because their location with respect to the mineralised horizon, was accurately known. Away from the adit, samples from outcrop were studied in preference to drill core samples because of their known location: much of the core intersecting the other three lenses (Map 1) was often split and not always complete, which therefore made its use questionable.

Surface mapping was aided by cut lines, now partly overgrown, and stream sections cut by two brooks draining the eastern and western parts of the area. A contoured, geological map of Tulks Hill (Cooper, 1968), which located both the cut lines and the major outcrops, was used as a topographic map only; the geology was reinterpreted and a new geological map produced (Map 1).

Where there is little outcrop a lens shape and/or interfingering relationship of the rock units is inferred, for two reasons: a) felsic volcanic-pyroclastic rocks, which predominate at Tulks Hill, are limited in their lateral extent and often interdigitate with adjacent

lithologies; and b) the dominant cleavage at Tulks Hill is subparallel to the bedding, trending NE-SW, and it is presumed that the rock units would have been deformed into lensoid shapes also oriented NE-SW.

1.3 PHYSIOGRAPHY

Two physiographic subdivisions comprise Tulks Hill: a gently rolling plateau-like area in the south, with an average elevation of approximately 400m, and an area of sloping ground in the north, locally with precipitously vertical cliffs (30m high). Tulks River, to the north of Tulks Hill, is the main drainage for the area, flowing east and emptying into Red Indian Lake; two small brooks, which have their source in the plateau-like area of Tulks Hill, drain north into Tulks River.

1.4 GLACIATION

Evidence for glaciation is generally absent although striae, oriented 330 degrees, were noted by Cooper (1968). A till of varying thickness, consisting predominantly of granite gneiss and granite boulders (Cooper, 1968), mantles the lower levels of the river valley and fills depressions within the plateau-like area. Erratics of sericite schist (local?) and mafic rock types are common in the plateau-like area.

1.5 PREVIOUS WORK

A brief report on the sulphide mineralogy at Tulks Hill (Jambohr, 1983) is the only published information that is directly relevant to the present study. Regional geological surveys by the Nfld Dept. of Mines and Energy (eg. Kean, 1977b) include brief descriptions of, and references to, the geology of Tulks Hill, which are useful in terms of the regional stratigraphic and structural setting (Chapter 3). The most recent (unpublished) detailed work at Tulks Hill is by geologists working for Abitibi-Price Mineral Resources whose reports are on file at the main company office in Buchans.

Cooper (1968) described the petrology and mineralisation at Tulks Hill and interpreted the mineralisation in terms of the genetic concepts of the day. For example, "Hydrothermal fluids appear to have deposited the sulphides in tabular porous tops of acid volcanic flows on the northwest limb of the central anticline. The deposit may be described as exogenetic and epigenetic."(p.2).

Brown (1964), Coward (1965), and Riley (1957) mapped either all or parts of Tulks Hill. All other mapping previous to Riley (1957) was performed by resident geologists of American Smelting and Refining Company (ASARCO); their reports are on file at the ASARCO office in Buchans.

In 1961 a copper anomaly was detected at the foot of

Tulks Hill after geochemical sampling of stream waters. In the following two years detailed soil sampling was undertaken which defined additional copper anomalies. Diamond drilling of the prospect was begun in 1963 and continued into 1964. Some of this drill core, housed at Buchans under the supervision of Abitibi-Price - ASARCO, was used in the present study.

1.6 AIMS OF THIS STUDY

Detailed mapping of both the surface and underground geology, as well as petrographic, geochemical and structural analysis of the host rocks and the sulphide mineralisation, were the prime objectives of the present study. The accumulated data are used to formulate a genetic model for the Tulks Hill sulphide deposit in terms of present day ideas and concepts; this includes determining the environment of deposition of the footwall rocks, their composition, style of alteration related to sulphide deposition, the relationship of the hangingwall lithologies to the sulphide deposit and the effects of post-mineralisation deformation. Also, an attempt is made to determine the chemical and fluid characteristics at the time of alteration and sulphide deposition.

CHAPTER 2

REGIONAL GEOLOGIC AND TECTONIC SETTING

2.1 INTRODUCTION

Known base metal volcanogenic massive sulphide deposits within the Central Volcanic Belt (CVB; Kean et al., 1981) are restricted to the Lower Palaeozoic (Cambrian-Silurian). Detailed studies of the Notre Dame Bay (NDB) deposits has led to a greater understanding of both the stratigraphy and metallogeny of the Lower Palaeozoic rocks of north-central Newfoundland (Dean, 1977, 1978; Kean and Strong, 1975; Strong, 1977). Consequently, NDB dominates the interpretations of the Cambrian-Silurian stratigraphy of central Newfoundland, and it may be useful to summarise its geology and metallogeny before describing the stratigraphically equivalent rocks of Tulks Hill.

2.2 GEOLOGY AND MINERALISATION OF NOTRE DAME BAY

Most of the information below is taken from Dean (1978), with some additibnal information from Strong (1977). A summary of the Lower Palaeozoic stratigraphy of NDB is given in Figure 2.1.

2.2.1 BASEMENT

The Betts Cove ophiolite in western Notre Dame Bay is the best exposed example of the presumed basement which

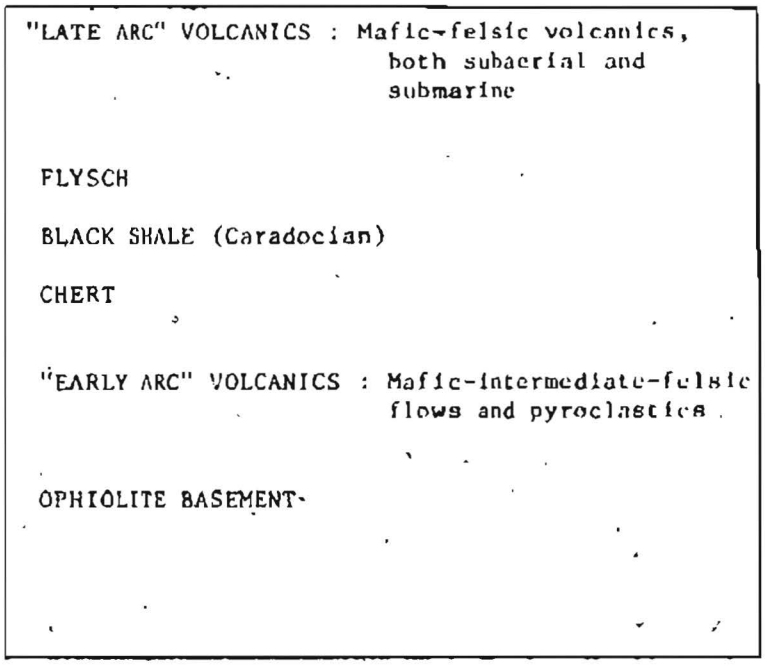

Figure 2.1: Simplified Lower Palaeozoic stratigraphy of Notre Dame Bay (compiled from Dean (1978))

numerous authors (Church and Stevens, 1971; Dewey and Bird, 1971; Upadhyay et al., 1971) interpret to represent oceanic crust. Closer to the study area, the ophiolitic occurrences of the Great Bend, Coy Pond, Pipestone Pond and Annieopsquotch complexes (see Fig. 3.1) are also remnants of the basement (Colman-Sadd, 1980; Colman-Sadd and Swinden, 1982; Dunning and Herd, 1980) although the timing of their emplacement is still disputed (Colman-Sadd, 1980; Pajari and Currie, 1978). Oceanic crustal basement is thought to have floored a wide Lower Palaeozoic ocean, called "Iapetus" (McKerrow and Ziegler, 1972), the closure of which produced ophiolite obduction and the Appalachian orogen through collision of the opposing margins (Williams, 1979).

Dunning and Krogh's (1983) U/Pb (zircon) age determinations for some of these Newfoundland ophiolite complexes give a narrow clustering of dates around upper Lower Ordovician (485 Ma.) suggesting either a synchronous time of formation or preferential preservation (obduction) of oceanic crust formed over a relatively short time range (Tremadoc-Arenig).

Sulphide deposits within ophiolite complexes typically have a relatively simple mineralogy, viz. pyrite, chalcopyrite and minor sphalerite, although gold and silver may also occur in significant quantities (Hutchinson, 1980). This mineralogy is typical of the CVB ophiolites, with chromite and magnetite as common accessories

(Colman-Sadd, 1980; Malpas and Strong, 1974).

2.2.2 PRE-CARADOCIAN VOLCANISM

Conformably overlying the ophiolitic basement are volcanic and pyroclastic rocks (hereafter referred to as volcanic(s) and pyroclastic(s) respectively) of mafic to intermediate composition with associated sediments. Locally, felsic horizons, chert and dyke rock are developed (Dean, 1978; Kean and Strong, 1975; Marten, 1971; Strong, 1977; Upadhyay, 1973; Upadhyay et al., 1971).

These rocks are thought to be related to subduction of Iapetus oceanic crust and the early stages of formation of an island arc system built upon that crust. This arc was centered near Wild Bight-Moretons Harbour (Fig. 1.1) and persisted through to late Ordovician-Silurian times (Kean and Strong, 1975; Payne and Strong, 1979; Strong, 1973).

A stratigraphically equivalent unit, the Dunnage Melange, is interpreted as a tectonic slump deposit of either existing lower Ordovician lithologies (southwest portion; Hibbard, 1976) formed during Caradocian times, or of more exotic and unique lithologies (northwest) for which no in-situ source terrain can be identified.

Copper (-zinc) mineralisation of the Consolidated Rambler mine is localised within felsic horizons of the Paquet Harbour Group (Tuach, 1976).

2.2.3 CARADOCIAN CHERT AND SHALE

Following the eruption of subduction-related volcanics there was a period of quiescence marked by the deposition of an extensive chert and black shale sequence which blanketed the volcanics. This lithology is interpreted by many authors to signal the closure of Iapetus (Dean, 1978; Dean and Strong, 1975; Strong, 1977; Williams, 1979) and in most areas deposition lasted for the whole of the Caradocian epoch. In western NDB however, only the lowest fossil zones are preserved (Nemagraptus gracilis) due to the deposition of easterly-prograding flysch derived from rocks exposed in the west during Taconic (middle Ordovician) uplift.

At most locations a basal red and green-black chert and cherty shale sequence is overlain by a black carbonaceous shale. Abundant radiolaria within the chert suggest that these are deep sea cherts, although it is possible that part of the chert is inorganic (Dean, 1978).

Pyritic horizons are locally developed within the shale which are currently the subject of a major metallogenic-geochemical investigation (Dean and Meyer, 1981, 1982, 1983, 1984).

2.2.4 FLYSCH DEPOSITS

An easterly prograding greywacke-conglomerate sequence of Upper Ordovician-Lower Silurian age overlies the Caradocian shale. Although the sequence is divisible into

two units, Sansom Greywacke overlain by the Goldson Conglomerate, they essentially represent different lithofacies of the same depositional episode.

The Sansom Greywacke is characterised by thickly-bedded arenaceous units, although basal argillaceous horizons are prominent in the more westerly localities. Turbidite deposition is indicated by scour channels, convolute bedding, and slump and intraformational breccias.

The Goldson Formation is present only in eastern NDB, with coralline fossils (Favosites, Halysites) indicating a Lower Silurian age. Massive, poorly-bedded conglomerates with plutonic, sedimentary and limestone clasts are characteristic, the latter suggesting the development of a reef system in the shallowing waters of the basin. Minor limy shale, argillite and sandstone occur at some localities.

This shallow water deposit marks the infilling of the "Caradoc basin" and denotes the final degradation of the island arc system of central Newfoundland (Hibbard and Williams, 1979).

On New World Island (Fig. 1.1) the flysch, black shale and Dunnage Mélange are suggested by McKerrow and Cocks (1977) to be part of a single stratigraphic "trench fill" sequence. They interpret the Sansom and Goldson "Groups" as an olistostrome and coarse-grained axial

channel facies respectively, both formed on the margin of the North American continent prior to the closure of Iapetus. Contrary to other publications (Dean, 1978; Dean and Strong, 1975; Strong, 1977; Williams, 1979), they suggest a Middle Devonian time of closure, using both faunal differences and the existence of "calc-alkaline" volcanics (post-Caradocian volcanics as used here) in Newfoundland, the Maritimes and Scotland as evidence. Williams (1979) suggests that the Reach Fault (between New World Island and the mainland) is not the suture zone for the closure of Iapetus, as suggested by McKerrow and Cocks (1977), but rather it represents the position of a local basin of deposition.

2.2.5 POST-CARADOCIAN VOLCANISM

A resurgence of volcanic activity in the CVB occurred immediately after the deposition of the chert-black shale-flysch sequence. It can be divided into three belts:

a) a central belt, known as the Roberts Arm-Buchans-Chanceport Belt, dominated by marine lithologies

b) two bounding belts, referred to as the Springdale Belt in the west and the Botwood Belt in the east, dominated by subaerial deposits.

a) Roberts Arm-Buchans-Chanceport Belt: The base of each group is marked by either an olistostrome or mafic-felsic volcanics. Blocks of volcanic rocks, conglomerate, greywacke and limestone set in an argillaceous matrix comprise the olistostrome, which probably resulted from either instability caused by the renewal of volcanism (Dean, 1978), or movement on the faults bounding the basin(s) of deposition (Arnott, 1983).

An overlying sedimentary unit, composed of slate, greywacke, sandstone, tuff and chert horizons with minor lavas, is capped by a volcanic assemblage of pillow lavas, agglomerates and tuffs. In most cases felsic volcanics are more abundant towards the top and locally-developed ignimbrites suggest subaerial conditions of deposition for some of the younger lithologies.

The important polymetallic sulphide deposits at Buchans are hosted by rocks of the Buchans Group (Thurlow et al., 1975) of probable middle Ordovician to early Silurian age (Bell and Blenkinsop, 1981; Bostock, 1978). Nowlan (unpub. information) did retrieve middle Ordovician conodonts from a limestone clast of a sedimentary unit in the Buchans Group but the fact that it is a clast introduces doubt for its significance with respect to the age of the Buchans Group.

b) Botwood and Springdale Belts: A lowermost sequence of alternating subaerial mafic-silicic lavas and pyroclastics, with interbedded red clastic sedimentary horizons, is an essential characteristic of each belt. A red, clastic sedimentary unit overlies all lithologies of the Botwood Belt but occurs only in the upper parts of the Springdale Group in the Springdale Belt. Ignimbritic volcanics, as well as cross bedding, ripple marks and mud cracks in the clastic lithologies, testify to a shallow water environment of deposition.

A marine sequence of lithologies, the Long Tickle Formation of the Cutwell Group (Kean, 1973), primarily consisting of interfingering lavas, agglomerate, tuff and limestone, is also correlated with rocks in the subaerial Springdale Belt (Dean, 1978).

2.3 DISCUSSION OF THE LITHOLOGIC AND METALLOGENIC EVOLUTION OF THE CVB

Figure 2.1 is a summary of the "typical" stratigraphic succession in the CVB: an ophiolite (oceanic) basement is overlain by two volcanic sequences, the latter being separated by a monotonous chert-black shale-flysch sequence.

At Betts Cove, Upadhyay (1973) documented a change from tholeiitic to calc-alkaline volcanism with a conformable progression into the overlying island arc lithologies. Dean and Strong (1975) expanded this idea to

propose a model, which is now generally accepted, of calc-alkaline volcanics overlying tholeiitic oceanic basement. The younger volcanic sequence, which post-dates continent-arc collision, is less easily explained and volcanism in a subduction (calc-alkaline) or rift-type environment is possible (Arnott, 1983; Thurlow, 1981 a,b).

It has been noted that the mineralogy of the sulphide deposits in Newfoundland changes with the composition of the host rocks (Stephens et al., in press; Swinden and Thorpe, in press), the NDB deposits (eg. Rambler) having less Zn and Pb than those deposits in central (Tulks Hill) and southern (Strickland) Newfoundland. This change in mineralogy corresponds to a change in host rock composition from mafic-dominated in NDB to felsic-dominated in central and southern Newfoundland. Hutchinson (1980) proposed that the mineralogy of sulphide deposits is a reflection of their tectonic environment: mineralisation in ophiolitic rocks, generated near spreading centres, has a relatively simple mineralogy (chalcopyrite-pyrite), whereas deposits in primitive island arcs are Cu-Zn rich. Deposits within the mature parts of the same island arc tend to be richer in Zn and Pb: a mixture of rifting and subduction volcanism is common in these environments, a fact noted by Cathles et al. (1983) for the Kuroko deposits. The change in mineralisation from the basement into pre-Caradocian volcanic rocks of NDB suggest that the tectonic environment may be a control on the type of mineralisation. This

implies that the tectonic environment at Tulks Hill, which has a Cu-Zn (-Pb) mineralogy, was dominated by a primitive arc, possibly with locally-developed rifting to account for the Pb in the deposit.

Mineralisation in the post-Caradocian volcanic sequences, which is distinctly polymetallic but localised in its distribution (eg. Buchans, Pilleys Island), is suggestive of a mature island arc environment with associated rifting. Both Thurlow (1981 a,b) and Strong (1973) have suggested that the post-Caradocian volcanic rocks were generated in an island arc setting, and Arnott (1983) has suggested that rifting was important in post-Caradocian times. It therefore seems likely that the post-Caradocian mineralisation was generated in a rifted, mature arc.

CHAPTER 3

VICTORIA LAKE GROUP

3.1 INTRODUCTION

The host rocks to the Tulks Hill deposit are the Victoria Lake Group (VLG; Kean, 1977b). It is an assemblage of volcanic and epiclastic rocks in central Newfoundland that crops out in a narrow, linear belt from King George IV Lake through to Grand Falls (Fig. 3.1), a distance of approximately 175km. Conodonts of Llanvirn-Llandeilo age, retrieved from a limestone horizon in the upper portions of the VLG (Kean and Jayasinghe, 1981), suggest that the VLG is correlative with pre-Caradocian volcanic rocks in Notre Dame Bay (Chapter 2). Model ages for Pb isotope data obtained for the Tulks Hill deposit suggest an age of 400-412 Ma for the Group (Swinden and Thorpe, in press): this age is too young since the VLG is known to underlie a Caradocian-age black shale and the conodont age is preferred.

The following generalised description of lithologies, stratigraphy and structural relationships is compiled from Dunning et al., (1982), Herd and Dunning (1979), Jayasinghe (1979), Kean (1976, 1977a, 1977b, 1978, 1979) Kean and Jayasinghe (1980, 1981), Kean and Mercer (1978) and Mercer (1978).

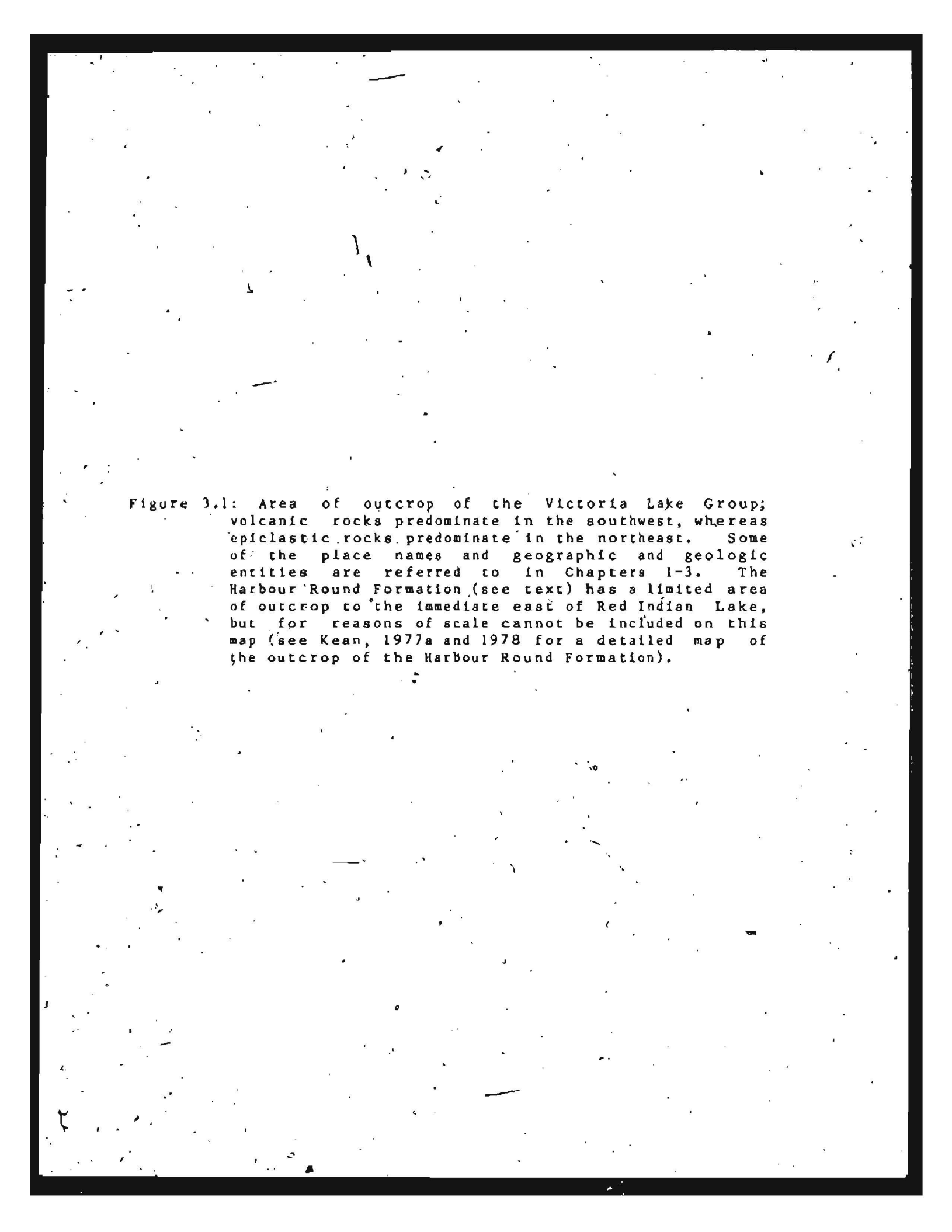

Figure 3.1: Area of outcrop of the Victoria Lake Group; volcanic rocks predominate in the southwest, whereas epiclastic rocks predominate in the northeast. Some of the place names and geographic and geologic entities are referred to in Chapters 1-3. The Harbour Round Formation (see text) has a limited area of outcrop to the immediate east of Red Indian Lake, but for reasons of scale cannot be included on this map (see Kean, 1977a and 1978 for a detailed map of the outcrop of the Harbour Round Formation).

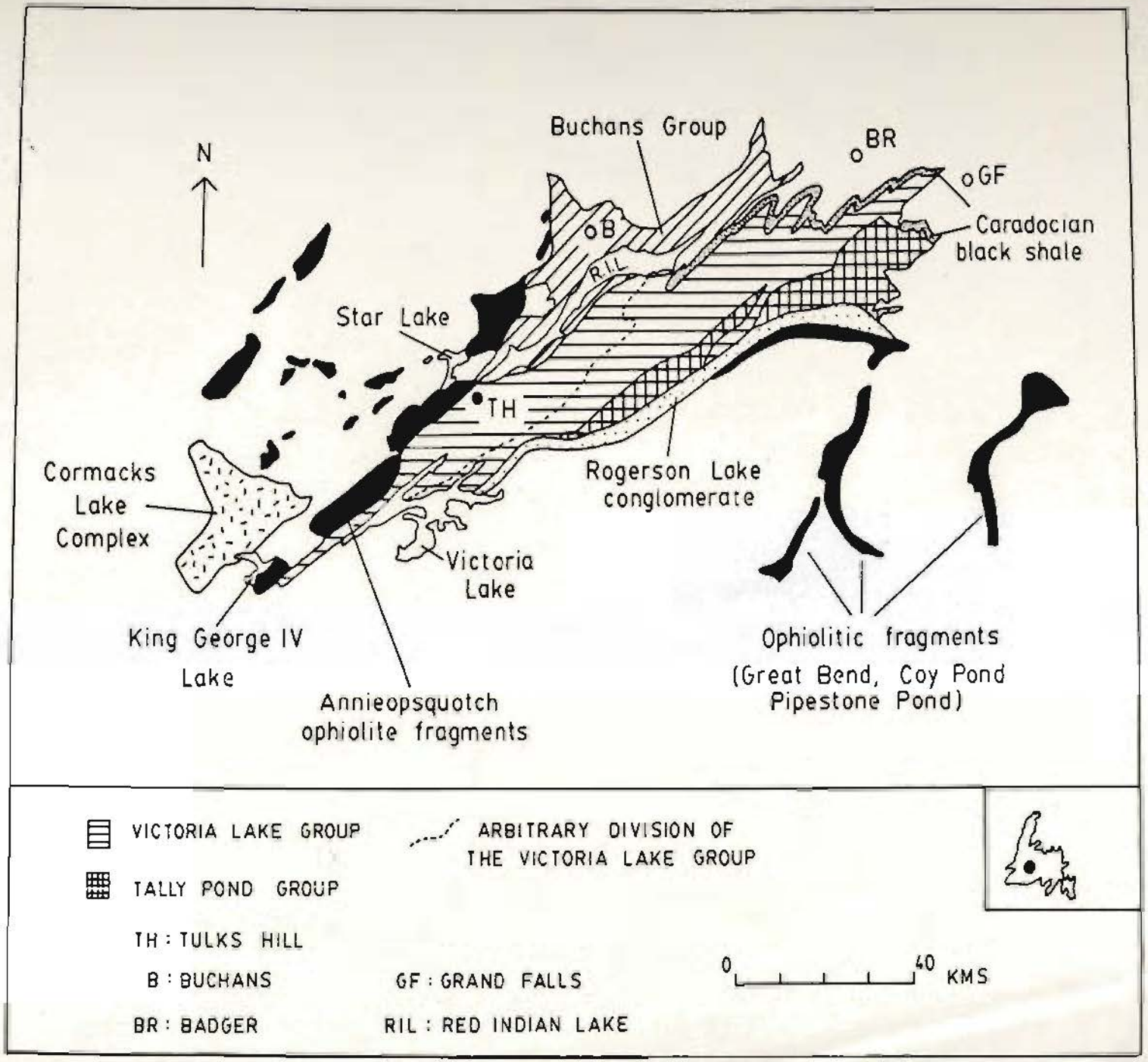
N
Buchans Group
BR
GF
Caradocian
black shale
B
RIL
Star Lake
TH
Cormacks
Lake
Complex
Rogerson Lake
conglomerate
Victoria
Lake
King George IV
Lake
Annieopsquotch
ophiolite fragments
Ophiolitic fragments
(Great Bend, Coy Pond
Pipestone Pond)
VICTORIA LAKE GROUP
ARBITRARY DIVISION OF
THE VICTORIA LAKE GROUP
TALLY POND GROUP
TH : TULKS HILL
B : BUCHANS
GF : GRAND FALLS
BR : BADGER
RIL : RED INDIAN LAKE
0
40
KMS

3.2 GENERAL GEOLOGY

A tentative correlation chart for the various map areas containing all or portions of the VLG is shown in Figure 3.2. Younging directions are seldom seen and it is only inferred that the silicic rocks overlie the mafic rocks. The dashed lines are not isochrons but connect similar lithologies or related facies. The thickness of these units is difficult to determine because of faulted contacts, poor outcrop, structural complexities and lithological similarity between and within units.

Two intrusive rock types are found: a) composite plutons comprising varible amounts of gabbro, diorite, granodiorite, quartz-monzonite and quartz porphyry, and b) medium to fine-grained gabbro-diorite. Both varieties of plutons have elliptical or linear outcrop patterns, suggesting post- or syn-tectonic periods of intrusion respectively. Some of these plutons intrude the VLG and are thought to represent the sub-surface feeders to the volcanic rocks of the VLG (Jayasinghe, 1979; Kean, 1978; Kean and Mercer, 1978; Mercer, 1978)

3.3 STRATIGRAPHY

An arbitrary two-fold lithological division of the Group is made as follows:

a) dominantly marine clastic sediments in the northeast outcrop area,

b) dominantly volcanic-pyroclastic lithologies in the

Figure 3.2: Tentative correlation chart for the Victoria Lake Group. The dashed lines connect similar lithologies or related facies. See text for references used in compilation.

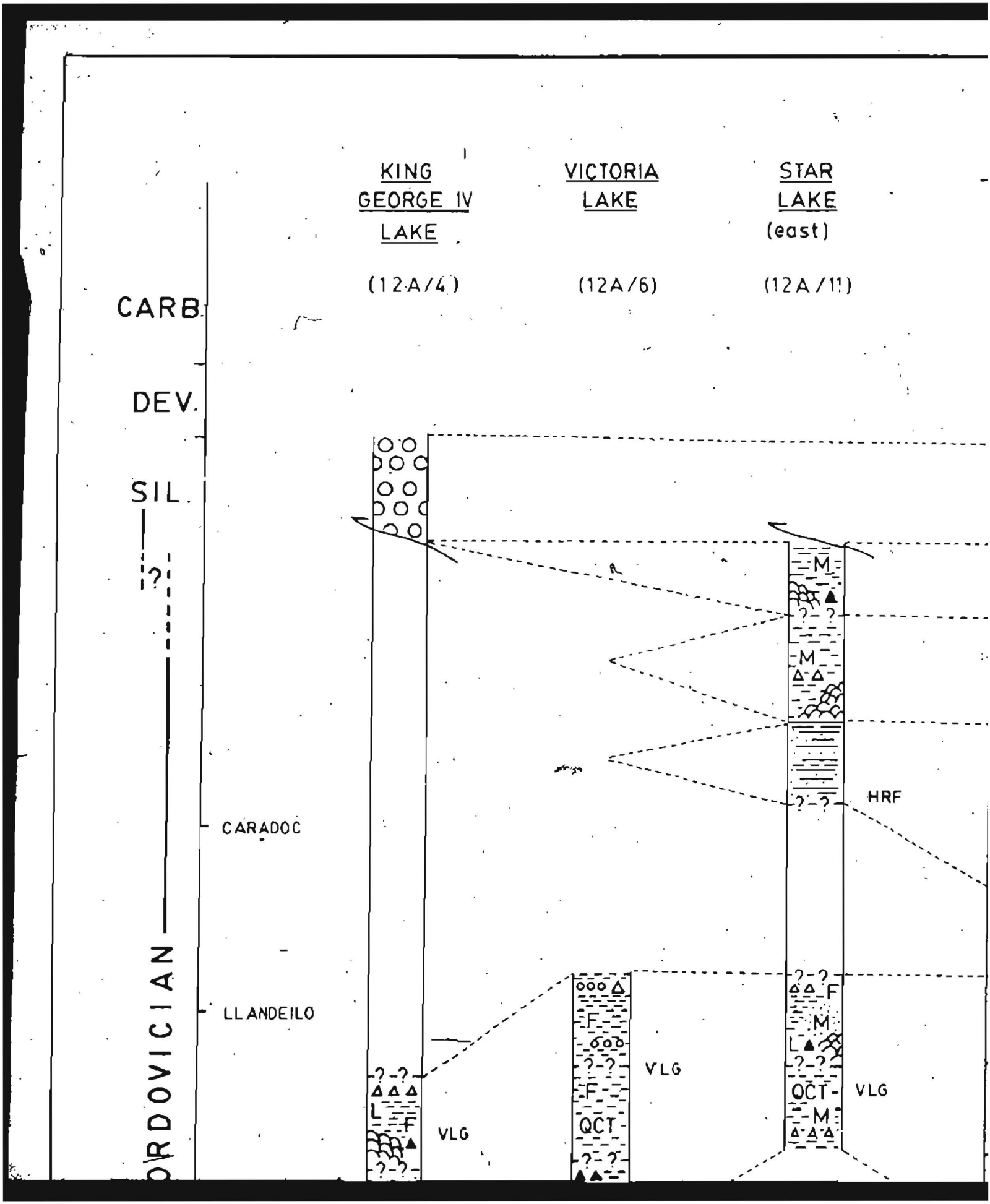
KING GEORGE IV LAKE
(12A/4)
VICTORIA LAKE
(12A/6)
STAR LAKE (east)
(12A/11)
CARB.
DEV.
SIL.
?
ORDOVICIAN
CARADOC
LLANDEILO
HRF
VLG
VLG
VLG
M
F
L
QCT

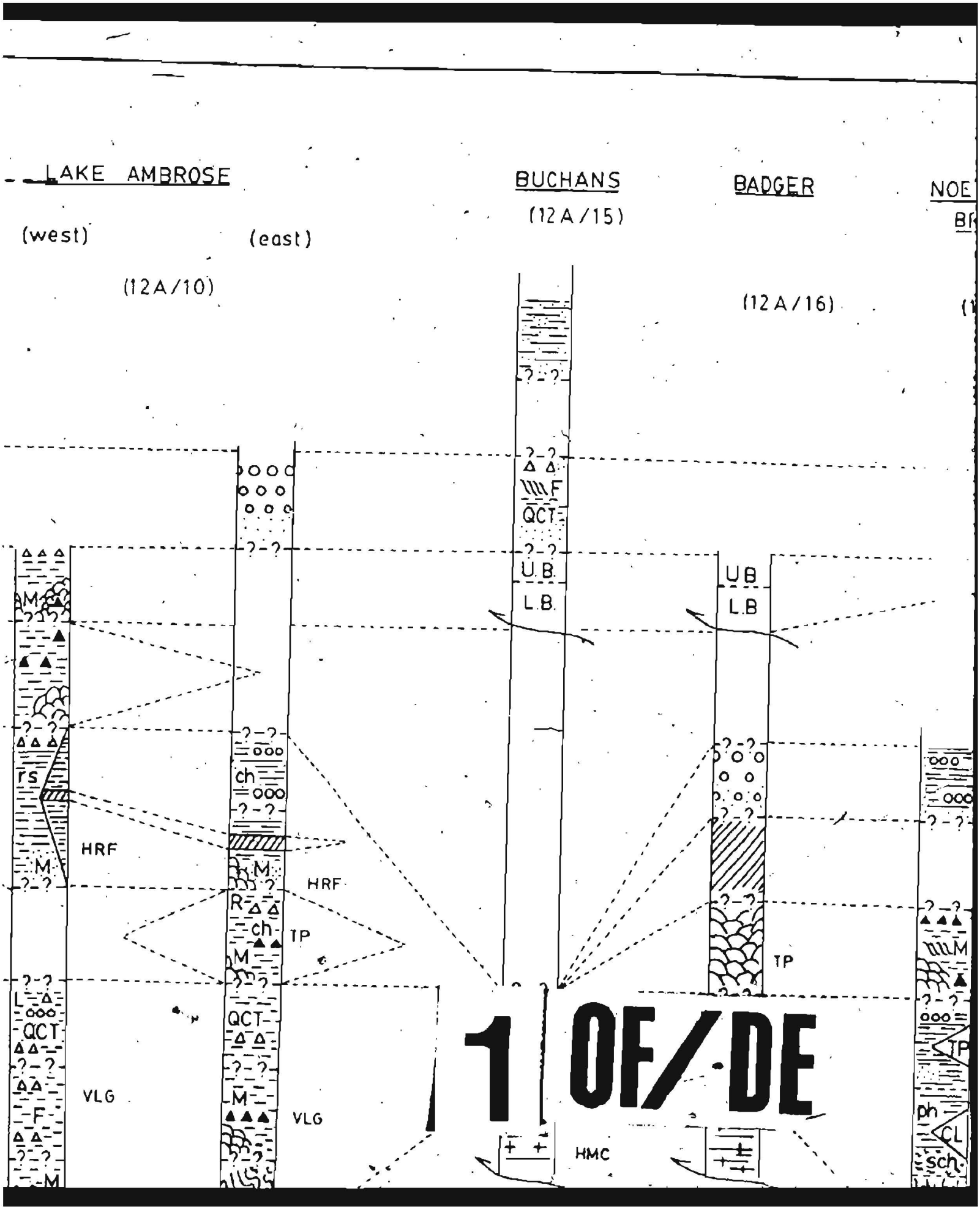
LAKE AMBROSE
(west)
(east)
(12A/10)
BUCHANS
(12A/15)
BADGER
(12A/16)
NOE
BR
(1
M
rs
HRF
M
L
QCT
VLG
F
M
ch
M
HRF
R
ch
TP
M
QCT
VLG
M
F
QCT
U.B.
L.B.
HMC
UB
LB
TP
TP
M
TP
ph
CL
sch.

1 OF/-DE

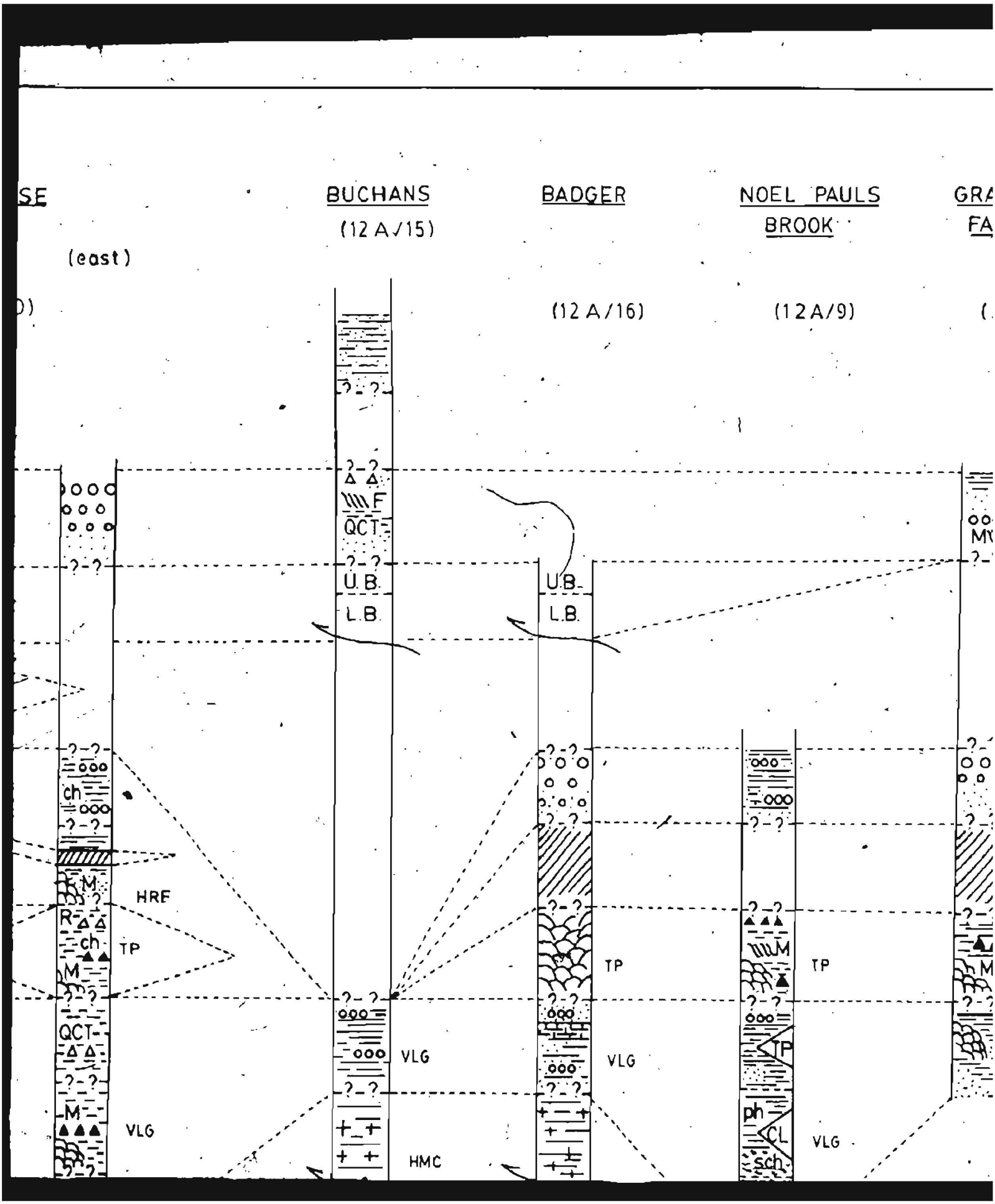
SE
(east)
)
BUCHANS
(12 A/15)
BADGER
(12 A/16)
NOEL PAULS
BROOK
(12 A/9)
GRA
FA
F
QCT
U.B.
L.B.
U.B.
L.B.
ch
M
HRF
R
ch
TP
M
QCT
M
VLG
VLG
HMC
TP
VLG
M
TP
TP
ph
CL
sch
VLG

ND
LLS

2 OF/DE

2D/13) ← NTS map sheet

LEGEND

UB Upper Buchans subgroup
LB Lower Buchans subgroup
HRF : Harbour Round Formation
TP Tally Pond Group
HMC : Hungry Mountain Complex
CL Carter Lake Volcanics
VLG : Victoria Lake Group

Breccia mafic/felsic
Tuff
Pillow lava
Sandstone / Greywacke
Siltstone
rs Red siltstone
Caradocian black shale
Conglomerate
Lava flow
ch Chert
Limestone
R Rhyodacite

P.C : Precambrian
QCT : Quartz crystal tuff
M : Mafic
F : Felsic
L : Lapilli
ph : Phyllite
sch : Schist
Gneiss
: Sheeted dykes
: Gabbro
: Pyroxenite
: Deformed plutonic rocks
: Thrust fault no direction implied
Cormacks Lake Complex

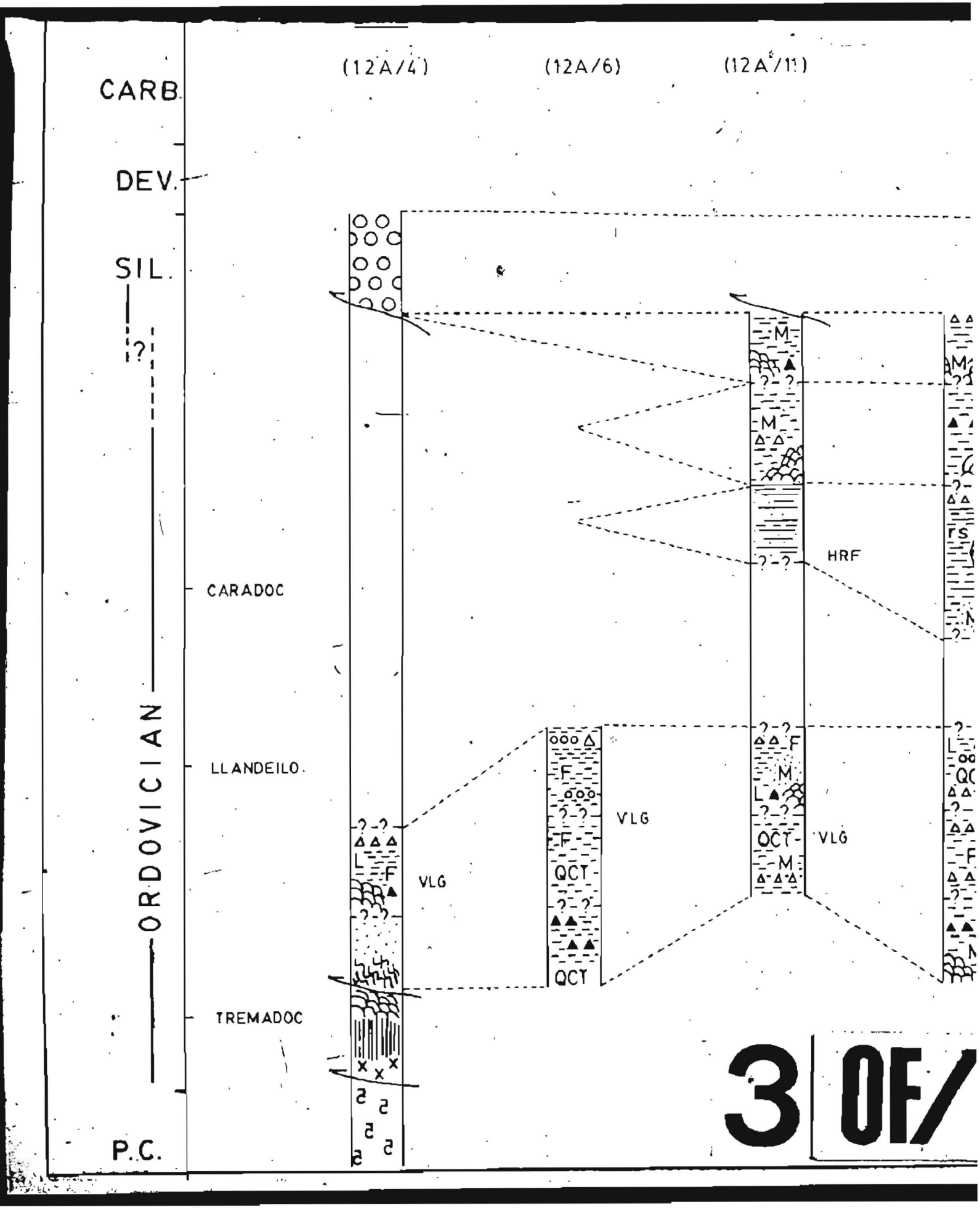
(12A/4)
(12A/6)
(12A/11)
CARB.
DEV.
SIL.
?
ORDOVICIAN
CARADOC
LLANDEILO
TREMADOC
P.C.
VLG
VLG
VLG
HRF
QCT
QCT
M
F
L
S
3 OF

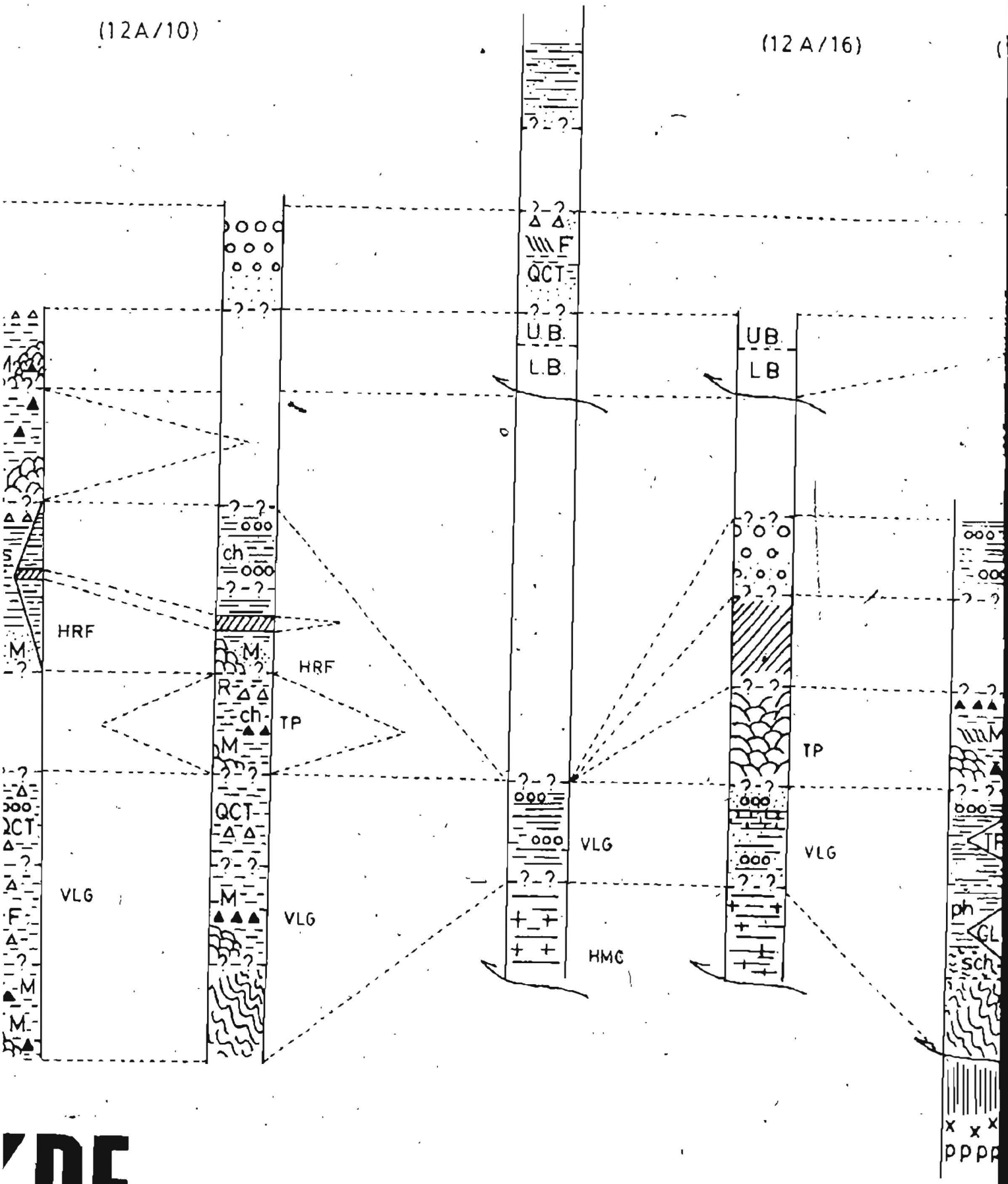
(12A/10)
(12A/16)
F
QCT
UB
LB
ch
HRF
M
R
TP
VLG
HMC
ph
GL
sch
x x x
p p p p

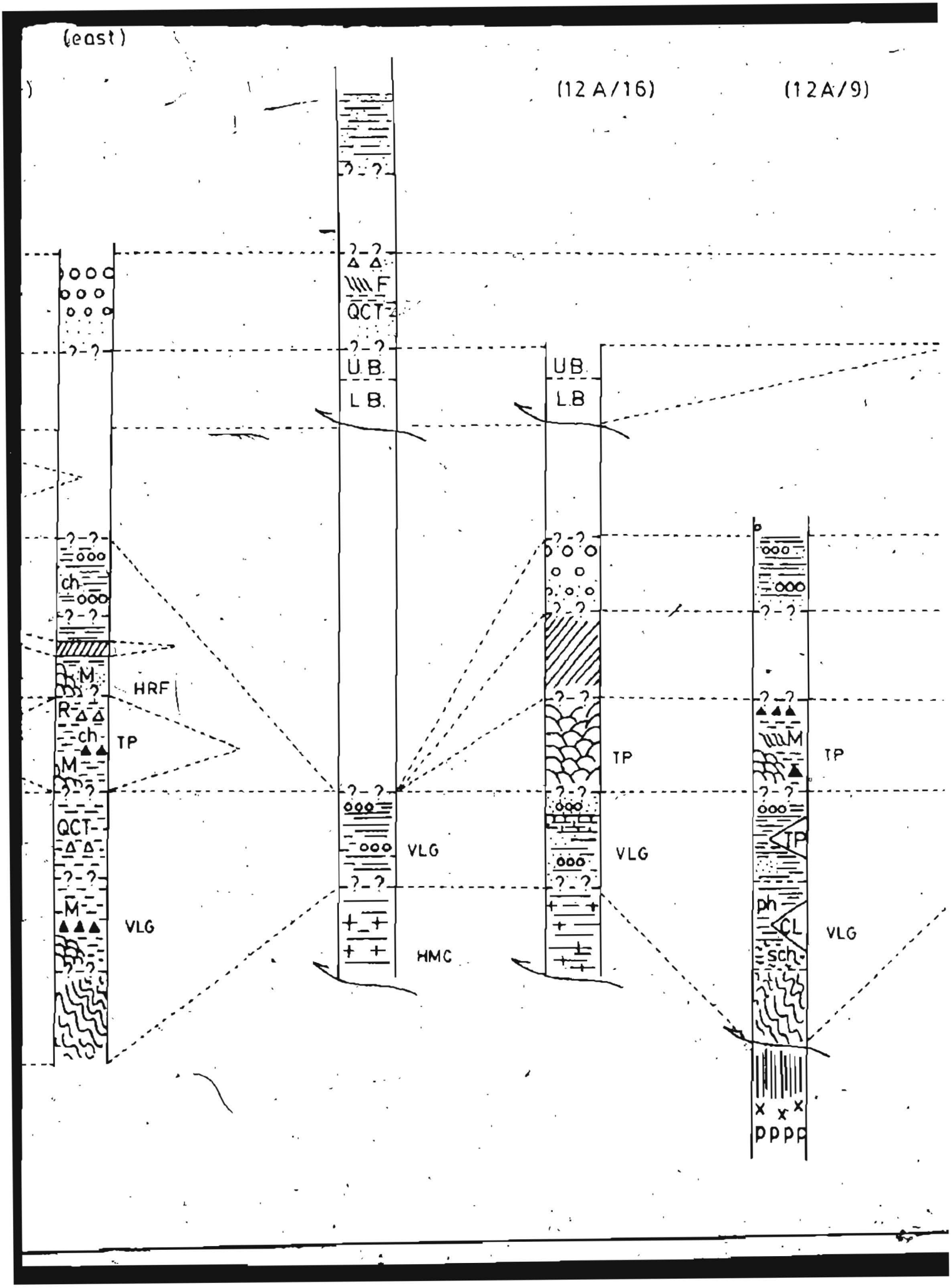
(east)
(12 A/16)
(12 A/9)
F
QCT
U.B.
L.B.
UB
LB
ch
M
HRF
R
TP
QCT
VLG
HMC
ph
CL
sch
x x x
p p p p

(2D/13) ← NTS map sheet

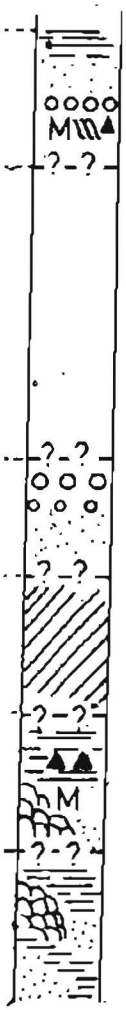

LEGEND

UB Upper Buchans subgroup
LB Lower Buchans subgroup
HRF : Harbour Round Formation
TP Tally Pond Group
HMC : Hungry Mountain Complex
CL Carter Lake Volcanics
VLG : Victoria Lake Group

Breccia mafic/felsic
Tuff
Pillow lava
Sandstone / Greywacke
Siltstone
rs Red siltstone
Caradocian black shale
Conglomerate
Lava flow
ch Chert
Limestone
R Rhyodacite

PC : Precambrian
QCT Quartz crystal tuff
M Mafic
F Felsic
L Lapilli
ph Phyllite
sch Schist
Gneiss
Sheeted dykes
Gabbro
ppp Pyroxenite
Deformed plutonic rocks
Thrust fault no direction implied
Cormacks Lake Complex

4 OF/DE 4

southwest outcrop area.

An approximate common boundary between these two groups may be drawn between the Lake Ambrose (east) and Buchans map sheets (see Fig. 3.2).

3.3.1 NORTHEAST OUTCROP AREA

Slates, siltstones, sandstones and greywackes, with minor interbeds of chert, red argillite and rare basic volcanics, characterise the Group in this area. Locally, conglomerate horizons and minor intermediate to felsic flows and agglomerates are present (Kean and Mercer, 1978). A single limestone horizon, exposed near the top of the sequence in the Badger map area, contains Llanvirn-Llandeilo age conodonts (Kean and Jayasinghe, 1980, 1981).

Sharp erosional bases and tops are associated with full or partial Bouma sequences within the clastic sedimentary units. Numerous localised sedimentary structures help to identify younging directions but the poor outcrop and repetitive lithological similarity hinders regional stratigraphic interpretations.

In the Noel Paul's Brook region the VLG is progressively metamorphosed towards the southeast where phyllites, schists and gneisses replace the typical greywacke-siltstone-chert sequence with increasing proximity to a granite-gneiss terrane (Jayasinghe, 1979).

A black shale, similar to that outcropping in NDB

(Chapter 2), overlies the VLG in central Newfoundland but its accurate delineation, mainly through geophysics, is hampered by interbedded greywacke, siltstone and chert which interfere with the geophysical signal. Caradocian graptolites within the shale confirm the pre-Caradoc age of the underlying Victoria Lake Group. In Figure 3.2 the Caradocian black shale and the overlying greywacke-conglomerate sequence is not included within the VLG, principally because of stratigraphic correlations with the Caradocian black shale and overlying flysch deposits in NDB (cf. Kean and Mercer, 1978). A similar, but apparently unfossiliferous, black shale in the Noel Paul's Brook region is also correlated with the Caradocian shale outcropping in the Grand Falls region.

3.3.2 SOUTHWEST OUTCROP AREA

Quartz-rich silicic rocks of rhyodacite composition, typically coarse pyroclastic breccias and crystal-lithic tuffs, are the most common lithologies, although massive flows and fine-grained tuffaceous rocks also occur (Kean, 1976, 1977a, 1977b, 1978).

Mafic to intermediate flows, agglomerates and tuffs are sporadically developed in the Star Lake (east) and Victoria Lake areas, typically occurring as intercalations within the silicic rocks (Kean, 1976, 1978). In the Lake Ambrose (west) area however, more extensive mafic-intermediate horizons occur (Kean, 1977a). Interbeds

of tuffaceous greywacke, sandstone, siltstone and black shale are present, particularly in the Victoria Lake area (Kean, 1976). Similar rock types outcrop in the King George IV and Lake Ambrose (east) map areas (Kean, 1978; Kean and Jayasinghe, 1981).

Altered mafic pillow lavas are faulted against the supposed basement (Annieopsquotch ophiolite) in the Victoria Lake region. If these pillow lavas mark the base of the VLG it provides a basis for suggesting a tentative correlation of the VLG with the pre-Caradocian volcanics of NDB, ie. the mafic rocks in the Victoria Lake area are equivalent to the Snooks Arm Group, for example, the latter conformably overlying the Betts Cove ophiolite (Chapter 2).

3.4 STRUCTURAL STYLE OF THE VICTORIA LAKE GROUP

All lithologies of the VLG, excluding some of the intrusions (Kean, 1976), possess a schistosity subparallel to the bedding (Herd and Dunning, 1979). It strikes parallel to the trend of the belt (NE-SW) and dips steeply to the northwest.

Rarely, distinct way-up and cleavage-bedding relationships can be defined and the units young to the northwest and "large-scale" tight to isoclinal folding is inferred (Kean, 1976, 1977b; Mercer, 1978). Faults parallel to the beds, associated with the probable isoclinal folding, are thought to be commonplace, although

it is difficult to document the amount and direction of displacement (Kean, 1976).

This deformation style and the accompanying greenschist grade of metamorphism are very typical of the VLG and serve to distinguish it from the overlying Buchans Group (Kean and Jayasinghe, 1980).

3.5 RELATIONSHIPS OF THE VLG TO THE BASEMENT.

The VLG is probably correlative with the pre-Caradocian volcanics of NDB (Kean et al., 1981) which implies an oceanic crustal basement (see Chapter 2). Possible ophiolitic basement outcrops in the King George IV and Noel Paul's Brook map sheet areas, although the contacts are either faulted or unexposed (Jayasinghe, 1979; Kean and Jayasinghe, 1981). Medium-grained gabbro, cumulate pyroxenite, and minor diorite occur in the Noel Paul's Brook area (Fig. 3.2), although intense deformation and alteration has converted the original pyroxenes to amphiboles (Jayasinghe, 1979). In the King George IV map area sheeted dykes, pillow lavas and gabbro occur, probably representing the upper portions of the oceanic crustal basement (Kean and Jayasinghe, 1981).

The Cormacks Lake Complex (King George IV area) may represent Grenville age continental basement (Herd and Dunning, 1979). It consists of polydeformed biotite gneiss, quartzite, amphibolite, mica-schist, calc-silicate

units and a foliated granite. Garnets, pyrite and magnetite are also sporadically developed. Multiple deformation patterns suggest that the complex is older than the less deformed ophiolitic material and it is therefore interpreted by Herd and Dunning (1979) to be a raft of Precambrian continental crust.

Amphibolite-grade metamorphic rocks mark the base of the VLG in parts of the Noel Paul's Brook, Lake Ambrose (east) and King George IV map areas (Kean and Jayasinghe, 1980, 1981) but are interpreted to represent locally-developed prograde metamorphic equivalents of VLG lithologies rather than basement; a lack of polyphase deformations distinguishes these rocks from the Cormacks Lake Complex.

3.6 ROCKS OVERLYING THE VLG

3.6.1 TALLY POND GROUP

The Tally Pond Group is probably the overlying lithological unit in the Badger, Noel Paul's Brook, Grand Falls (west) and Lake Ambrose (west) map sheet areas (Fig. 3.2). Fine-grained clastic and volcanogenic sediments, overlain by mafic pillow lavas, flows, and breccias, with intercalated felsic flows and pyroclastics, crop out in the type area (Lake Ambrose (west)). Laminated siltstones, red chert and shales are interbedded with the volcanics.

Mafic to intermediate flows, breccias and tuffs with interbedded siltstones and greywacke, which crop out in the

Grand Falls (west) and Noel Paul's Brook regions (Jayasinghe, 1979; Kean and Mercer, 1978) which are also referred to as the Tally Pond Group; although Jayasinghe (1979) does not use the term "Tally Pond" for the units in the Noel Paul's Brook region, the similarity in lithology suggests a probable equivalence with those in the type area. In the Noel Paul's Brook region felsic rocks of the Tally Pond Group are intercalated with the VLG suggesting that the base of the Tally Pond Group is diachronous and that its lowest members are equivalent to the uppermost portions of the VLG.

3.6.2 HARBOUR ROUND FORMATION

Finely-laminated grey-green siltstone, red siltstone and chert, and minor mafic tuffaceous rocks constitute the Harbour Round Formation (Fig. 3.2). It has a limited outcrop distribution and is present only in the Star Lake (east) and Lake Ambrose (west) map areas (Kean, 1977a, 1978). No contact relationships are seen with the underlying VLG. Younger rocks in the Lake Ambrose (east) area are separated from the VLG by members of the Tally Pond Group suggesting that the Harbour Round Formation is stratigraphically equivalent to the Tally Pond Group.

The southwestern extremity of the area has no outcrops of Harbour Round Formation. Instead, the Silurian(?) polymict Rogerson Lake conglomerate probably overlies the Victoria Lake Group (Kean, 1983; Kean and Jayasinghe,

1981) suggesting uplift and erosion, and/or non-deposition, of post-Caradocian rocks in this area.

3.7 LITHOLOGICAL COMPARISONS WITH THE ROCKS OF NOTRE DAME BAY

A Caradocian black shale in both central Newfoundland and NDB suggests a connection of the two areas in middle Ordovician times. Pre-Caradocian lithological sequences in the two areas are, however, quite different: there is a relative abundance of felsic pyroclastics and volcanics in the southern portions of the VLG which may, in part, be related to a difference in the basement type. It has been suggested (Colman-Sadd, 1980; Swinden, 1982; Swinden and Thorpe, in press) that continental crust may have played a more significant role in determining the magma type in central and southern Newfoundland, the felsic magmas possibly being generated by crustal assimilation and/or palingenesis. In south central Newfoundland the Cormacks Lake Complex is an obvious candidate as evidence of such continental crust. It is interesting to note that no outcrops of Cormacks Lake equivalents are found in Notre Dame Bay.

3.8 SUMMARY, INTERPRETATION AND STYLE OF MINERALISATION IN THE VLG

Two lithological facies comprise the linear belt of rocks known as the Victoria Lake Group: felsic volcanic

and pyroclastic rocks predominate in the southwest whereas epiclastic, sedimentary rocks outcrop in the northeast. Caradocian age graptolites within the overlying black shale confirm the pre-Caradocian age of the VLG and therefore correlate the Group with the pre-Caradocian volcanic rocks of NDB (Chapter 2).

Basement relationships are not clear-cut and both oceanic (Annieopsquotch ophiolite) and continental (Cormacks Lake Complex) crustal basement are possible; this separates the evolution of the VLG from the stratigraphically equivalent lithologies in NDB. Pb isotope data (Swinden and Thorpe, in press) favour continental crustal involvement during magma genesis. An unusual tectonic environment is therefore required to explain the change in volcanism to the south of NDB; one such environment involves the transgression of island arc volcanism across a continental boundary, as suggested by Swinden and Thorpe (in press; see Fig. 3.3).

Mineralisation within the VLG also reflects the change in both the style of magma genesis and the related volcanic rocks; volcanogenic massive sulphide deposits in central and southern Newfoundland have increased proportions of Zn and Pb relative to Cu, a feature that is thought to reflect an increased involvement of continental crust (Stephens et al., 1983; Swinden and Thorpe, in press).

Figure 3.3: Island arc migration across a continental boundary. This tectonic interpretation has been suggested by Swinden and Thorpe (in press) to explain the abundance of felsic volcanic rocks, increased Zn and Pb contents of volcanogenic massive sulphide deposits in central and southern Newfoundland, and changes in Pb isotope values (redrawn).

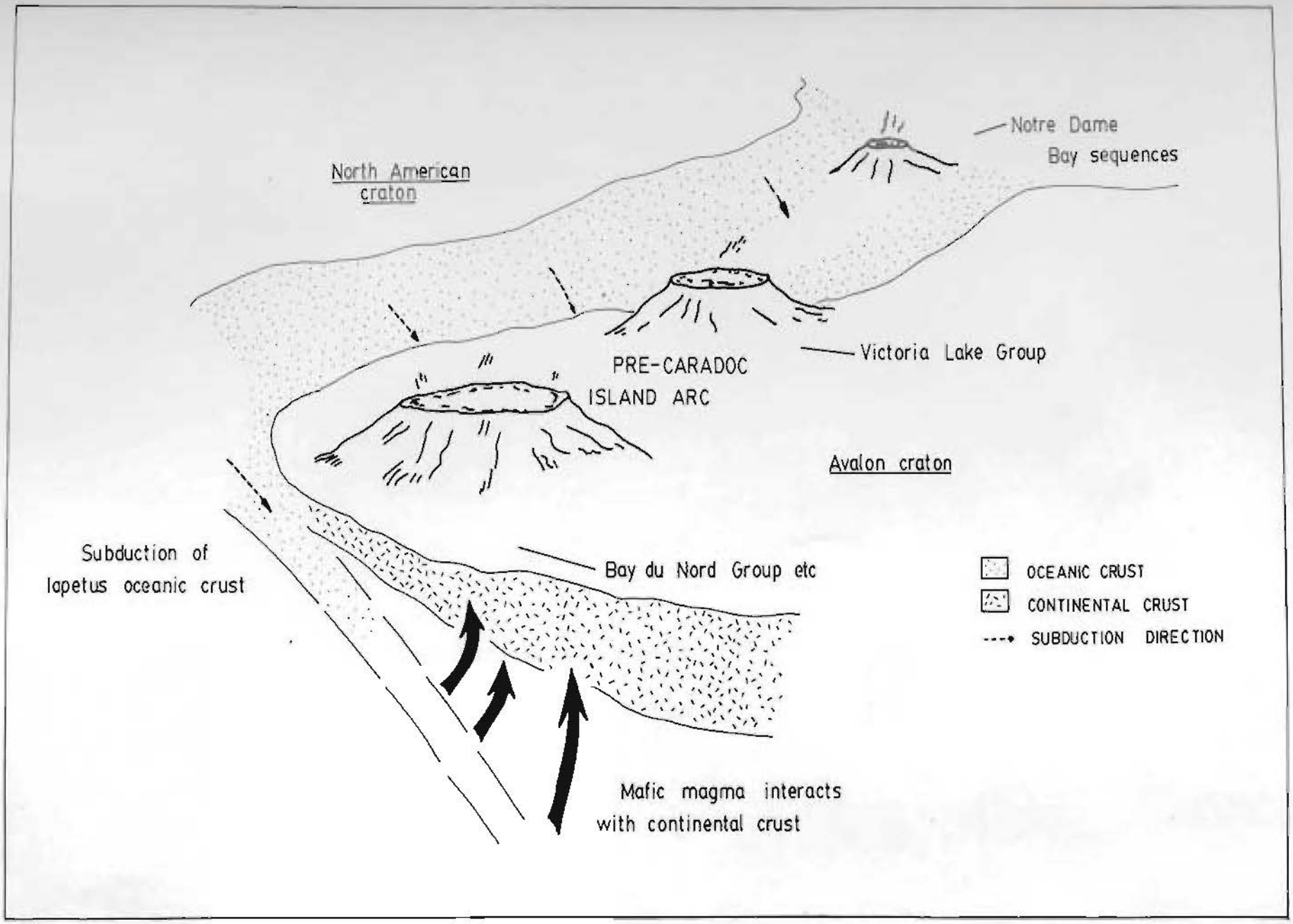
North American craton
Notre Dame Bay sequences
Victoria Lake Group
PRE-CARADOC ISLAND ARC
Avalon craton
Subduction of Iapetus oceanic crust
Bay du Nord Group etc
Mafic magma interacts with continental crust
OCEANIC CRUST
CONTINENTAL CRUST
SUBDUCTION DIRECTION

CHAPTER 4

THE GEOLOGY AND PETROGRAPHY OF THE TULKS HILL ROCKS

4.1 INTRODUCTION

The Tulks Hill rocks crop out in the Dunnage tectonostratigraphic zone of the Appalachians (Williams, 1979) and more specifically within the Star Lake (east) map sheet (Kean, 1978). They are part of the southwest portion of the VLC in which felsic volcanics and pyroclastics are dominant.

4.2 GENERAL STATEMENT

Table 4.1 compares the unit names used in this study with those of Cooper (1968). Cooper's geological map is too generalised for the present study and was used only as a topographic and outcrop-location map. Maps of the surface (revised) and underground (new) geology can be found in the back pocket of this thesis (Maps 1 and 2, respectively).

In this chapter the geology and petrography of the Tulks Hill rocks are described and interpreted. The sulphides of the "mineralised horizon" (see Fig. 4.1) are discussed in Chapter 5.

4.3 ROCK DESCRIPTIONS

Table 4.2 summarises the primary and secondary mineralogy of the 11 rock types that crop out at Tulks

Table 4.1 : Unit names used in this study and by Cooper (1968)

THIS STUDY	COOPER (1968)
Quartz crystal tuff Large quartz crystal tuff	Sericitic acid volcanics
Quartz crystal tuff	Porphyritic chloritic acid volcanics
Biotite quartz crystal tuff	Biotitic acid volcanics
Rhyolitic breccia	Fragmental acid volcanics
Iron formation	? Non porphyritic chloritic acid volcanics
Iron formation	? Intermediate volcanics
Siliceous stockwork	Pyritic acid volcanics
Black shale	Black slate
Not recognised	Metaconglomerate
Not recognised	Black chert breccia
Not recognised	Metasiltstone breccia
Mafic dyke	Diabase dyke
Quartz veins	Quartz veins

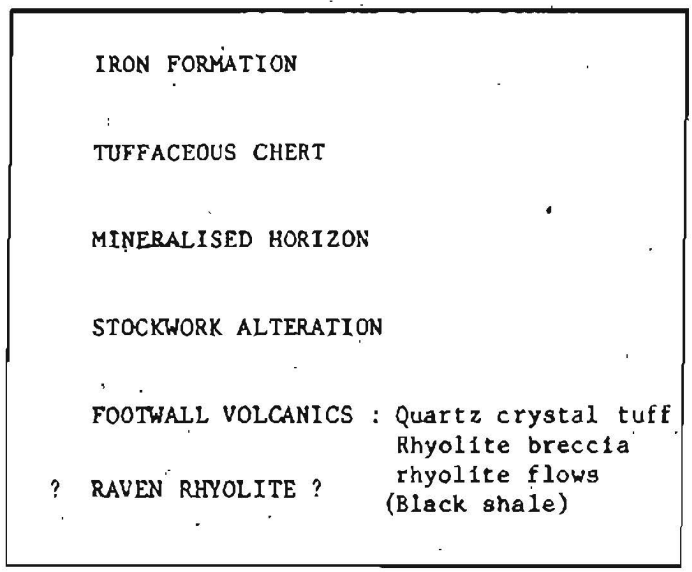

Figure 4.1 :Tentative stratigraphy for Tulks Hill.

Table 4.2 : Summary of the primary and secondary mineralogy of the 11 rock types that outcrop at Tulks Hill

	PRIMARY		SECONDARY		
Rock type	Matrix	Phenocrysts	Phenocrysts	Matrix	Comments
Quartz crystal tuff	Qtz Ab	Qtz (2mm) Ab → Ep Bi → Ser;Chl		Chl;Ser	Some lithic clasts
Large-quartz crystal tuff	Qtz	Qtz (2mm) Ab → Chl;Bi; Qtz Hem ← Pyt		Qtz Chl-Ser Ep Ab	Porphyritic rhyolite lithic clasts Graded albite beds
Biotite-quartz crystal tuff	Qtz Bi Ab(?) Kspar(?)	Qtz Ab → Ser,Bi Bi(?) → Chl		Ser	Lithic clasts
Alkali-enriched rhyolite	Qtz Bi →	Qtz Ab		Ser,Carb Chl Microcline	Secondary Microcline surrounds sericitic alteration
Altered rhyolite	Qtz Bi (Zrcn)	Qtz (Ab) → Ser,Chl		Ser, Chl Carb, Qtz	
Volcanic breccia	Qtz Ab(?)	Qtz Ab(?) → Ser,ep Kspar → Ser Bi → Chl		Qtz Ser-chl Bi Qtz Ab	Chequerboard albite in matrix Possible primary albite in fragments

Table 4.2 (contd)

Chloritic Stockwork	? (Zrcn)	? ?	Chl (Qtz) (Ser) Carb Pyt-cp-sph	Post-deformational mus covite
Siliceous stockwork	Qtz Fdspar(?) (Zrcn)	Fdspar(?) → Carb,ep Qtz(?) qtz Bi → Chl Hem ← Pyt	Qtz,ser, carb,ep pyt-cp-sph	Deformation destroys original paragenetic sequence
Tuffaceous chert	Qtz Tuff Zrcn (Barite?)	Qtz Ab → Ep,qtz	Qtz-chl-pyt ser,chl carb	High MgO High Na_2O
Iron formation	Qtz Zrcn Bi Apte (Ab) (Carb?)	Qtz Ab → Ser,ep Bi → Chl Sid.	Qtz-Fechl-pyt-carb Ser	Chequerboard albite 2 chlorite types

Abbreviations : Qtz : quartz
Fdspar : feldspar
Zrcn : Zircon
Bi : Biotite
Apte : Apatite
Chl : Chlorite
Cp : Chalcopyrite
Ab : Albite
Carb : Carbonate
Ep : Epidote
Sid : Siderite
Ser : Sericite
Hem : Hematite
Sph : Sphalerite
Kspar : K-feldspar
Pyt : Pyrite

Hill.

4.3.1 VOLCANIC ROCKS

Even though intense deformation and hydrothermal alteration have transformed the majority of the volcanic rocks into "quartz-eye" sericite-schists, volcanic features are still recognised. For example, virtually all quartz, feldspar and biotite crystals are broken, fractured and, locally, exhibit graded bedding (Plate 4.1). Also, coarse rhyolite breccias are interbedded with these schists, and many of the quartz crystals within both the rhyolites and the pyroclastic units have resorption margins and/or bipyramidal shapes (high temperature beta quartz) typical of volcanic rocks (Plate 4.2).

A fine-grained felsic matrix is common to all rock types. Albite is the dominant feldspar, it's pure composition suggesting a secondary hydrothermal replacement origin (see Chapter 8 and section 4.4.2.2.1).

4.3.1.1 Quartz-sericite-chlorite crystal tuff

This is the dominant lithology at Tulks Hill (including it's subgroups) occurring both as individual units and as a matrix component to rhyolite breccias (Map 1). Alteration to siliceous stockwork, with accompanying iron staining, is sporadically developed.

A bleached, grey-white weathering colour is

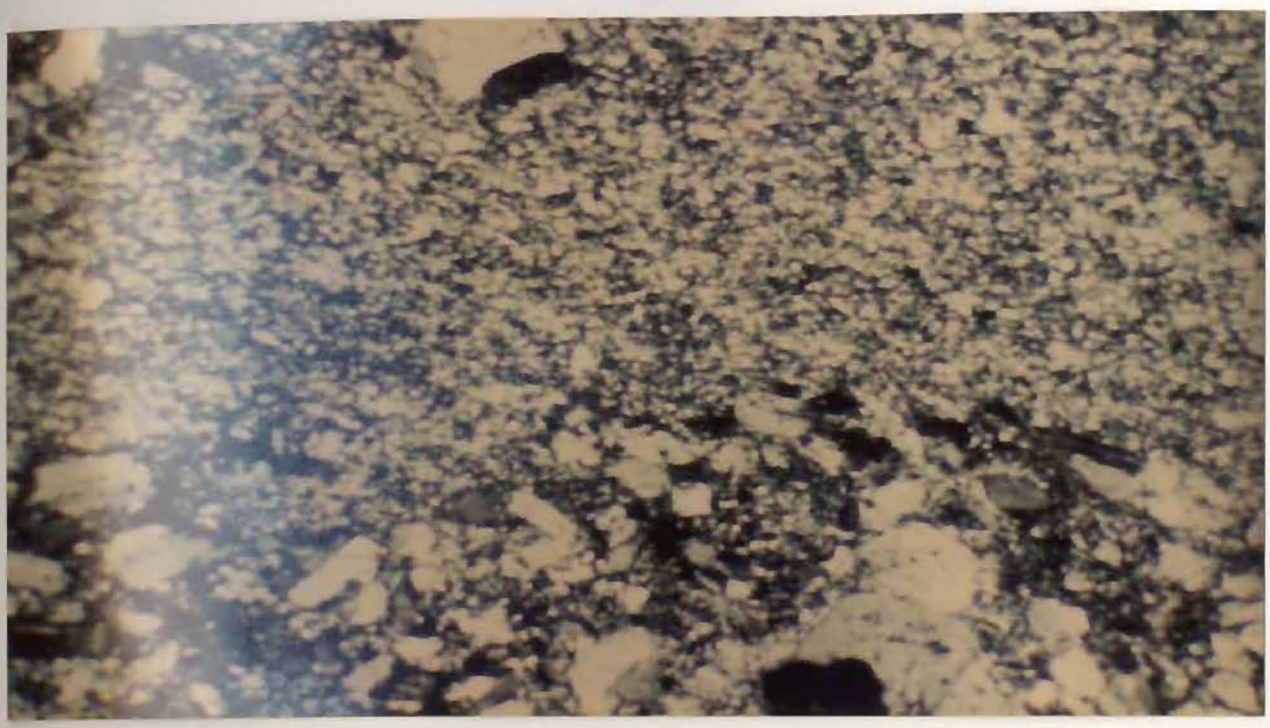

Plate 4.1: Graded beds of albite within the large quartz crystal tuff. Field of view 2mm x 1.5mm (12x magnification).

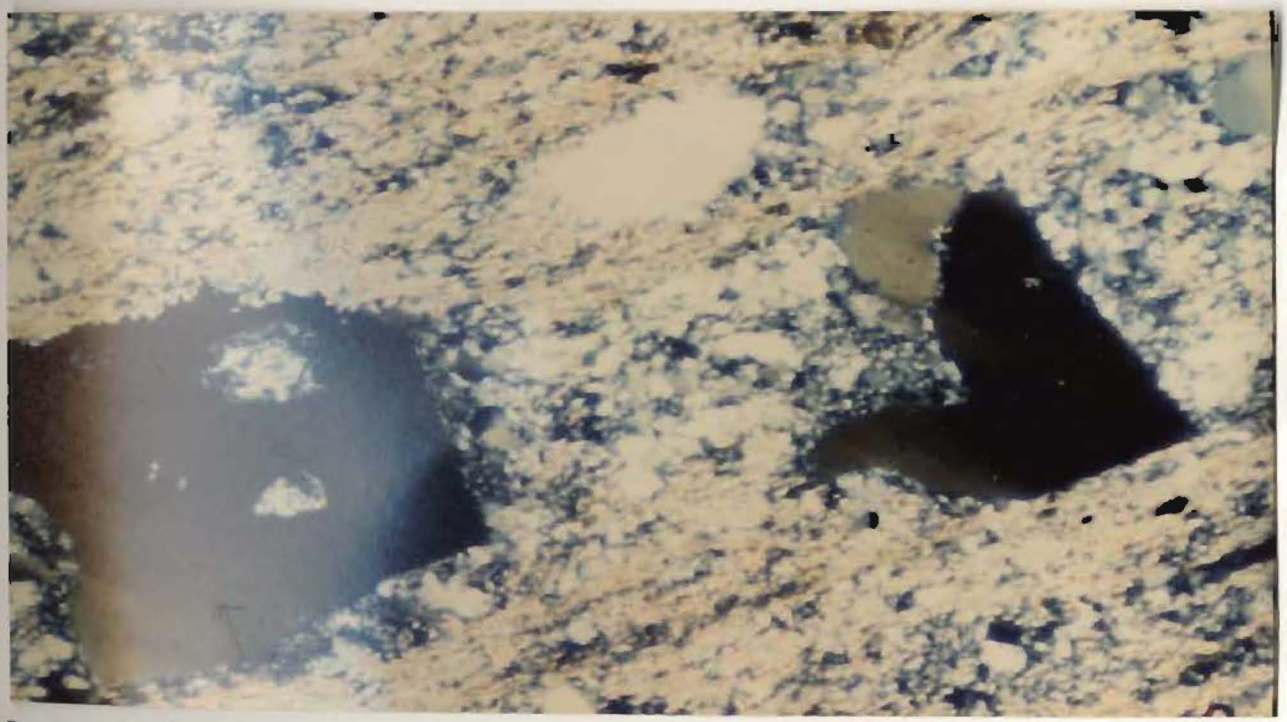

Plate 4.2: High temperature (beta) quartz typical of volcanic rocks. Recrystallisation of the central portion of the crystal (lapilli) is noteworthy. Sericite and quartz comprise the matrix. Field of view 2mm x 1.5mm (12x magnification).

distinctive (Plate 4.3), with locally-developed green patches of chloritic alteration (Plate 4.4). Quartz phenocrysts (<2mm.) and a prominent schistosity, reflecting the abundance of fine-grained sericite and chlorite, are characteristic features of the outcrop. Feldspar phenocrysts, although present in thin section, are not distinct in the hand sample.

Both recrystallised anhedral, and strain-free bipyramidal quartz, are present. Albite crystals (approx. 2mm in length) are both broken and whole, and locally have their long axes oriented subparallel to the Si fabric (Chapter 9); discontinuous, dagger-like twinning is a typical feature of some albite crystals (Plate 4.5). Chloritised biotite phenocrysts are similarly oriented and, locally, have a rim of iron oxide. A matrix of fine-grained quartz, albite and chloritised biotite is typical.

A lack of distinct silica banding and heavy iron oxide stains, as well as smaller quartz phenocrysts, distinguish this rock from the siliceous stockwork and the large-quartz crystal tuff, respectively.

Two sub-units are identified:

4.3.1.1.1 Large-Quartz Crystal Tuff

Its best development is in the southern part of Tulks Hill where it is interbedded with rhyolite breccias and flows(?), quartz crystal tuffs and iron formation (Map 1).

Plate 4.3: Quartz-sericite-chlorite crystal tuff. Abundant quartz phenocrysts, a grey weathering colour and a prominent schistosity are characteristic. Sharpener is approx. 3.5 cm. long.

Plate 4.4: Chloritic alteration within the quartz-sericite-chlorite crystal tuff. Hammer is approx. 33 cm. long.

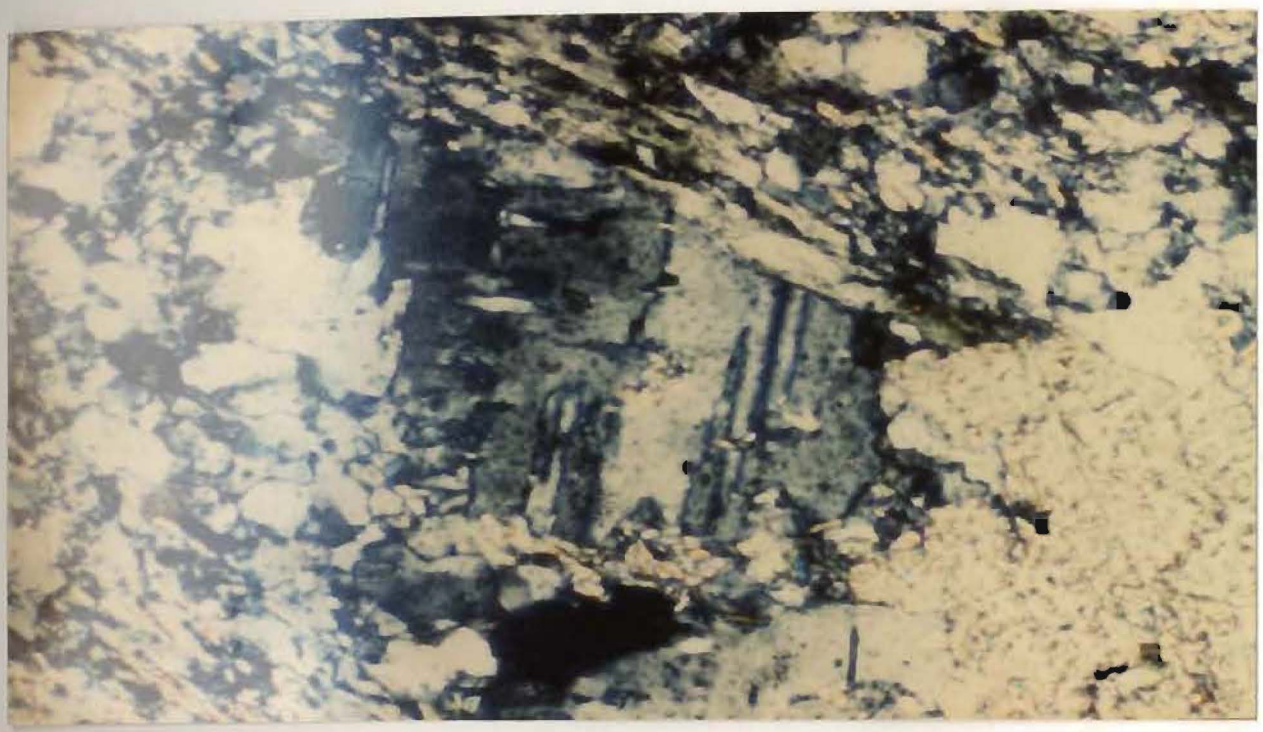

Plate 4.5: Photomicrograph of dagger-like twinning in secondary albite. Associated minerals include calcite, sericite, recrystallised quartz and green chlorite. Field of view 0.1mm x 0.07mm (25x magnification).

Plate 4.6: Two fragments of large quartz crystal tuff within a similar rock matrix. Note the large, grey coloured quartz phenocrysts within the sericitised fragments. Pencil is approx. 12 cm. long and is aligned subparallel to the S1 schistosity.

Gradational relationships with the quartz crystal tuffs are common and consequently the thickness is difficult to determine. Alteration to siliceous stockwork is variably developed in the southern outcrop; the boundary between the altered and unaltered rock is distinct and the limits of the alteration are easily mapped. Similar alteration in the northern part of Tulks Hill is less distinct and a patchwork outcrop pattern is produced. Included fragments of porphyritic rhyolite and the large-quartz crystal tuff itself are locally developed distinctive variations (Plate 4.6).

Large, rounded, "glassy" quartz phenocrysts (=> 2mm.) distinguish this sub-unit from the other quartz crystal tuffs. Most phenocrysts are internally strained but not recrystallised. Quartz overgrowths on smaller (< 2 mm.) quartz phenocrysts invariably contain randomly oriented sericite inclusions. The overgrowth is in optical continuity with the host phenocryst and is approximately 0.5mm. thick (Plate 4.7). Fine-grained quartz, with sericite-muscovite and chlorite, comprise the matrix. A fabric occurs only when the component of platy minerals is greater than the quartz component; if the reverse occurs then the chlorite and sericite are aligned along the quartz grain boundaries.

Graded beds of randomly oriented albite and minor quartz crystals (1mm. diameter), in a reduced matrix of fine-grained quartz, chlorite and epidote, are locally

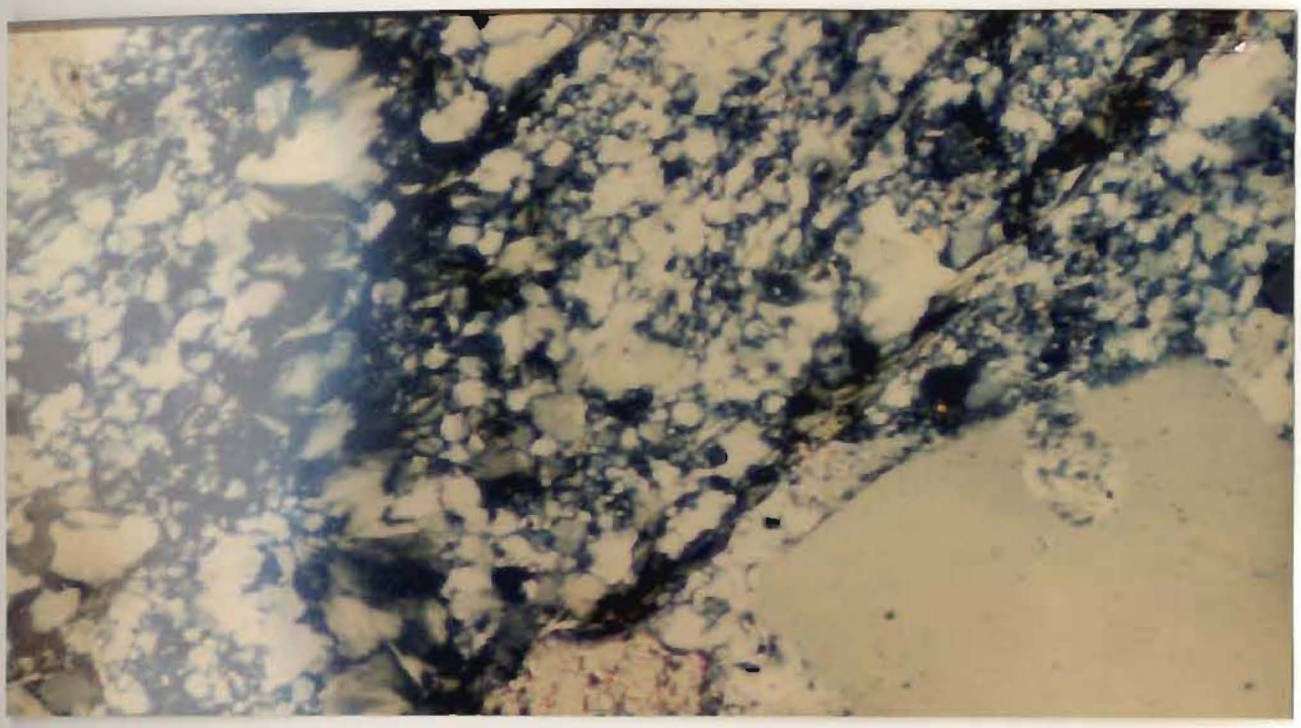

Plate 4.7: Photomicrograph showing a quartz overgrowth on a high temperature (beta) quartz phenocryst. Chlorite, recrystallised quartz and locally-developed calcite, comprise the matrix. Field of view 0.1mm x 0.07mm (25x magnification).

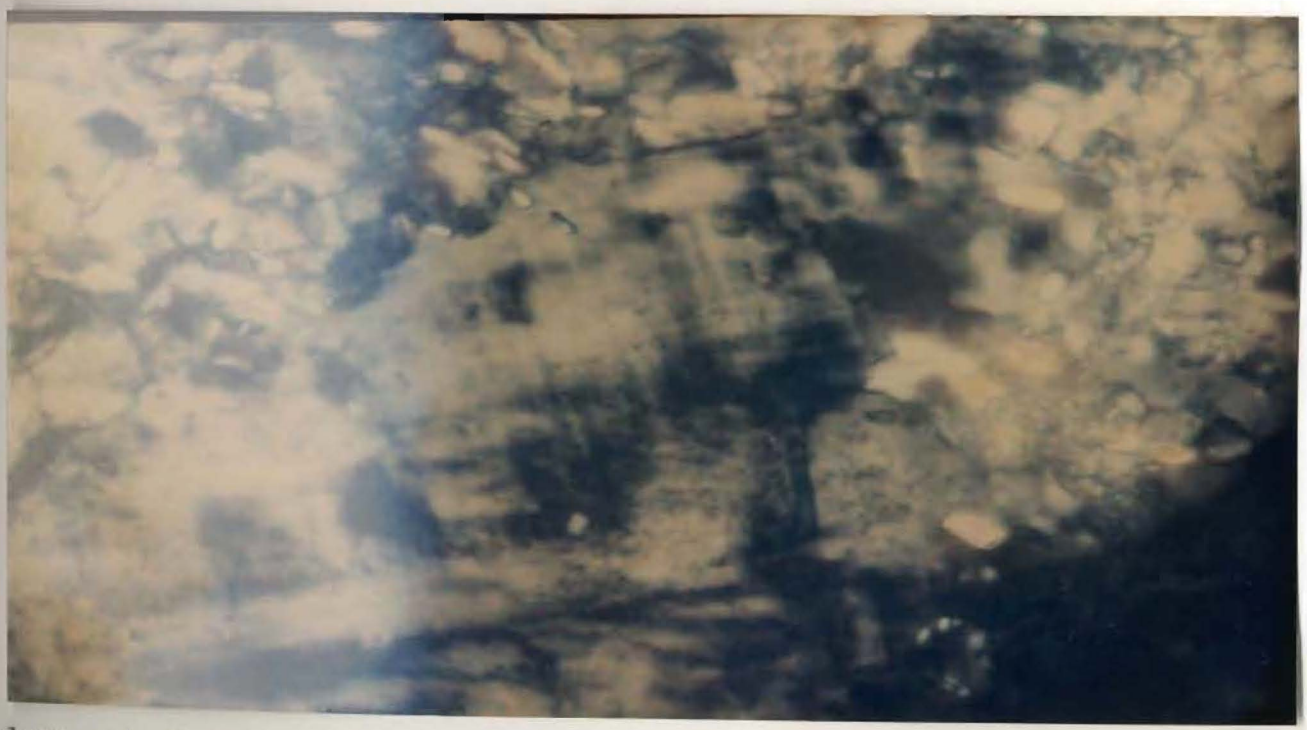

Plate 4.8: Photomicrograph of fine-grained secondary microcline in the alkali-enriched Raven rhyolite. Twinning is poorly developed. 125x magnification.

developed (Plate 4.1). Commonly, the overlying unit consists of finer-grained quartz, with minor phenocryst material. Albite-rich rip-up clasts may be present in these overlying units.

Epidote, zircon, carbonate and iron oxide are common accessory minerals.

4.3.1.1.2 Biotite-Quartz Crystal Tuff

A biotite-rich unit is locally developed in the northwest part of Tulks Hill (Map 1). It is thought to be a hydrothermally altered, facies variation of the adjacent lithologies, viz. rhyolite breccia, quartz crystal tuff and large-quartz crystal tuff. Its southern contact is not exposed; however, towards the north it grades into a chloritic quartz crystal tuff. It has a minimum width of 10m. but its lateral extent is unknown.

Abundant, fresh-looking biotite and a khaki-brown weathering colour distinguish this rock from the quartz crystal tuff; quartz and albite phenocrysts however, have similar textural characteristics to the latter. Sericite occurs as a matrix component and as a dusting to the albite phenocrysts. Locally, the albite contains quartz inclusions. Myrmekitically intergrown plagioclase and quartz occur as the only lithic fragments.

4.3.1.2 Massive felsic volcanic rocks ("rhyolites")

Any massive felsic volcanic rock at Tulks Hill is referred to as rhyolite (here and throughout the thesis). Three sub-types are identified on the basis of their alteration: alkali-enriched, bleached and chloritised-sericitised. The last two sub-types are combined under the generalised term of "altered rhyolite". This subdivision is for convenience only and is not meant to imply that the alkali-enriched rhyolite is fresh.

Rhyolite crops out in the northern part of Tulks Hill, herein named the Raven rhyolite, in both underground and surface exposures and as smaller outcrops (unnamed) of flows(?) interbedded with pyroclastic rocks in the southern part of the map area (Maps 1 and 2). Lithological characteristics are similar in the two occurrences but because of chemical and genetic considerations they are treated separately (Chapters 6 and 10).

Aphanitic rhyolite is most common. In general, mafic minerals and quartz and feldspar phenocrysts are poorly developed. The matrix is fine-grained quartz and consequently textural features are invisible to the naked eye. In all cases the lack of a distinct fabric is characteristic. Parts of the Raven rhyolite, however, are strongly schistose in zones that are thought to represent discrete faults (Chapter 9).

4.3.1.2.1 Alkali-enriched rhyolite

Hand samples are massive and are coloured grey, orange to off-white or pale green. Bleaching (as defined below) is minimal although chlorite, sericite and quartz veinlets may occur.

Well-developed jointing and a wide exposure (> 15m.) distinguish the alkali-enriched portion of the Raven rhyolite (Map 2). Poor surface exposure does not permit its accurate delineation to the east and west, although topographic considerations suggests that its lateral extent is minimal.

Quartz phenocrysts, carbonate and/or quartz veinlets, with or without pyrite-chalcopyrite mineralisation, are locally developed. Feldspar phenocrysts are rare in hand samples. In thin section, microcline overgrows a mixed assemblage of sericite and/or carbonate, but is only visible at high magnification. Microcline has a cloudy appearance in plane polarised light and distinctive twinning is poorly developed (Plate 4.8).

Surface exposures of the alkali-enriched rhyolite are interbedded with volcanic breccias and both varieties of quartz crystal tuff. Abundant albite phenocrysts (secondary) and a lack of K-feldspar are the only obvious mineralogical differences from the alkali-enriched samples of the Raven rhyolite.

4.3.1.2.2 Altered rhyolite

4.3.1.2.2.1 Bleached rhyolite

A creamy-white weathering colour with faint iron-staining is distinctive for this rock (Plate 4.9). It is best developed at the contact of the Raven rhyolite and iron formation (Map 2). Aphanitic, bleached rhyolite also outcrops in the west part of the map area to the south of a black shale-pyrite mineralised horizon (Map 1).

Scattered calcite crystals within a fine-grained quartz-sericite matrix is a typical mineral assemblage of the bleached rhyolite (Plate 4.10). Albite is sporadically developed. Samples of bleached rhyolite from the western part of Tulks Hill contain local concentrations of calcite, associated with either sinuous zones of recrystallised quartz or as overgrowths of the matrix.

4.3.1.2.2.2 Chloritised-sericitised rhyolite

Underground exposures of the Raven rhyolite show the best development of this rhyolite type. The colours of the hand sample depend upon the style of alteration; for example, extensive chloritic alteration produces a green colour, whereas sericitic alteration produces a pale white colour comparable to the bleached rhyolite (Plate 4.11). Commonly, unaltered portions of the Raven rhyolite (alkali-enriched?) are interspersed with these horizons but they are not easy to sample.

Mineralogically the alteration is defined by chlorite

Plate 4.9: Slightly schistose, bleached rhyolite. This outcrop is to the west of lens T3 and is approximately along strike from the Raven rhyolite. Hammer is approx. 33 cm. long.

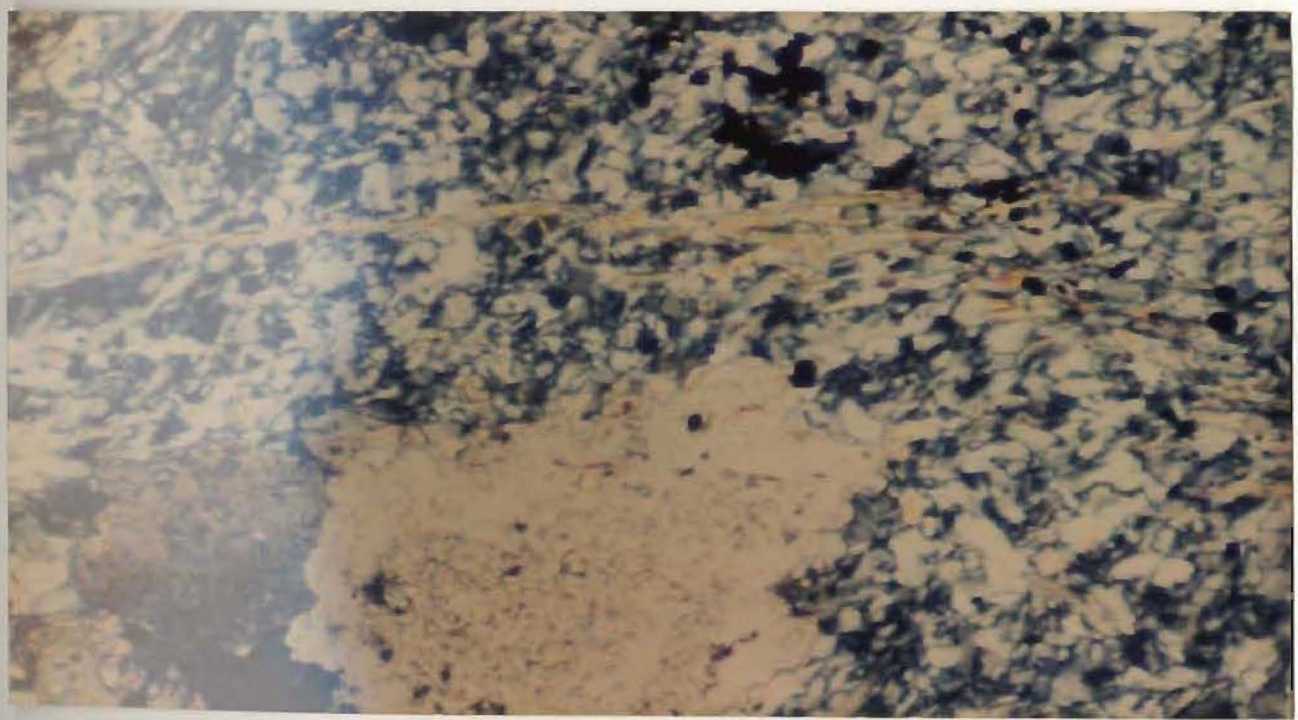

Plate 4.10: Typical bleached rhyolite assemblage of quartz, sericite and carbonate. Pyrite is scattered throughout this sample. Field of view 0.1mm x 0.07mm (25x magnification).

and sericite, occurring as either veinlets or individual needle-like crystals within a felsic matrix. Locally, biotite and albite phenocrysts are present. Quartz phenocrysts, some with overgrowths, are sporadically developed.

Pyrite is prominent in the Raven rhyolite within carbonate-, chlorite- and quartz-rich veinlets; however, chalcopyrite is rarely observed. These veinlets, in some case up to 50 cm. thick, are probably related to deformation.

4.3.1.3 Rhyolite Breccia

The largest outcrop of rhyolite breccia is in the southeast part of Tulks Hill, although its boundaries are undefined because of a lack of outcrop. More typically it occurs as smaller, isolated horizons with a limited lateral extent (Map 1). All breccias are matrix supported and have an average fragment length of 12 cm; certain horizons have fragments up to 40 cm. in length, or rarely, 2m. in length (Plate 4.12). Alteration effects, such as quartz veinlets and bleaching, are more pronounced in the southeast outcrops.

Weathering colours depend upon the extent of hydrothermal alteration: breccias with a low degree of alteration have a grey to off-white matrix colour and pale yellow fragments, whereas intense alteration bleaches both

Plate 4.11: Mixed sericite-chlorite alteration of the Raven rhyolite. Pencil is approx. 12 cm. long.

Plate 4.12: Volcanic breccia fragment, approximately 2m long. The metal clip board is approximately 25 cm. long. This photograph looks west and shows the Tulks River Valley (possibly a fault zone) and orange-coloured oxidised iron of the siliceous stockwork (far side of the gorge).

the matrix and the edges of the fragments. Pyrite deposition during such alteration is suggested by extensive goethite development in the oxidised portions of the surface exposures (Plate 4.13). Extreme alteration may deposit silica and sericite/chlorite within the fragments of an altered breccia (Plate 4.14).

Certain outcrops of the quartz crystal tuff contain orange-coloured, lens-shaped, siliceous horizons that bear a superficial resemblance to the rhyolite breccias. These "fragments" have indistinct outlines and typically lack quartz phenocrysts. Oxidised iron within the fine-grained recrystallised quartz matrix produces the orange colour. These horizons could represent either deformed and hydrothermally altered fragments, or more likely, deformed zones of hydrothermal silicification.

a) Fragments: Sericitic alteration of orthoclase and albite-oligoclase phenocrysts is common; apart from this, the phenocrysts have a fresh appearance. Biotite phenocrysts, partially altered to chlorite, accompany recrystallised quartz in the pressure shadows of strained and fractured quartz phenocrysts. Larger biotite crystals occur in association with glomeroporhyritic plagioclase possibly reflecting a primary magmatic association.

b) Matrix: Quartz phenocrysts, as well as clasts showing vermicular intergrowths of quartz and plagioclase

Plate 4.13: Goethite staining of a volcanic breccia horizon. Fragments are oriented subparallel to the S1 schistosity. Pencil is approx. 9 cm. long.

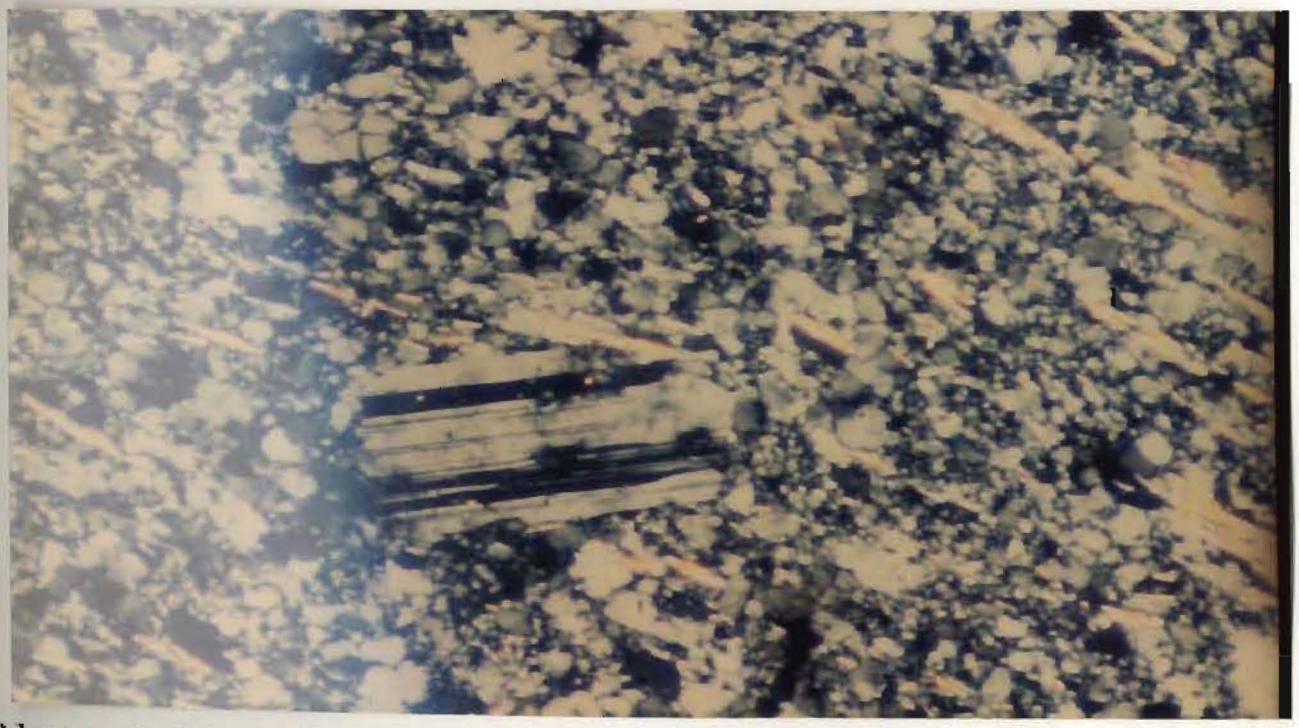

Plate 4.14: "Fresh" magmatic albite and sericite veinlet alteration in a volcanic breccia fragment. Matrix is predominantly recrystallised quartz. Note the continuous twin planes of the albite (cf. Plate 4.5). Field of view 0.1mm x 0.07mm (25x magnification).

(myrmekite), accompany iron-stained sericite, minor chlorite and recrystallised fine-grained quartz in the matrix. Chequerboard albite phenocrysts (secondary) are prominent.

4.3.2 ROCK TYPES RELATED TO ALTERATION

Intense hydrothermal alteration and deformation has produced two rock types, the protolith to which is thought to be a tuffaceous unit.

4.3.2.1 Siliceous Stockwork

This distinctive rock type is defined by abundant chert-like quartz, with sericite, minor chlorite and either oxidised or fresh mineralisation. Surface exposures have developed a gossan which aids in locating zones of siliceous stockwork. A lack of silica bands and/or extensive mineralisation distinguishes the host rocks from the siliceous stockwork.

Siliceous stockwork occurs in both surface and underground exposures (Maps 1 and 2); gradational contacts are typical, although faulted contacts are observed underground. Grey quartz bands (approx. 5.0cm thick) alternate with thinner (0.5cm thick) white, sericite (-chlorite) horizons. A ribbed pattern, produced by differential erosion and removal of sericite, is a distinctive characteristic of the surface exposures and is

continuous over many metres (Plate 4.15). Cubic cavities in the siliceous horizons, as well as extensive iron staining, suggests oxidation and removal of pyrite.

In thin section, fractured anhedral and bipyramidal quartz phenocrysts (0.5mm.), decayed biotite (0.3mm.) and rarely, broken albite pherocrysts, resemble those of the quartz crystal tuffs (Plate 4.16). Larger quartz phenocrysts occur where alteration has affected the large-quartz crystal tuff.

Deformation structures, such as polygonal and seriate grain boundaries, are common in the matrix quartz, as is pressure shadow growth of secondary quartz, sericite and chlorite in the low strain areas of phenocrysts. Typically, two cleavages can be identified in the sericite horizons (Plate 4.17).

The freshest exposures of the siliceous stockwork alteration are found underground. Here, quartz veinlets with pyrite and sphalerite are oriented subparallel to the silica-sericite bands, although locally they may transect this banding (Plate 4.18). Chalcopyrite is a minor component within the siliceous stockwork.

In thin section the sulphide veinlets are intergrown with quartz, chlorite and Mn-rich carbonate. Within the matrix the pyrite is often granulated whereas sphalerite is smeared parallel to the dominant fabric. Zircon-rich layers are prominent and probably represent heavy mineral layers within the tuffaceous protolith.

Plate 4.15: Siliceous stockwork alteration. Deformation has oriented the silica-sericite bands subparallel to the S1 schistosity. Differential erosion has removed the sericite to give a ribbed pattern. Hammer is approx. 33 cm. long.

Plate 4.16: Recrystallised quartz phenocryst within the siliceous stockwork. Chlorite and quartz occupy the pressure shadows of the phenocryst. Sericite, quartz and goethite "veinlets" comprise the matrix. Field of view 2mm x 1.5mm (12x magnification).

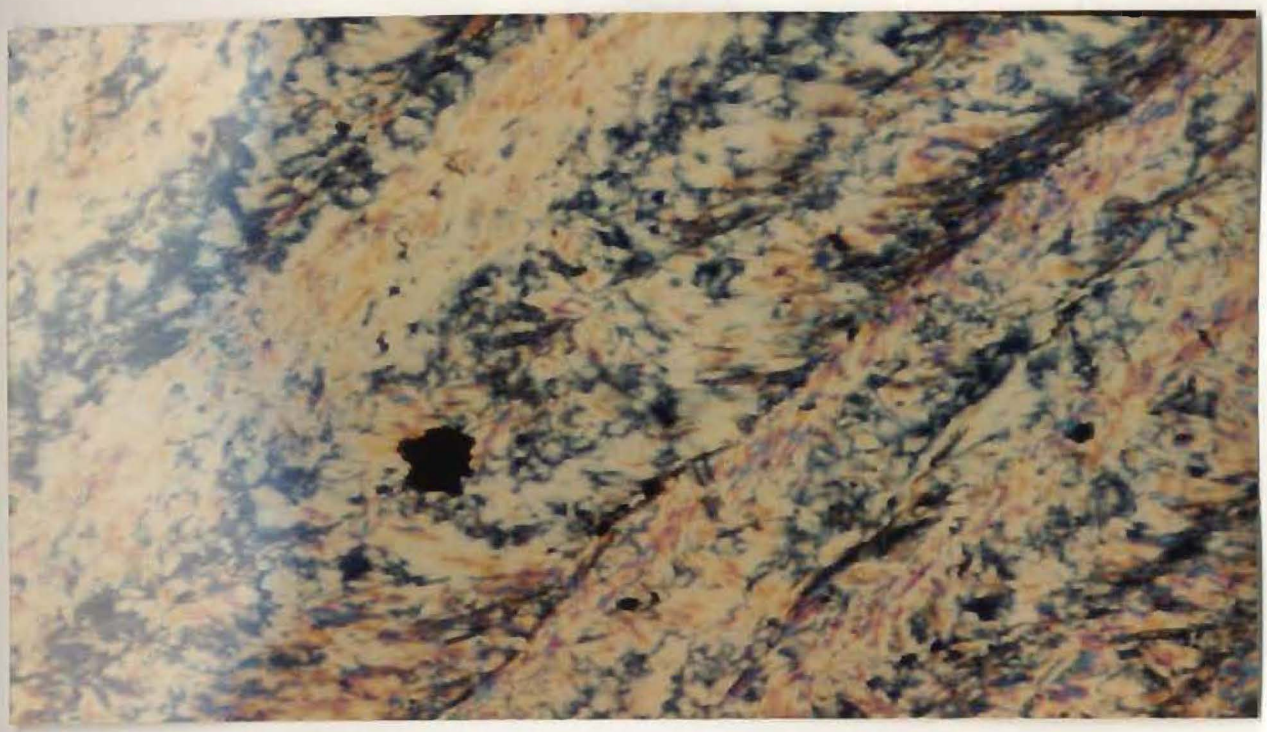

Plate 4.17: Sericite portion of the siliceous stockwork alteration. Two cleavges are present, the later one (oriented NE-SW) crenulating an earlier fabric (oriented NW-SE). Field of view 0.1mm x 0.07mm (25x magnification).

Plate 4.18: Pyrite-rich veinlets cross-cut a quartz-rich band in the siliceous stockwork. Other veinlets are oriented subparallel to the S1 schistosity. Pen cap is approx. 4 cm. long and is oriented subparallel to S1.

Peripheral parts of the stockwork alteration consist of a mixed (not banded) sericite-silica alteration cross-cut by a network of iron oxide veinlets (Plate 4.19). It marks the boundary between the host rocks and the banded siliceous stockwork type, although it is not differentiated on Map 1.

4.3.2.2 Chloritic stockwork

This unit has a relatively narrow (approx. 2m. thick) underground exposure. Its upper and lower contacts, bounded by the siliceous stockwork, are faulted (Map 2).

Hand samples are green to black in colour due to the dominance of chlorite, although green coloured sericite is locally prominent. Euhedral-anhedral pyrite and sinuous chalcopyrite veinlets occur in sporadic concentrations (Plate 4.20). Quartz phenocrysts and veinlets are generally a minor component.

Siderite-rich carbonate is more common in samples taken from the eastern and western extremities of the unit where it is interbedded with sericite horizons of the siliceous stockwork (Plate 4.21). At these locations pyrite porphyroblasts (up to 2 cm. square), in both the sericite and chlorite horizons, are aligned subparallel to the S1 schistosity (Chapter 9).

The only known occurrence of randomly oriented muscovite crystals overgrowing the fabric is contained

Plate 4.19: Peripheral portion of the stockwork alteration where mineralogical banding is absent. A network of goethite veinlets (originally pyrite?) cross-cut a mixed silica-sericite rock. Pencil is approx. 12 cm. long.

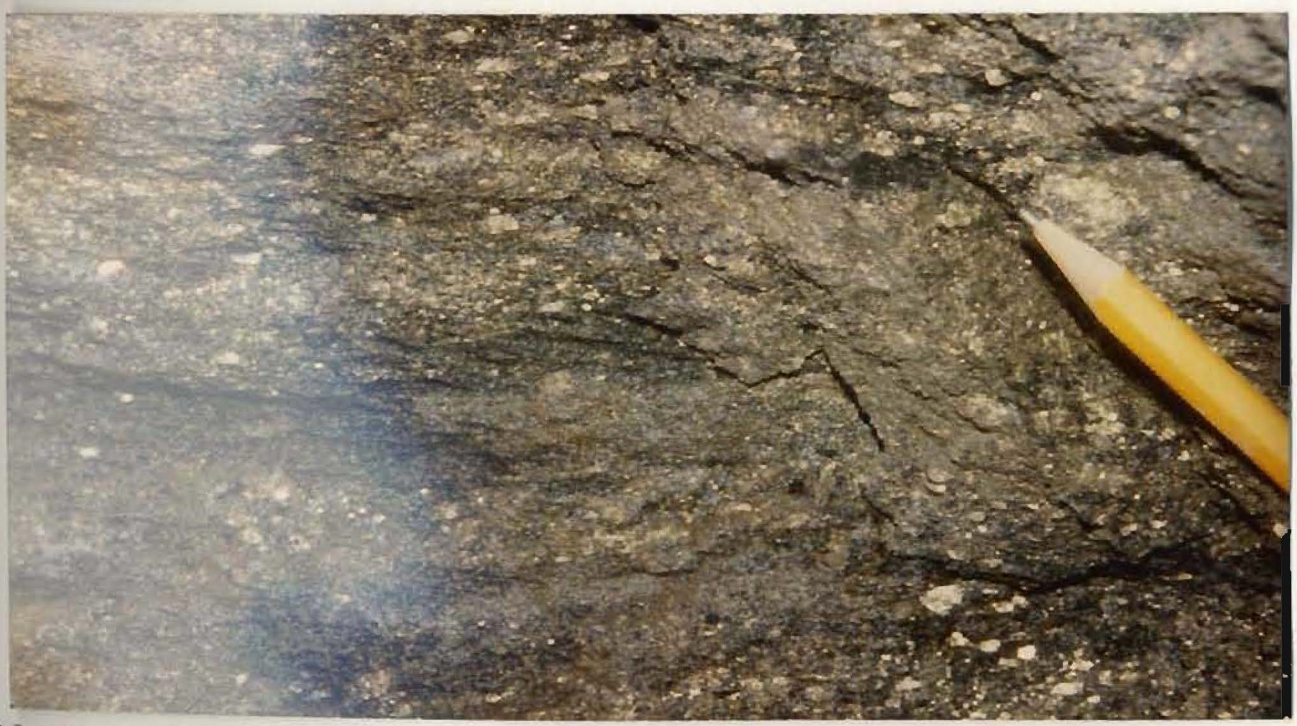

Plate 4.20: Chloritic stockwork alteration. Prominent pyrite porphyroblasts and chalcopyrite are set in a fine-grained, green coloured chlorite matrix. Secondary covellite (blue) is also present. Pencil tip is approx. 3 cm. long.

Plate 4.21: Interbedded chloritic (black) and sericitic (white) alteration, West Adit. Tight to isoclinal folding can be discerned. Pyritic mineralisation is restricted to the chloritic alteration and is most abundant near the pencil (upper left). Pencil is approx. 12 cm. long.

Plate 4.22: Tuffaceous chert in the North Adit. Oxidised mineralisation at upper left is a recent feature related to adit construction. Pencil is approximately 12 cm. long.

within a sample of the chloritic stockwork. This feature must have formed during post-deformational metamorphism.

A narrow (0.6m thick) mineralised, chloritic horizon is exposed in the North Adit (Map 2). Its southern contact is faulted against siliceous stockwork. Iron staining obscures its northern contact but it too is thought to be faulted (against iron formation).

Magnesian carbonate (sideritic adjacent to the mineralisation) is relatively abundant in a quartz-chlorite-muscovite matrix. Abundant sphalerite mineralisation contrasts this chloritic stockwork with the sphalerite-poor footwall chloritic stockwork and suggests a greater similarity to the siliceous stockwork, which has a relative abundance of sphalerite. Zircon and epidote are minor components.

4.3.3 CHEMICAL SEDIMENTS

4.3.3.1 Tuffaceous chert

This rock type occurs in underground exposures only, immediately to the north of a mafic dyke (Map 2). Its northern contact is faulted against siliceous stockwork while the contact with the dyke is marked by a zone of brecciation.

Thin (approx. 2 cm.), white, sericite (-chlorite) horizons alternate with thicker (approx. 10 cm.), grey

chert-like horizons so that its physical appearance is similar to the siliceous stockwork (Plate 4.22). Unlike the siliceous stockwork, however, it lacks sphalerite mineralisation and has a relative abundance of oriented albite crystals. Anhedral Mg-rich carbonate and minor barite(?) are distinctive components. Zones of recrystallised quartz and profuse zircon mats may reflect primary tuffaceous material, that is, phenocrysts and heavy mineral lag-type deposits, respectively. Aligned (bedded?), euhedral pyrite overgrows two cleavages, a feature that is interpreted to represent post-deformational annealing (Chapter 9).

A related rock type, here called the siliceous ash, has two small exposures in the East and West Adits, adjacent to the Main Hall (Map 2). In both cases the upper and lower contacts are faulted. A grey colour and a fine, gritty texture are characteristic. Mineralisation is limited to discontinuous stringers of euhedral and granular pyrite, the latter type suggesting possible microshearing along the bedding plane (Chapter 9).

A minor chloritised biotite component accompanies the laminations of fine-grained quartz and sericite. Samples from the western exposure have a similar mineralogy but are more deformed and contain minor amounts of carbonate (Plate 4.23).

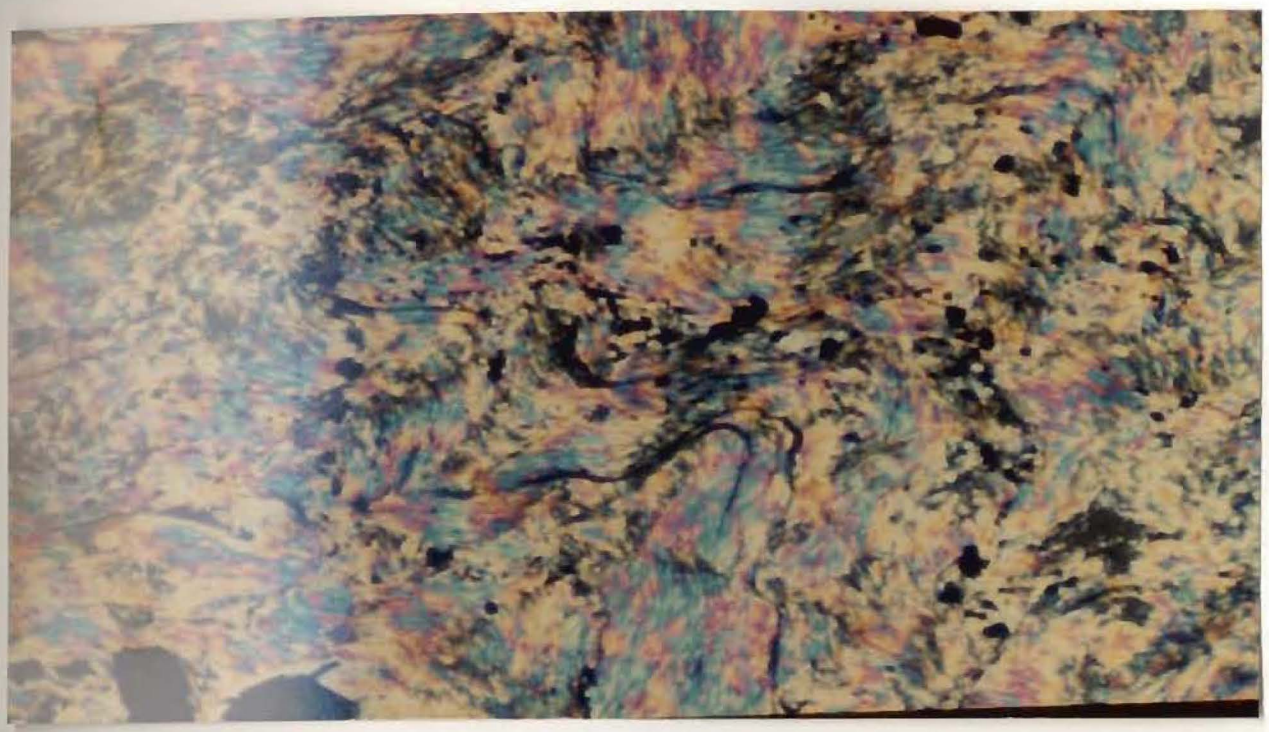

Plate 4.23: Photomicrograph of a sample of siliceous ash. Bedded pyrite is folded with the sericite. An earlier fabric is weakly crenulated. Field of view 0.1mm x 0.07mm (25x magnification).

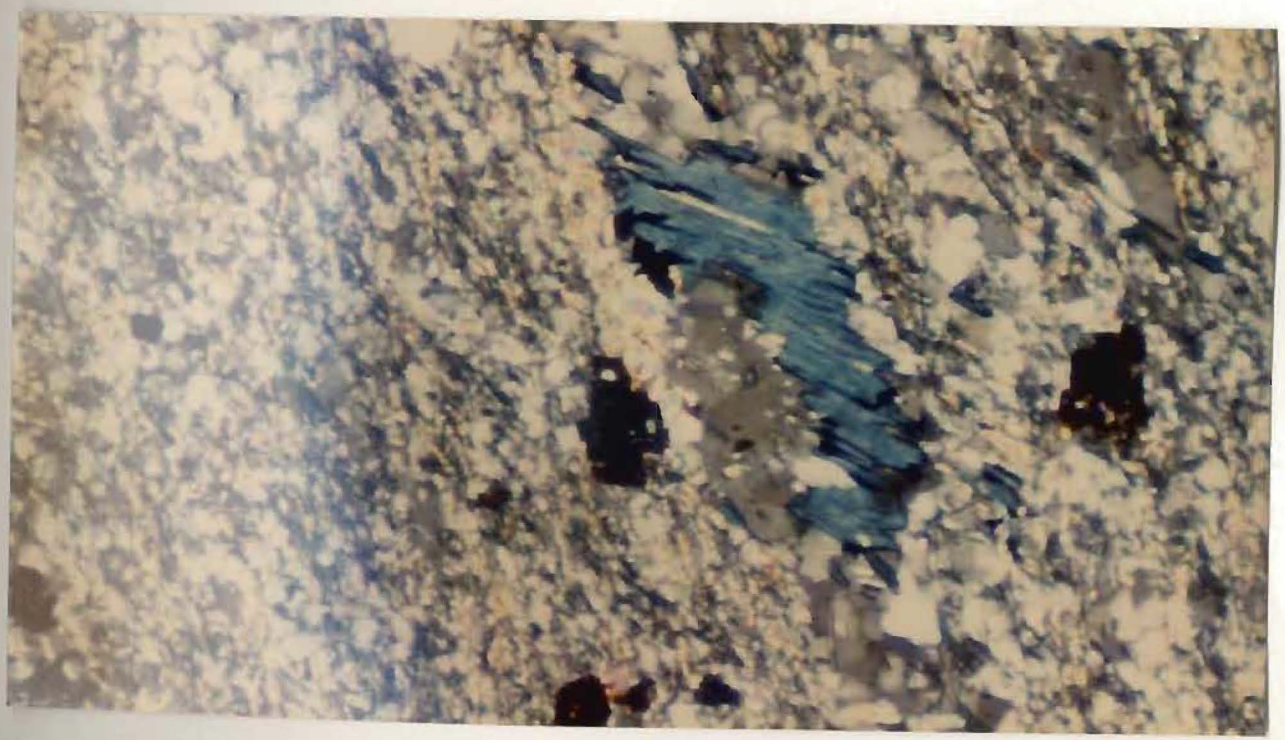

Plate 4.24: Large, ragged chlorite within a quartz-sulphide veinlet of the iron formation showing anomalous blue birefringence. Quartz, sericite and pyrite comprise the matrix. Associated mineralisation is fresh. Field of view 0.1mm x 0.07mm (25x magnification).

4.3.3.2 Iron formation

The largest surface exposure of the iron formation (see addendum 2) in the south-central part of Tulks Hill, is bounded by a quartz crystal tuff in the north and a rhyolite breccia horizon in the south (Map 1). Its eastern and western terminations are not exposed and an interfingering relationship is inferred. All other outcrops of it are small (less than 10m. long), linear- to lens-shaped bodies interbedded with quartz crystal tuffs. In all cases contacts are conformable.

A distinctive, brown-red weathering colour contrasts with the olive to dark green fresh surfaces. A speckled appearance to some surfaces appears to be related to the oxidation of sulphide mineralisation. Unlike most rocks at Tulks Hill a cleavage is rarely seen, except in the finer-grained portions of the unit.

Two types of chlorite are developed in a siliceous matrix:

a) Large, ragged crystals, associated with veinlets of coarse-grained quartz, showing distinctive anomalous blue birefringence (Plate 4.24). Most cleavage trace orientations are perpendicular to the rock fabric. Sulphide inclusions are fresh.

b) Finer-grained, lath- to needle-shaped matrix chlorite, showing anomalous olive-green colours in plane polarised light (Plate 4.25). Associated mineralisation is

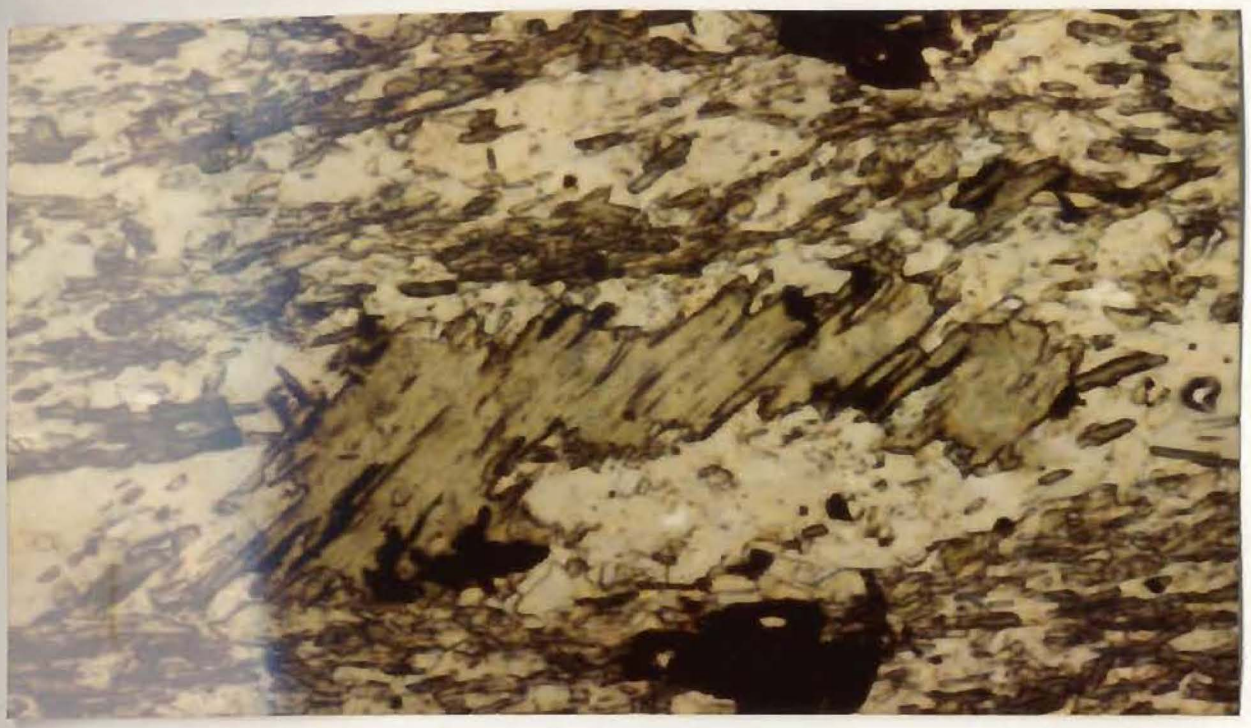

Plate 4.25: Fine-grained, needle-shaped chlorite within the matrix of the iron formation. Associated mineralisation is oxidised. Field of view 0.1mm x 0.07mm (25x magnification).

Plate 4.26: Chert-siderite "stringers" within the iron formation (underground outcrop). Green chlorite+quartz comprise the bulk of the matrix. The pencil is approx. 12 cm. long.

oxidised.

Quartz phenocrysts are not prominent, although locally-developed zones of recrystallised quartz (approx. 1.0 mm.) probably represent such phenocrysts subsequently deformed into a mosaic of sub-grain boundaries. Fractured albite phenocrysts (<= 1 mm.), kinked biotite, sericite, carbonate, iron oxide pseudomorphs of pyrite and epidote are locally prominent components.

Faulted upper and lower contacts are inferred for the underground exposures (Map 2). An olive-green matrix with thin stringer-like horizons (< 10 cm. thick) of grey chert and orange-coloured siderite-rich carbonate is characteristic (Plate 4.26). These "stringers" are continuous over a distance of 0.5m. or more, and invariably terminate as tight folds.

Thin sections of samples from the underground exposure contain abundant, coarse-grained, subhedral siderite-rich carbonate augens, associated with Fe (-Mg) chlorite and/or quartz, enclosed by a matrix of quartz and needle-like sericite crystals (Plate 4.27). A crude alignment of the siderite-rich carbonate in samples from the southern part of the outcrop is less visible in the north because of a decrease in the carbonate content.

Both fractured and whole albite crystals, elongated subparallel to define a crude fabric, are common in the northern exposures as are thin sericite beds (<= 1 mm.) which overlie some of the broken feldspar phenocrysts and

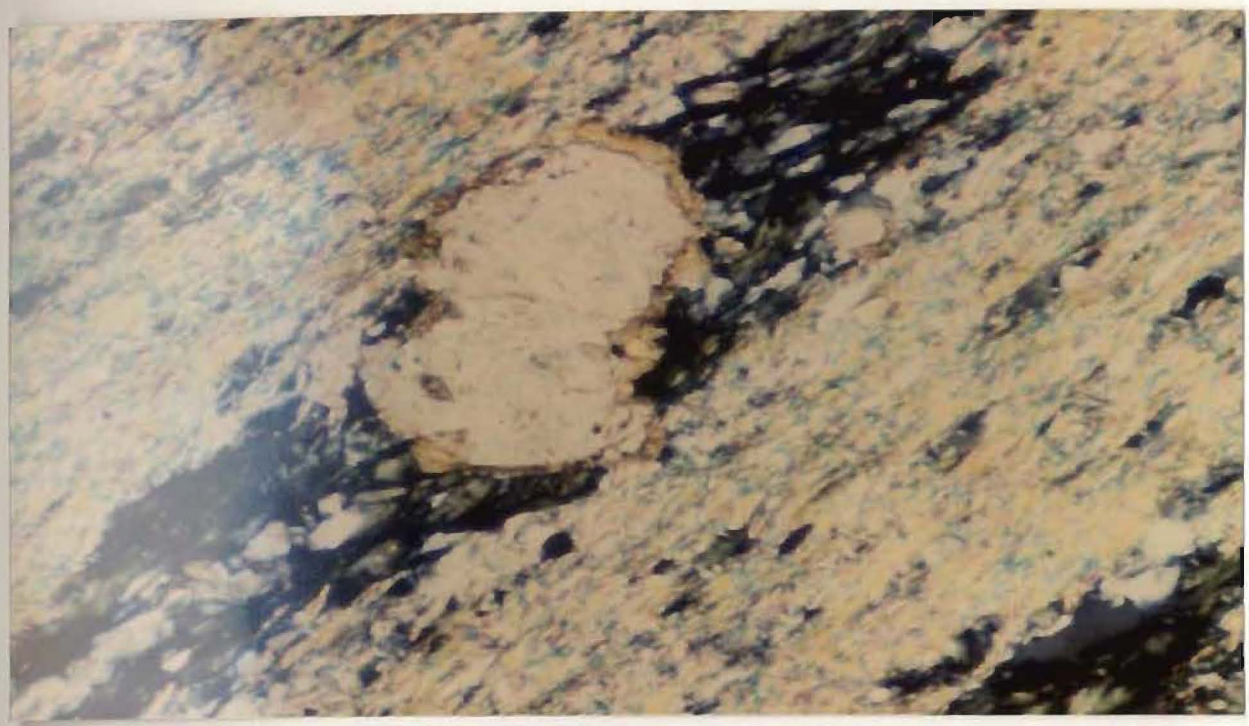

Plate 4.27: Subhedral siderite augens, with chlorite-quartz pressure shadows, in the iron formation. The matrix consists of sericite and quartz. Field of view 0.1mm x 0.07mm (25x magnification).

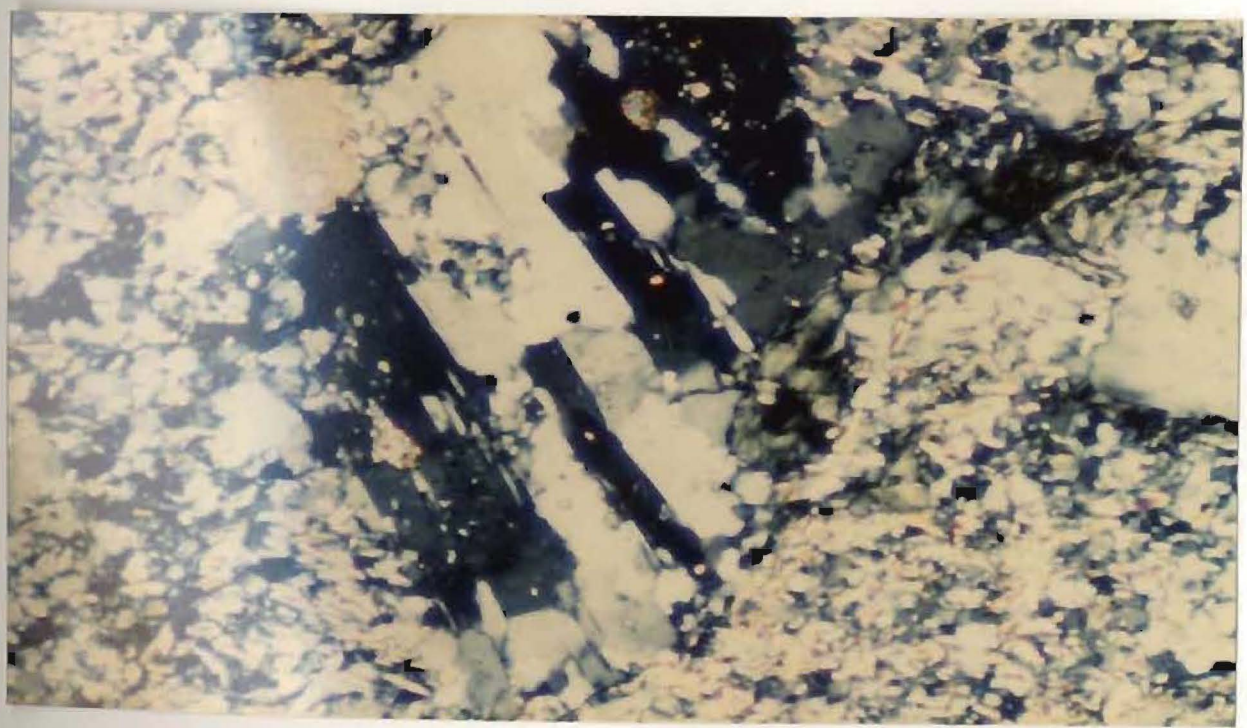

Plate 4.28: Well-developed chequerboard pattern of the twin planes of secondary albite. Quartz, sericite and chlorite comprise the matrix. Calcite and epidote are locally developed alteration minerals associated with the albite. Field of view 0.1mm x 0.07mm (25x magnification).

locally grade into more massive sericite horizons without any distinct break. The latter is thought to represent primary grading of fine-grained tuffaceous material. Apparently, the sericite (tuff) increases at the expense of the carbonate in the northerly outcrops.

Zircon, epidote and sericite are accessory minerals.

4.4 INTERPRETATION AND DISCUSSION

4.4.1 INTRODUCTION

Apart from the sulphide deposit itself (Chapter 5), two types of rock predominate at Tulks Hill: volcanic-pyroclastic deposits and chemical sediments. Mineralogically and chemically they are distinct: alteration within the volcanics is extensive whereas the chemical sediments contain a relatively "fresh" mineralogy. Since sulphide deposition is a hydrothermal phenomenon (Hutchinson, 1982), alteration is an inherent feature so that the volcanics must be older than the sulphides and chemical sediments, and hence, are termed the Footwall Volcanics.

4.4.2 FOOTWALL VOLCANICS

4.4.2.1 Environment of deposition

A felsic protolith to the hydrothermally altered rocks at Tulks Hill is implied by the fractured quartz phenocrysts, siliceous matrices and relatively abundant

rhyolite breccias. Chemical data, using the less mobile trace elements, suggest a rhyolite to dacite composition for the volcanic rocks (Chapters 6 and 7).

Within the tuffaceous rocks, graded beds of albite crystals, as well as albite-rich rip-up clasts and minor interbeds of black shale (not differentiated on Map I), indicate an aqueous environment of deposition, with locally-developed scour currents. Since whole and fractured phenocrysts are intermixed, and the feldspar phenocrysts have a subparallel alignment, it may suggest deposition by submarine debris flows which could effectively provide fluidised flow-protection of some, but not all, phenocrysts and would probably align the phenocrysts subparallel to the flow direction. Scour currents within these debris flows could rip-up albite crystals and any unconsolidated rocks over which the debris flow passed (eg. quartz crystal tuff). This mode of deposition may also explain the general lack of grading within the tuffaceous rocks --- airfall pyroclastic rocks should be sorted due to differential settling in seawater (Schermerhorn, 1970). Schermerhorn (1970) also suggests that a submarine debris flow mechanism is the best way to explain the presence of isolated, sharply bounded, volcanic blocks within finer-grained tuffaceous material; such blocks occur at Tulks Hill (Plate 4.12).

A debris flow mechanism of deposition is preferred for the rhyolite breccias since they are interbedded with the

tuffaceous units. Flow-top brecciation of rhyolite lava flows is thought to be an unlikely method of formation since lithic clasts are included in the matrix and graded bedding is locally-developed.

A debris flow origin has been suggested for the quartz-eye porphyry of the Bathurst camp (Davies, 1980), the quartz crystal tuffs at Jerome, Arizona (Anderson and Nash, 1972) and the crystal tuffs at the Woodlawn Cu-Zn deposit, Australia (Petersen and Lambert, 1979), all of which have volcanogenic massive sulphides. Initiation of these flows could be through caldera collapse, a process that may be common in mineralised felsic volcanic terranes (Ohmoto, 1978; Ohmoto and Takahashi, 1983; Scott, 1978). This topic is discussed further in Chapter 10.

4.4.2.2 Hydrothermal alteration

Mineralogical, chemical and textural reconstitution are inherent features during hydrothermal alteration. Within the footwall volcanics two distinct types of alteration are recognised: relatively weak alteration, characterised by alkali-enrichment, and moderate to intense alteration with obliteration of the primary rock fabric (*eg.* siliceous stockwork alteration).

4.4.2.2.1 Alkali-enrichment

4.4.2.2.1.1 Secondary albite

This mineral is extensively developed in the tuffaceous rocks and the matrix to the breccias; chemical analyses of such rocks always give high Na2O values (Chapter 6). Therefore, a more correct term for these rocks would be quartz-keratophyres (Hughes, 1973) but the igneous terminology is retained because it is more informative.

Most albite crystals display one or more of the following characteristics: a) quartz, epidote and/or calcite inclusions; b) chequerboard twin planes (Plate 4.28); c) pure composition (Chapter 6). All three features are characteristic of albite crystals formed by Na metasomatism of pre-existing feldspars (Battey, 1955); the presence of Ca-rich minerals (eg. epidote) as inclusions probably reflects albite replacement of a more calcic plagioclase, such as oligoclase or andesine.

Experimental studies of hydrothermally altered basalts have produced albite at temperatures > 150 degrees centigrade (Bischoff and Dickson, 1975; Hajash, 1975; Mottl and Holland, 1978). All of the Na necessary for the formation of albite is extracted from seawater. In these same experiments however, it was shown that seawater:rock ratios >10 inhibit albite formation. Assuming that the experimental data for basalts can be applied to altered felsic rocks, and of course that the albite at Tulks Hill is hydrothermal (as is suggested by its pure composition;

Chapter 8), it suggests that low seawater:rock ratios (<10) characterised those areas distant from the mineralisation. Also, the temperature of formation of albite, and therefore the temperature of the hydrothermal fluid, must have been greater than 150 degrees centigrade. Rosenbauer et al. (1983) showed that albitisation occurs only when H+ ions are present in the hydrothermal solution; the presence of albite in the Tulks Hill rocks suggests that the fluid contained H+ ions. Indirectly, this also suggests that the hydrothermal fluid was probably a variation of seawater since base fixing (removal of Mg etc., and the formation of smectites with concomitant release of H^+ ions to the solution) can be best accomplished if seawater dominates the fluid composition (Rosenbauer et al., 1983). The generation of H+ ions will also lead to base metal leaching, mobilisation and transportation (Bischoff et al., 1981).

In some instances, sericite occurs as a dusting of albite. As shown in Figure 4.2 sericite formation reflects a lower Na+/H+ ratio than that needed for albite formation. A lower ratio could result from albite formation when Na was removed from the solution. Note also that albite and sericite can coexist simply by varying the H+ ion ratio: an increase in the H+ ion activity can result from base fixing, as described above.

Secondary albite is associated with chlorite, sericite and sulphide mineralisation which may indicate a genetic

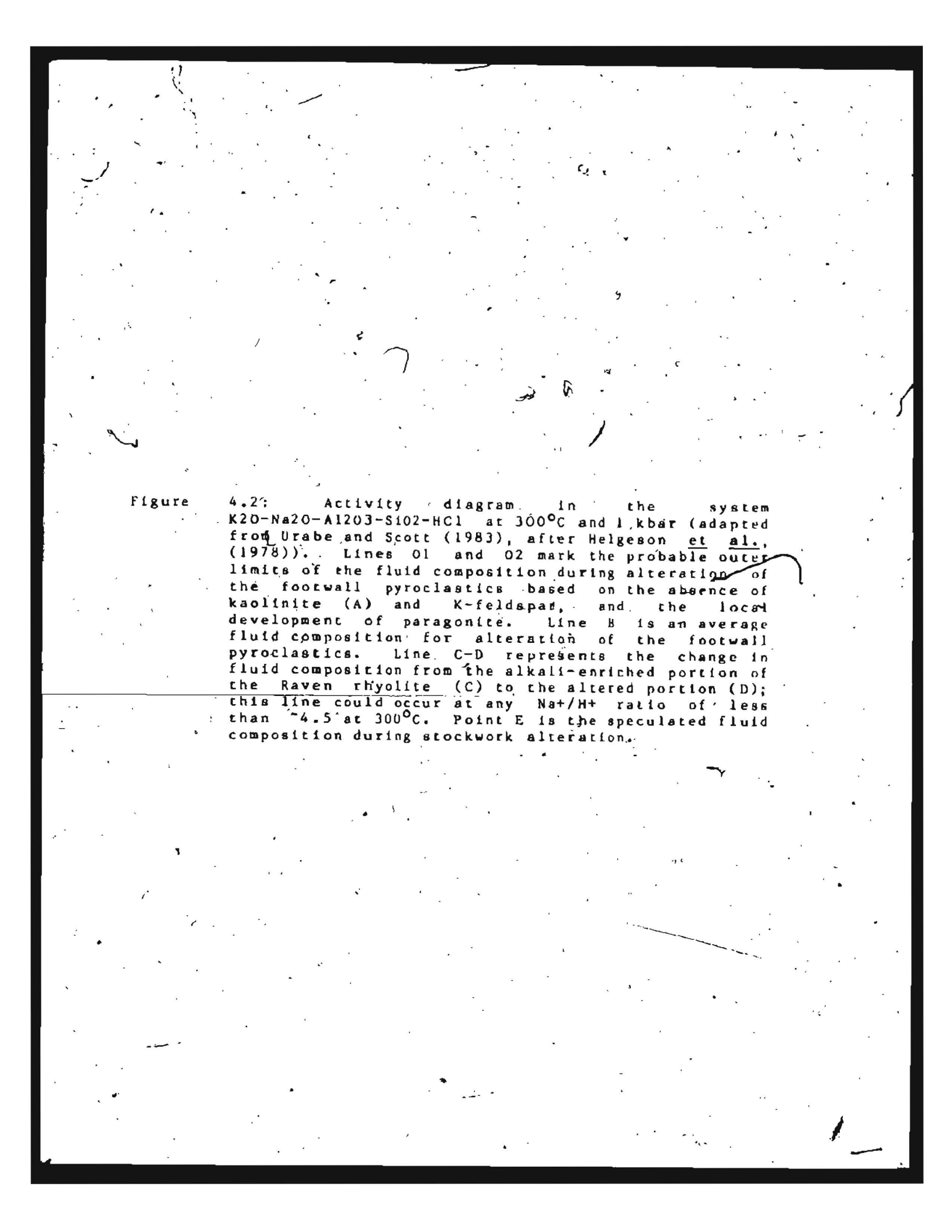

Figure 4.2: Activity diagram in the system K_2O-Na_2O-Al_2O_3-SiO_2-HCl at 300°C and 1 kbar (adapted from Urabe and Scott (1983), after Helgeson et al., (1978)). Lines O1 and O2 mark the probable outer limits of the fluid composition during alteration of the footwall pyroclastics based on the absence of kaolinite (A) and K-feldspar, and the local development of paragonite. Line B is an average fluid composition for alteration of the footwall pyroclastics. Line C-D represents the change in fluid composition from the alkali-enriched portion of the Raven rhyolite (C) to the altered portion (D); this line could occur at any Na^+/H^+ ratio of less than ~4.5 at 300°C. Point E is the speculated fluid composition during stockwork alteration.

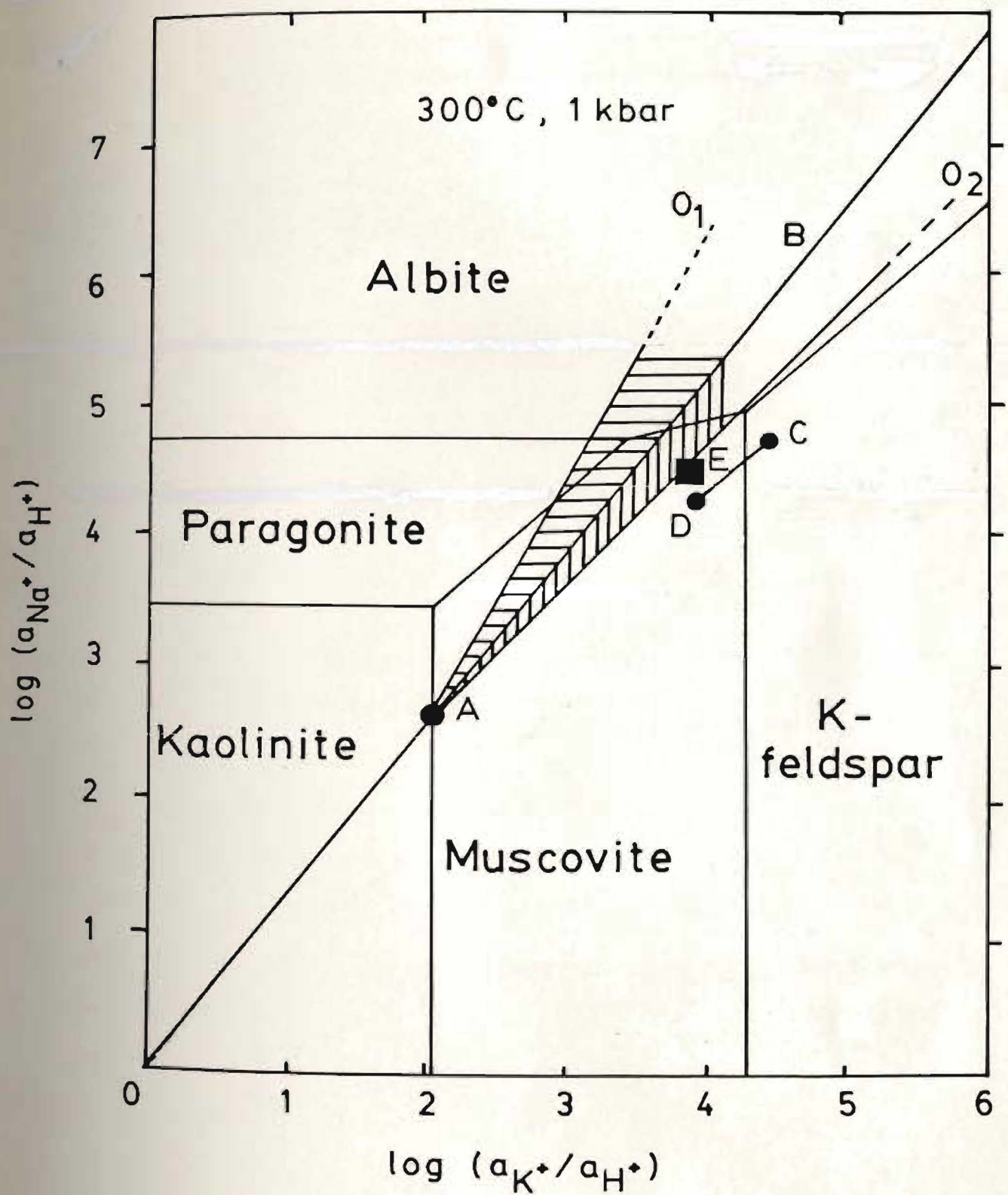
300°C, 1 kbar
Albite
Paragonite
Kaolinite
Muscovite
K-feldspar
A
B
C
D
E
O1
O2
log (aNa+/aH+)
log (aK+/aH+)
0
1
2
3
4
5
6
7

link of Na-metasomatism with at least one phase of hydrothermal alteration and sulphide deposition. Quartz-keratophyres outcrop in the footwall of the Iberian Pyrite deposits (Schermerhorn, 1970), the Stekenjokk-Levi deposit of the Scandinavian Caledonides (Stephens, 1982) and the Seneca deposit, British Columbia (Urabe et al, 1983) suggesting that albitisation is a common accompaniment to sulphide deposition in some areas.

4.4.2.2.1.2 Secondary microcline

The Raven rhyolite is thought to be temporally and spatially related to the footwall volcanics, not only because of trace element similarities (Chapter 6), but because it has suffered alteration. However, its alkali-enrichment is typically sericite or, locally, secondary microcline, rather than albite, and consequently it is separated from the footwall volcanics.

In the northern portions of the Raven rhyolite, where chloritic alteration and bleaching are minimal, microcline predominates over sericite, and locally, it overgrows a mixed assemblage of sericite and carbonate. This suggests that K^+ ion activity in the fluid(s) became dominant in the northern portions after a period of time when H^+ and CO_3^{--} ions dominated the fluid(s) composition (Meyer and Hemley, 1967; Rose and Burt, 1979; see line C-D in Fig. 4.2). It is suggested that the initial period of hydration and carbonation of the Raven rhyolite correlates with a period

of Na-enrichment in the tuffs, whereas microcline growth reflects a later phase of alteration dominanted by K-addition, in a manner similar to the K-addition in the tuffs.

K-enrichment of the Raven rhyolite may indicate a genetic link with the siliceous stockwork which also has a high K content, and it is conceivable that the Raven rhyolite is analogous to either the "white rhyolite lava domes" of Kuroko deposits (Sato, 1977) or the sub-volcanic intrusions that are commonly associated with Precambrian sulphide deposits (Campbell et al., 1981; Franklin and Thorpe, 1982). It is interesting to note that carbonate - chlorite - quartz - sulphide veinlets are relatively common in the Raven rhyolite; this may be evidence in support of a genetic connection with sulphide deposition and hydrothermal alteration.

4.4.2.2.2 Zones of intense alteration

Extreme alteration of the felsic footwall volcanics is typified by the siliceous and chloritic stockwork alteration. In both cases shattered quartz phenocrysts and quartz pseudomorphs of feldspar (siliceous stockwork only) suggest a crystal tuff protolith: a high permeability and mineral surface area probably aided increased fluid-mineral reactions within the tuffaceous rock.

4.4.2.2.2.1 Siliceous Stockwork

Within the East Adit (Map 2), the quartz-sericite stockwork alteration grades into a massive pyrite bed through an increase in the number of pyritic horizons, providing evidence of the genetic link of alteration and mineralisation (Plate 4.29). Since the sulphides accumulated on the seafloor (Hutchinson, 1982) the stockwork alteration must also have formed close to the seawater - rock interface so that the stockwork alteration marks a zone of hydrothermal fluid expulsion and intense alteration where chemical change and mineral reaction are maximised. Similar alteration rock types are recognised at most Precambrian and Phanerozoic (Kuroko) deposits: for example, Riverin and Hodgson (1980) noted that the Millenbach pipe has both sericite alteration and localised zones of silicification; Shirozu (1974) discusses a sericite-quartz zone of alteration surrounding Keiko ore in Kuroko deposits.

At Tulks Hill the presence of [illegible] carbonate suggests that the chemical conditions during alteration were slightly alkaline. Since seawater is typically alkaline this feature adds strength to the suggestion of formation close to the seawater - rock interface.

4.4.2.2.2.2 Chlorite Stockwork

This rock, composed of Mg-rich chlorite, is restricted to areas of siliceous stockwork and sulphide mineralisation

Plate 4.29: Mineralised layers within the siliceous stockwork (right) increase towards the hangingwall (left) and eventually grade into a massive pyrite bed. Siliceous ash is faulted against the mineralisation. Hammer length is approx. 33 cm.

(Map 2) implying a genetic link with mineralisation. Recent experimental work by Mottl (1983) has shown that Mg-chlorites can form in hydrothermal environments when seawater dominates the fluid, the required Mg being extracted from the seawater (Chapter 8). Thus, the location of a Mg-rich chlorite horizon in the footwall of the sulphide deposit is compatible with the alteration zones forming at or close to the seawater - rock interface. Chlorite formation probably post-dates albitisation as suggested by the lack of albite within this rock type. A possible reaction to explain the absence of albite is given below:

$$2NaAlSi_3O_8 + 5FeS_2 + 2H+ + 13H_2O$$

(Froese, 1981)

$$\rightleftharpoons (Fe_5Al)Si_3AlO_{10}(OH)_8 + 2Na+ + 10H_2S + 3SiO_2 + 5/2O_2$$

Chloritic alteration is as common in volcanogenic massive sulphide deposits as siliceous stockwork alteration (eg. Roberts and Reardon, 1978), typically defining a pipe shape (Franklin et al., 1981; Sangster, 1972). At Tulks Hill, however, deformation has reoriented the alteration zone into an elongate horizon trending subparallel to the S1 foliation (Chapter 9).

4.4.2.2.3 Other evidence for alteration

Mineralogical evidence of alteration is dispersed throughout the footwall volcanics: sericite and chlorite occur in all rock types and locally become dominant (eg.

quartz crystal tuff). The variation in composition of the chlorite within different rocks at Tulks Hill, and its significance in terms of hydrothermal alteration, is discussed in Chapter 8.

Quartz overgrowths on phenocrysts (phenoblasts) are sporadically developed; in all cases, sericite crystals are randomly oriented within the overgrowth but are absent from the host crystal. This association with the hydrothermal sericite, as well as their augen texture, suggests that the overgrowth is a pre-deformational phenomenom and is not a metamorphic feature (cf. Berge (1981) and Hopwood (1976)). It is thought to have formed during hydrothermal alteration through deposition of quartz from a silica-saturated brine. An identical feature is discussed by Frater (1983) for the Golden Grove Cu-Zn deposit in Western Australia. Overgrowths on quartz phenocrysts within the Raven rhyolite suggests that the rhyolite suffered a similar phase of hydrothermal alteration, and it is possible that the intrusion of the Raven rhyolite was synchronous with the deposition of the footwall volcanics. Of course, this implies that the Raven rhyolite is an integral part of the mineralising event(s).

Orange-coloured zones of silicification within the quartz crystal tuffs, now deformed into lens shapes, as well as diffuse edges to some rhyolite breccia clasts, are taken as evidence of quartz deposition and hydrothermal alteration during the passage of a hydrothermal fluid

through the volcanic pile.

4.4.3 CHEMICAL SEDIMENTS

A tuffaceous chert and an iron formation, which, by analogy with Kuroko deposits (Kalogeropoulas and Scott, 1983), must overlie the mineralisation, are examples of chemical sediments formed as precipitates from the hydrothermal solution. Slightly alkaline conditions during deposition and/or alteration is suggested by the presence of carbonate in both rock types. The spatial relationship of these chert-rich rocks to the mineralised horizon suggests a hydrothermal origin for the chert: silica supersaturation within the hydrothermal fluid, caused by mixing of the brine with cold seawater, is invoked to explain silica retention (and not dispersion) at the site of mineralisation (Rimstidt and Barnes, 1980).

4.4.3.1 Tuffaceous Chert

Quiescent conditions during deposition is suggested by a relative lack of volcanic material: minor sericite horizons (2-3cm thick), which are thought to be tuff, and a few phenocrysts, are the only evidence of volcanic activity. The thickness of the tuffaceous chert at Tulks Hill (Map 2) far exceeds the thickness of the Kuroko tuffaceous cherts (20-30 cm; Kalogeropoulas and Scott, 1983), which may suggest overthickening of the horizon

during deformation (Chapter 9).

Hangingwall alteration is relatively minor, when compared to the footwall volcanics, and manifests itself as dolomitic carbonate and chlorite, both minerals producing relatively high MgO values in the whole rock chemical analysis (Chapter 6). Mg-enrichment is relatively common in the hangingwall of the Kuroko deposits (Urabe, 1978) which is attributed to a "leakage" of hydrothermal fluids after deposition of the chert. Such a mechanism is likely at Tulks Hill, probably with mixing of the hydrothermal solution with seawater to produce the alkaline conditions for carbonate deposition. Recent theoretical modelling of sulphide deposition and paragenesis, these late fluids typically have high temperatures (>300 degrees centigrade); at such temperatures tuffaceous beds within the chert, consisting of K clay minerals, could be converted to sericite.

A tuffaceous chert, termed the Key tuffite, outcrops in the hangingwall of deposits at Mattagami Lake, Quebec (Roberts, 1975). Its banded appearance is identical to the tuffaceous chert at Tulks Hill.

4.4.3.2 Iron Formation

An abundance of iron-rich minerals, specifically siderite-rich carbonate and Fe (-Mg) chlorite, in a recrystallised quartz matrix (chert), is interpreted as a

mixed silicate-carbonate facies of an iron formation, analogous to certain iron formations at the Bathurst camp (Saif, 1983).

Whether or not the siderite-rich carbonate is primary or metamorphic is difficult to prove on textural grounds alone, since any carbonate is susceptible to solution and mobilisation during deformation (Ramdohr, 1969): the isoclinal folding at Tulks Hill (Chapter 9) would have realigned the carbonate subparallel to the schistosity, a mechanism that may have been responsible for the production of a "pseudo-augen" texture. However, since iron-rich minerals are restricted to the iron formation it suggests that primary Fe-Ca-Mg -rich minerals were present within this rock.

4.5 BRIEF SUMMARY AND STRATIGRAPHIC SUCCESSION

Structural complexities at Tulks Hill are a hinderence to the establishment of an unequivocal stratigraphy. However, by analogy with other mining camps the spatial and temporal relationships of the Tulks Hill rocks can be determined. Also, genetic models for volcanogenic massive sulphide deposits are useful for determining both the cause and probable relative timing of alteration, which indirectly, also helps to establish the possible sequence of deposition. Figure 4.1 is constructed using these lines of reasoning.

Na-enrichment in the footwall volcanics separates them

from the remaining rock types. Extreme alteration of the volcanics (stockwork) is localised at the base of the mineralised horizon which implies a genetic link of the stockwork to the mineralising event(s). K-enrichment in the Raven rhyolite is similar to the siliceous stockwork which suggests not only a genetic link to the mineralising event(s), but also that intrusion predates alteration and mineralisation (ie. it is probably comagmatic with the footwall volcanics). Sulphide veinlets within the alkali-enriched portion of the Raven rhyolite support the latter contention. It is speculated that the rhyolite is comparable to the lava domes and subvolcanic intrusions (sills) associated with other volcanogenic massive sulphide deposits.

The tuffaceous chert and the iron formation have both a relatively fresh mineralogy and a low sulphide content, which separates them from the remaining rock types. Contacts are faulted, but by analogy with other deposits they are thought to post-date the main mineralising event. Volcanic rocks interbedded with the distal portions of the iron formation (see Map 1), as well as phenocrysts within the tuffaceous chert, suggest that explosive volcanism did not cease completely during the deposition of the chemical sediments but rather it waned slightly. Thus, the sulphide deposit, since it contains no obvious evidence of explosive volcanic activity, was deposited during a brief hiatus in volcanism.

CHAPTER 5

SULPHIDE MINERALOGY

5.1 INTRODUCTION

Pyrite constitutes at least 70 % of the total sulphide content at Tulks Hill. It occurs as massive lenses at the mineralised horizon (Plate 5.1) and as disseminations within all rock types. Oxidation to goethite is common in the surface outcrops (Plate 5.2). Sphalerite is the most abundant economic mineral and is restricted to the mineralised horizon and the underlying stockwork alteration. Chalcopyrite and galena are present in roughly equal amounts, the former decreasing at the expense of galena towards the chemical sediments (hangingwall). Arsenopyrite, tennantite, bornite, covellite and digenite are variably distributed accessory sulphide minerals. Jambohr (1983) identified electrum (av. 68% Au) and minor amounts of marcasite, magnetite and ilmentite. Cubanite(?) may also be present (Cooper, 1968).

The following description of the sulphide mineralogy and textures is based on samples taken from the T3 lens (Map 2), as well as DDHs T60 and T90, the latter cross-cutting T3 lens (Map 3). Compositional variations and implications are discussed in Chapter 8.

Plate 5.1: Massive pyrite at the mineralised horizon. Blue-black mineral is probably covellite. Pencil is approx. 12 cm. long.

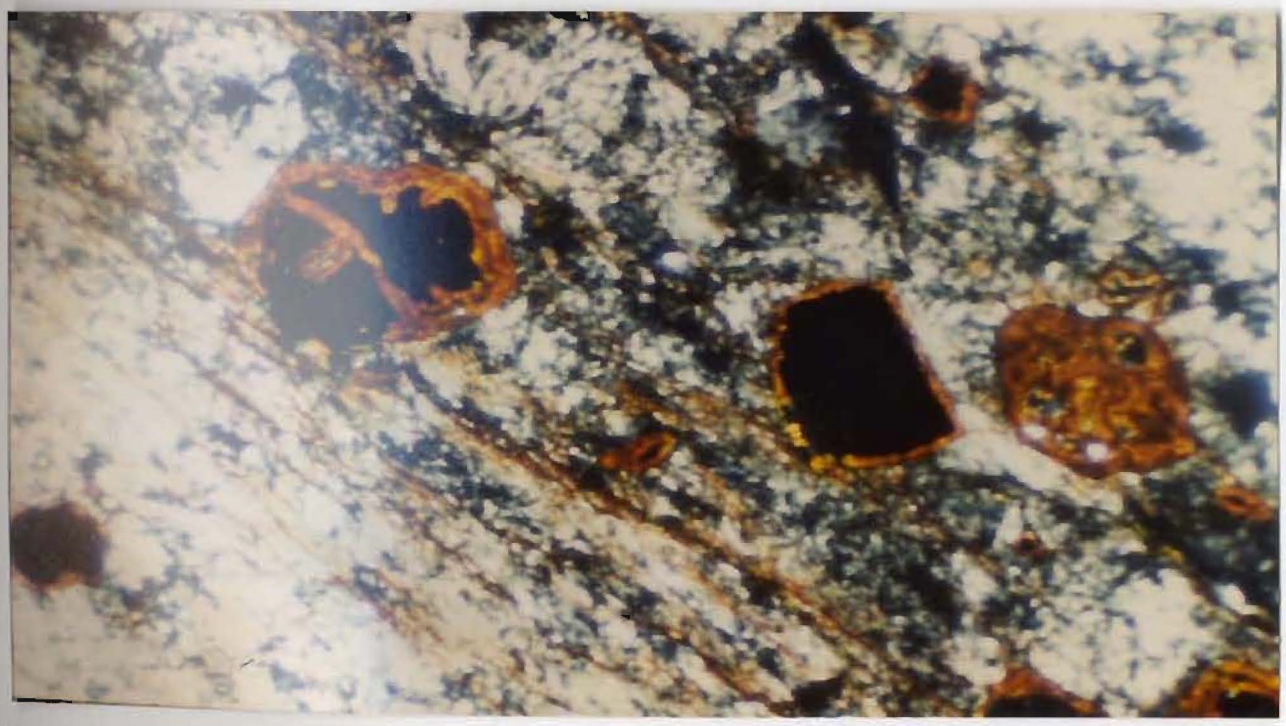

Plate 5.2: Variably developed oxidised pyrite within the siliceous stockwork alteration. Oxidation ranges from complete pseudomorphs (right) to rim alteration (centre). Field of view 2mm x 1.5mm (12x magnification).

5.2 PYRITE

Two pyrite types are identified: a) massive lenses, and b) veinlets and disseminations within the remaining rock types.

5.2.1 Massive pyrite

If the pyrite content exceeds 50 % of the rock it is termed massive. This effectively restricts massive pyrite to the underground outcrops (Map 2), although small (< 3m in length) bedded pyrite horizons occur in the quartz crystal tuff to the south of the mineralised horizon.

Two subtypes are differentiated in underground outcrop: (1) relatively fine-grained with prominent closely-spaced joints, and (2) relatively coarse-grained with no joints. Both types may occur in the same outcrop, the boundary between them being sharp (Plate 5.3).

5.2.2 Veinlet and disseminated pyrite

Pyrite within veinlets typically is euhedral and coexists with quartz, iron-rich chlorite and, locally, iron-rich carbonate. In the siliceous stockwork, where such veinlets are best developed, they contain sphalerite and sericite. These veinlets may cross-cut the siliceous bands (Plate 4.18).

Disseminated pyrite is either euhedral or fractured and broken. Pressure shadows associated with euhedral pyrite suggest that annealing, to produce the euhedral

Plate 5.3: Sharp contact between recrystallised pyrite (beneath pen), interpreted to be a fault zone, and well-jointed pyrite (to the left of pen) in the East Adit. Folding has isolated a "fragment" of chloritic alteration in the recrystallised pyrite. Siliceous stockwork alteration outcrops to the right of the mineralisation. Pen is approx. 12 cm. long.

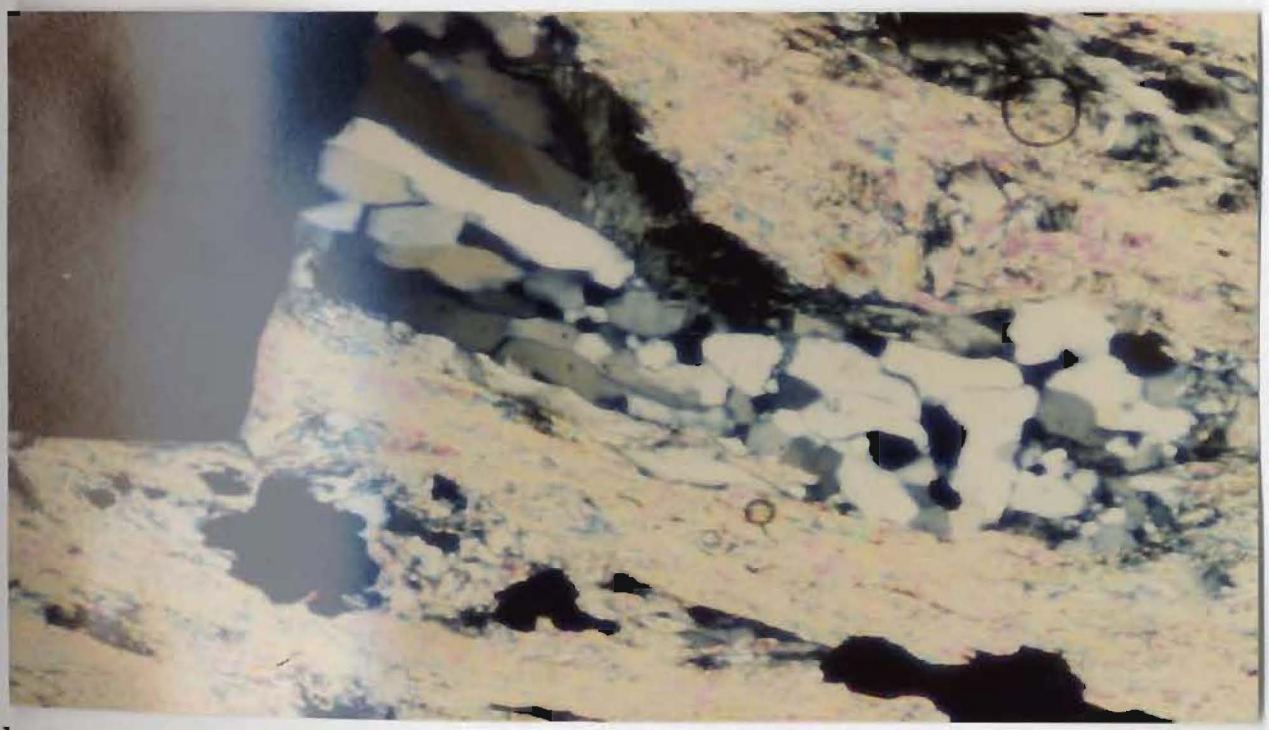

Plate 5.4: Euhedral pyrite overgrows the S1 schistosity. Quartz-chlorite pressure shadows associated with the pyrite are oriented subparallel to the S1 schistosity and locally have a sinuous shape. Field of view 2mm x 1.5mm (12x magnification).

pyrite, post-dates the deformation (Plate 5.4). In these instances pressure fringes of chlorite, sericite and/or quartz are well-developed subparallel to the schistosity (Plate 5.4). Granular, or crushed, pyrite typically occurs in zones adjacent to the euhedral pyrite suggesting a period of faulting after euhedral pyrite growth.

5.3 SPHALERITE

Sphalerite is restricted to the siliceous stockwork and massive zones within the mineralised horizons (Map 2). In the former case, it is associated either with veinlets of pyrite (see above) or in thicker, milky-coloured quartz veins cross-cutting the stockwork banding. The latter are thought to be deformation-induced (Chapter 9).

Relatively thick beds of sphalerite are shown on Map 2, where sphalerite comprises at least 50 % of the rock (Plate 5.5). In hand sample, the sphalerite is brown to deep red and is locally banded (bedded?) due to alternating pyrite (-chalcopyrite) horizons. Flexuring of some banded mineralisation is not uncommon. A honey-brown or pale yellow colour is distinctive when viewed with transmitted light, the latter possibly reflecting its low Fe content (Chapter 8).

Invariably, sphalerite is interstitial to any pyrite although it may occur as bleb-like inclusions within pyrite and chalcopyrite. This is thought to result from pyrite porphyroblastesis and chalcopyrite mobilisation,

Plate 5.5: Bed of massive sphalerite bounded by siliceous stockwork (South Adit). Right-hand contact is faulted. Hammer is approx. 33 cm. long.

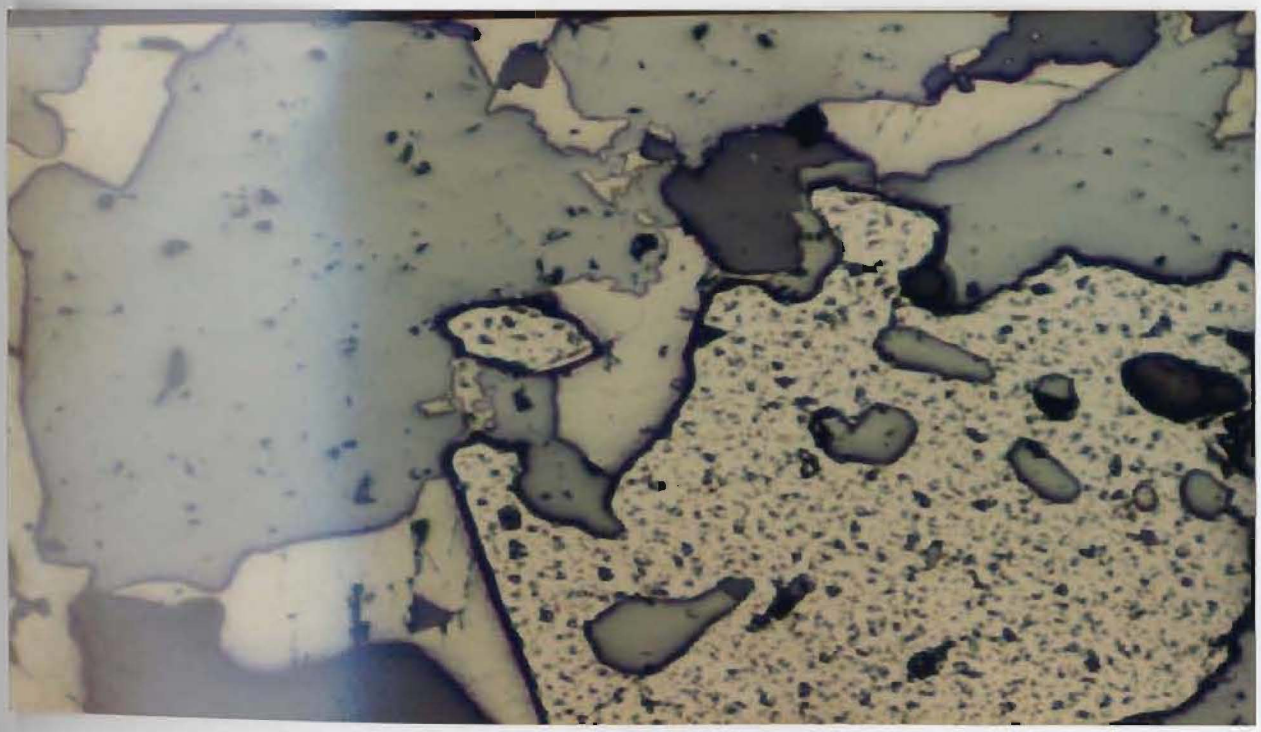

Plate 5.6: Inclusions of chalcopyrite (golden yellow) and galena (white) in sphalerite (grey). Sphalerite is also included within pyrite (pale yellow). Silicate minerals are dark grey. Field of view 0.1mm x 0.07mm (25x magnification).

respectively (Chapter 9). Locally, chalcopyrite and galena occur as inclusions within sphalerite (Plate 5.6). In samples of the siliceous stockwork that have a high matrix:sulphide content the sphalerite is oriented subparallel to the fabric.

5.4 CHALCOPYRITE

Chalcopyrite is most abundant in the chloritic stockwork, although minor amounts are sporadically distributed in the siliceous stockwork and the footwall portions of the massive mineralisation. It decreases in abundance within the mineralised horizon towards the contact with the tuffaceous chert, that is, towards the hangingwall. Centimetre-thick veinlets of chalcopyrite, quartz and carbonate occur in the alkali-enriched portion of the Raven rhyolite.

Invariably, chalcopyrite forms selvages to pyrite. Millimetre-size recrystallisation zones within massive pyrite often host mobilised chalcopyrite (Plate 5.7), as do fractures within individual pyrite crystals (Plate 5.8).

Locally, chalcopyrite is associated with pyrrhotite (Plate 5.8), which is a unique mineral association in the T3 lens at Tulks Hill. Pyrrhotite is a minor mineral and rarely occurs in any other association, and therefore does not permit the use of sphalerite as a geobarometer.

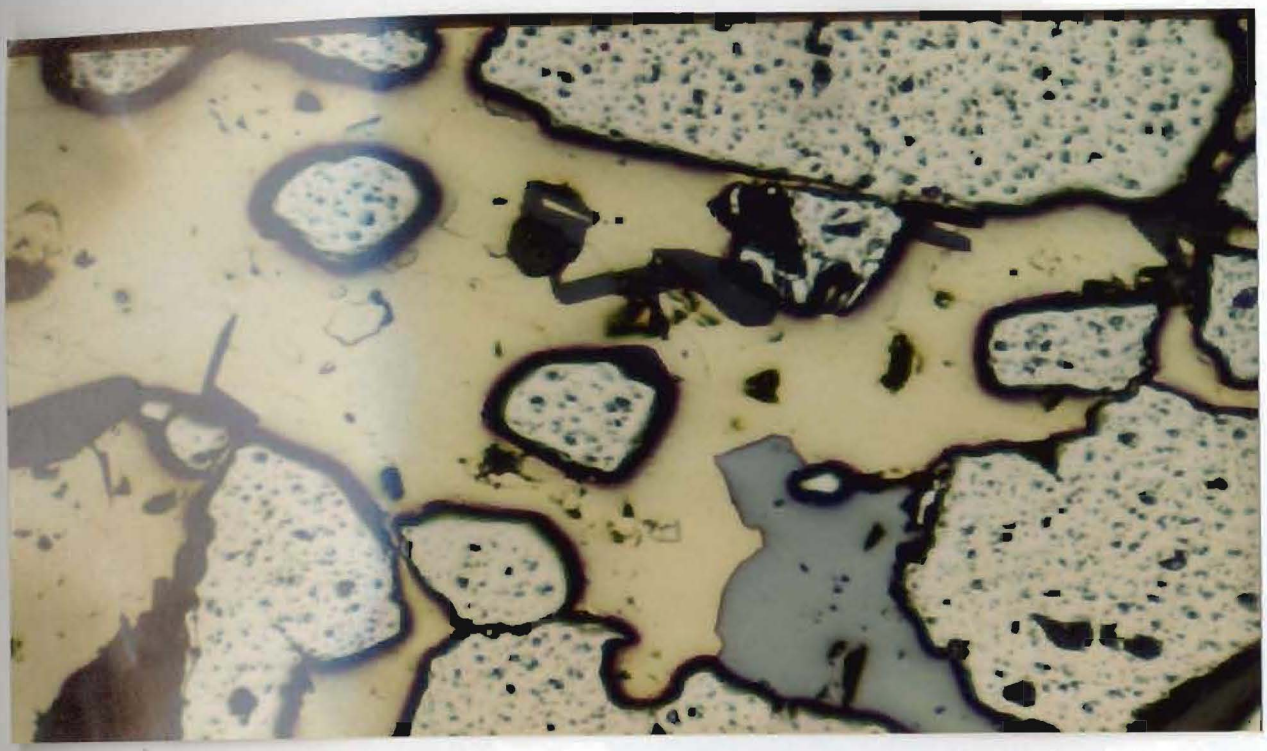

Plate 5.7: Fractured and granulated pyrite (pale yellow) host mobilised chalcopyrite (golden yellow). Sphalerite (grey) and silicate minerals (dark grey) are also present. Field of view 0.1mm x 0.07mm (25x magnification).

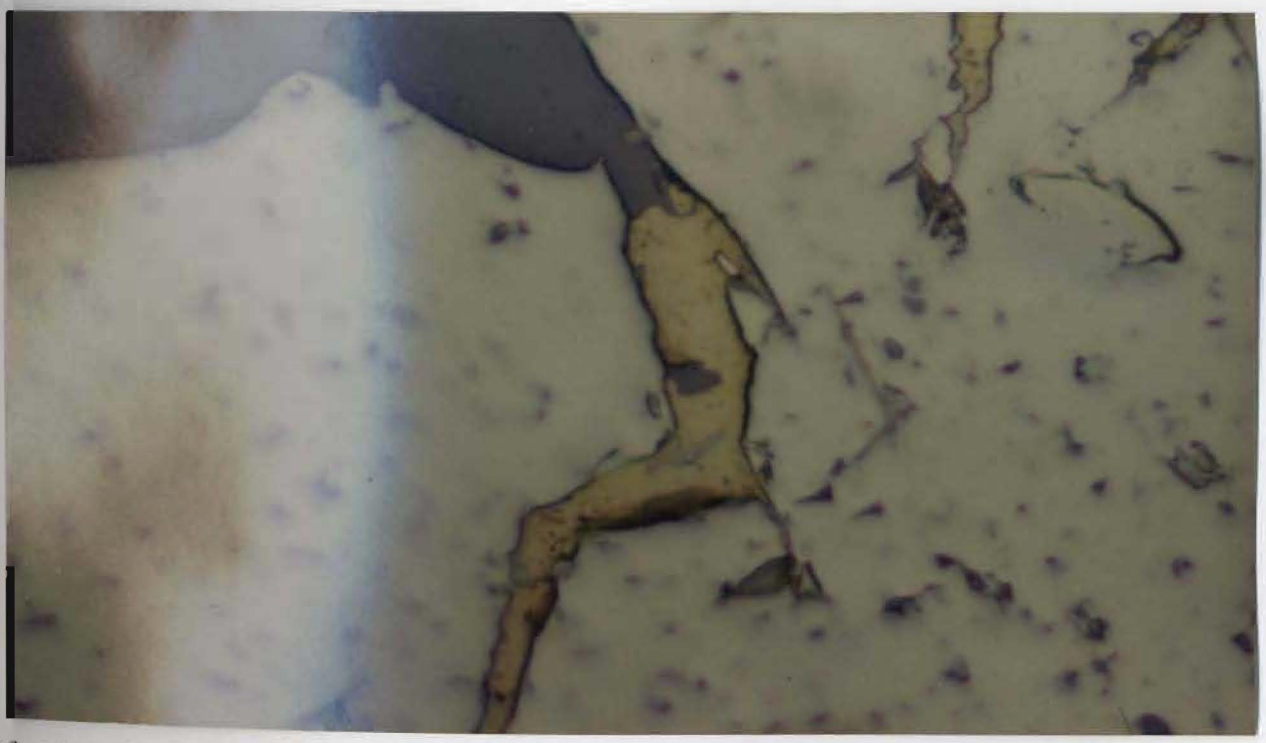

Plate 5.8: Chalcopyrite (golden yellow) fills a fracture in the pyrite (yellow). Pyrrhotite (pink) is associated with the chalcopyrite only (centre of the photograph). Dark grey to black mineral is silicate gangue. 125x magnification.

5.5 GALENA

Megascopic galena is identified only in samples taken from the hangingwall or distal portions (lens T3b on Map 3) of the mineralised horizon. Locally, thin (< 1 mm.), wisp-like galena is visible in samples of banded sphalerite-pyrite. Microscopic occurrences are found in some massive pyrite and sphalerite-rich samples. However, it is rare, if not absent, in the siliceous stockwork. Quartz veins cross-cutting the S1 schistosity contain minor galena, typically with ankeritic(?) carbonate, as in the Main Hall fault zone (Map 2).

Galena, like chalcopyrite and sphalerite, occurs as an interstial mineral to pyrite, although in samples from the hangingwall the pyrite component is reduced and galena is interstitial to sphalerite (Plate 5.6). It may occur as distinct bleb-like inclusions in pyrite but more commonly it is interstial to the three main sulphide minerals. The latter may completely surround the galena to produce a sieved texture (Plate 5.6).

5.6 TENNANTITE (Fahlore Group)

This mineral, which has a complex mineralogy (Chapter 8), is only identified in drill core samples of the distal portions of the mineralised horizon. It contains inclusions of chalcopyrite, but is surrounded by galena. The difference in polishing hardness between galena and tennantite, as well as its brown to pink colour, aid in the

identification of tennantite.

Unlike most tennantites, which undergo brittle deformation (Ramdohr, 1969), this sample shows no signs of cataclastic deformation (unetched), reflecting the inhomogeneous style of deformation at Tulks Hill (Chapter 9). Its matrix position therefore, is thought to be primary suggesting a "late" time of formation relative to the other sulphide minerals.

5.7 ARSENOPYRITE

This mineral is scattered throughout the mineralised horizon, without any consistency to its location. It has a fractured, brittle appearance in polished section, often occurring as "islands" within the more plastically deformed sulphides (chalcopyrite, galena and sphalerite).

5.8 MINOR SULPHIDE MINERALS

Pyrrhotite, bornite, covellite and polybasite-pearceite(?) occur in accessory amounts. The latter mineral pair is intergrown with coarse chalcopyrite, but is too fine-grained to be analysed with the electron microprobe.

Bornite may be present as a primary mineral associated with chalcopyrite in the main sulphide assemblage. Both bornite and covellite occur as relatively coarse crystals associated with chalcopyrite in quartz-vein boudins within the S1 schistosity (Chapter 9), strongly suggesting that

their presence is pre-deformational (Plate 5.9). Some of the covellite and bornite however, is found on the rims and in cracks of chalcopyrite and pyrite, suggesting formation during weathering and/or supergene alteration.

5.9 INTERPRETATION AND DISCUSSION

The sulphide mineralogy at Tulks Hill is dominated by massive pyrite but it also has significant accumulations of sphalerite, chalcopyrite and galena. Assuming that the local stratigraphy of Tulks Hill is correct, there is a mineralogical zoning of the deposit, both vertically and laterally, from a chalcopyrite-rich footwall through sphalerite-rich horizons into a galena-tennantite-rich horizon (the lateral, distal portions of the T3 lens is repeated by isoclinal folding, as shown in Map 3). This is the typical sequence of mineral deposition in volcanogenic massive sulphide deposits (Large, 1977) which is borne out further by the systematic decrease in the mole % FeS content of sphalerites with increasing proximity of the hangingwall (Chapter 8). This sequential deposition of sulphides is thought to reflect their decreased solubility in the hydrothermal fluid (Pb>Cu>Zn; Barnes and Czamanske, 1967) probably caused by a simple temperature drop (Solomon and Walshe, 1979). Four mechanisms are commonly proposed for this temperature drop: a) mixing with cold (sea)water; b) adiabatic decompression (throttling); c) heat loss through contact with the wall rocks; d) boiling (Skinner,

Plate 5.9: Bornite (violet), chalcopyrite (yellow) and minor covellite (blue) in a quartz-vein boudin. Pen cap is approx. 3 cm. long.

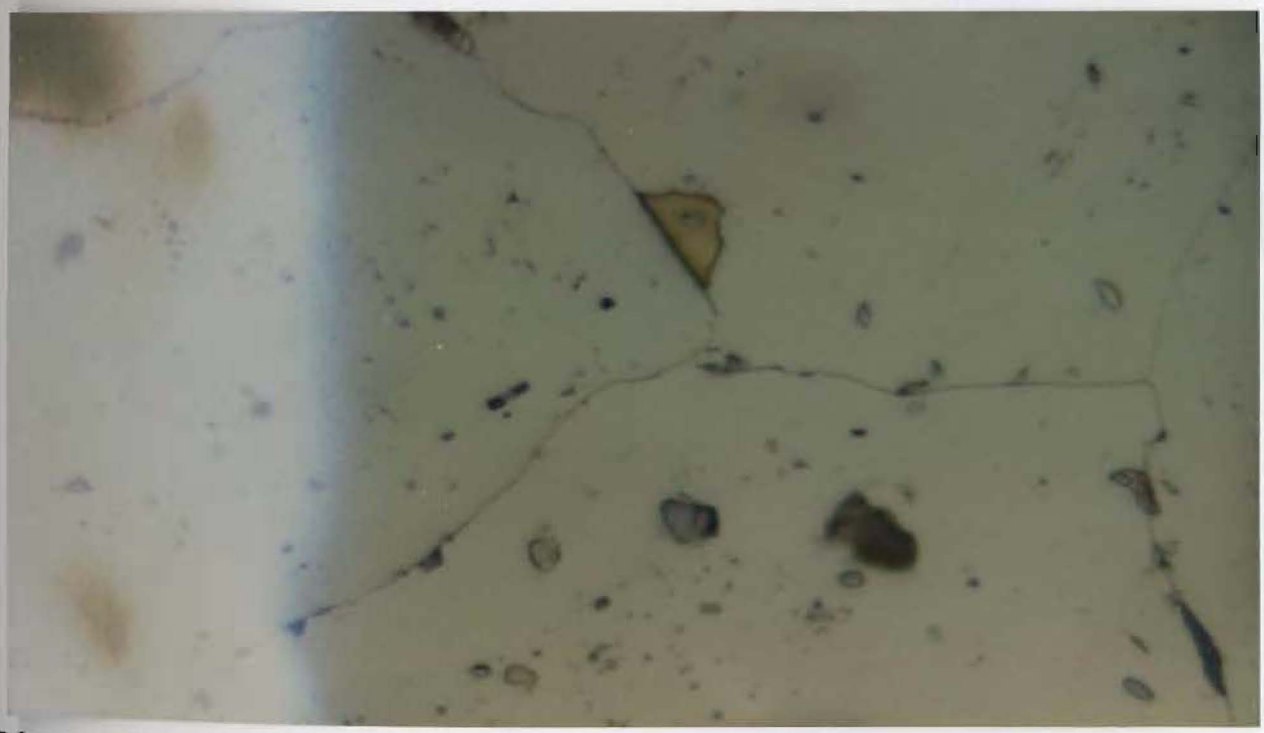

Plate 5.10: Equilibrium triple junction developed in massive pyrite (yellow), probably as a result of annealing. Silicates and unidentified sulphides are included within the pyrite. Deformation has mobilised chalcopyrite (golden yellow) along pyrite grain boundaries. 125x magnification.

1979). Mechanism (c) is unlikely to seriously affect the fluid temperature because rates of heat conduction are too slow. Either of the three other mechanisms (or a combination) could precipitate the sulphides. Carbonate within the siliceous stockwork suggests that boiling probably occurred (Holland and Malmin, 1979) although the severe Ce depletion in the siliceous stockwork, as well as the Mg chlorites within the stockwork, imply seawater interaction and therefore probable cooling by mixing (Graf, 1977; Mottl, 1983).

Epigenetic mineralisation occurs as pyrite-sphalerite veinlets within the siliceous stockwork. Although these veinlets are subparallel to the S1 schistosity it is thought that they originally defined a network of veinlets within the siliceous stockwork, as shown by the local occurrences of sulphide veinlets cross-cutting the siliceous horizons (Plate 4.18). This feature is comparable to the keiko ore zone (undeformed) of the Japanese Kuroko deposits (Sato, 1977) where the epigenetic mineralisation has been interpreted to represent a fossil feeder zone for the hydrothermal fluids, immediately beneath the seawater-rock interface and the area of sulphide deposition. The location of similar epigenetic mineralisation at Tulks Hill, immediately beneath the sulphide mineralisation, as well as the cross-cutting relationship of some sulphide veinlets suggests that the siliceous stockwork marks a (deformed) feeder zone for the

mineralising hydrothermal fluid.

All sulphide textures are thought to reflect either deformation, metamorphism or a combination of the two. Annealed pyrite, as well as pyrite porphyroblasts within the stockwork and the tuffaceous chert, probably reflect growth during higher metamorphic temperatures. Such growth would explain the numerous inclusions of silicate matrix and lower temperature sulphides (eg. galena) within pyrite (Plate 5.6): because of its high form energy (Craig and Vaughan, 1981; Stanton, 1972) pyrite will always recrystallise as euhedra when growing in free space or when against minerals of a lower form energy (eg. silicates). If free space is not available, then the pyrite crystals impinge upon each other at interfacial angles of 120 degrees, as shown in Plate 5.10. Metamorphic overgrowth of chalcopyrite by sphalerite, and vice-versa, is a probable explanation of the inclusions in these minerals; exsolution is not thought to be an appropriate mechanism for such a vast amount of bleb-like inclusions (Barton, 1978; Wiggins and Craig, 1980). Wide zones (approx. 1m.) of recrystallised pyrite, without a joint system, and micro-scale fault zones of granulated pyrite-arsenopyrite, both trending subparallel to the S1 schistosity, define zones of brittle deformation (Plate 5.3). Such deformation must post-date annealing (Chapter 9). It is possible that these fault zones represent primary porosity within the massive pyrite: according to Atkinson (1975) pore spaces

within a deforming rock act as zones of stress relief. Consequently, highly porous pyrite would suffer the ravages of deformation more than adjacent horizons of massive pyrite, ie. it may act as a fault zone. Elongate pyrite within these zones may have grown by a process of fluid or stress assisted diffusion, the porosity of the layer aiding the fluid movement (Atkinson, 1975).

Plastic deformation features of chalcopyrite, sphalerite and galena, are common at Tulks Hill; stringers of mineralisation are aligned subparallel to the S1 schistosity, typically occupying areas of pyrite recrystallisation (cleavage) where the strain is lower (Plate 5.11). Polished sections of these cleavage zones contain granulated sulphides "floating" in the plastically deformed sulphides (eg. chalcopyrite).

Experimental work by Kelly and Clarke (1975) determined that chalcopyrite will not "flow" until at least 100°C, at which time polysynthetic deformation twins develop, leading to a loss of strength and consequent failure enabling plastic flow. At the pressures and temperatures of greenschist facies metamorphism (approx. 3 kbar and 300-500°C) ductility is the required mode of deformation.

Although such factors as grain size, strain rate and impurities affect the relative timing of plastic deformation in sulphides, a crude ranking of strength is possible: at the temperatures and pressures of greenschist

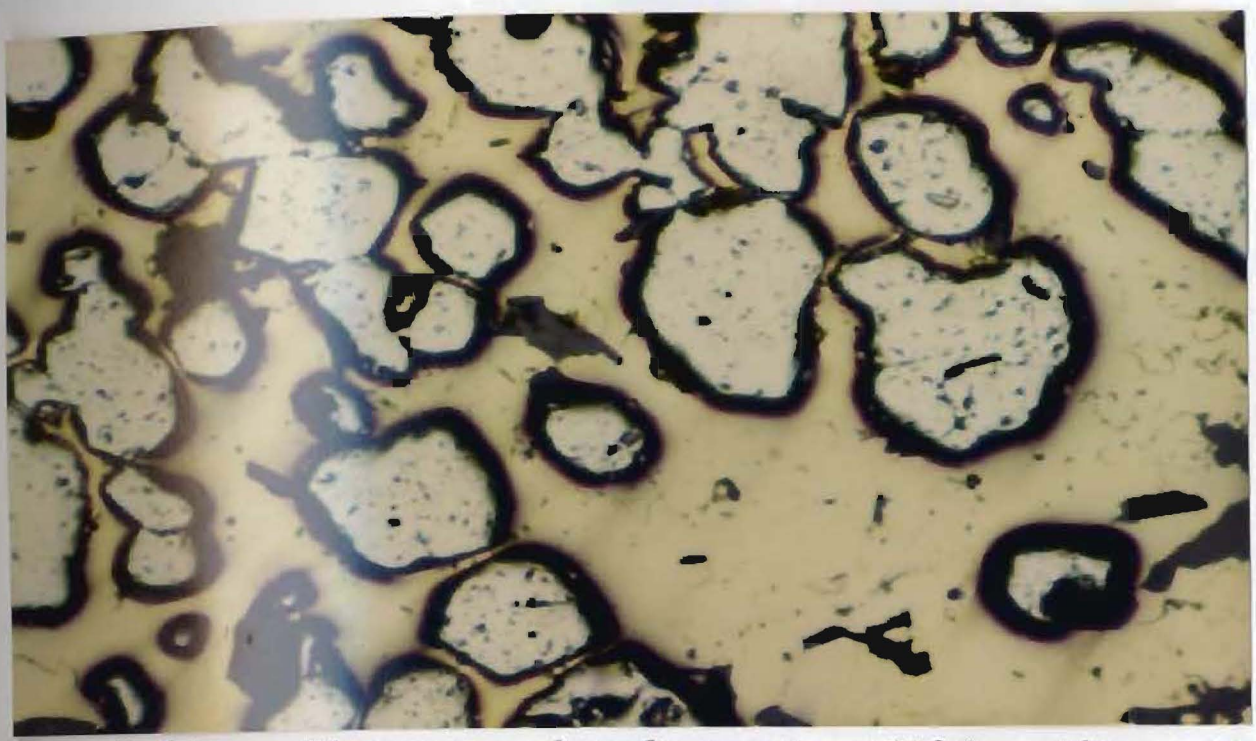

Plate 5.11: Cleavage development within the massive pyrite (yellow) causes granulation. Mobilised chalcopyrite (golden yellow) occupies these low strain areas. Field of view 0.1mm x 0.07mm (25x magnification).

facies metamorphism sphalerite > chalcopyrite > pyrrhotite > galena. Under similar conditions pyrite will deform cataclastically (Atkinson, 1975).

CHAPTER 6

PETROCHEMISTRY

6.1 INTRODUCTION

Sixty five samples were analysed for major and trace elements to determine the chemistry of the Tulks Hill rocks. At least one sample from each rock type was analysed. The analytical techniques, precision and accuracy are given in Appendix II.

Hydrothermal alteration is extensive in the footwall rocks and the primary mineralogy and rock textures are usually absent; this precludes the use of a modal classification for the rocks. Only the chemical sediments, which stratigraphically overlie the mineralisation, can be termed "fresh" because their deposition post-dated the main alteration event(s).

Most of the footwall rocks are waterlain pyroclastic deposits which therefore introduces a high risk for alteration and the incorporation of "anomalous" material for example, heavy mineral lag-type deposits (zircon). This precludes their use in petrogenetic studies. The chemistry of the massive felsic volcanic rocks however, can be used to approximate the primary rock-type because they should be relatively freer from such effects.

Five natural groupings are used for easier comparison of the chemical characteristics. These are:

1) rhyolite: a) alkali-enriched rhyolite
b) altered rhyolite
2) pyroclastics
3) chemical sediments
4) stockwork alteration
5) mineralised horizons

This chapter is divided into 3 sections: the first section describes the major and trace element contents within each group, the second section discusses and interprets these data in terms of the primary and secondary mineralogy and the possible chemical environment, and the third section uses the less mobile trace elements to discriminate the possible primary rock type.

6.2 MAJOR AND TRACE ELEMENT CHEMISTRY

Tables giving mean, standard deviation, and minimum and maximum values for each oxide in each group are contained within this chapter. Since the effects of hydrothermal alteration are best appreciated when the LOI is given, the data are not normalised to a volatile-free basis. Complete lists of the data can be found in Appendix I.

6.2.1 RHYOLITE

Two rhyolite types are differentiated by their physical appearance and chemistry: one type is fresh-looking and alkali-enriched, and the second type is

altered (including bleached) with no significant alkali-enrichment. Both may occur within the same unit, for example the Raven rhyolite (Map 2), or as isolated occurrences within the tuffaceous rocks (see Map 1).

6.2.1.1 Alkali-enriched rhyolite

Most of the samples are taken from the Raven rhyolite (Table 6.1). Unfortunately there is only one suitable surface outcrop of alkali-enriched rhyolite.

Major elements: Contrasting Na2O and K2O contents produce two subtypes corresponding to surface (Na-rich) and Raven (K-rich) rhyolite analyses (Fig. 6.1E). Total alkali contents, however, are similar.

Silica content varies between 67.8 and 81.3 wt.% (Fig. 6.2E) with respective Al2O3 values of 15.5 and 9.24 wt.%. In general, Al2O3 decreases with increasing SiO2 content.

A ternary plot of CaO : Fe2O3 : MgO shows that CaO is enriched relative to the other two oxides (Fig. 6.3E). Absolute values for CaO range from 0.1 to 6.25 wt.%, whereas MgO and Fe2O3 are never greater than 1.87 and 1.89 wt.% respectively.

Trace elements: Lead, Th, U, V, Ni and Cr show only a limited variation between 0.1 and 11 ppm; the latter two elements invariably are absent. Zinc is always greater

Table 6.1 : Summary of the major and trace element chemistry of the alkali-enriched rhyolites

	ALKALI-ENRICHED RHYOLITE				
	Mean	SD	Min	Max	No.
SiO_2	75.21	4.77	67.80	81.30	8
TiO_2	0.11	0.07	0.04	0.23	8
Al_2O_3	11.42	2.09	9.67	15.50	8
Fe_2O_3	1.29	0.38	0.78	1.89	8
MnO	0.06	0.05	0.01	0.16	8
MgO	0.80	0.48	0.30	1.87	8
CaO	1.79	1.98	0.10	6.25	8
Na_2O	0.92	1.46	0.07	4.44	8
K_2O	4.46	1.95	0.95	6.97	8
P_2O_5	0.02	0.02	0.01	0.05	6
LOI	3.09	1.96	0.76	7.19	8
Pb	6	3	3	11	7
Th	7	2	3	10	7
U	4	2	2	8	7
Rb	39	15	9	63	8
Sr	42	34	13	118	8
Y	66	14	43	85	8
Zr	145	39	115	233	8
Nb	6	2	2	9	8
Zn	30	9	21	48	8
Cu	14	2	10	16	8
Ni	0	0	0	1	2
La	7	2	4	12	7
Ba	677	257	241	1110	8
V	2	2	0	8	6
Ce	17	6	9	26	8
Cr	0	0	0	0	1
Ga	9	2	7	13	8

Figure 6.1: Na_2O vs. K_2O diagram for the 6 rock groups identified at Tulks Hill.

A: Pyroclastics
B: Siliceous stockwork
C: Mineralised horizon
D: Chemical sediments
E: Alkali-enriched rhyolite
F: Altered rhyolite

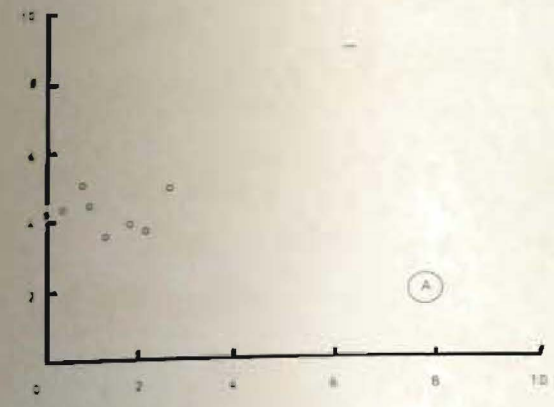
A

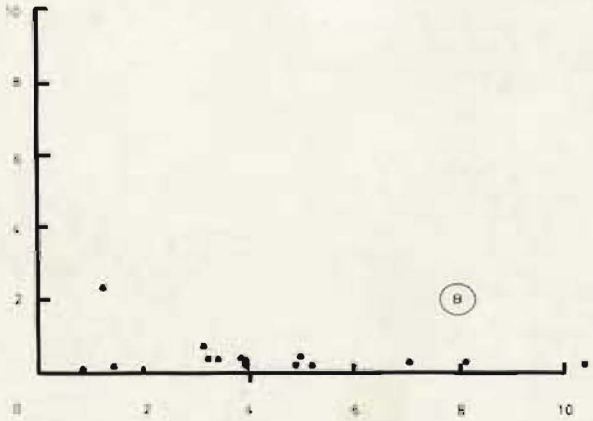
B

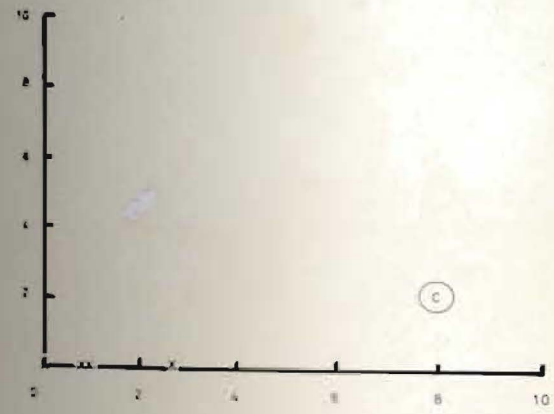
C

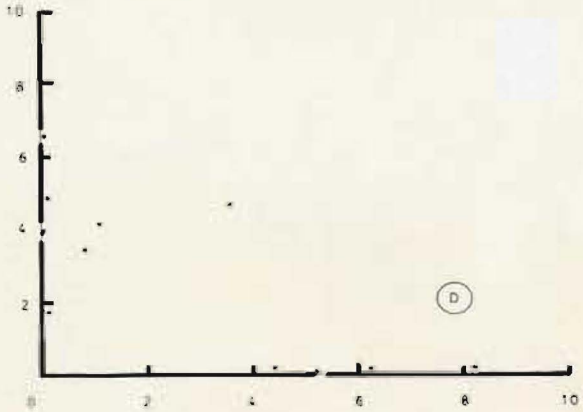
D

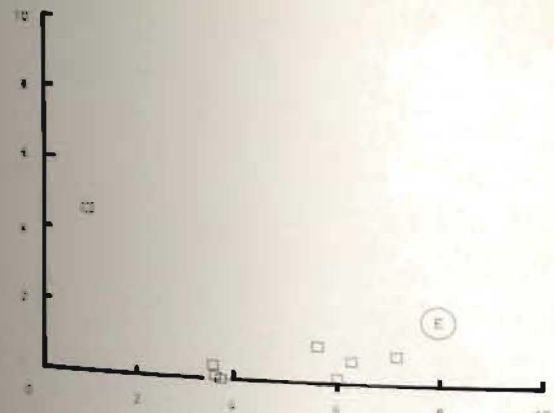
E
Na2O (wt %)
K2O (wt %)

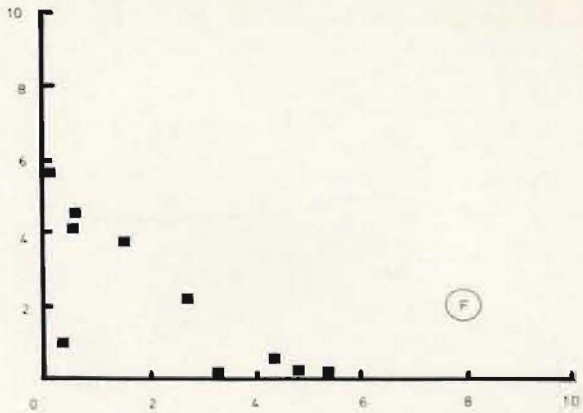
F

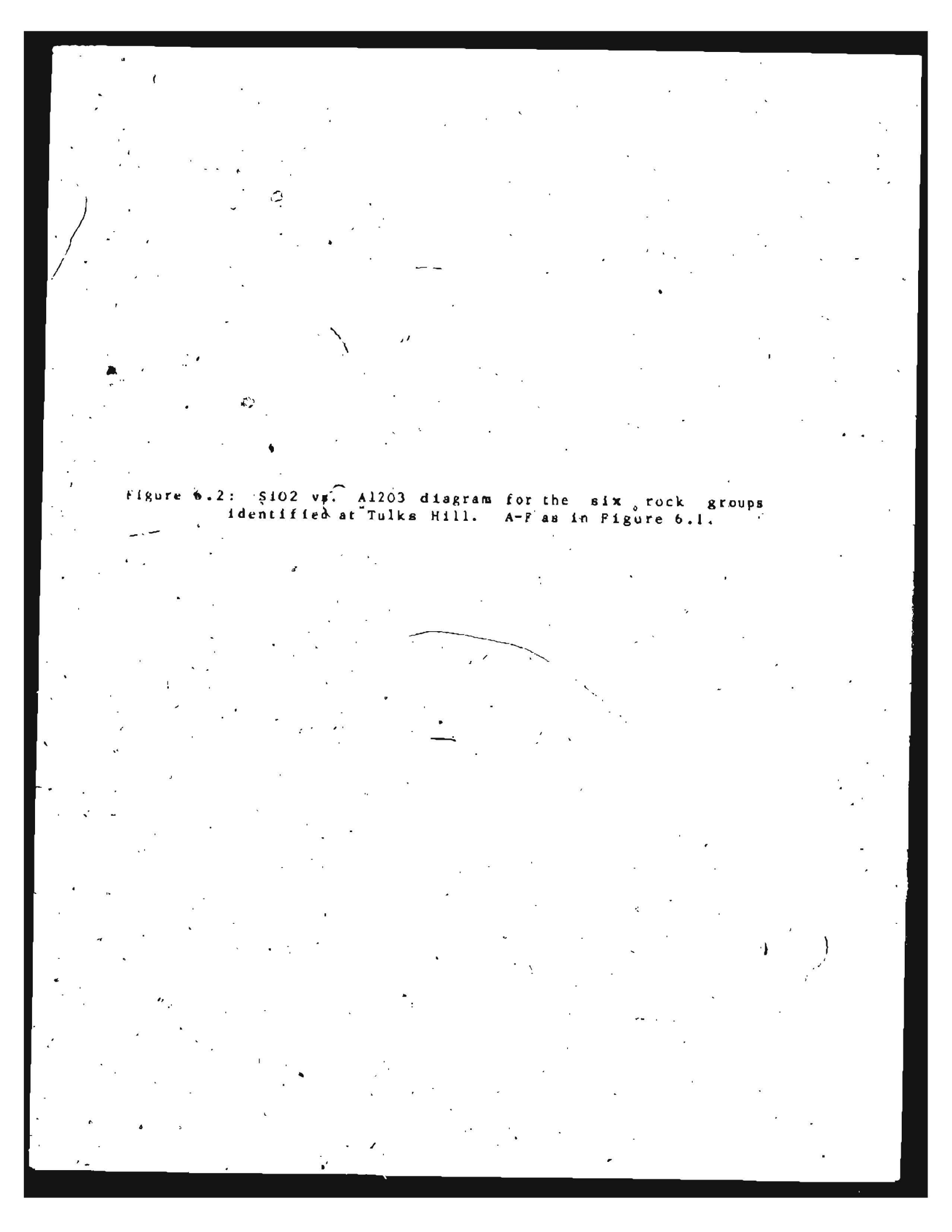

Figure 6.2: SiO2 vs. Al2O3 diagram for the six rock groups identified at Tulks Hill. A-F as in Figure 6.1.

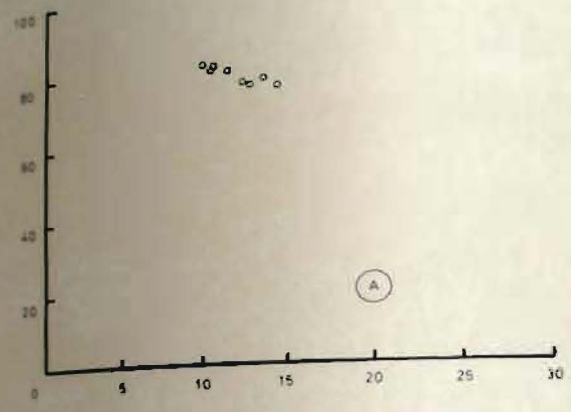
A

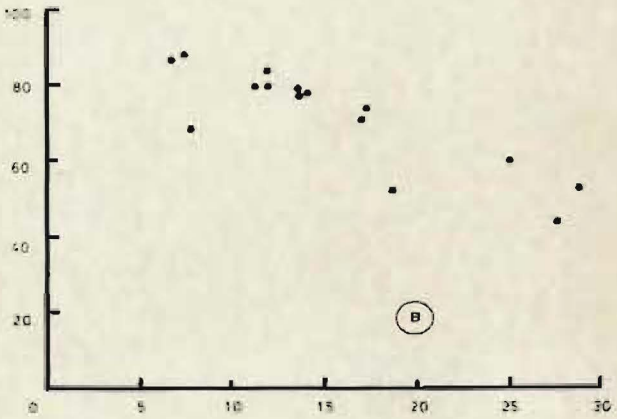
B

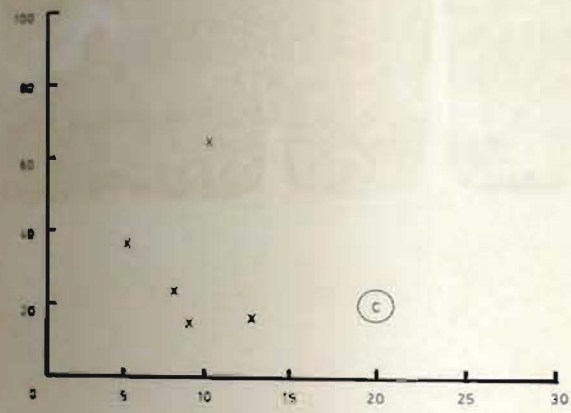
C

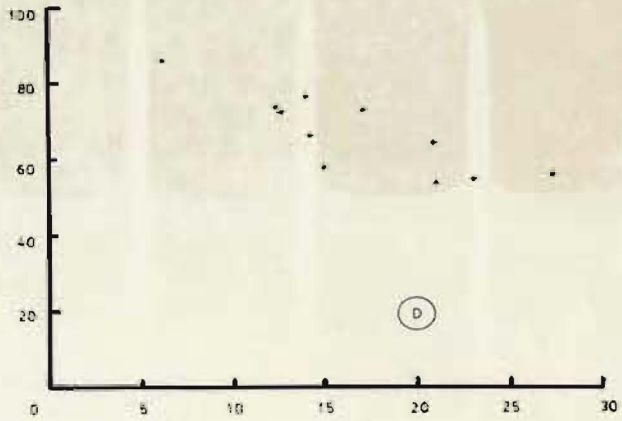
D

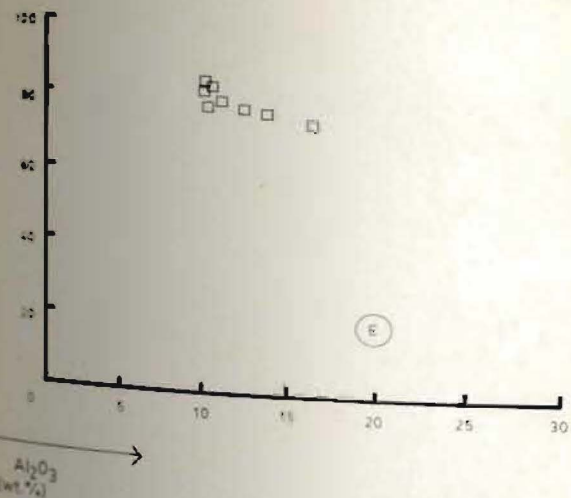
E
SiO2 (wt %)
Al2O3 (wt %)

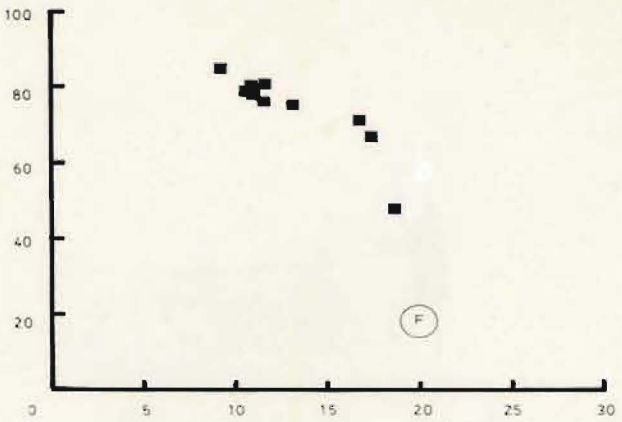
F

Figure 6.3: CaO : Fe2O3 : MgO plot for the six rock groups identified at Tulks Hill. A-F as in Figure 6.1.

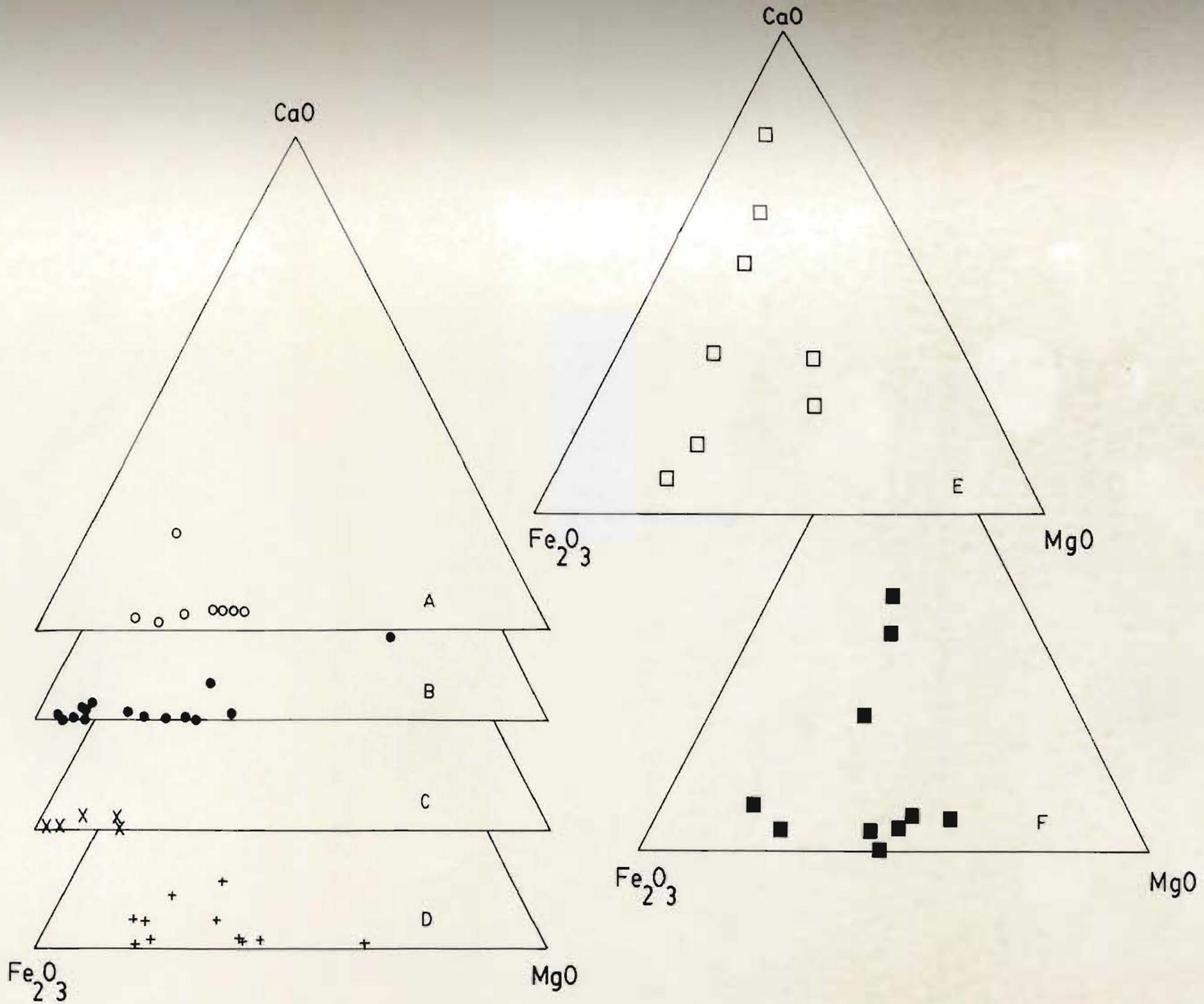
CaO
A
B
C
D
Fe_2O_3
MgO
CaO
E
Fe_2O_3
MgO
F
Fe_2O_3
MgO

than Cu, the former ranging from 21 to 48 ppm whereas the latter has a restricted range from 10 to 16 ppm. Barium ranges from 241 to 1110 ppm.

6.2.1.2 Altered rhyolite

Two of the ten samples are from surface outcrops; the remainder are from the Raven rhyolite (Table 6.2). Sericitic and/or chloritic alteration is common to many samples. Sulphide micro-veinlets are intimately related to intense alteration zones and, for this reason, were not removed prior to the chemical analysis.

Major elements: Total alkalis range from 3.23 to 5.68 wt.%, although sample 12NA-82 contains only 1.23 wt.% combined alkalis. A higher Na2O:K2O ratio for the surface samples differentiates them from the Raven rhyolite samples, which have lower Na2O:K2O ratios (Fig. 6.1F). Their Na2O:K2O ratio is similar to the alkali-enriched rhyolite surface samples (Fig. 6.1E).

Silica content ranges from 44 wt.% (12NA-82) to 84.2 wt.% (Fig. 6.2F), although the mode is between 64 and 80 wt.%. Alumina decreases from 17.3 to 9.24 wt.% with increasing SiO2 content.

Ferric iron oxide and MgO contents have a positive linear relationship (Fig. 6.4F). The highest Fe2O3 and MgO contents (15.82 and 14.25 wt.%., respectively) are

Table 6.2 : Summary of the major and trace element chemistry of the altered rhyolite

	ALTERED RHYOLITE				
	Mean	SD	Min	Max	No.
SiO_2	70.77	11.19	44.00	84.20	10
TiO_2	0.13	0.07	0.06	0.27	10
Al_2O_3	12.57	2.98	9.24	17.30	10
Fe_2O_3	3.65	4.39	0.81	15.82	10
MnO	0.06	0.05	0.01	0.13	9
MgO	3.39	4.07	0.20	14.25	10
CaO	1.00	1.30	0.05	3.64	10
Na_2O	2.15	2.10	0.09	5.58	10
K_2O	2.27	1.91	0.10	5.19	10
P_2O_5	0.06	0.05	0.01	0.12	8
LOI	3.46	2.15	0.84	6.98	10
Pb	7	4	3	12	5
Th	4	3	1	12	8
U	4	3	1	11	8
Rb	29	19	6	58	9
Sr	38	17	15	70	10
Y	48	18	17	78	10
Zr	126	46	38	202	10
Nb	4	2	1	8	10
Zn	77	112	12	366	9
Cu	15	2	12	19	10
Ni	5	25	5	5	1
La	6	3	1	12	9
Ba	1152	1725	27	5201	10
V	36	50	1	123	8
Ce	75	11	3	41	10
Cr	0	0	0	0	0
Ga	12	4	7	20	10

Figure 6.4: Fe_2O_3 vs. MgO diagram for the six rock groups identified at Tulks Hill. A-F as in Figure 6.1. Note the change in Fe_2O_3 scale for Figure 6.1C (Mineralised horizon)

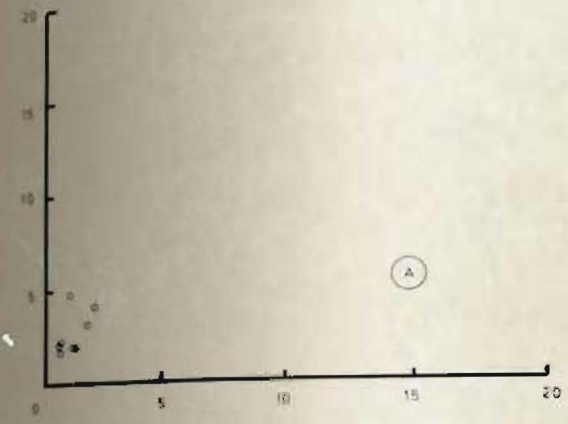

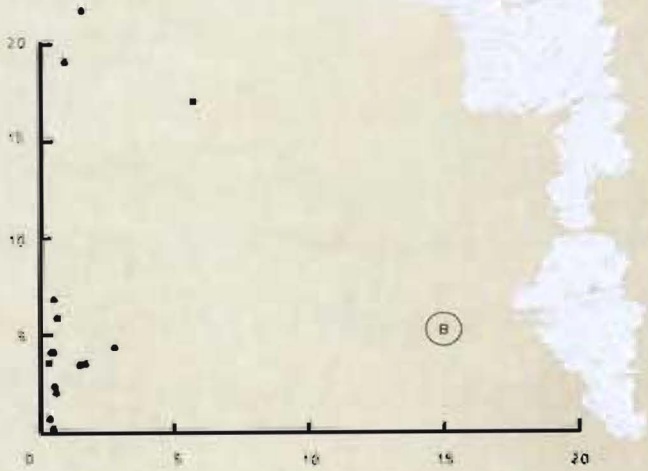

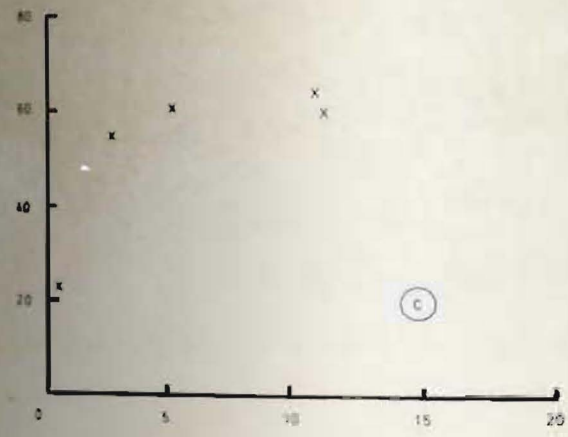

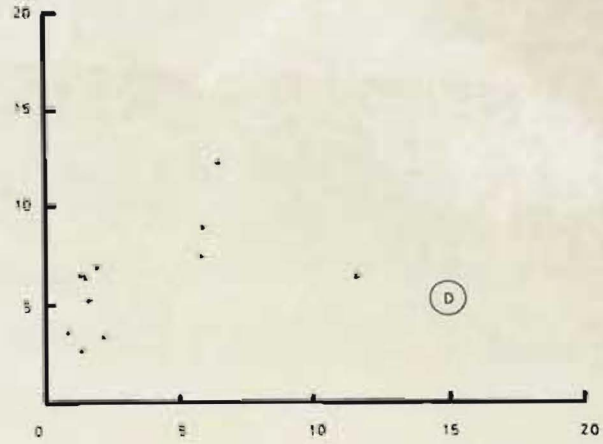

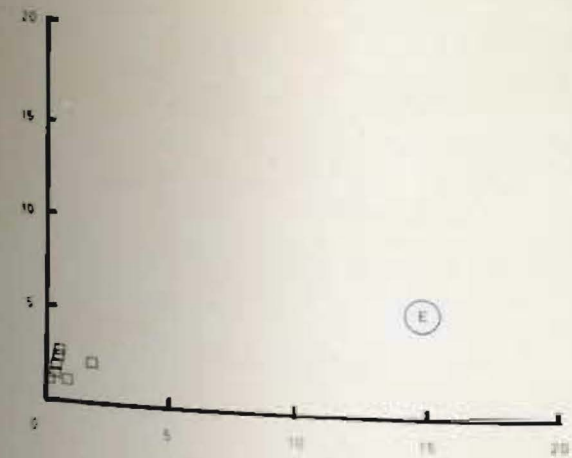

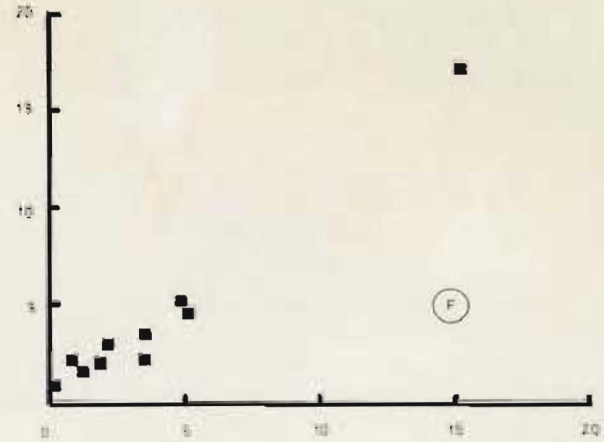

MgO (wt%)

associated with sample 12NA-82 (chloritised rhyolite); most values fall within the range 0.3 to 5.03 wt.%. A ternary plot of CaO : Fe2O3 : MgO shows that the latter two oxides are enriched relative to CaO (Fig. 6.3F), which is in marked contrast to the alkali-enriched rhyolite.

Trace elements: Lead, Th, U, Ni and Cr show a limited range of abundance from 0 to 12 ppm, which is similar to the alkali-enriched rhyolite; V however, varies between 0 and 123 ppm. Zinc values range from 0 to 91 ppm, although a higher value (366 ppm) is associated with sample 12NA-82 (44 wt.% SiO2). Copper is restricted in its abundance, with values between 13 and 19 ppm, which is similar to the copper range in the alkali-enriched rhyolite. Barium has a wide range of values with a minimum of 27 ppm and a maximum of 5201 ppm.

6.2.2 PYROCLASTICS

Three distinct mappable units, the large-quartz crystal tuff, biotite tuff and quartz crystal tuff, are here combined to form one group. Eight samples were analysed (Table 6.3).

Major Elements: Total alkalis in 5 samples never exceed 5.62 wt.%, and Na2O is more abundant than K2O. The remaining three samples, 82-12A, -12B and -12C are from the biotite tuff and have higher total alkali contents (5.67,

Table 6.3 : Summary of the major and trace element chemistry of the pyroclastics

	PYROCLASTICS				
	Mean	SD	Min	Max	No.
SiO_2	76.08	2.87	73.00	79.60	8
TiO_2	0.10	0.03	0.06	0.15	8
Al_2O_3	11.74	1.54	9.85	14.20	8
Fe_2O_3	2.69	1.08	1.68	4.63	8
MnO	0.05	0.03	0.02	0.10	8
MgO	1.18	0.55	0.57	2.11	8
CaO	0.20	0.19	0.05	0.64	8
Na_2O	4.14	0.51	3.46	4.86	8
K_2O	1.23	0.89	0.01	2.62	8
P_2O_5	0.02	0.01	0.01	0.02	2
LOI	1.59	0.39	0.90	2.13	8
Pb	3	2	2	6	5
Th	3	2	1	8	4
U	2	1	1	4	3
Rb	19	10	6	35	7
Sr	51	17	36	88	8
Y	53	17	27	85	8
Zr	127	44	46	193	8
Nb	3	1	1	6	8
Zn	71	66	12	213	8
Cu	13	1	12	17	8
Ni	1	1	1	1	1
La	9	3	4	15	7
Ba	274	104	10	512	8
V	44	74	2	192	6
Ce	24	10	12	47	8
Cr	0	0	0	0	0
Ga	12	3	9	17	8

5.62 and 7.36 wt.% respectively) and higher K2O:Na2O ratios (Fig. 6.1A).

Minimum and maximum silica contents of 73.0 and 79.6 wt.% are accompanied by Al2O3 values of 12.5 and 9.85 wt.%, respectively (Fig. 6.2A). In general, an increase in Fe2O3 content is matched by increasing MgO, the former ranging from 1.68 to 4.63 wt.% while the latter ranges from 0.57 to 2.11 wt.% (Fig. 6.4A). All samples contain less than 0.64 wt.% CaO (Fig. 6.3A).

Trace Elements: Lead, Th, U, Ni and Cr all fall below the detection limit of analysis, which probably reflects both their primary felsic nature and hydrothermal leaching within these porous rocks. Vanadium is sporadically distributed, ranging from 0 to 192 ppm. Zinc values are greater than Cu in all but one sample (82-1), with a minimum value of 13 ppm and a maximum of 213 ppm. Copper varies between 0 and 17 ppm. Barium has a maximum value (512 ppm) in sample 82-12C; the other two biotite tuffs (samples 82-12A and -12B) also have higher (> 300 ppm) Ba contents than the other pyroclastics.

6.2.3 SILICEOUS STOCKWORK

Of the fifteen samples analysed, ten were from underground outcrop, the remainder from surface outcrops (Table 6.4).

Table 6.4 : Summary of the major and trace element chemistry of the siliceous stockwork

	SILICEOUS STOCKWORK				
	Mean	SD	Min	Max	No.
SiO_2	67.67	14.87	36.90	86.20	15
TiO_2	0.14	0.08	0.03	0.33	12
Al_2O_3	14.45	6.10	6.60	27.40	15
Fe_2O_3	6.03	6.01	0.16	19.82	15
MnO	0.02	0.01	0.01	0.05	12
MgO	1.10	1.29	0.31	5.18	15
CaO	0.07	0.06	0.01	0.20	15
Na_2O	0.41	0.54	0.04	2.27	15
K_2O	4.08	2.34	0.77	9.88	15
P_2O_5	0.07	0.03	0.04	0.11	9
LOI	4.77	3.40	1.08	11.65	15
Pb	471	723	2	2188	14
Th	10	8	2	29	14
U	6	6	0	24	12
Rb	78	41	15	157	15
Sr	33	18	7	74	15
Y	38	30	12	133	15
Zr	187	89	88	391	15
Nb	6	3	2	15	15
Zn	2082	4664	3	17030	15
Cu	387	474	5	1285	15
Ni	2	1	1	4	3
La	9	4	2	21	15
Ba	1464	1469	207	6393	15
V	28	31	0	104	14
Ce	15	7	6	28	15
Cr	38	54	0	77	2
Ga	22	13	7	48	15

Major Elements: Total alkalis typically range between 3.48 and 5.09 wt.% although two samples, T63-81 and 82-8, have low values of 0.81 and 1.55 wt.%, respectively. Samples 82-A1b and 9MH-82 have high total alkali contents of 10.9 and 7.01 wt.%, respectively. In all cases, except sample 82-B1a, K2O is higher than Na2O (Fig. 6.1B).

Silica content varies from 36.9 to 86.2 wt.%, the lower silica values corresponding to higher Al2O3 contents (Fig. 6.2B). Fe2O3 and MgO show no correlation, the former ranging up to 19.82 wt.% while the latter has a maximum value of 5.18 wt.% (Fig. 6.4B). CaO contents are negligible (Fig. 6.3B).

Trace Elements: Lead contents vary from 0 to 2188 ppm. Thorium, V, Ni, U, and Cr have restricted values up to a maximum of 24 ppm. Nine samples have zinc contents less than 100 ppm; sample 9MH-82 has the greatest zinc content (17030 ppm). In general, Cu values are higher than Zn, the maximum Cu content (1285 ppm) being found in sample 3SA-82. Most Ba values range from 750 to 1350 ppm, although two samples, T63-81 and 82-B1a, have lower values of 207 and 241 ppm respectively. Sample 9MH-82 contains 2646 ppm Ba.

6.2.4 MINERALISED HORIZONS

Six heavily mineralised samples were analysed; one analysis was discarded because of its high total (Table 6.5).

Table 6.5 : Summary of the major and trace element chemistry of the mineralised horizon

	MINERALIZED HORIZON				
	Mean	SD	Min	Max	No.
SiO_2	20.36	18.99	10.90	54.30	5
TiO_2	0.10	0.00	0.10	0.10	4
Al_2O_3	6.36	3.36	1.71	9.99	5
Fe_2O_3	32.38	14.05	17.49	47.15	5
MnO	0.17	0.14	0.02	0.35	5
MgO	4.26	4.03	0.46	8.89	5
CaO	0.45	0.51	0.07	1.17	5
Na_2O	0.04	0.04	0.01	0.09	4
K_2O	0.77	1.06	0.02	2.33	4
P_2O_5	0.06	0.04	0.03	0.10	5
LOI	19.63	5.75	10.88	25.93	5
Pb	64924	119988	208	278524	5
Th	282	499	15	1170	5
U	3	2	0	7	4
Rb	64	76	5	192	5
Sr	13	10	5	26	3
Y	12	14	1	30	5
Zr	158	90	94	317	5
Nb	6	4	2	10	3
Zn	135621	188762	392	438274	5
Cu	5191	3927	98	9114	5
Ni	0	0	0	0	2
La	20	13	7	41	5
Ba	235	240	51	649	5
V	35	21	19	72	5
Ce	10	4	5	16	5
Cr	0	0	0	1	2
Ga	542	971	2	2267	5

Major Elements: Total alkalis in all but one sample are less than 0.5 wt.%; sample 2WA-82 however, contains 2.42 wt.% combined total alkalis and K2O >> Na2O (Fig. 6.1C). Three samples have an average SiO2 content of 11.95 wt.% but sample 2WA-82 contains 54.3 wt.% silica (Fig. 6.2C). All Al2O3 values are < 10 wt.%. Fe2O3 varies from 19.38 to 47.15 wt.%, and shows no consistent relationship to the MgO content; the latter varies from 0.46 to 8.89 wt.% (Fig. 6.4C). CaO contents are less than 1.17 wt.% (Fig. 6.3C).

Combined metal contents (Pb + Zn + Cu) vary from 0.06 to 24.3 wt.%. In all cases Zn is the dominant metal; three samples (5ES-82, 2WA-82, 10WA-82) have Pb > Cu.

Trace Elements: Thorium, U, and V range up to 48 ppm although sample 5ES-82 contains 149 ppm Th. Nickel and Cr are absent. Barium contents range from 51 to 649 ppm.

6.2.5 CHEMICAL SEDIMENTS

Six tuffaceous cherts from underground outcrop and 5 iron formation samples from surface outcrops (Table 6.6) were analysed.

Major Elements : Total alkali contents in both chemical sediments vary between 1.78 and 7.71 wt.% with roughly equal amounts of Na2O and K2O (Fig. 6.1D).

Silica values range from 50.6 to 82.9 wt.% (Fig.

Table 6.6 : Summary of the major and trace element chemistry of the chemical sediments

	CHEMICAL SEDIMENTS				
	Mean	SD	Min	Max	No.
SiO_2	63.33	11.18	49.60	82.90	11
TiO_2	0.27	0.17	0.07	0.73	11
Al_2O_3	15.70	5.30	5.95	25.00	11
Fe_2O_3	5.96	2.55	2.52	11.40	11
MnO	0.08	0.08	0.01	0.29	11
MgO	3.49	3.10	0.84	10.75	11
CaO	0.49	0.77	0.05	2.74	11
Na_2O	2.58	2.19	0.09	6.05	11
K_2O	2.55	2.73	0.02	7.51	11
P_2O_5	0.08	0.08	0.02	0.29	10
LOI	4.13	1.71	1.87	6.20	11
Pb	67	58	1	138	8
Th	13	2	10	17	6
U	5	3	1	12	10
Rb	66	61	2	163	9
Sr	55	29	17	117	11
Y	43	21	21	96	11
Zr	148	92	42	296	11
Nb	5	3	1	11	11
Zn	122	68	53	303	11
Cu	21	10	8	37	11
Ni	6	0	6	6	2
La	8	4	2	16	11
Ba	2395	3406	57	11299	11
V	80	178	3	585	10
Ce	17	9	1	32	11
Cr	0	0	0	0	0
Ca	16	6	7	28	11

6.2D) with Al2O3 values of 21.4 and 5.95 wt.%, respectively. Both Fe2O3 and MgO are variable, ranging from 2.52 to 11.4 and 0.84 to 10.75 wt.%, respectively. CaO values are typically less than 1.0 wt.% (Fig. 6.3D), although sample 82-14 has a higher value of 2.74 wt.%.

Trace Elements: Thorium, U, Ni, Cr and V never exceed values of 71 ppm, except for V in sample 82-14 (585 ppm); Pb contents however, range up to 138 ppm. Typically, the zinc content is at least twice that of Cu, the former ranging from 53 to 303 ppm and the latter from 8 to 37 ppm. Barium content in the tuffaceous chert is high (range 2812 to 11299 ppm) although one sample (19MH-82) contains only 64 ppm; the iron formation has a maximum Ba content of 558 ppm.

6.3 INTERPRETATION AND DISCUSSION

6.3.1 INTRODUCTION

No fresh rocks crop out at Tulks Hill (Fig. 6.5) and consequently the chemistry described above reflects the style of hydrothermal alteration and, to a certain extent, their original composition. Three alteration styles are identified on chemical and petrographic evidence: a) K enrichment, b) Na enrichment, and c) Fe2O3 and MgO enrichment.

Although the chemical sediments are not igneous rocks they do contain an igneous-derived component (tuff). Since

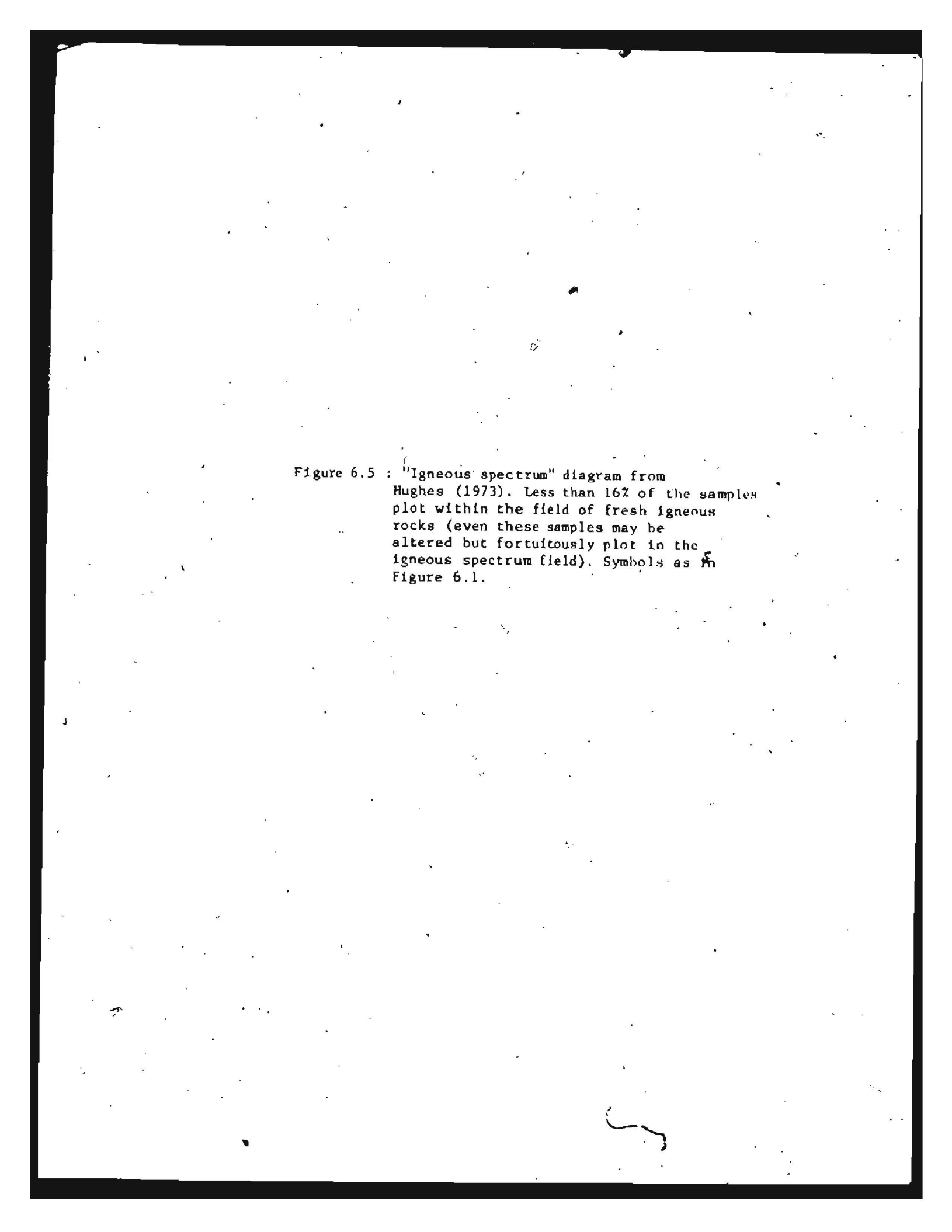

Figure 6.5 : "Igneous spectrum" diagram from Hughes (1973). Less than 16% of the samples plot within the field of fresh igneous rocks (even these samples may be altered but fortuitously plot in the igneous spectrum field). Symbols as in Figure 6.1.

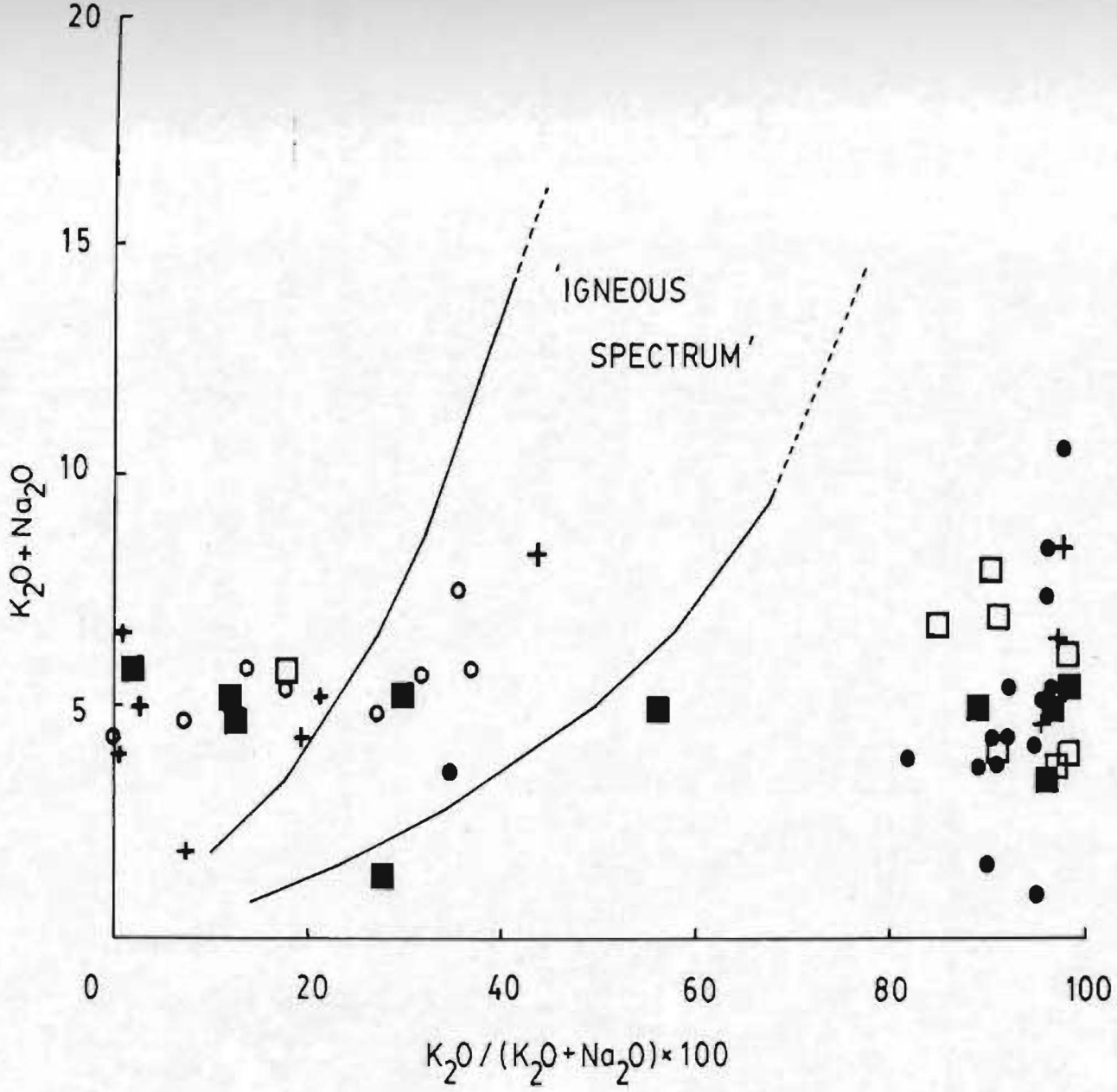
20
15
10
5
0
20
40
60
80
100
K_2O+Na_2O
$K_2O/(K_2O+Na_2O)\times 100$
'IGNEOUS
SPECTRUM'

the composition of the volcanic rocks erupted after sulphide deposition can change abruptly (eg. in the Bathurst camp; Whitehead and Goodfellow, 1978) it is of interest to see whether the tuffaceous layers in the chemical sediments record a similar change at Tulks Hill. Consequently, the chemical sediments are discussed with the volcanic rocks.

6.3.2 ALKALI METASOMATISM

Three subgroups are defined, based on their K2O and Na2O contents (Fig. 6.6):

a) High K2O:Na2O ratios distinguish the siliceous stockwork, mineralised horizons and the alkali-enriched portion of the Raven rhyolite,

b) Low K2O:Na2O ratios characterise the pyroclastics and the interbedded (surface) alkali-enriched rhyolite,

c) Intermediate K2O:Na2O ratios distinguish the altered rhyolite and chemical sediments

Sericite and/or microcline (Raven rhyolite) secondary overgrowths account for the high K2O content in subgroup (a), whereas Na2O enrichment in subgroup (b) reflects abundant secondary albite. A mixture of sericite and albite (secondary and primary?) produces the variable Na2O:K2O ratio in the altered rhyolite and chemical sediments.

Figure 6.6: Log Na2O vs. log K2O diagram. Three broad groups are identified: K enrichment characterises the mineralised horizon, alkali-enriched rhyolite (Raven rhyolite only) and the siliceous stockwork, whereas Na enrichment characterises the pyroclastic units and the surface outcrop of alkali-enriched rhyolite (this analysis plots within the pyroclastic units field). The altered rhyolite (filled squares) and the chemical sediments have variable amounts of Na2O and K2O and plot on both sides of the K2O = Na2O line.

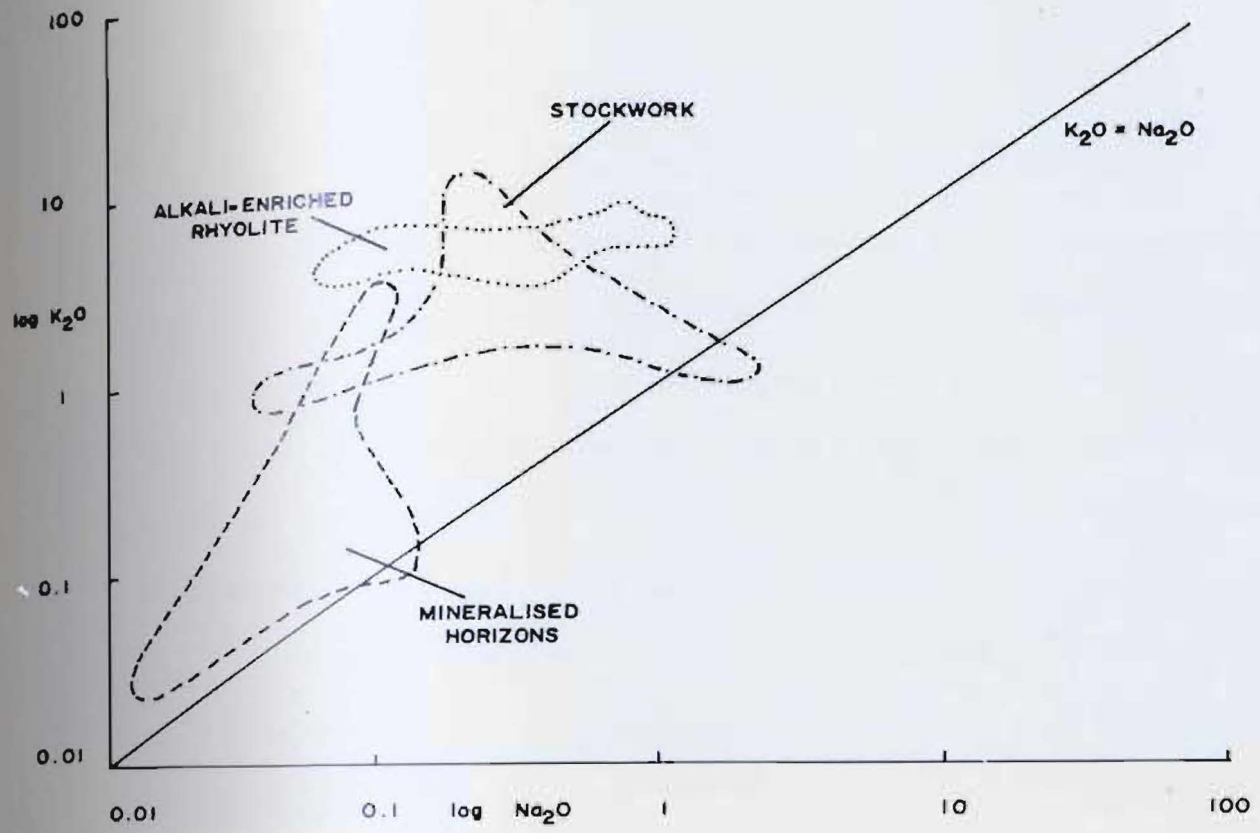
100
10
log K_2O
1
0.1
0.01
0.01
0.1
log Na_2O
1
10
100
STOCKWORK
$K_2O = Na_2O$
ALKALI-ENRICHED RHYOLITE
MINERALISED HORIZONS

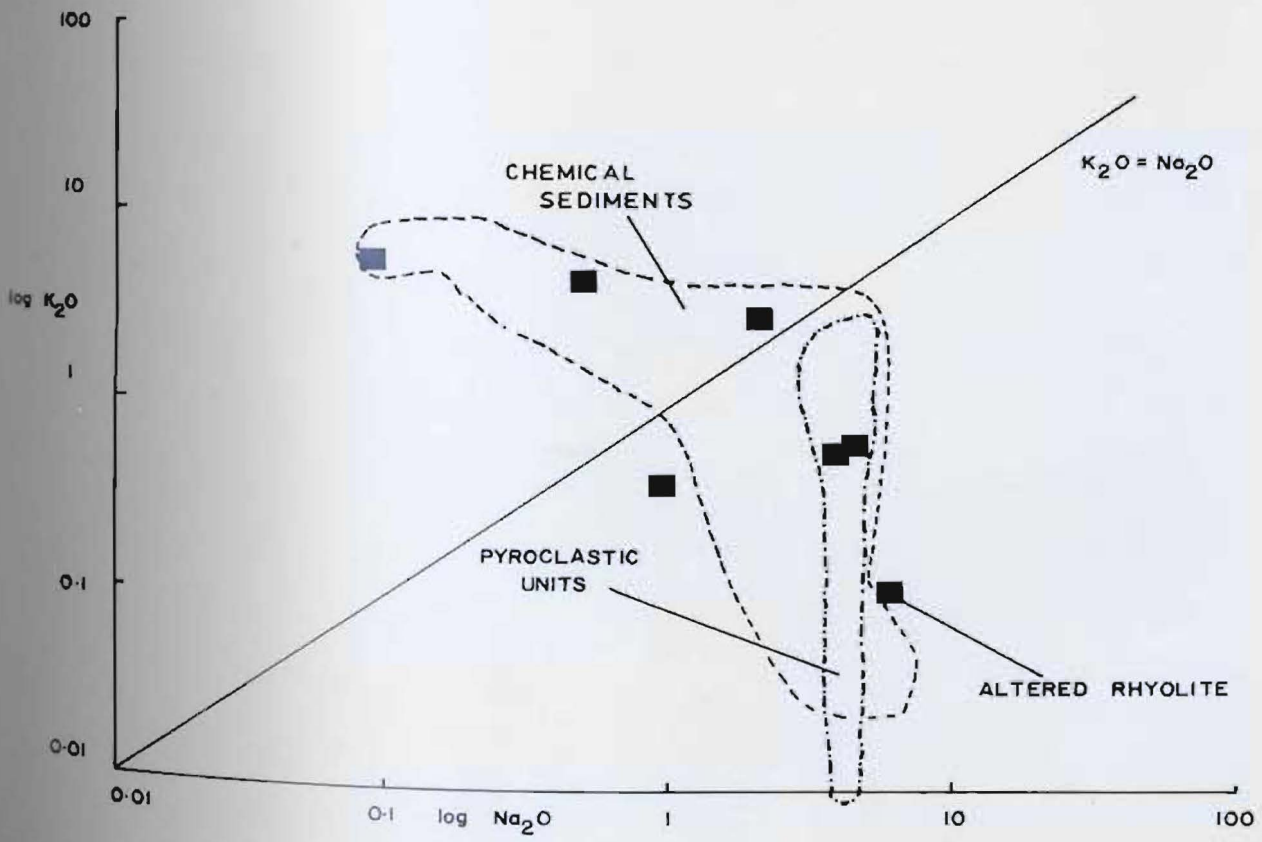
100
10
log K_2O
1
0·1
0·01
0·01
0·1
log Na_2O
1
10
100
CHEMICAL SEDIMENTS
$K_2O = Na_2O$
PYROCLASTIC UNITS
ALTERED RHYOLITE

6.3.2.1 K enrichment

Potassium enrichment appears to be genetically related to sulphide deposition, as suggested by the high K2O:Na2O ratio of the siliceous stockwork and mineralised horizons.

Current theories of sulphide deposition suggest that metal precipitation occurred at or near the seawater-rock interface (Hutchinson, 1982; Ohmoto and Skinner, 1983). This interface is thought to mark a critical zone of chemical reaction between the hot, acid, saline fluids and the cold, slightly alkaline seawater (Skinner, 1979). The restriction of K enrichment to only the siliceous stockwork and the mineralised horizons, two genetically related rock types (Chapter 4), suggests their formation close to the seawater-rock interface where fluid mixing produced conditions favourable to sericite formation and consequent "dumping" of potassium. The importance of the seawater-rock interface is shown by the lack of K enrichment zones in other rock types. K-feldspar destruction is usually given as the source of K in the fluid (Riverin and Hodgson, 1980) and this is probably the mechanism of K enrichment in the hydrothermal fluid at Tulks Hill, since the altered footwall rocks are thought to have had a rhyolitic composition (section 6.4).

Potassium enrichment is common in the footwall of Archaen Cu-Zn volcanogenic massive sulphide deposits, for example, the Millenbach deposit, Louvem deposit, Mattagami

Lake, Sturgeon Lake and the numerous deposits in the Flin-Flon - Snow Lake area (Koo and Mossman, 1975; Riverin and Hodgson, 1980; Roberts and Reardon, 1978; Sangster and Scott, 1976; Spitz and Darling, 1975; Walford and Franklin, 1982). The Japanese Kuroko deposits also have K-enrichment surrounding the footwall siliceous ore (Izawa et al., 1978).

Potassium enrichment in the Raven rhyolite may imply that it is genetically linked with the mineralising episode(s) (also see Chapters 4 and 10).

6.3.2.2 Na enrichment

This affects rock types that are presently more distant from the mineralisation. All pyroclastic rocks and the surface rhyolite contain pure albite (locally chequerboard), have high Na2O:K2O ratios and lack primary Fe-Mg minerals. These features typify quartz-keratophyres and are taken as evidence of alteration with accompanying Na metasomatism (Schermerhorn, 1973; Smith and Jackson, 1974). Quartz-keratophyres form during low-grade metamorphism and alkali metasomatism of pre-existing felsic rocks (Hughes, 1973).

Na enrichment adjacent to the K enrichment zone (siliceous stockwork) at Tulks Hill is anomalous in comparison to most other volcanogenic massive sulphide deposits: Na depletion is well documented by Date et al.

(1983) and Hashiguchi et al. (1983), for certain Japanese Kuroko-type deposits, and by Wynne (1983), for the Strickland deposit in southern Newfoundland. Hashiguchi et al. (1983) defined a Na depletion zone that ranged in areal extent from 10m to 1000m distant from the ore zone; it is conceivable that either a restricted Na depletion zone at Tulks Hill was overlooked during the present study, or that it was faulted out during later deformation so that the Na enrichment zone was juxtaposed against K enrichment (see Chapter 9 for the structural style at Tulks Hill). However, according to Date and Watanabe (1979) the Na depletion zone is equivalent to the chlorite-sericite alteration zone, and since the bulk of the footwall pyroclastic rocks at Tulks Hill fall into this category Na depletion should be evident. This is not the case suggesting that Na enrichment within the footwall rocks is anomalous. A possible implication is that the chequerboard albite formed during later regional metamorphism, although the association with sulphide veinlets would be difficult to explain in this case.

Footwall sodium enrichment is documented at the Anderson Lake deposit (Walford and Franklin, 1982), where it occurs beneath a K-enriched zone and passes, in its lower levels, into a wider area of Na-depletion (as documented above), and at the Uwamuki deposit in Japan and the Seneca and Corbet deposits of Canada (Urabe et al., 1983).

6.3.2.3 Soda-potash relationships

A comparison of the Tulks Hill volcanics with average values for felsic rocks (Table 6.7; Le Maitre, 1976) shows that extensive Na:K metasomatism, and probably K removal, must have occurred since the Tulks Hill rhyolites have a lower total alkali content, but a higher Na:K ratio. Widespread Na enrichment, but restricted areas of K enrichment (siliceous stockwork and mineralised horizons), suggest that the chemical environment was, in general, favourable to Na deposition. However, total alkali contents within the contrasting subgroups are similar suggesting alkali redistribution, rather than addition, during alteration. It is possible therefore, that Na and K enrichment formed virtually simultaneously, although in different areas, possibly as a result of a variation in pH within the volcanic pile (Fig. 4.2): an increase in the Na^+/H^+ and K^+/H^+ ratio within the fluid would allow the formation of both albite and muscovite. Since muscovite is stable within the stockwork and albite is stable within the footwall volcanics it implies an increase in H^+ ion activity towards the seawater-rock interface. This increase could result from chloritisation within the stockwork since Mg-chlorite formation is accompanied by base fixing and H^+ ion release (Rosenbauer et al., 1983).

Table 6.7: Average major element compositions for three felsic volcanic rocks (from Le Maitre, 1976).

	Rhyolite	Rhyodacite	Dacite
SiO_2	72.82	65.55	65.01
TiO_2	0.28	0.60	0.58
Al_2O_3	13.27	15.04	15.91
Fe_2O_3	1.48	2.13	2.43
FeO	1.11	2.03	2.30
MnO	0.06	0.09	0.09
MgO	0.39	2.09	1.78
CaO	1.14	3.62	4.32
Na_2O	3.55	3.67	3.79
K_2O	4.30	3.00	2.17
H_2O^+	1.10	1.09	0.91
H_2O^-	0.31	0.42	0.28
P_2O_5	0.07	0.25	0.15
CO_2	0.08	0.21	0.06

6.3.2.4 Rb content and alkali metasomatism

In high potash rock-types a positive linear relationship exists between K and Rb because of their comparable geochemical characteristics (Fig. 6.7). Alteration of the rhyolite (sericitisation, chloritisation etc.) decreases the K:Rb ratio, suggesting K-depletion during hydrothermal alteration which may simply reflect sericite formation.

6.3.3 MgO AND TOTAL Fe DISTRIBUTION

Some samples at Tulks Hill have MgO and/or total Fe contents that are comparable to basalts (eg. 12NA-82). If these samples are basalts then other oxides, such as TiO_2, should display a certain amount of geochemical coherency. The scatter in Figures 6.8 and 6.8a shows that this is not the case. Also, the low values of Ni and Cr, all below the detection limits of the XRF machine, are not compatible with a magmatic origin for the MgO. This implies that the MgO has been enriched by secondary processes. Figure 6.9 suggests that the MgO content may be related to hydration/carbonation (chlorite/dolomite formation) rather than primary magmatic processes. In addition, petrographic and trace element data, as used in section 6.4, suggest a felsic, rather than a mafic, protolith for these rocks prior to alteration: sample 12NA-82 is an altered portion of the Raven rhyolite.

Fresh, magmatic, Fe-Mg minerals are absent from the

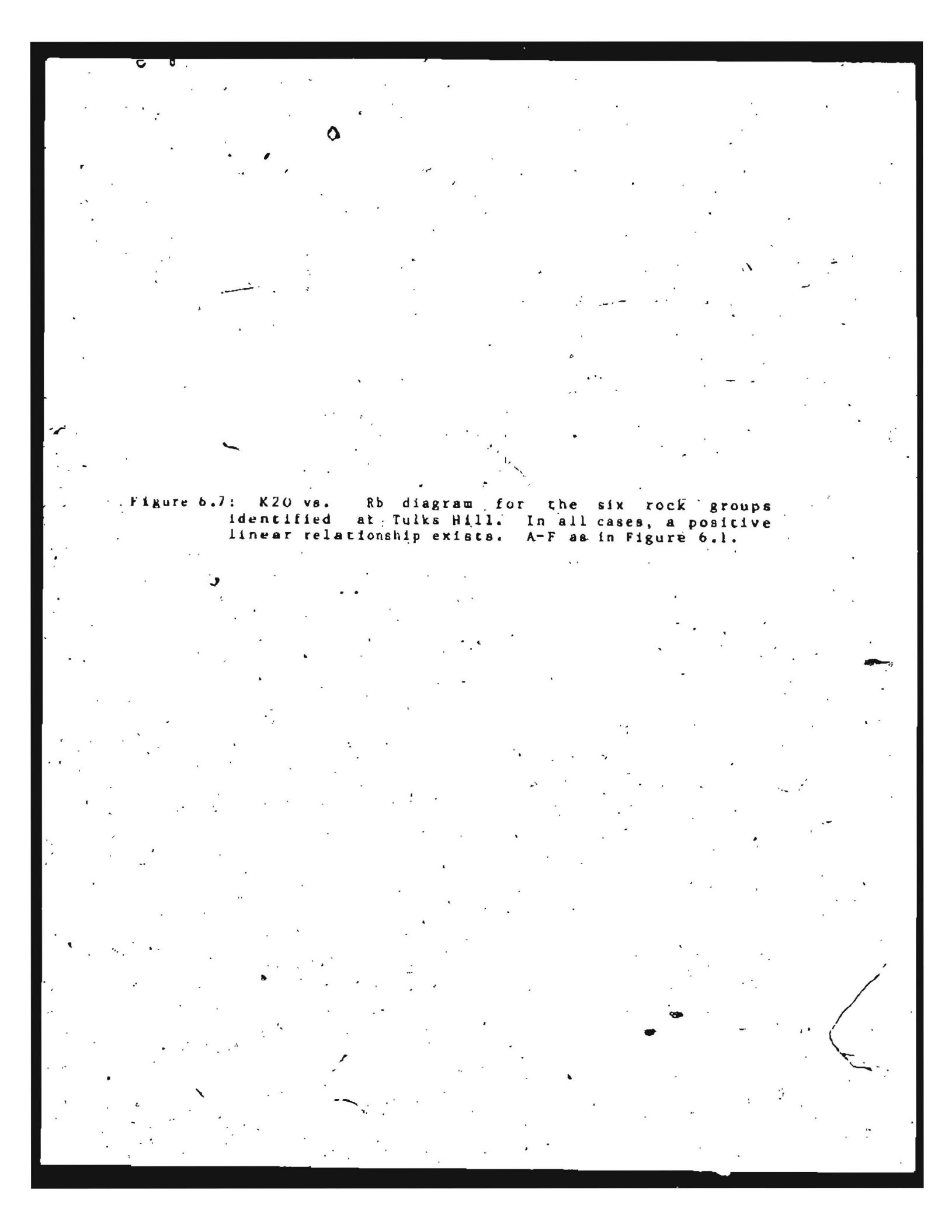

Figure 6.7: K2O vs. Rb diagram for the six rock groups identified at Tulks Hill. In all cases, a positive linear relationship exists. A-F as in Figure 6.1.

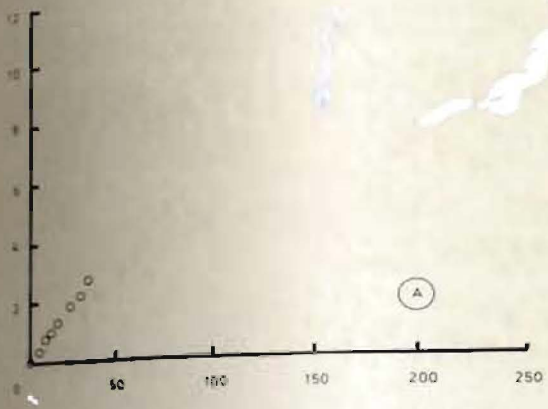
A
0
50
100
150
200
250

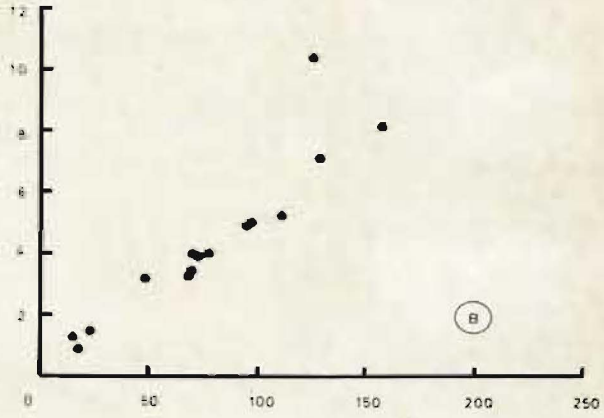
B
0
50
100
150
200
250

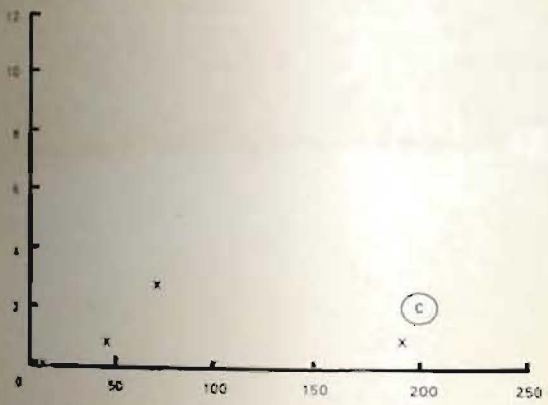
C
0
50
100
150
200
250

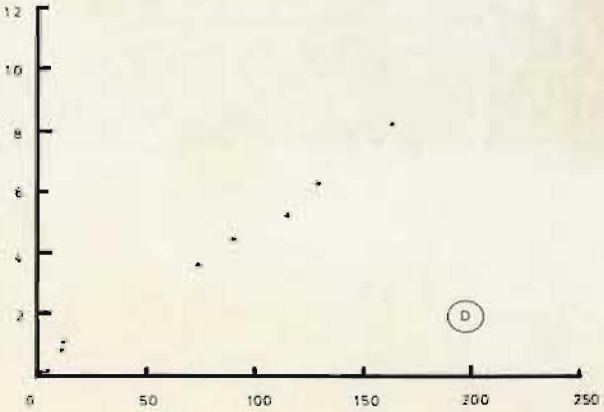
D
0
50
100
150
200
250

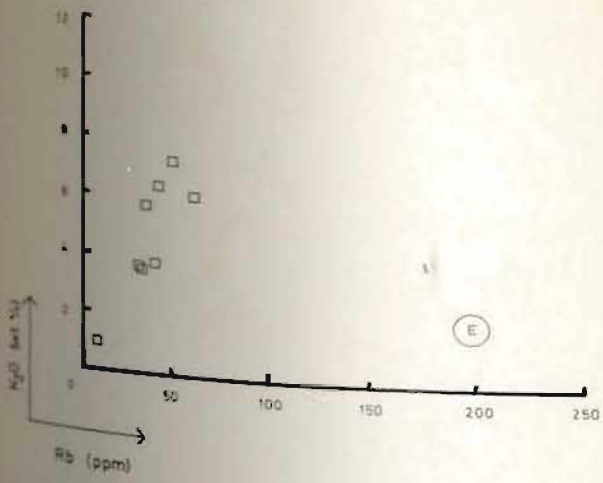
E
0
50
100
150
200
250
Rb (ppm)

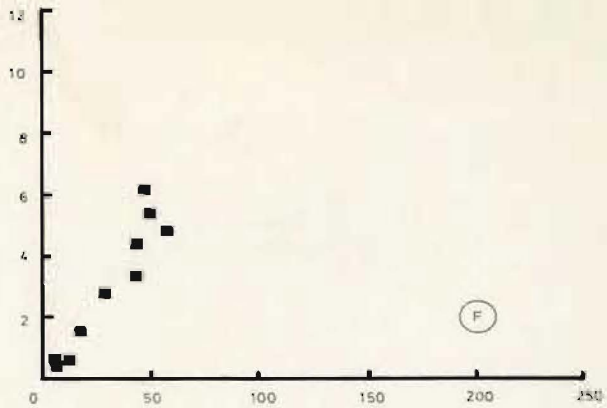
F
0
50
100
150
200
250

Figure 6.8: MgO vs. TiO2 diagram. A lack of geochemical coherency between these two oxides suggests that MgO has been enriched by secondary processes. A-F as in Figure 6.1.

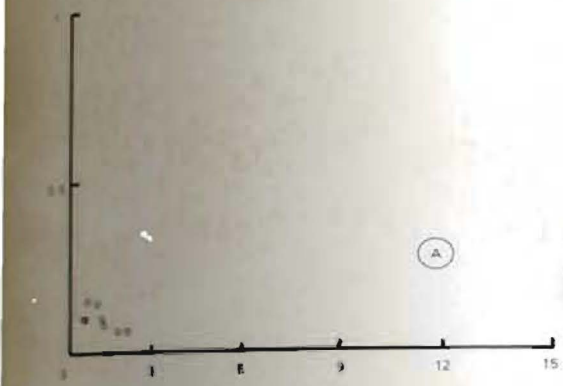
A
0
3
6
9
12
15

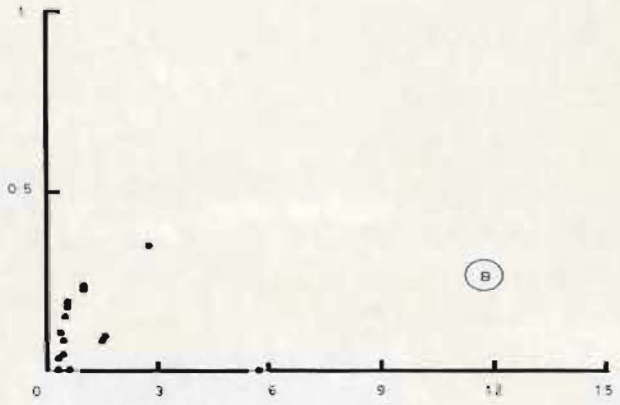
1
0.5
B
0
3
6
9
12
15

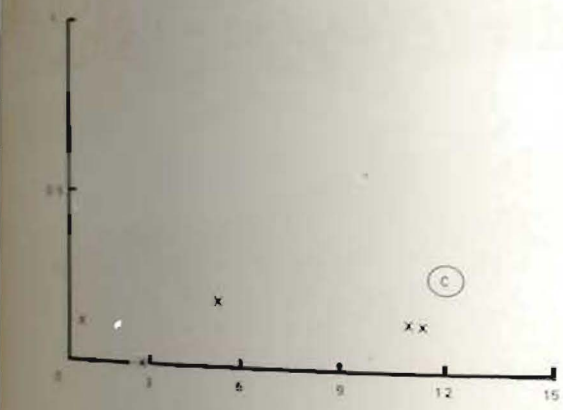
C
0
3
6
9
12
15

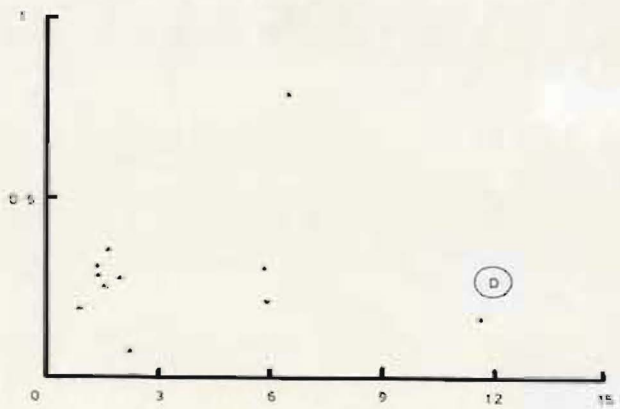
1
0.5
D
0
3
6
9
12
15

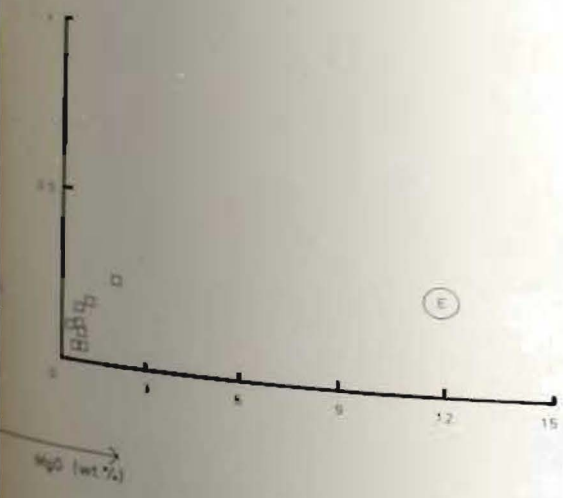
E
0
3
6
9
12
15
MgO (wt%)

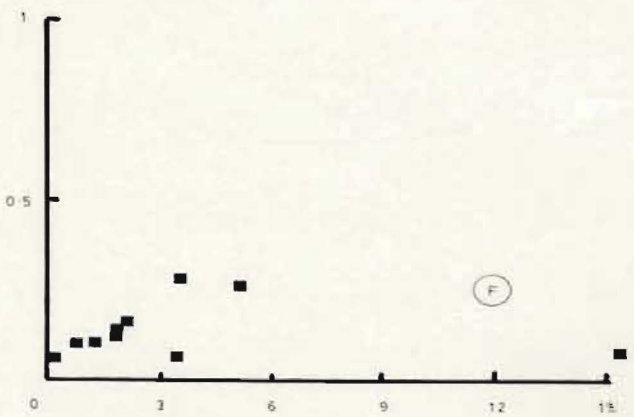
1
0.5
F
0
3
6
9
12
15

Figure 6.8a: Fe2O3 vs. TiO2 diagram. A-F as in Figure 6.1.

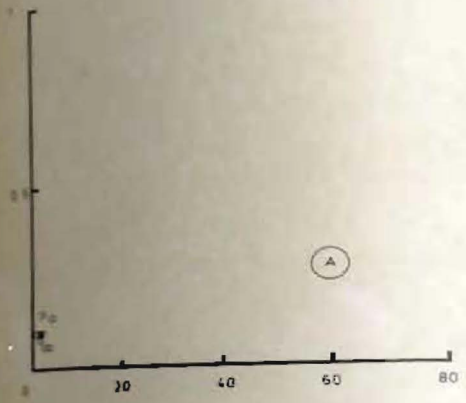
A
20
40
60
80

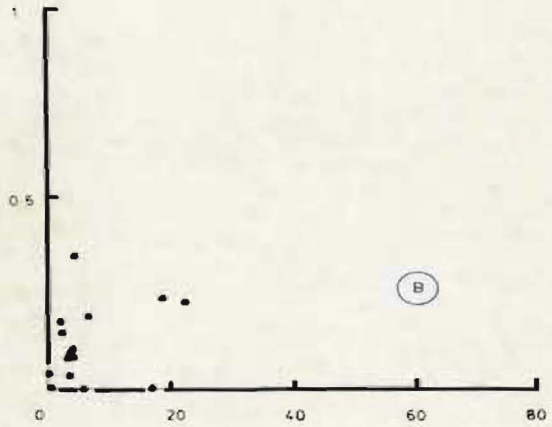
1
0·5
B
0
20
40
60
80

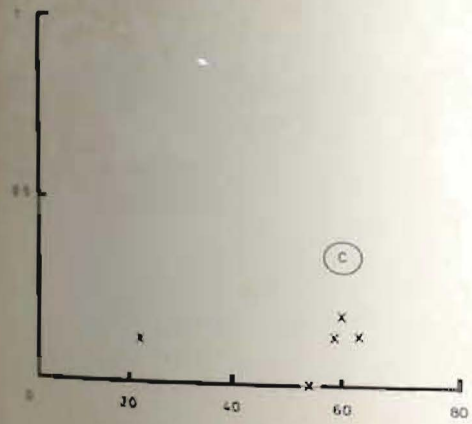
C
20
40
60
80

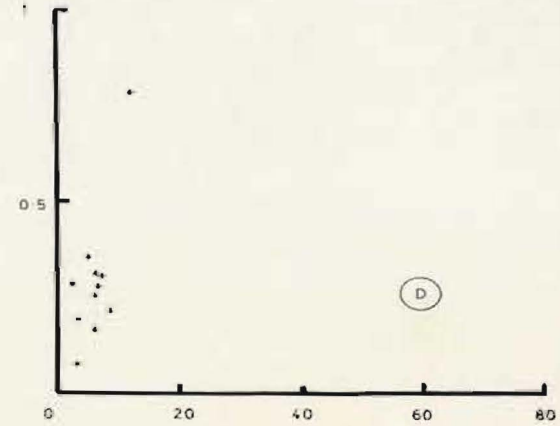
1
0·5
D
0
20
40
60
80

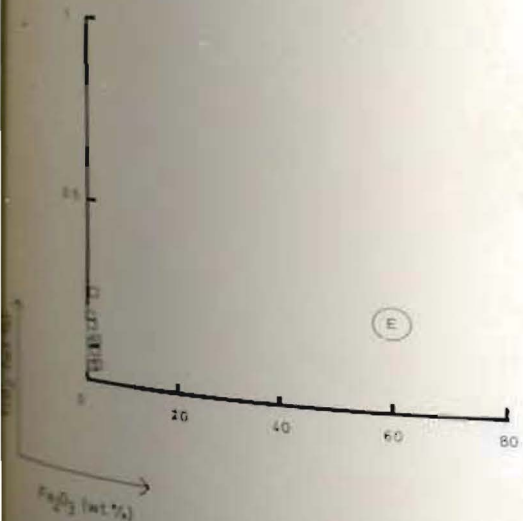
E
20
40
60
80
Fe2O3 (wt.%)

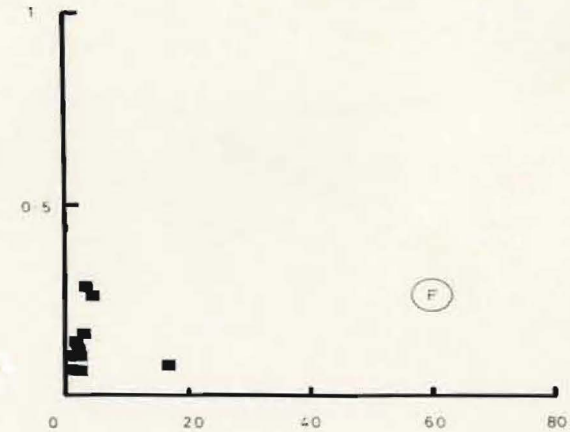
1
0·5
F
0
20
40
60
80

Figure 6.9: MgO vs. LOI. The moderately positive linear relationship between these two oxides suggests that MgO was enriched by hydration and/or carbonation.

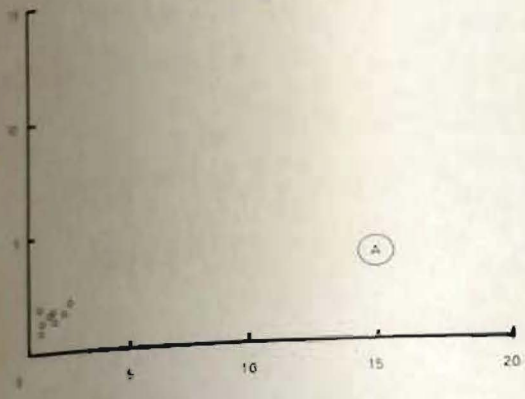
A
0
5
10
15
20

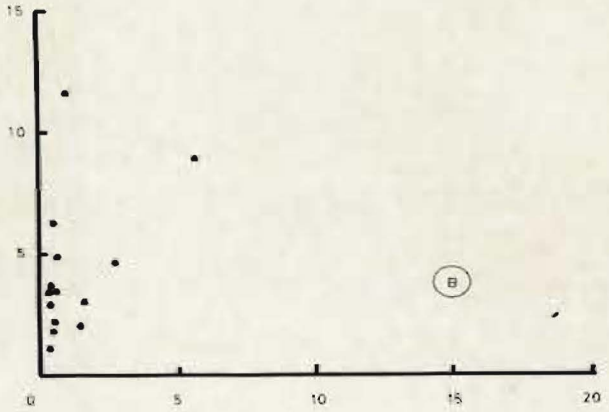
15
10
5
B
0
5
10
15
20

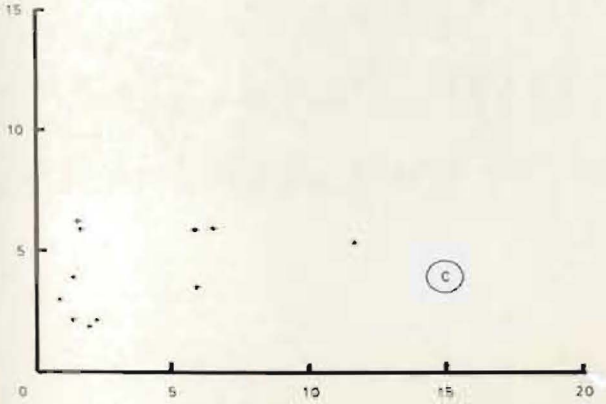
15
10
5
C
0
5
10
15
20

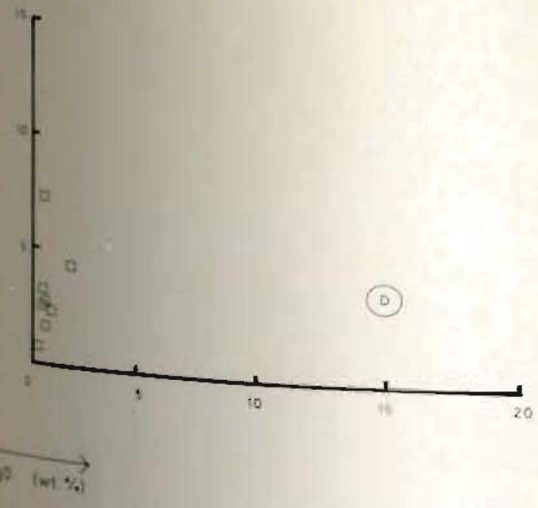
15
10
5
D
0
5
10
20
MgO (wt %)

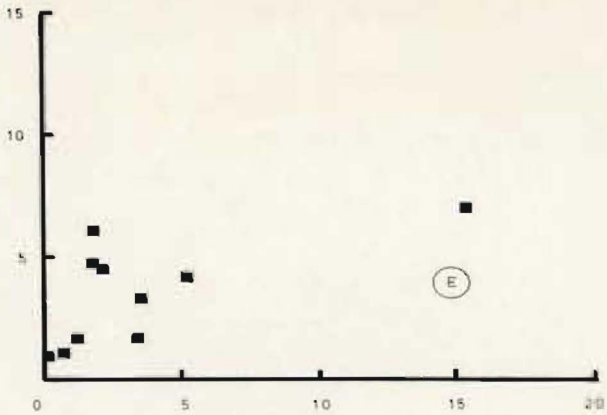
15
10
5
E
0
5
10
15
20

Tulka Hill rocks. Pervasive chlorite alteration, with or without epidote, suggests replacement of pre-existing Ca-Fe-Mg minerals. Although this mineralogy is unknown, biotite, fayalitic olivine and orthopyroxene are likely candidates (Carmichael et al., 1974). Data for the mineral chemistry of the chlorites (Chapter 8) prove that they are Mg- and/or Fe-rich and thus, the chemical composition and variation of a chlorite in an altered rock would vary the total Fe and MgO contents for that rock. Samples of the altered rhyolite (Table 6.2) or the footwall pyroclastics (Table 6.3) are good examples of this: similar rock types have different amounts of total Fe and MgO simply because of their variable chloritic alteration. According to Mottl (1983), the variation in the chlorite chemistry, and consequent total Fe and MgO enrichment/depletion, reflects the passage of hydrothermal fluids en route to or from the seawater-rock interface. The application of Mottl's (1983) ideas to the chlorite chemistry at Tulks Hill is discussed further in Chapter 8.

Disseminated pyrite also increases the total Fe content which explains the high values for samples from the siliceous stockwork and mineralised horizon.

6.3.4 CaO DISTRIBUTION

Both rhyolite types (alkali-enriched and altered) are enriched in CaO; low CaO reflects the lack of calcite in the remaining groups (Fig. 6.3).

Calcite precipitation is best effected by boiling of a CO2-rich hydrothermal fluid (Holland and Malinin, 1979). However, in most cases its formation is also dependant upon the partial CO2 pressure of the fluid, H+ metasomatism with the wall-rock (which affects the fluid pH), and possibly fluid mixing and NaCl content (Holland and Malinin, 1979).

In a felsic volcanic pile, such as at Tulks Hill, clinopyroxene and/or plagioclase destruction could provide Ca ions to the solution or, alternatively, there could be an extraneous source for the calcium. This would lead to precipitation of calcite if that fluid was CO2-rich. This appears to be the case with the rhyolites.

Two possibilities explain the lack of calcite within the pyroclastic lithologies; 1) primary Ca minerals were absent, thus eliminating a Ca supply (unlikely) or, 2) primary Ca minerals were destroyed but calcite was not precipitated because of inappropriate chemical conditions (ie. fluids too acid).

A corollary of (2) is that the hydrothermal fluids within the rhyolites probably had a lower H+ ion activity and/or NaCl content: an increase in both of these parameters would prohibit calcite precipitation (Holland and Malinin, 1979). Sericite and albite formation in the footwall occurs when the H+ ion activity is increased (see Fig. 4.2); this would favour calcite dissolution and may explain the absence of calcite in the footwall volcanics.

Pervasive loss of CaO within the alteration pipe at

the Millenbach deposit (Riverin and Hodgson, 1980) and Mattabi deposit (Franklin et al., 1977) is similar to that observed at Tulks Hill, yet is opposite to that observed at the Mattagami Lake deposit (Roberts and Reardon, 1978), where high CaO and carbonate contents are characteristic. This difference in alteration chemistry within similar types of sulphide deposits suggests local, rather than regional, chemical controls on carbonate deposition: the localisation of calcite within the rhyolite at Tulks Hill is evidence of this.

6.3.5 BARIUM DISTRIBUTION

Barite ore-horizons, up to several metres thick, are typical of the black ore, hangingwall portions of Kuroko deposits (Sato, 1977). At the Iwami mine a barite-rich stockwork alteration zone is present (Mukaiyama et al., 1974). Thurlow (1981 a) identified microscopic barite within the matrix of the ore horizon dacite tuffs at Buchans, and in fractures within plagioclase, amphibole and quartz phenocrysts. Thus, barite is a common mineral in volcanogenic massive sulphide deposits, in both footwall and hangingwall locations, and is probably an intrinsic characteristic of the hydrothermal environment of sulphide deposition (Holland and Malinin, 1979). Barium is present in all rock-types at Tulks Hill but shows a wide variation in abundance between the major groups. Two arbitrary sub-groups are defined:

1) Altered rhyolite, siliceous stockwork and chemical sediments. Mean Ba >= 1150 ppm; maximum Ba content: range 5201 - 11299 ppm.

2) Pyroclastic rocks, alkali-enriched rhyolite and mineralised horizons. Mean Ba <= 1150 ppm; maximum Ba content: range 284 - 1110 ppm.

From these data it is apparent that the sulphide horizon is Ba-poor, yet the immediate footwall and hangingwall are relatively Ba-rich. Ba depletion at the mineralised horizon must be controlled by the conditions during sulphide deposition: the reduced environment during sulphide precipitation may have prohibited barite formation allowing Ba to be dispersed in seawater (Hanor, 1979). Since barite is absent (apparently) in the other two rock types Ba must be stabilised by another mechanism: one method of Ba enrichment is as an exchange ion within the interlayer lattice of K-mica (Hanor, 1979), and since sericite is abundant within the stockwork alteration and the chemical sediments it may be a possible mechanism of Ba enrichment. Sericite is a minor component of the gangue mineralogy of the massive sulphides which would explain the low Ba values.

According to Ohmoto and Lasaga (1982), sulphates are stable in a reducing environment if, 1) the temperature is below 250 degrees centigrade and if, 2) there was enough oxygen to precipitate sulphates prior to the onset of reducing conditions. This is because the reaction

$$2\ O2(g) + H2S(aq) \longrightarrow SO4(--) + 2H(+)$$

will proceed to the left only at very slow rates; this allows sulphate metastability in a reduced environment. Since sulphates are absent at Tulks Hill it implies that either the temperature was greater than 250 degrees centigrade and/or the environment was reduced. It is suggested that both the high temperature (>250 degrees centigrade; Chapter 10) and the reduced environment during sulphide deposition influenced Ba distribution by not allowing barite to precipitate so that Ba either substituted for K within sericite, or was dispersed in seawater.

6.3.6 BASE METAL DISTRIBUTION

Figure 6.10 outlines the base metal distribution in the Tulks Hill rocks. Arbitrary divisions are shown to highlight the dominance of one or more of the base metals.

Zinc is common to all rock groups, being relatively more abundant in the footwall volcanics, iron formation and 8 siliceous stockwork alteration samples. Six siliceous stockwork samples are relatively Cu rich, and surprisingly, one sample is rich in Pb. Cu > Zn+Pb characterises the mineralised horizon. All three base metals occur in roughly equal amounts in the tuffaceous chert.

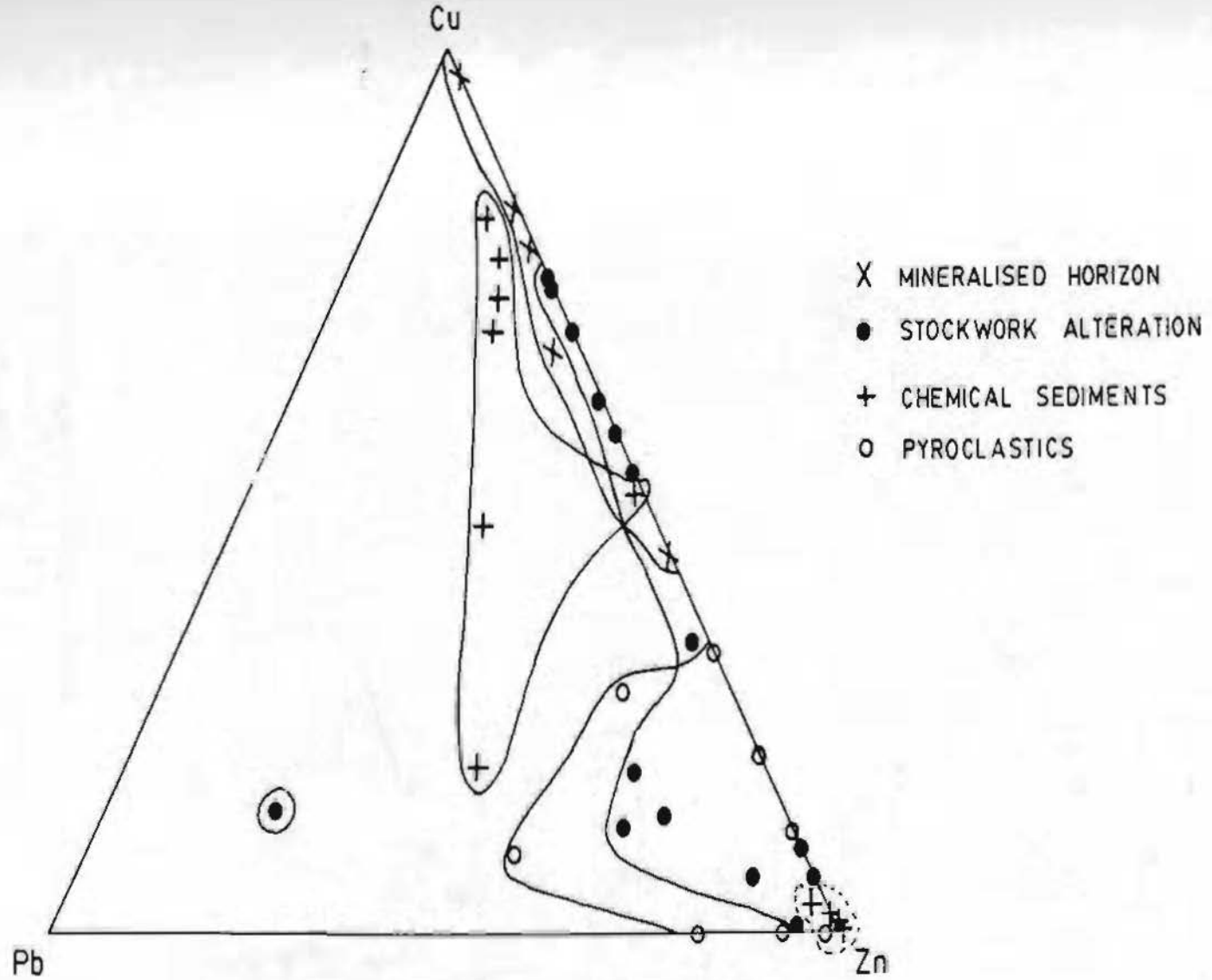

Figure 6.10 : Cu : Pb : Zn ratio diagram for
the 6 rock groups identified at Tulks Hill.

6.4 PRIMARY ROCK CHEMISTRY

6.4.1 INTRODUCTION

In any environment of hydrothermal alteration, major element mobility is a hindrance to rock classification. For example, at Tulks Hill the K2O content within similar rock types is comparable to potash trachytes or banakites (Fig. 6.11), yet petrographic data (Ghapter 4) do not support an original magmatic cause for their high K composition, suggesting that K2O addition has occurred. This therefore makes Ewart's (1979) rock classification inappropriate for the Tulks Hill rocks. To overcome this problem trace elements are used (eg. Zr, Nb, Y) because their mobility is more restricted which allows a tentative classification of metavolcanic rocks by comparison with fresh volcanic rocks. Discrimination diagrams, which outline fields for fresh rock types with known trace element contents, are used for this purpose (eg. Pearce and Cann, 1973; Winchester and Floyd, 1977).

Recent papers concerned with the classification of metavolcanic rocks have concentrated on those with mafic affinities (eg. Gale and Pearce, 1982) because, unlike felsic rocks, they are geochemically less variable, due to the lack of abundant late-stage minerals, such as zircon. Studies using trace element contents of metafelsic rocks are few (eg. Dudas et al., 1983; Hill and Thomas, 1983; Kay, 1982; Taylor et al., 1981) even though Winchester and Floyd (1977) have published discrimination diagrams

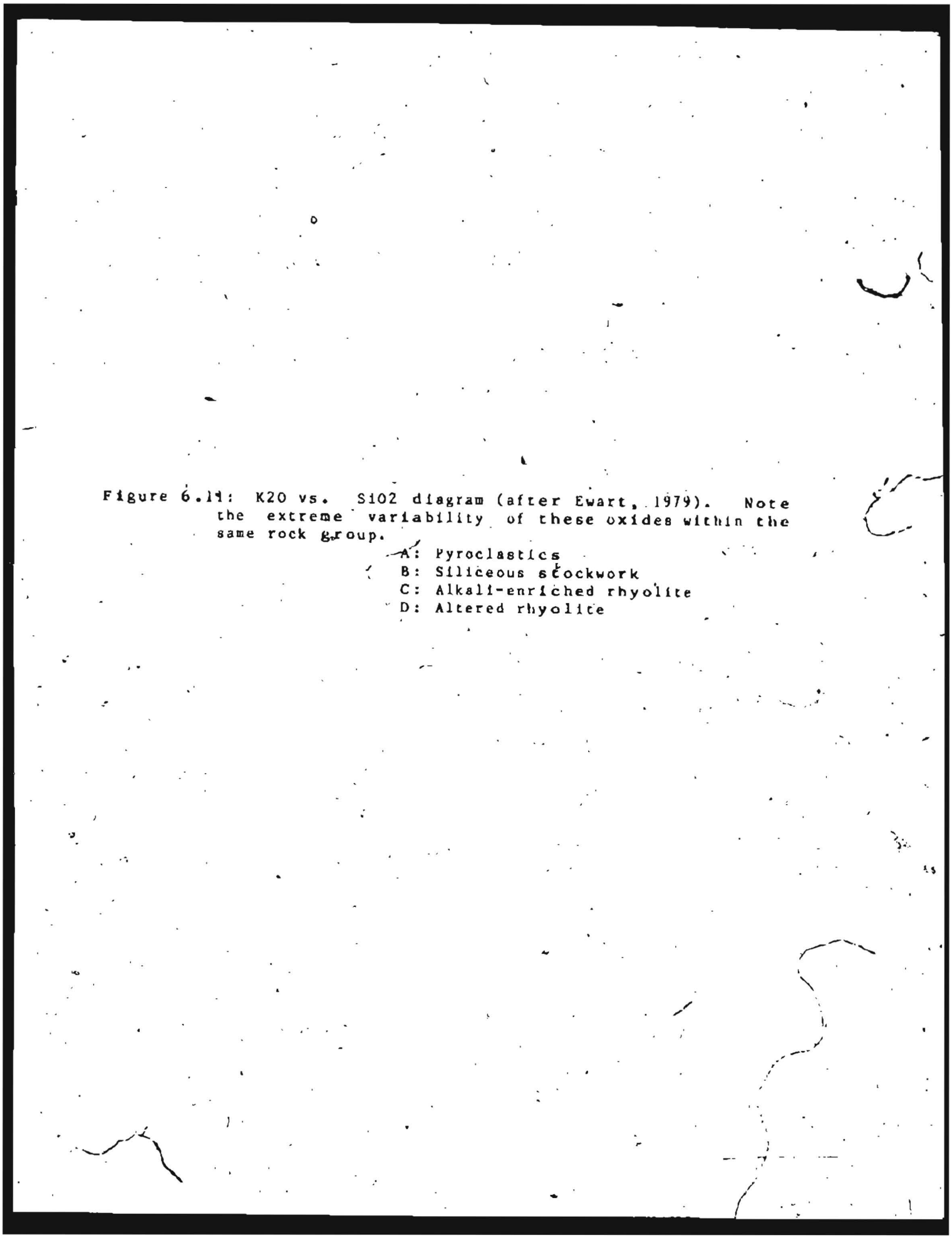

Figure 6.14: K2O vs. SiO2 diagram (after Ewart, 1979). Note the extreme variability of these oxides within the same rock group.

A: Pyroclastics
B: Siliceous stockwork
C: Alkali-enriched rhyolite
D: Altered rhyolite

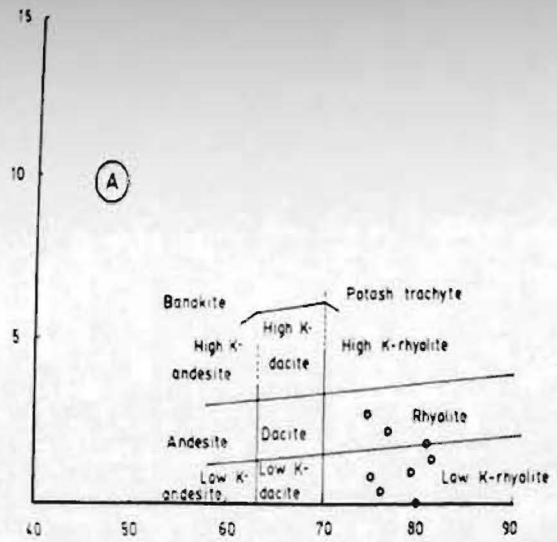
A
Banakite
Potash trachyte
High K-andesite
High K-dacite
High K-rhyolite
Andesite
Dacite
Rhyolite
Low K-andesite
Low K-dacite
Low K-rhyolite
15
10
5
40
50
60
70
80
90

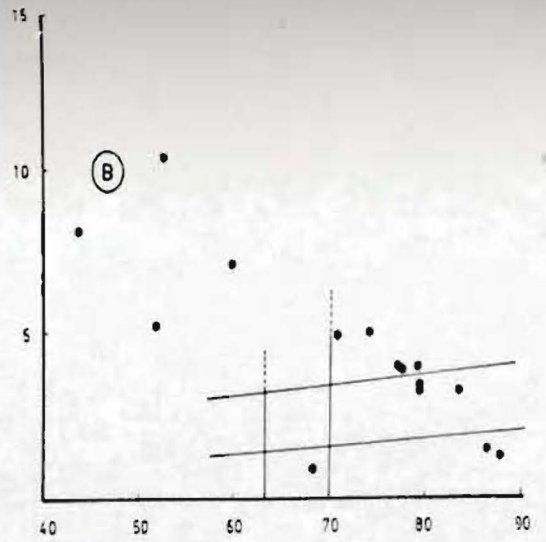
B
15
10
5
40
50
60
70
80
90

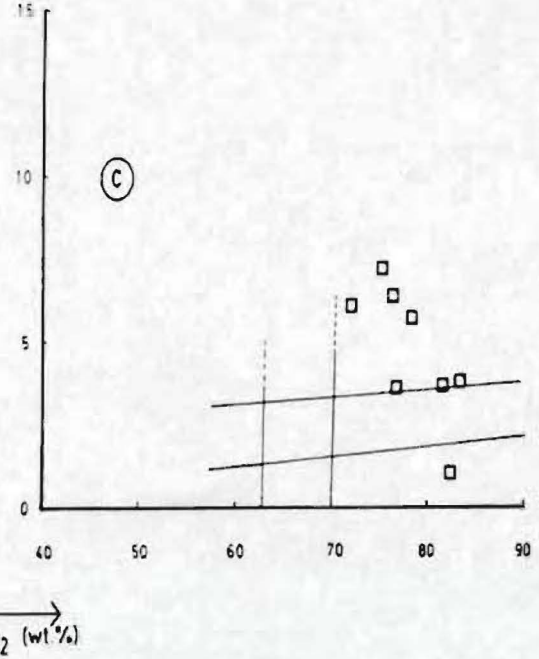
C
15
10
5
0
40
50
60
70
80
90
K2O (wt.%)
SiO2 (wt.%)

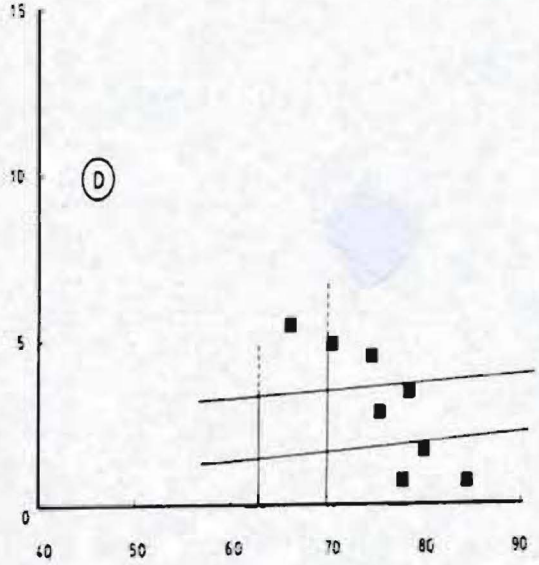
D
15
10
5
0
40
50
60
70
80
90

applicable to these rocks (up to, and including, greenschist grade). Since only felsic rocks outcrop at Tulks Hill the discrimination diagrams of Winchester and Floyd (1977) are used below.

6.4.2 Zr/TiO2 VS. Nb/Y

Winchester and Floyd (1977) determined that the trace element content of common mafic to felsic rocks varied according to their extent of differentiation or alkalinity: the Zr/TiO2 ratio was discovered to be a good measure of differentiation while Nb/Y varied with alkalinity.

The majority of samples for every group at Tulks Hill, excluding the chemical sediments, are sub-alkaline and have trace element characteristics that are comparable to rhyolite-rhyodacite-dacite; the latter two rock-types are more common (Fig 6.12). One pyroclastic sample plots within the trachyte field (Fig. 6.12A) and three stockwork alteration samples have alkalic affinities, plotting within the commendite-pantellerite and trachyandesite fields (Fig. 6.12B). Four samples from the chemical sediments plot within the andesite and/or basalt fields which suggests that the volcanic activity underwent a compositional change after sulphide deposition, becoming more intermediate with time.

Figure 6.12: Zr/TiO2 vs. Nb/Y diagram (from Winchester and Floyd, 1977). Most samples plot within the rhyolite-dacite field. See text for further discussion.

A: Pyroclastics
B: Siliceous stockwork
C: Chemical sediments
D: Alkali-enriched rhyolite
E: Altered rhyolite

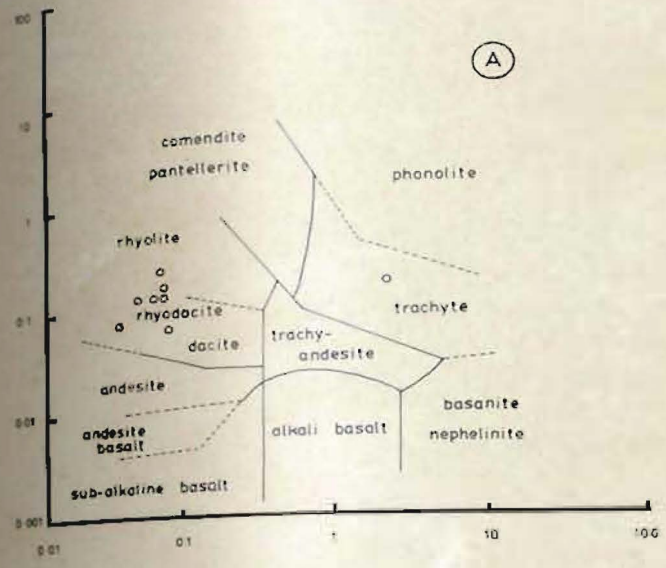
A
comendite
pantellerite
phonolite
rhyolite
trachyte
rhyodacite
dacite
trachy-
andesite
andesite
basanite
andesite
basalt
alkali basalt
nephelinite
sub-alkaline basalt

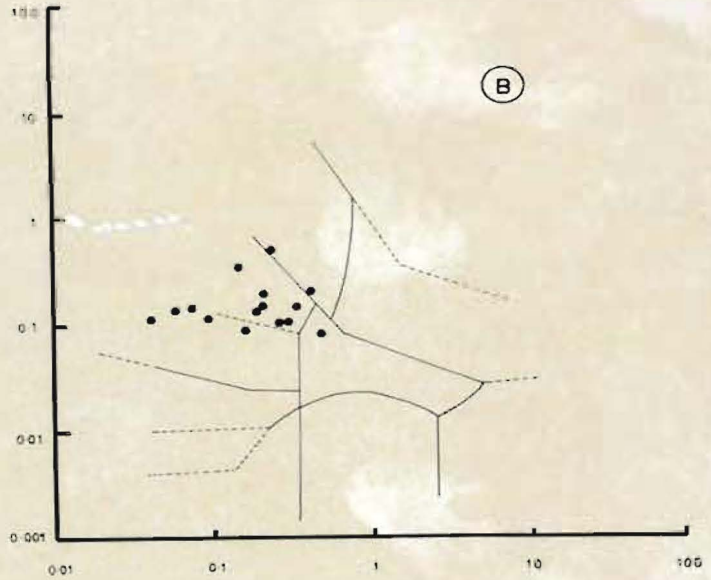
B

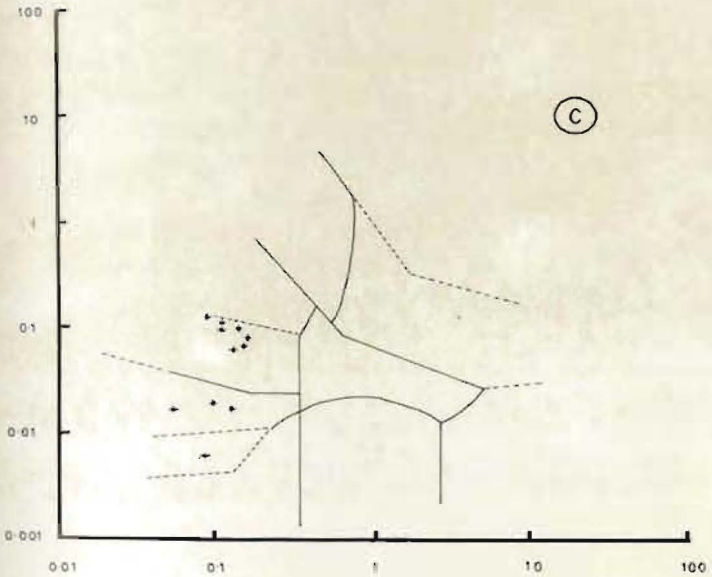
C

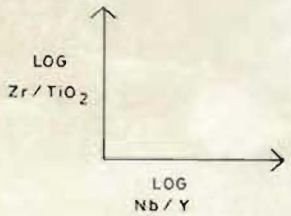
LOG
Zr / TiO2
LOG
Nb / Y

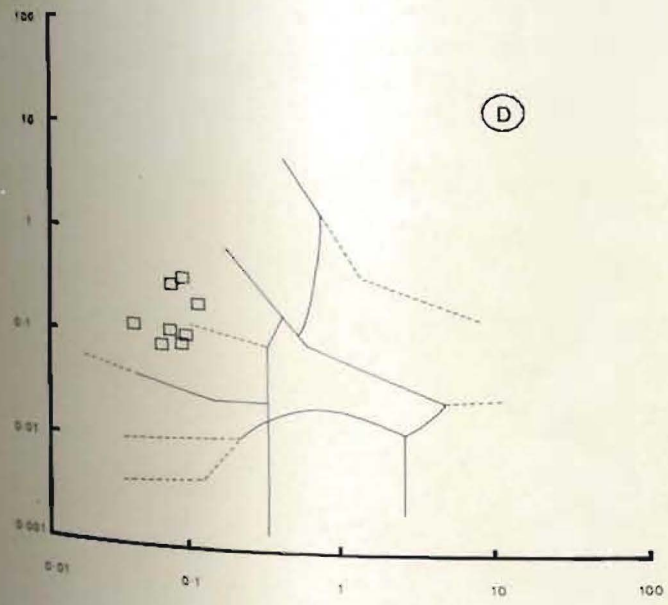
D

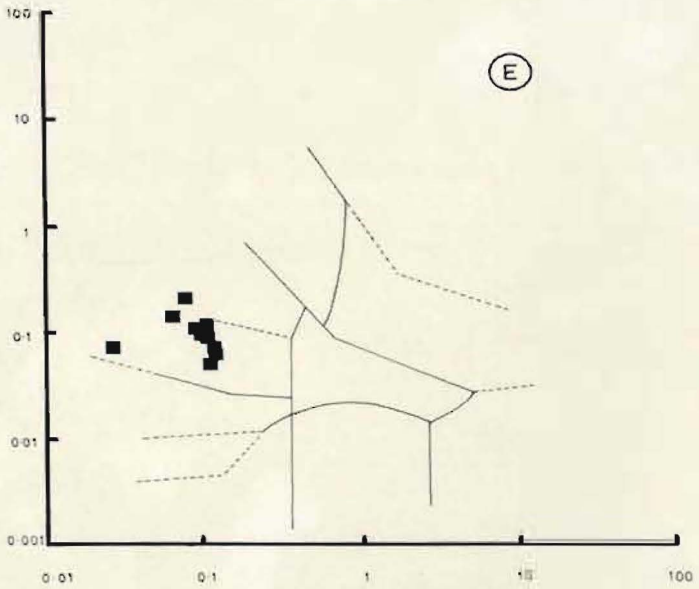
E

6.4.3 Ga VS. Zr/TiO2

According to Winchester and Floyd (1977), Ga is an indicator of rock alkalinity; in this respect it is similar to the Nb/Y ratio. Most samples plot within the rhyolite-rhyodacite-dacite fields (Fig 6.13). However, 5 stockwork alteration samples plot within the pantellerite and phonolite-trachyte fields.

The above data (sections 6.4.2/3) reinforce the petrographic evidence by suggesting that the majority of the rocks at Tulks Hill are felsic, and probably had a calc-alkaline, rhyodacitic chemistry prior to hydrothermal alteration. The occurrence of alkalic rocks at Tulks Hill is not substantiated by petrographic studies; only samples of stockwork alteration appear to have definite alkalic chemistry --- they are thought o form in an extreme chemical environment where alkali enrichment is common (sericite is abundant). Such an environment is thought to have mobilised those elements that are normally thought to be immobile, ie. Ga, Nb and/or Y. Further, these samples have relatively high Pb contents which may have influenced the detection of Ga since the peaks for Pb interfere with Ga giving erroneous readings for Ga.

6.4.4 Zr VS. TiO2

Pearce (1980) devised this diagram to illustrate the tectonic settings of different (not necessarily felsic)

Figure 6.13: Ga vs. Zr/TiO2 diagram (from Winchester and Floyd, 1977). Most samples plot within the rhyolite-dacite field. See text for discussion concerning "alkalic" rock types. A-D as in Figure 6.11.

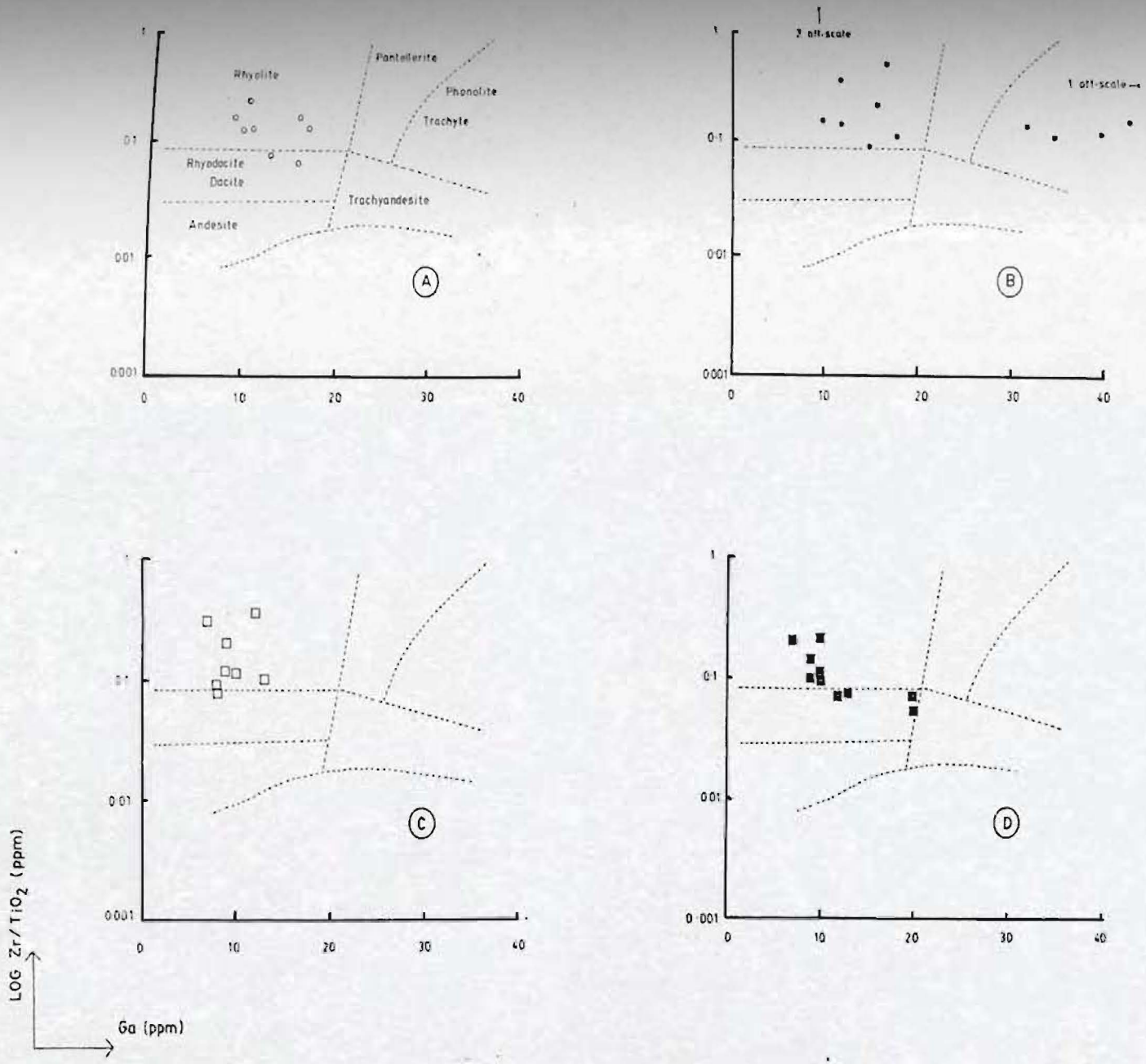
Rhyolite
Pantellerite
Phonolite
Trachyte
Rhyodacite
Dacite
Trachyandesite
Andesite
A
B
C
D
2 off-scale
1 off-scale
LOG Zr/TiO2 (ppm)
Ga (ppm)

rock types (Fig 6.14). All igneous rocks plot within the "arc lava" field, as do other dacitic pyroclastics of the Victoria Lake Group (Dunning, 1984). However, the different Zr and TiO2 contents for the Tulks Hill felsic rocks suggests a different magma batch, possibly more evolved (eg. fractionated) than those rocks analysed by Dunning (1984) in the Victoria Lake area.

Figure 6.14: Zr vs. TiO2 diagram (from Pearce, 1980). All samples plot within or close to the "arc lava" field; A-D as in Figure 6.11. Shaded area is data from Dunning (1984) for other samples of the Victoria Lake Group.

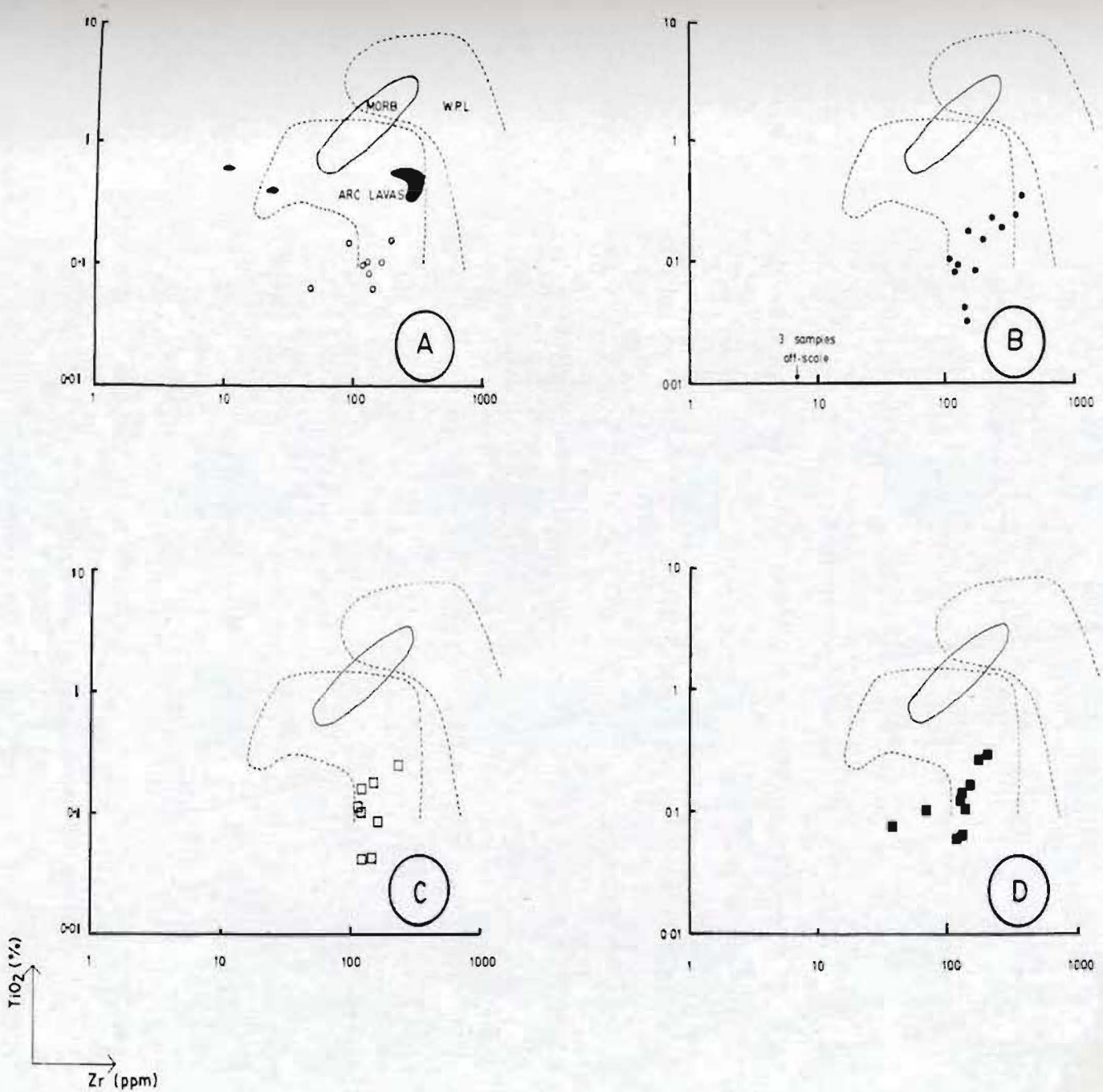
10
1
0·1
0·01
1
10
100
1000
MORB
WPL
ARC LAVAS
A
B
3 samples
off-scale
C
D
TiO2 (%)
Zr (ppm)

CHAPTER 7

RARE EARTH ELEMENTS

7.1 INTRODUCTION

The rare earths are a geochemically coherent group of trace elements whose predictable behaviour is often used to elucidate the processes of magma genesis (Hanson, 1978). Certain rare earth elements (REE) are preferentially incorporated into particular rock-forming minerals (Fig. 7.1); for example the heavy REE (HREE) are concentrated in zircon, garnet and amphibole, whereas the light REE (LREE), and particularly europium (Eu), are enriched relative to the HREE in feldspar. Consequently, the REE abundance and variation (pattern) for a fresh igneous rock depends upon its mineralogy, which in turn reflects the large-scale processes of partial melting, fractional crystallisation and/or assimilation of country rocks (eg. Cameron and Hanson, 1982; Hanson, 1978, 1980).

Each REE value is normalised to the corresponding value in chondrite, the latter assumed to represent primitive terrestrial material with primordial REE abundances (Haskin et al., 1966). A flat REE pattern and low total abundances are characteristic of chondrites; igneous processes, such as those discussed above, variably fractionate the REE to give different absolute values in different rock types depending on the minerals involved in fractionation. Fresh felsic volcanic rocks typically have

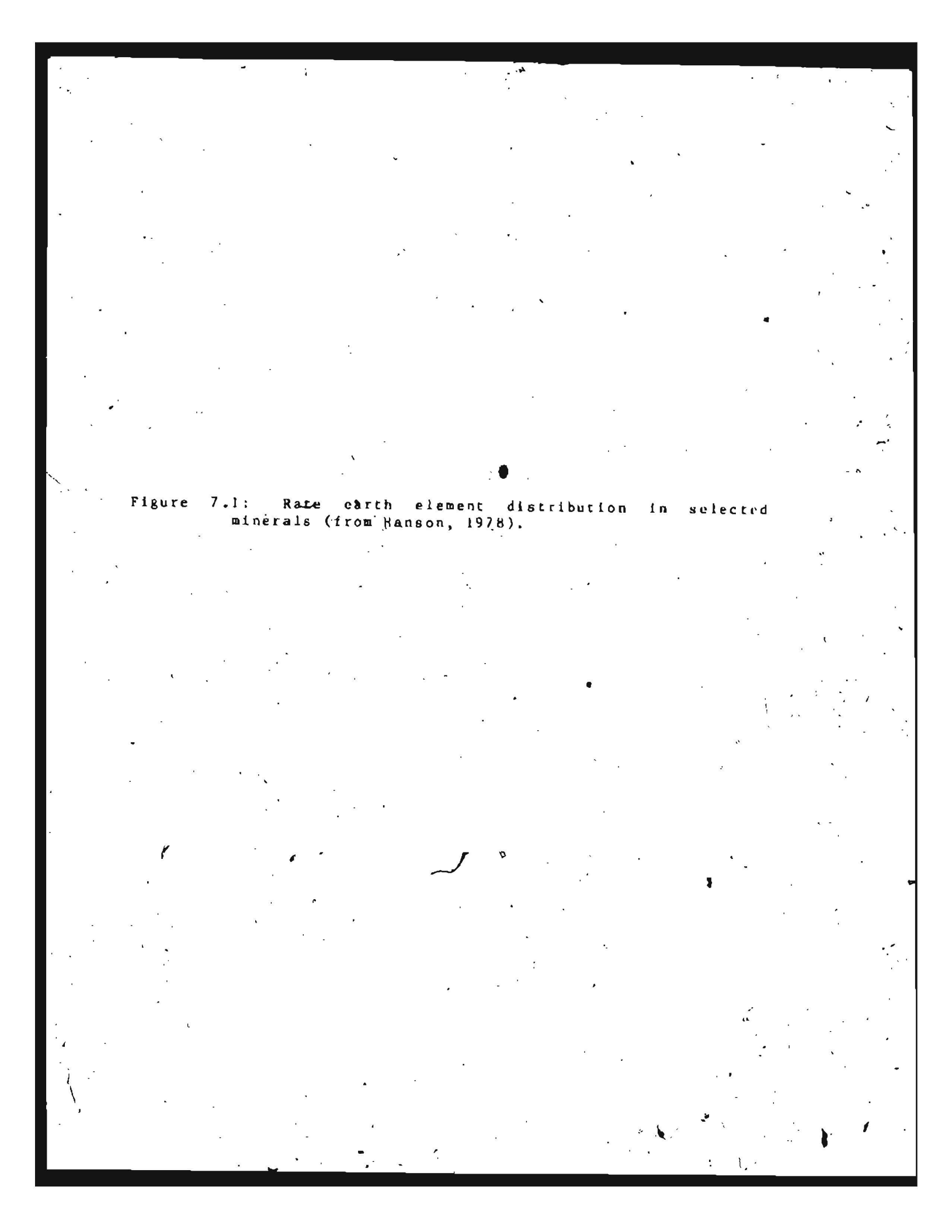

Figure 7.1: Rare earth element distribution in selected minerals (from Hanson, 1978).

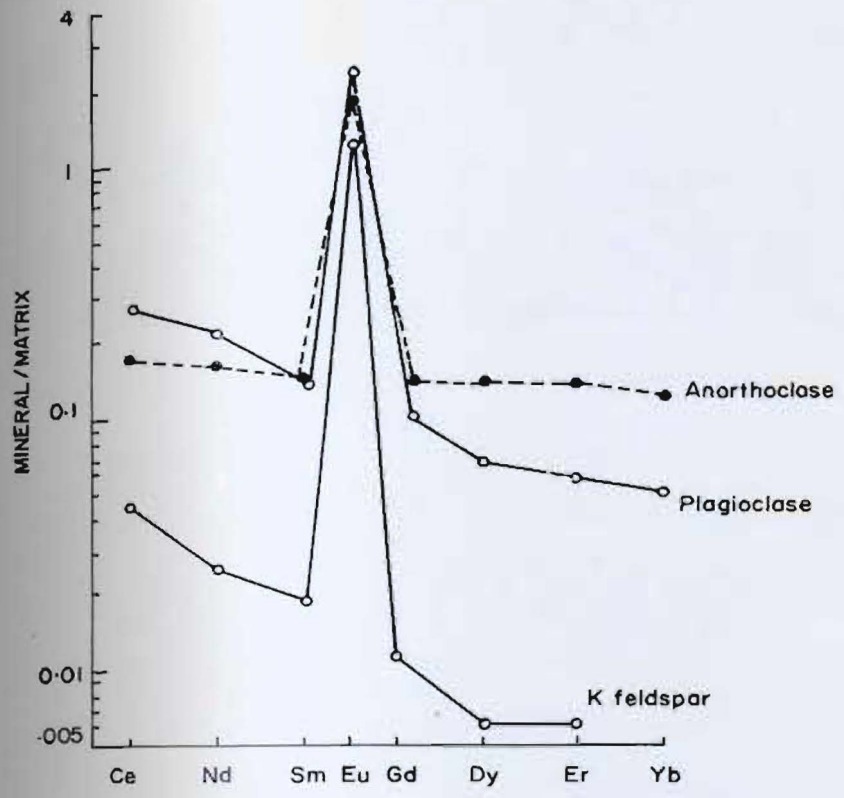
4
1
0·1
0·01
·005
MINERAL / MATRIX
Anorthoclase
Plagioclase
K feldspar
Ce
Nd
Sm
Eu
Gd
Dy
Er
Yb

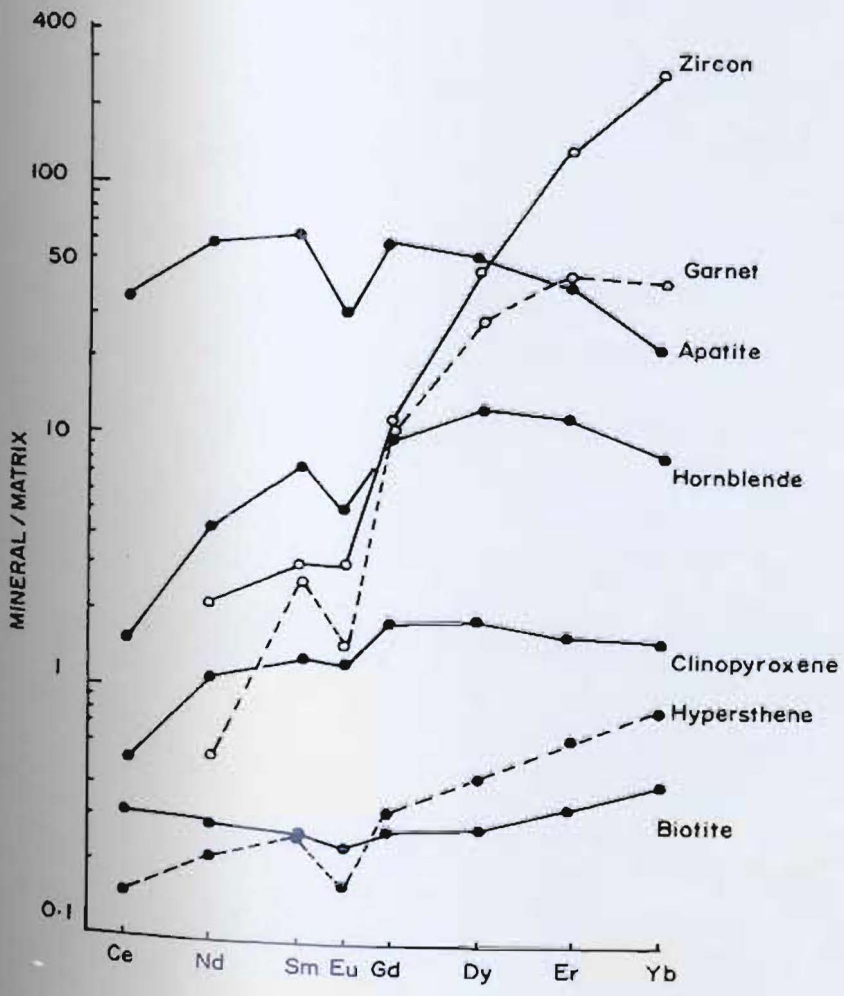
400
100
50
10
1
0·1
MINERAL / MATRIX
Zircon
Garnet
Apatite
Hornblende
Clinopyroxene
Hypersthene
Biotite
Ce
Nd
Sm
Eu
Gd
Dy
Er
Yb

flat to negative slopes, LREE enrichment and a negative Eu anomaly.

Hydrothermal alteration may have a profound effect on the primary REE distribution: partial or complete destruction of magmatic minerals releases variable amounts of REEs to form complexes with chloride, fluoride, carbonate or sulphate ions within the hydrothermal fluid (Flynn and Burnham, 1978; Hanson, 1978; Haskin et al., 1966; Taylor and Fryer, 1983). Chloride preferentially leaches LREE (La-Sm) whereas $CO_3^{=}$ and F^- leach HREE (Gd-Lu) (Collerson and Fryer, 1978; Taylor and Fryer, 1982; Taylor et al., 1981). Consequently, altered igneous rocks, such as those at Tulks Hill, may show a variety of REE patterns dependent upon the extent of mineral breakdown and the relative activity of the anionic species (F^-, $CO_3^{=}$, Cl^-) in the fluid. Fluid inclusions and the secondary mineralogy are used in conjunction with the REE pattern to identify the relative importance of the anionic species during alteration (Taylor and Fryer, 1980, 1982).

As a reference, and in part for comparison, a field of REE patterns for seven ore-bearing felsic volcanic rocks is shown (from Campbell et al., 1982). The location of the seven samples that comprise the field is given in the caption to Figure 7.2.

7.2 REE ABUNDANCES AND ASSOCIATED ELEMENT TRENDS

Except where shown, the absolute values are those obtained after normalising to the chondrite values of Taylor and Gorton (1977). Complete REE analyses are listed in Appendix I. REE values listed below (eg. 345.45 in the alkali-enriched rhyolite) are enrichment factors above chondrite, listed as ppm.

7.2.1 RHYOLITE

All samples were from the Raven rhyolite. Four had a relatively fresh physical appearance, but a chemical analysis showed them to be K-enriched. Five were bleached, chloritised and/or partially sericitised.

7.2.1.1 Alkali-enriched rhyolite.

Moderate LREE enrichment characterises all samples (Fig. 7.2). Total REE contents in the four samples range from 345.45 to 280.13. La varies between 79.05 and 44.62 while Yb varies between 31.75 and 18.29. Note that the lower La content corresponds to the highest Yb content to produce the flattest pattern (sample 24NA-82).

A consistent increase in the K/Rb ratio corresponds to a decrease in the REE pattern slope (Fig. 7.3).

Figure 7.2: REE variations within samples of the alkali-enriched rhyolite. The shaded area encompasses 7 REE analyses of ore-bearing felsic volcanic rocks from different mining camps:

Kam Kotia, Ontario
South Bay, Ontario
Kidd Creek, Ontario
Sturgeon Lake, Ontario
Matagami, Quebec
Golden Grove, Western Australia
Kuroko, Japan

Source of data is Campbell et al. (1982) except for Matagami, Quebec (MacGeehan and MacLean, 1980).

Figure 7.3: Ratioed components plotted as a function of LREE depletion in 4 samples of alkali-enriched Raven rhyolite. Only the K/Rb ratio shows a consistent increase with LREE depletion.

ALKALI-ENRICHED RHYOLITE

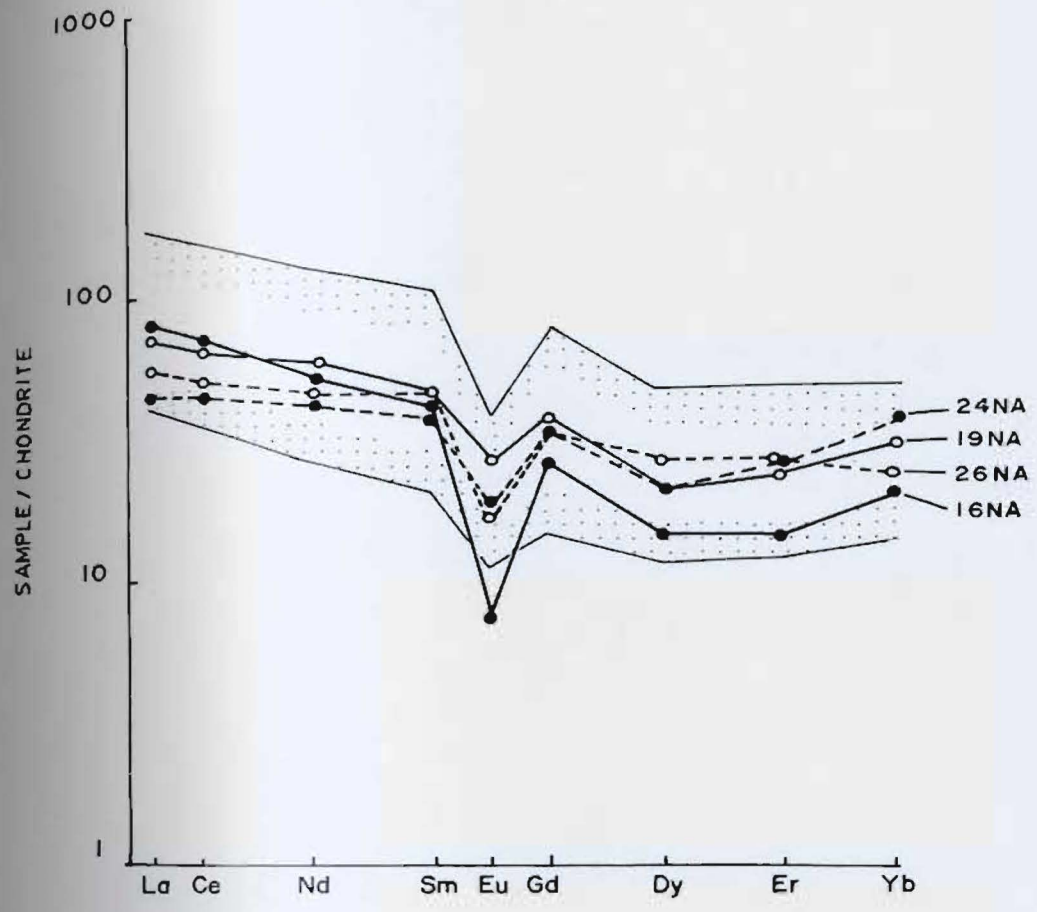

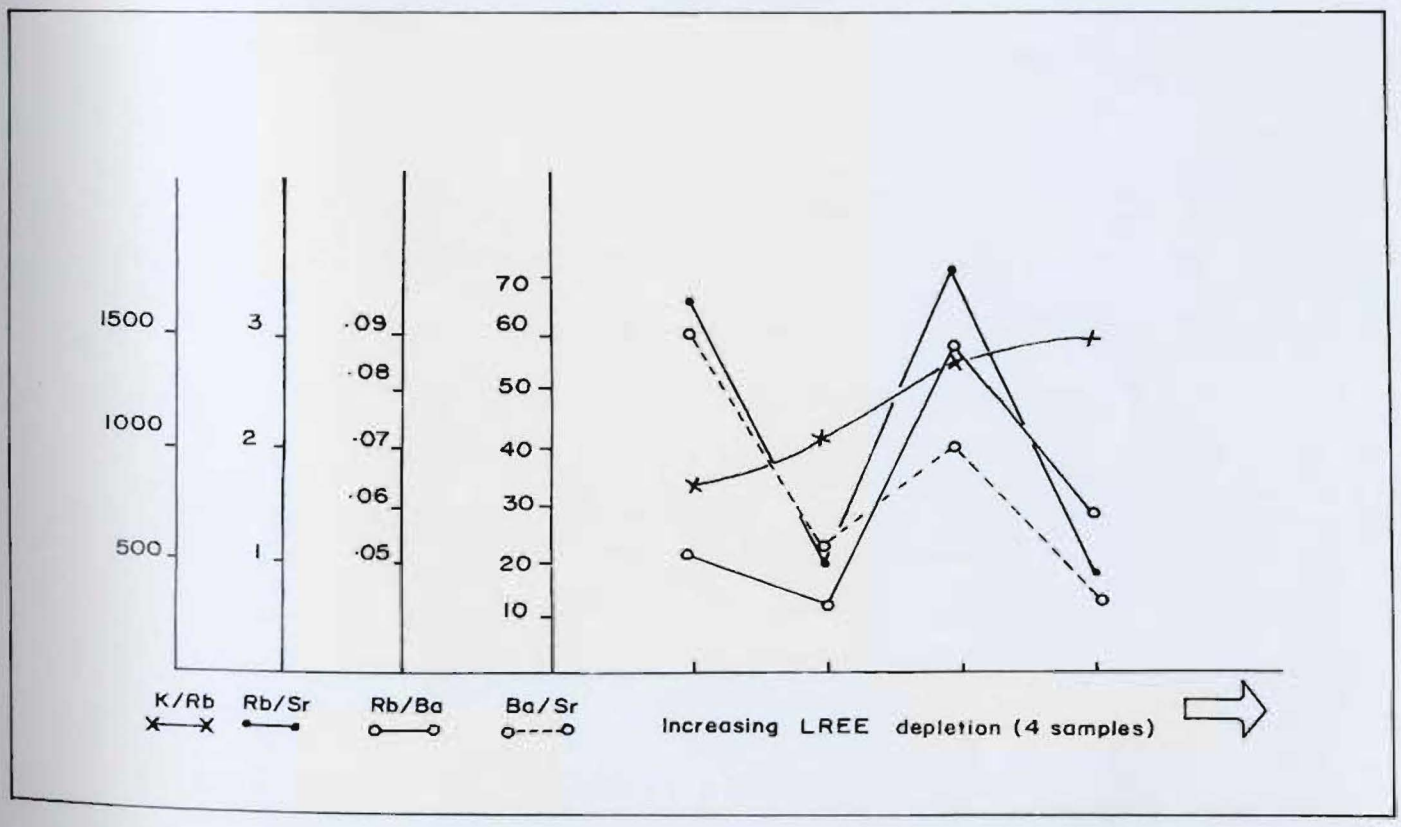

7.2.1.2 Altered rhyolite.

Least and most altered types are identified (Fig. 7.4); samples 11NA- and 20NA-82 are more sericitised and chloritised compared to the remaining samples.

Flat REE patterns distinguish the most altered samples from the least altered ones (17NA-, 18NA-, 20NA-82), the latter showing moderate negative slopes similar to the alkali-enriched rhyolite. Eu depletion anomalies are less pronounced in the most altered samples. Also, averaged total REE abundances decrease from 340.66 for the least altered samples, to 136.6 for the most altered ones. Averaged total LREE and total HREE contents decrease respectively from 216.48 to 60.98 and 107.3 to 62.32 with increasing alteration. Note that the difference in total LREE between the least and the most altered samples is much greater than in the total HREE.

Higher ratios of Ba/Sr, Ba/Na, Rb/Sr and perhaps K/Rb are characteristic in the most altered samples; higher Na/Sr characterises the least altered samples (Fig. 7.5).

7.2.2 SILICEOUS STOCKWORK

Two groups, each consisting of three samples, can be identified by their REE concentrations and associated patterns.

Figure 7.4: REE variations within samples of altered rhyolite. Two groups are identified corresponding to least altered (17NA-, 18NA- and 20NA-82) and most altered types. The least altered samples compare favourably with the alkali-enriched rhyolite. Sources for the shaded field are given in Figure 7.2.

Figure 7.5: Ratioed components plotted to show their variation with respect to alteration in 5 altered rhyolite samples. LREE abundances increase towards the right, ie. from sample 20NA-82 to 18NA-82.

ALTERED RHYOLITE

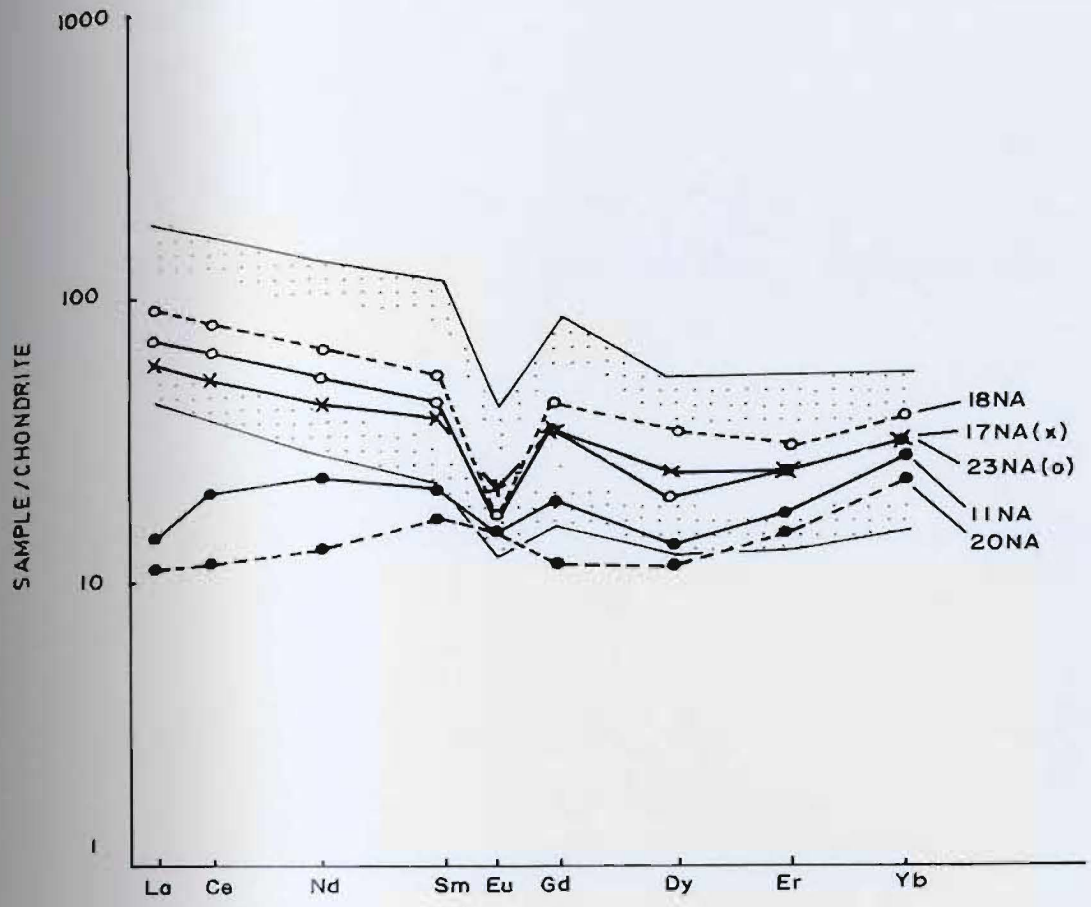

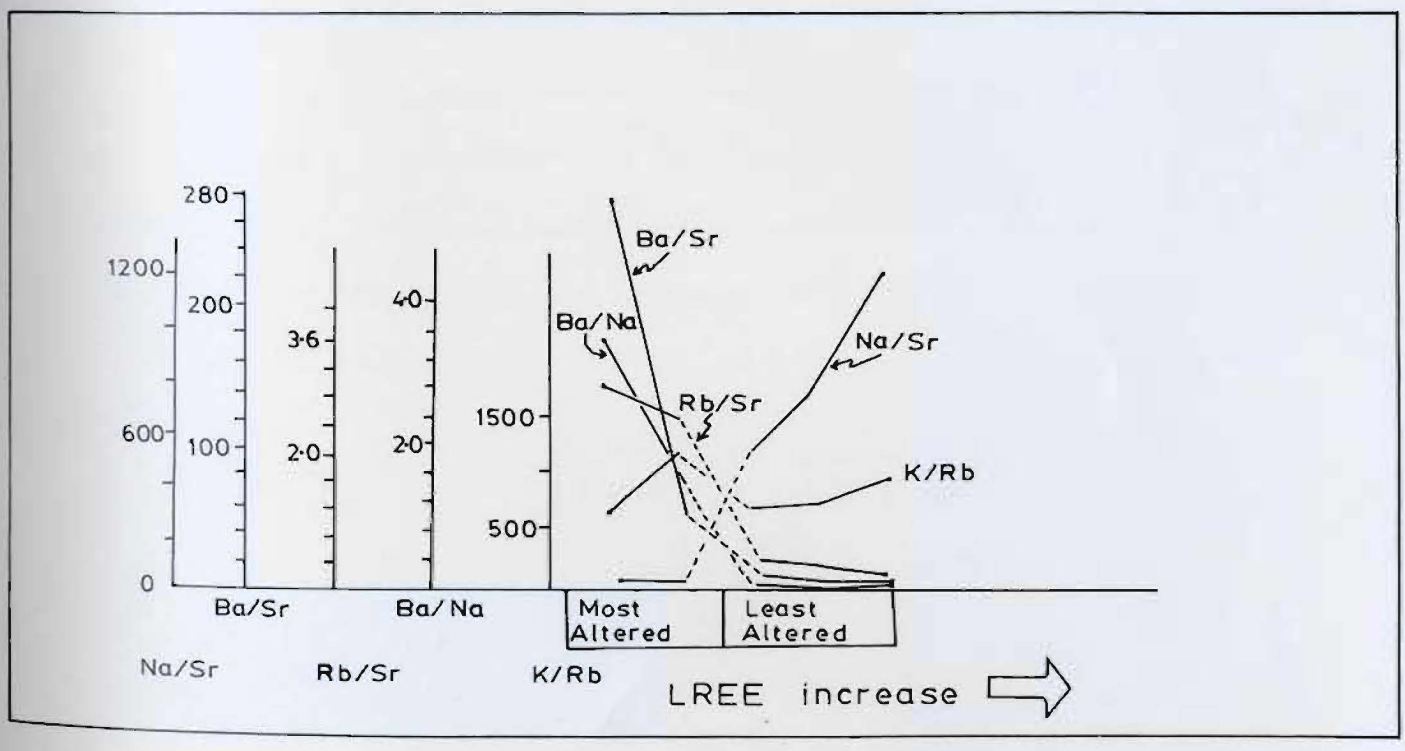

Group (a): Three samples, from widely spaced locations, have similar patterns and abundances showing pronounced Eu depletion anomalies and negative slopes (Fig.. 7.6). Total REE concentrations range from 287.34 to 176.18 with La varying between 72.73 and 40.14. Yb ranges from 19.3 to 10.3. Eu varies between 10.84 and 9.18.

Increasing SiO2 and depletion of Al2O3 accompanies a slight REE enrichment. Trace element contents in the three samples are similar except for the base metals; the sample with the highest metal content (Pb + Zn + Cu) has a higher total REE (sample 14EN-82).

Group (b): Flat to positive slopes, diverse LREE contents, ranging from 99.17 to 17.53, but similar HREE concentrations, varying from 59.06 to 49.83, characterise the three remaining siliceous stockwork alteration samples (Fig. 7.7). Samples 2SA- and 4NA-82 have total REE contents of 154.82 and 175.52 respectively; sample 3SA-82 has a reduced total REE content of 87.05 because of extremely low values for the LREEs. Eu is depleted in sample 4NA-82 only.

LREE depletion in sample 3SA-82 is accompanied by a lower SiO2 content, but higher Al2O3 and Fe2O3 contents. Trace element contents are similar in all three samples except for Ba and the base metals: a high metal content

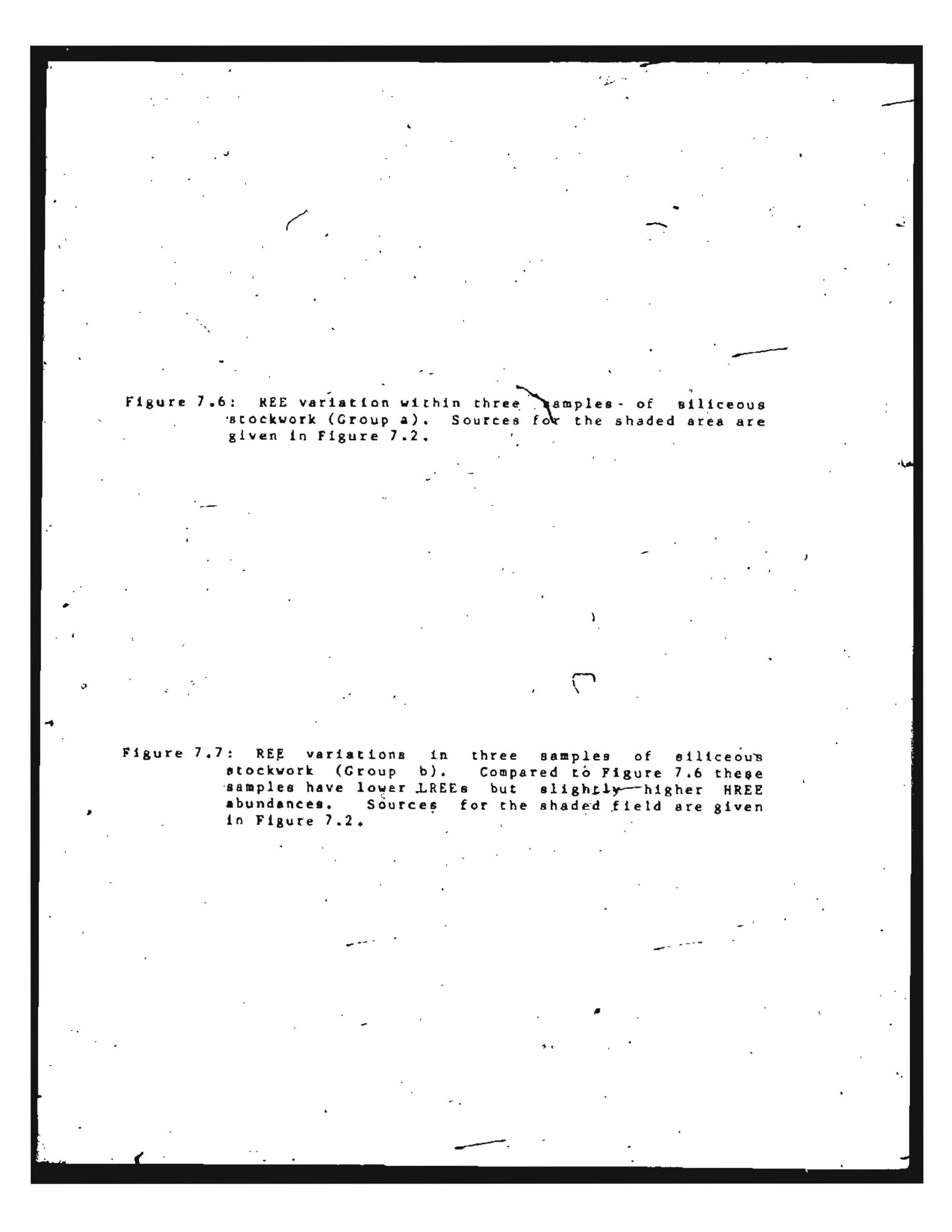

Figure 7.6: REE variation within three samples of siliceous stockwork (Group a). Sources for the shaded area are given in Figure 7.2.

Figure 7.7: REE variations in three samples of siliceous stockwork (Group b). Compared to Figure 7.6 these samples have lower LREEs but slightly higher HREE abundances. Sources for the shaded field are given in Figure 7.2.

SILICEOUS STOCKWORK (a)

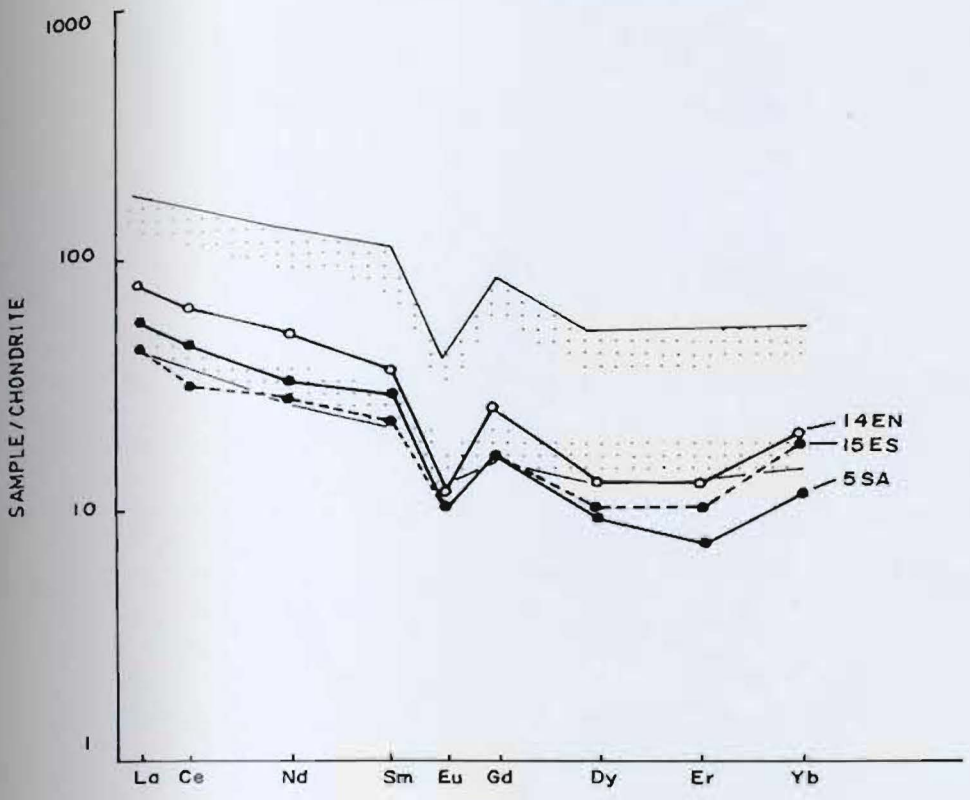

SILICEOUS STOCKWORK (b)

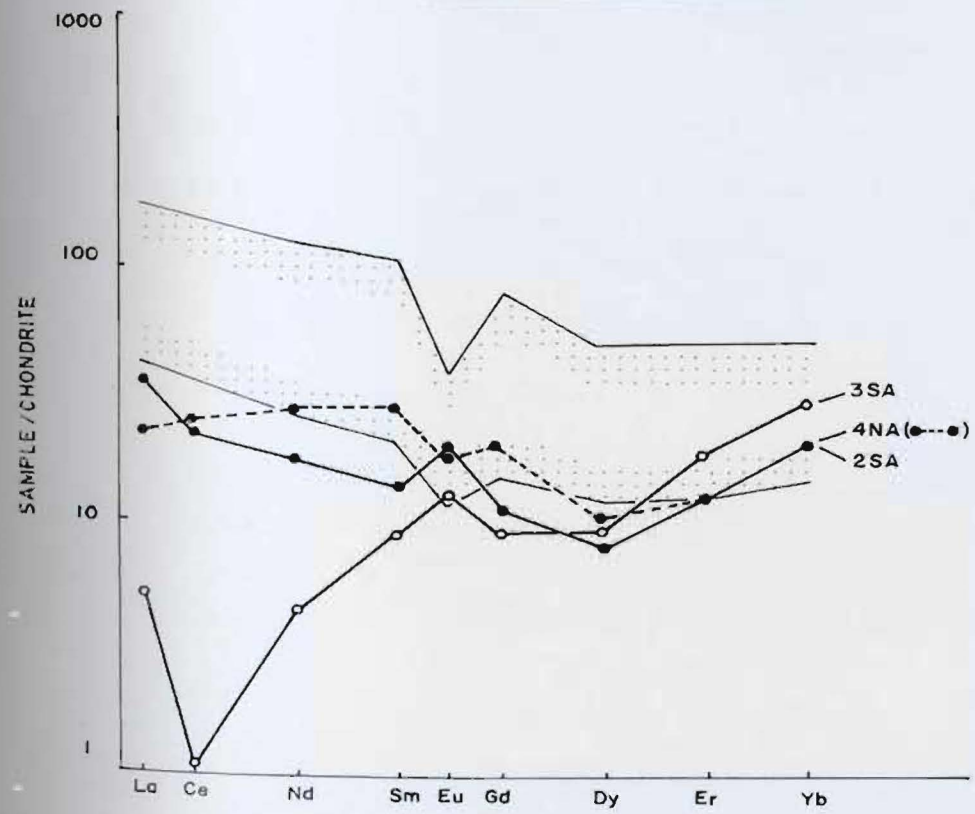

(av. Pb+Zn+Cu, 1136 ppm) but relatively low Ba (av. 1054 ppm) characterises samples 2SA-82 and 3SA-82; conversely, sample 4NA-82 has extreme Ba enrichment (6393 ppm) but low base metals (54 ppm).

7.2.3 MINERALISED HORIZONS

Two heavily mineralised samples and one mineralised chlorite-schist have been analysed (Fig. 7.8). Flat or slightly negative slopes are characteristic; only sample 10WA-82, which has combined base metals in excess of 70 wt.%, contains a Eu enrichment anomaly, which may be a reflection of the relative lack of albite as a gangue to the mineralisation (see Fig. 7.1).

Total REE concentrations range from 187.76 to 41.33. La varies between 46.35 and 6.14, while Yb ranges from 16.3 to 14.37. An average value for the LREE is 57.94 whereas the averaged HREE concentration is 28.45 producing an averaged enrichment factor of 2 for the LREEs.

Total REE depletion with increasing mineralisation is accompanied by a decrease in SiO2, Al2O3, K2O and Ba, and increases in LOI, Rb, Zr and Th. However, the trace element results for sample 10WA-82 may be spurious because of the poor calibration (XRF) for samples with a High sulphide content, so that the absolute values should be viewed with caution.

Figure 7.8: REE variations for three mineralised samples. Samples 5ES and 10WA are heavily mineralised and have lower total REE abundances than the mineralised chloritic stockwork (2WA). Sources for the shaded area are given in Figure 7.2.

Figure 7.9: REE variations for a sample of biotite tuff and tuffaceous chert. Also shown is a REE pattern for an average of 10 analyses of oxide-rich samples from the New Brunswick mining camp (source: Graf, 1977). Graf's (1977) data are normalised to the values of Taylor and Gorton (1977).

MINERALISED HORIZON

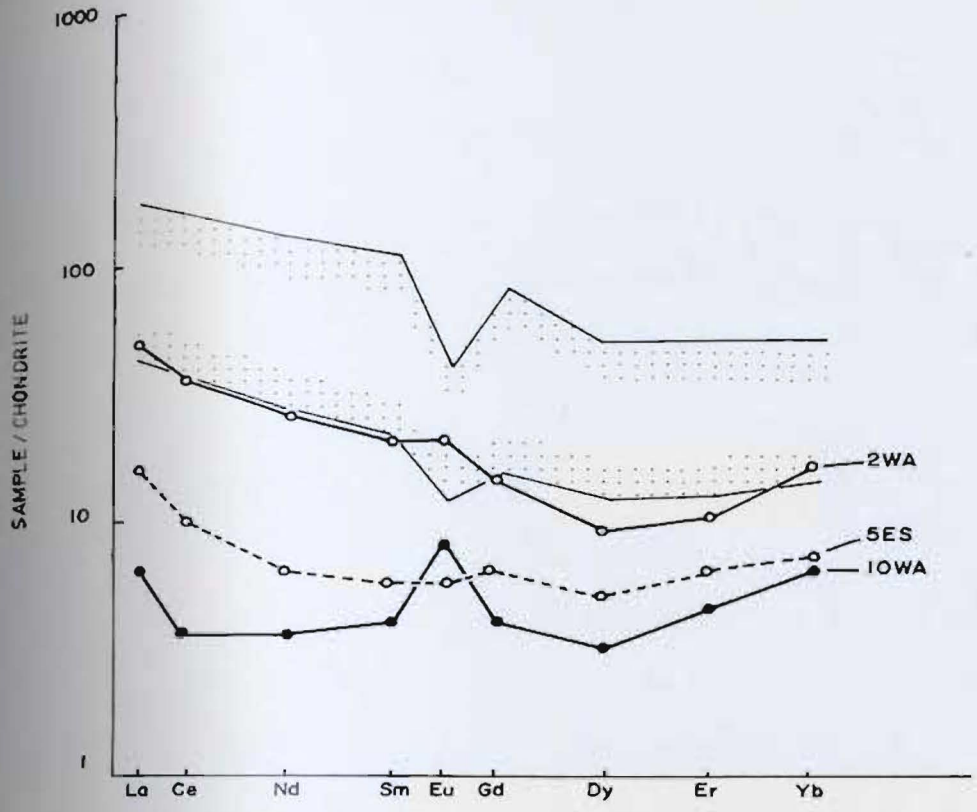

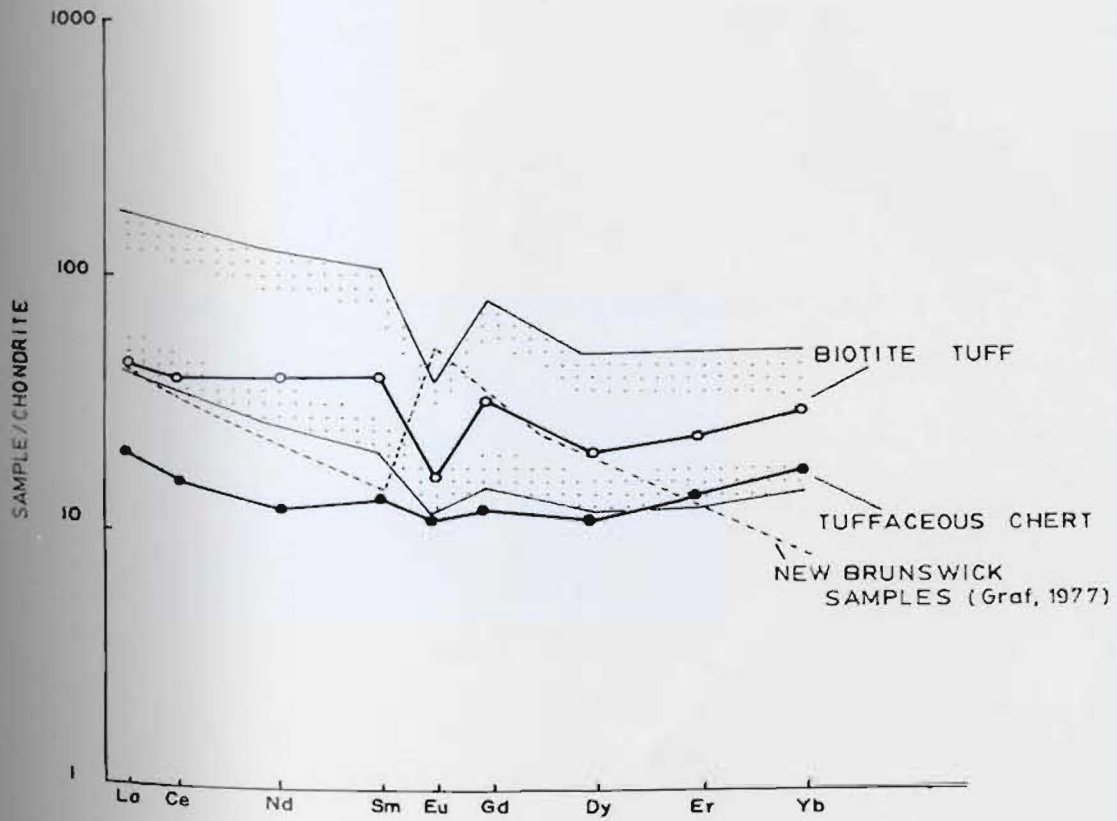

7.2.4 TUFFACEOUS CHERT

Total LREE and HREE abundances are similar which produces a flat pattern with no Eu anomaly, similar to certain mineralised samples (Fig. 7.9). Total REE abundance of 124.49 is within the range for the mineralised horizons.

7.3 INTERPRETATION AND DISCUSSION

In a recent paper, Campbell et al. (1982) suggested that the REE concentrations for ore-bearing felsic volcanic rocks differ from barren felsic volcanic rocks because of a different genetic history. According to the authors, lower REE abundances, flat patterns and distinct Eu depletion anomalies characterise ore-bearing felsic volcanic rocks, whereas steeper slopes and no Eu anomaly distinguish barren rocks. A critical argument in their theory is REE immobility during alteration. Their data for the ore-bearing felsic volcanic rocks are plotted on Figures 7.2 through to 7.9. (excluding Figs. 7.3 and 7.5).

Taylor and Fryer (1980, 1982, 1983) and Graf (1977) have suggested that REE mobility during hydrothermal alteration is real. Specifically, Cl^- ions within a mineralising solution are capable of complexing LREE while $CO_3^{=}$ and F^- ions complex HREE. A necessary requirement therefore, is that mineral destruction releases REEs to the solution. Selective mobilisation of LREE or HREE, depending upon the chemical characteristics of the

solution, will alter the primary magmatic signature.

The following section discusses and interprets the Tulks Hill REE data with respect to the above ideas. The terms enrichment and depletion are used relatively; for example, the LREE in samples 11NA-82 and 20NA-82 are depleted relative to the remaining rhyolites.

7.3.1 RHYOLITES

Both rhyolite types have similar REE abundances and are discussed together.

All samples have virtually identical HREE abundances. The LREE are equally enriched in all but two samples (11NA-, 20NA-82) ---- severe LREE depletion in the latter is accompanied by a loss of the characteristic Eu depletion anomaly. Apart from the LREE of these two samples, the REE plots for the Tulks Hill rhyolites fall within the "ore-bearing felsic volcanic field" of Campbell et al. (1982).

Both steep and shallow slopes, with or without Eu depletion anomalies, occur in the two rhyolite types, and since the samples are from the same intrusive body the data suggest that REE mobilisation during alteration of the rhyolite is real. LREE depletion in samples 11NA- and 20NA-82 probably reflects their mobilisation by Cl-rich brines, whereas HREE "stabilisation" may reflect the presence of unaltered zircon: this mineral is known to concentrate HREEs (Hanson, 1978) and is present in all

samples.

7.3.2 SILICEOUS STOCKWORK, MINERALISED HORIZON AND TUFFACEOUS CHERT

The three groups are discussed together because of their presumed genetic link with the hydrothermal fluid and sulphide deposition.

The protolith to the siliceous stockwork alteration is thought to have been a rhyolite tuff and as such should have similar REE concentrations to a rhyolite if the REEs are immobile. LREE concentrations within the siliceous stockwork however, are highly variable, which is unlikely to reflect primary magmatic processes. Rather, it suggests LREE complexing with chloride ions in the solution during alteration (Taylor and Fryer, 1982).

Unlike the siliceous stockwork, the mineralised horizons and tuffaceous chert do not have protoliths because they are chemical precipitates. As such, their REE concentration should reflect that of the hydrothermal fluid (Graf, 1977). Similar REE patterns and abundances for the tuffaceous chert and the mineralised horizon imply a similar origin (ie. hydrothermal fluid). The oxide-rich samples (chemical sediments) studied by Graf (1977) have relatively low REE abundances and positive Eu anomalies (see Fig. 7.9), the latter reflecting the Pb-rich nature of the distal portions of the mineralisation: K-feldspar destruction releases Pb and Eu to the mineralising solution

to produce the enrichment in the chemical sediments. The REE data for the chemical sediments (mineralised horizon and tuffaceous chert) at Tulks Hill are consistent with Graf's (1977) model, particularly the Eu enrichment anomaly in the Pb-enriched sample (10WA-82): an average REE analysis for the oxide-rich iron formations analysed by Graf (1977) is shown on Figure 7.9 for comparison. The lower total REEs in the mineralised horizon and the tuffaceous chert, compared to the rhyolite and the siliceous stockwork, is also consistent with Graf's (1977) model.

Virtually identical HREE concentrations in all three groups probably reflects the primary zircon distribution (Hanson, 1978), since all groups have similar Zr contents (Table 7.1). Kalogeropoulos and Scott (1983) suggest that the clastic (volcanic) component of the tetsusekiei horizons in the hangingwall of Kuroko deposits may have controlled the REE in the coexisting chemical (chert) layers through a "chemical homogenisation" process during later hydrothermal alteration. At Tulks Hill, the similarity of the trace element data in both the stockwork and the tuffaceous chert suggests that such a process probably operated at Tulks Hill during hydrothermal alteration.

Seawater interaction during alteration is suggested by the low Ce content of sample 3SA-82: Ce anomalies are characteristic of samples from ophiolitic suites that have

Table 7.1: Mean Zr contents for the Tulks Hill rock groups.

All groups have similar Zr abundances which may explain the similar HREE contents in the rocks.

ALKALI-ENRICHED RHYOLITE:		145 ppm
ALTERED RHYOLITE	:	126 ppm
PYROCLASTICS	:	127 ppm
SILICEOUS STOCKWORK	:	187 ppm
MINERALISED HORIZON	:	158 ppm
CHEMICAL SEDIMENTS	:	148 ppm

undergone seafloor alteration/metamorphism (eg. Heming and Rankin, 1979; Ludden and Thompson, 1978; Masuda and Nagasawa, 1976; Menzies et al., 1977). Such alteration by seawater-dominated fluids would remove Ce to the solution since Ce is strongly depleted in seawater (Graf, 1977). Ce depletion also occurs during weathering (Ronov et al., 1977) but this is not thought to have occurred at Tulks Hill since the samples show no effects of weathering and therefore the Ce anomaly is probably a primary feature (ie. seawater interaction).

7.3.3 SULPHIDE PRECIPITATION AND REE CONCENTRATIONS

From the REE patterns in the above three groups it is apparent that substantial sulphide deposition is accompanied by decreases in the LREE only (eg. 3SA-82). A possible relationship exists between the two phenomena: metal ions are thought to be transported as chloride complexes and under high S^{--} conditions these complexes break down to precipitate as sulphides. This precipitation releases Cl ions to the solution (Barnes, 1979; Skinner, 1979)

$$MeCl^{-}_{(aq)} + H_2S_{(aq)} \rightleftharpoons MeS + 2H^{+} + 2Cl^{-}$$

which may scavenge, and remove, LREEs. Increasing the pH, through such mechanisms as fluid boiling or mixing with more alkaline solutions (eg. seawater), causes metal

precipitation (Barnes, 1979) and under alkaline conditions carbonate, and therefore HREEs, are stabilised. Carbonate within the stockwork alteration and the tuffaceous chert strongly suggests that the pH was increased at the seawater-rock interface; this would permit sulphide deposition and Cl- ion release. Thus, at least one controlling factor for LREE depletion at Tulks Hill is the extent of sulphide precipitation.

7.4 SUMMARY

REE concentrations within the altered felsic volcanic rocks and the chemical sediments are thought to reflect a combination of hydrothermal and magmatic processes. For example, LREE depletion in the stockwork probably reflects selective leaching of these elements by a fluid rich in Cl- ions. The HREE distribution however, probably reflects the primary zircon distribution in both the volcanic rocks and the younger tuffaceous cherts.

REE mobilisation during alteration associated with Kuroko deposits is implied by Dudas *et al.* (1983) when they say "The postore group is generally less altered than the preore samples, suggesting that the flatness of the rare earth element pattern is not an artifact of alteration" (p.129). It is apparent that REE mobilisation during alteration is a normal phenomenon.

CHAPTER 8

MINERAL CHEMISTRY

8.1 INTRODUCTION

Sulphides, silicates and carbonates were analysed using the electron microprobe. Complete analyses and analytical techniques are given in Appendices I and II.

8.2 SILICATES AND CARBONATES

8.2.1 CHLORITE

Fourteen samples have been analysed to determine if the Fe/Fe+Mg ratio varies with respect to the rock type and/or the location in relation to mineralisation. At least two points were analysed in each sample. Chemical formulae were calculated on the basis of 28 oxygen atoms, and the molecular proportions of Mg and Fe were used to determine the Fe/Fe+Mg ratio.

Most chlorites have similar optical properties showing 1st order grey colours or anomalous green birefringence. Certain samples contain chlorites that have a violet birefringence but these are not extensively developed. Locally, the chlorites exhibit a pale green pleochroism. Chlorites with a distinctive (anomalous) blue colour (PPL) occur in sulphide+quartz-rich veinlets within the iron formation. In the same sample the matrix chlorites have a green colour but there is no correlation between the difference in the optical properties and a difference in

the chemical composition: the matrix chlorites have a virtually identical chemistry to the veinlet chlorites. This is the reverse to Wynne (1983) who found a correlation between the chemical composition of the chlorites and their optical properties.

Table 8.1 summarises the variation in the Fe/Fe+Mg ratio and lists the rock type analysed. The ratio for each sample is an average of the total number of chlorite analyses for that particular sample. Four groups are defined: lowest ratios occur in samples of massive mineralisation, whereas the highest ratios (that is, Fe-rich) occur in sample 82-13, the iron formation. Intermediate values distinguish the chloritised portions of the quartz crystal tuff and 3 mineralised samples, the latter having a weak to well-developed foliation of the sulphides. Using the criteria of Hey (1954), the chlorites range from ripidolite (iron formation) through to clinochlore, with only one sample plotting as diabantite (Fig. 8.1). It is obvious from this diagram that the mineralised samples (squares) plot in the Mg- and Si-rich (Al-poor) part of the diagram defining a crude trend from least mineralised to most mineralised. A similar trend of Mg enrichment in the chlorites with increasing mineralisation is highlighted on a molecular proportions diagram (Fig. 8.2). Figure 8.1 shows that the Tulks Hill chlorites are more aluminous than the Buchans chlorites and only overlap the Buchans ore zone chlorites (Henley and

Table 8.1: Summary of the variation in Fe/Fe+Mg ratio with respect to the rock type analysed.

Mg-rich**	Fe-Mg**		
0 - 0.3	0.3 - 0.7		
	LOW	MED	HIGH
6NA-82 10WA-82 T52-81 T74-81 T53-81	82-30 82-C5 82-C16 5ES-82	13Wa-82* T48-81 * 10ES-82*	82-13

* Foliated sulphides
**Calculated from the Fe/Fe+Mg ratio of the formula ions

Figure 8.1: Chlorites classified according to the criteria of Hey (1954). A crude trend is defined by a decrease in the Fe/Fe+Mg ratio with increasing sulphide content. Also shown are the compositional fields for chlorites from the Buchans rocks (Henley and Thornley, 1981). See Figure 8.2 for an explanation of the symbols.

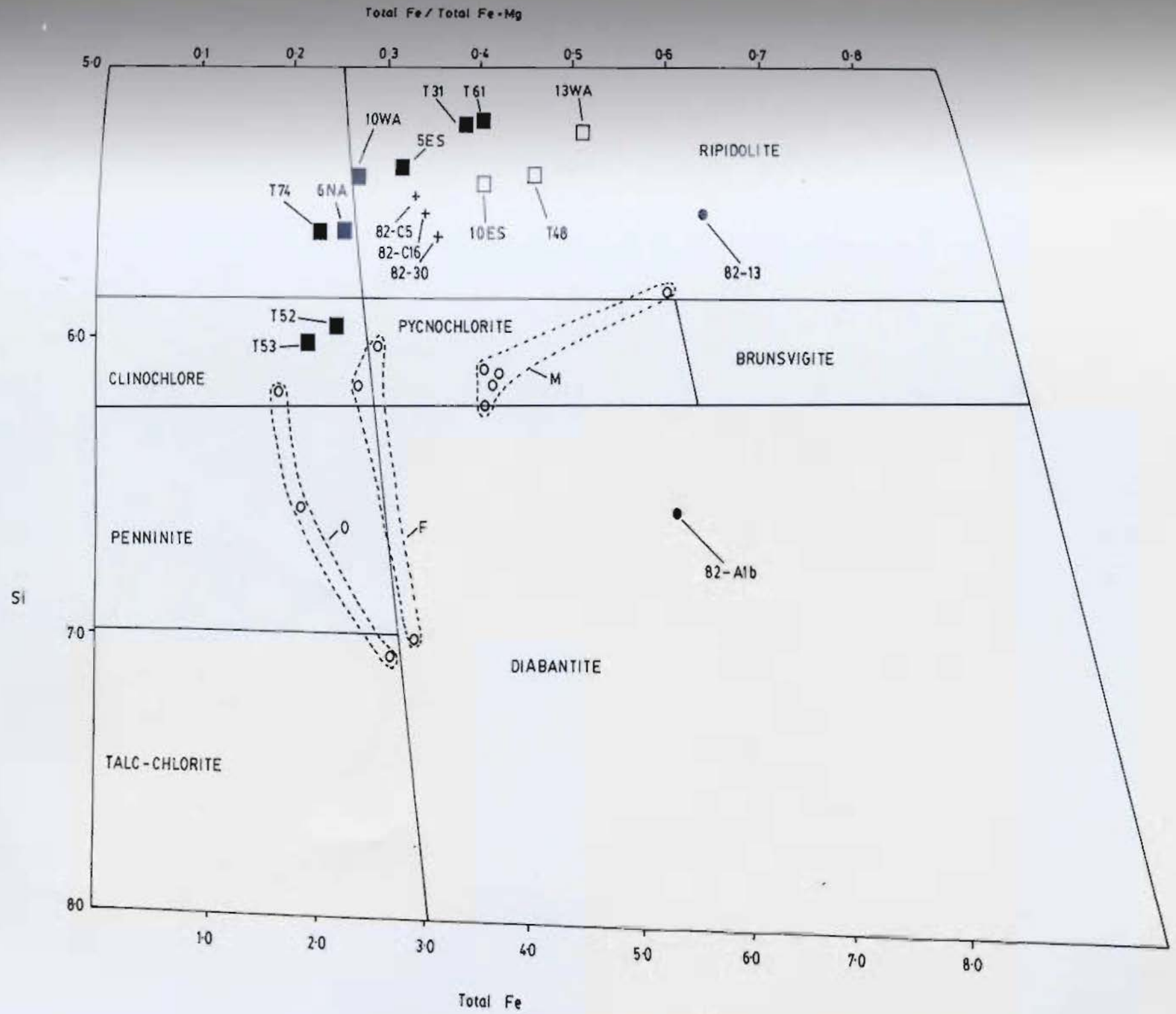
Total Fe / Total Fe+Mg
0·1
0·2
0·3
0·4
0·5
0·6
0·7
0·8
5·0
6·0
7·0
8·0
Si
1·0
2·0
3·0
4·0
5·0
6·0
7·0
8·0
Total Fe
T31
T61
13WA
10WA
5ES
RIPIDOLITE
T74
6NA
82-C5
82-C16
82-30
10ES
T48
82-13
T52
T53
PYCNOCHLORITE
BRUNSVIGITE
CLINOCHLORE
M
O
F
PENNINITE
82-A1b
DIABANTITE
TALC-CHLORITE

Figure 8.2: Chlorite compositions plotted on a portion of the Al-Mg-Fe system molecular proportion diagram. Also shown are the fields for the Buchans chlorites (from Henley and Thornley, 1981).

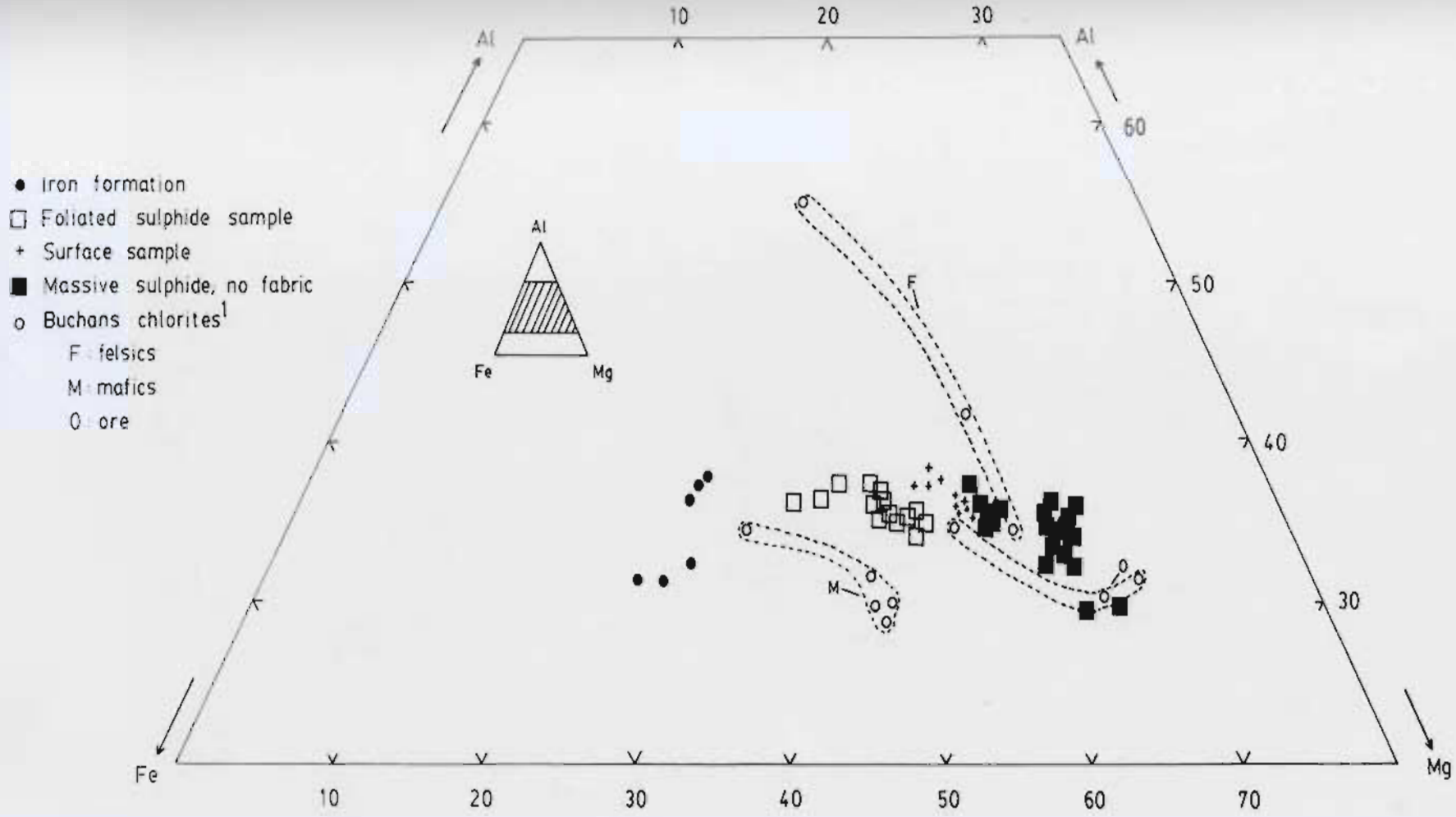
Iron formation
Foliated sulphide sample
Surface sample
Massive sulphide, no fabric
Buchans chlorites[1]
F felsics
M mafics
O ore
Al
Fe
Mg
10
20
30
40
50
60
70
F
M
O

Thornley, 1981) when Si:Al substitution is ignored. An interesting feature shown by both diagrams is the intermediate positions of chlorites in samples distant from the mineralisation (crosses), separating two clusters of chlorite analyses for heavily mineralised samples. This aberration in the trend of decreasing Fe content of chlorites with increasing proximity to the mineralised horizons is explained below.

These data indicate that Mg-enrichment distinguishes the mineralised horizon from the remaining rock types, with the samples from the West Adit (Map 2) being more Mg-rich. This feature is characteristic of both Precambrian and Phanerozoic (Kuroko type) deposits (Petersen and Lambert, 1979; Riverin, 1977; Roberts and Reardon, 1978; Shirozu, 1974, 1978 a,b). At the Seneca and Corbet deposits (Canada) the Fe/Fe+Mg ratio increases with increasing distance from the deposit, from 0.282 to 0.510 and 0.35 to 0.59 respectively (Urabe et al., 1983).

Fe-Mg chlorites within some mineralised samples are unusual because the majority of the mineralised samples contain chlorites that are Mg-rich. It is suggested that the higher Fe content of these chlorites reflects metamorphic re-equilibration with pyrite, possibly localised in a fault zone (these samples have a weak to well-developed fabric). Alternatively, a form of desulfidation during the mineralising event could have converted the Mg chlorites to Fe-Mg chlorites:

$$\text{(Mg) chlorites} + FeS_2 \longrightarrow \text{(Fe,Mg) chlorites} + 2(S)$$

This mechanism has been proposed by Bachinski (1976), Kalogeropoulos and Scott (1983) and Vokes (1970) to explain "atypical" chlorites within a Mg rich zone and is used here to explain the shift in chemical composition of the "ore zone" chlorites at Tulks Hill.

Mottl (1983) discusses the variation in chemical composition of experimentally produced chlorites in basalts and compares his data with the observed chlorite chemistry formed in altered basalts at mid-ocean ridges. In essence, the major controlling factor of the chlorite chemistry is the seawater/rock mass ratio (SW/R); higher ratios (up to 50:1) allow Mg-chlorite formation whereas lower ratios (less than 10:1) favour the formation of Fe-rich chlorites. Apparently, all of the Mg can be extracted from seawater and it is not necessay to have primary Mg minerals in felsic rocks. Deeper levels of a hydrothermal system have a lower SW/R ratio, as well as less Mg because of reactions involving Mg uptake at shallower levels, and consequently, Fe chlorites predominate in the deeper levels of the hydrothermal system. At Tulks Hill, Mg-rich chlorites occur at the mineralised horizon or in the immediate footwall whereas iron chlorites predominate within the footwall felsic volcanics (ignoring the "atypical" chlorites). This suggests that a high SW/R ratio characterises the footwall to the sulphide deposit, which

is compatible with the chlorite stockwork representing a deformed palaeofeeder vent. However, according to Mottl (1983), Mg chlorites are produced at the sites of downward fluid flow, which is the reverse to the model proposed for sulphide genesis (Hutchinson, 1982), a difference that is difficult to reconcile.

It has been suggested (Urabe *et al.*, 1983) that chloritic alteration, which commonly occurs at the base of many sulphide deposits, is not truly hydrothermal: seawater within the pore spaces of brecciated tuffaceous rocks produce a Mg chlorite assemblage by ion exchange with seawater (*cf.* Mottl, 1983); this assemblage is not necessarily related to hydrothermal activity. Once a hydrothermal system develops, a sericite-dominant assemblage is produced at the location of fluid discharge by a process of outward replacement of the already formed chlorite. In this manner a sericite-dominant assemblage, surrounded by a chloritic alteration zone, is produced. Urabe *et al.* (1983) suggested this mechanism of replacement because they observed that chlorite did not occur within the ore, and concluded that the chlorite was in disequilibrium with the hydrothermal fluid and hence must have formed through some other process. Since chlorite is a gangue mineral to the mineralisation at Tulks Hill the hydrothermal solution must have been in equilibrium with the fluid (*ie.* the reverse to the Uwamuki deposit). Although the chlorite at Tulks Hill is

hydrothermal the method of outward replacement may be the best explanation of the alteration zoning since sericitic replacement of chlorite is locally observed.

8.2.2 SERICITE

Thirty-nine sericite analyses are listed in Appendix I. There is little variation in the chemistry, although MgO and FeO are present in significant quantities, varying from 0.72 to 2.74 wt.% and 0.53 to 6.04 wt.%, respectively. Two samples, 81-74 and 82-30, contain 2.71 and 1.25 wt.% Na_2O respectively, probably substituting for K_2O, which has a lower value in this sample.

Texturally, the sericite occurs either in scaly aggregates, which locally become coarse enough to warrant the term muscovite, or as finer grains aligned subparallel to the S1 fabric. Some samples contain green coloured sericite (PPL) that shows weak pleochroism. Typically the birefringence of sericite is upper second order.

Sericite formation in volcanogenic massive sulphide deposits is as common as chlorite formation although, as at Tulks Hill, the zone of sericite formation tends to be more widespread. Hydrolysis of K-feldspar is a commonly proposed mechanism of generation of K for the solution (Meyer and Hemley, 1967) with sericite formation in the footwall occurring by a method of outward replacement of already formed chlorite. This is thought to be the mechanism of sericite formation at Tulks Hill, at least

within the siliceous stockwork, since partial sericite replacement of chlorite is seen in some samples.

Froese (1981) has shown that sericite may have restricted conditions of formation: at 300 degrees centigrade, which is approximately the temperature of sulphide deposition at Tulks Hill (see Chapter 10) sericite is stable at a pH of 4.41 or less (under specified conditions; see Chapter 10). Since sericite is abundant in the footwall of the Tulks Hill deposit a maximum pH of approximately 4.41 is probable during sulphide deposition.

8.2.3 BIOTITE

Three analyses of biotite within one sample from the biotite tuff are listed in Appendix I. All analyses are Fe-rich but show a slight variation in K2O content.

According to Beane (1974), igneous biotites have molecular Mg/Fe ratios of < 1, whereas hydrothermal biotites of porphyry systems have ratios > 1.5. If the hydrothermal systems associated with porphyry copper and volcanogenic massive sulphide deposits can be equated, then the Tulks Hill biotites are igneous since the Mg/Fe ratio is < 1. However, secondary albite is found in the biotite tuff which suggests that the rock has been hydrothermally altered. Preservation of magmatic biotite is unlikely during hydrothermal alteration so that the low Mg/Fe ratio probably reflects an earlier (pre-biotite) development of an Fe-rich mineral (chlorite?). This mineral could have

ected as a precursor to the biotite that is present in the tuff; the biotite would form during later K metasomatism.

8.2.4 FELDSPAR

Electron microprobe analyses of the Tulks Hill feldspars indicate no variation in the Ab-An content: all are pure albite with only a 1% (maximum) difference from the core to the rim (Appendix 1). This purity is unlikely to result from magmatic processes (Carmichael et al., 1974) although a metamorphic or hydrothermal origin is possible. In the absence of a regional survey of the VLG, which may show that albite is a common mineral (ie. it is metamorphic), it is suggested that the albite is hydrothermal.

Feldspar alteration to aluminosilicates (epidote, sericite-chlorite) is variably developed and may be caused by the same hydrothermal fluid event(s) responsible for the albitisation.

A paucity of calcium-rich minerals in most altered samples (except carbonate-rich ones) suggests that feldspar compositions more calcic than oligoclase did not exist prior to alteration, supporting a rhyolite-rhyodacite composition for the rocks (Chapter 6).

8.2.5 CARBONATE

The average carbonate mineralogy for four samples is plotted on Figure 8.3.

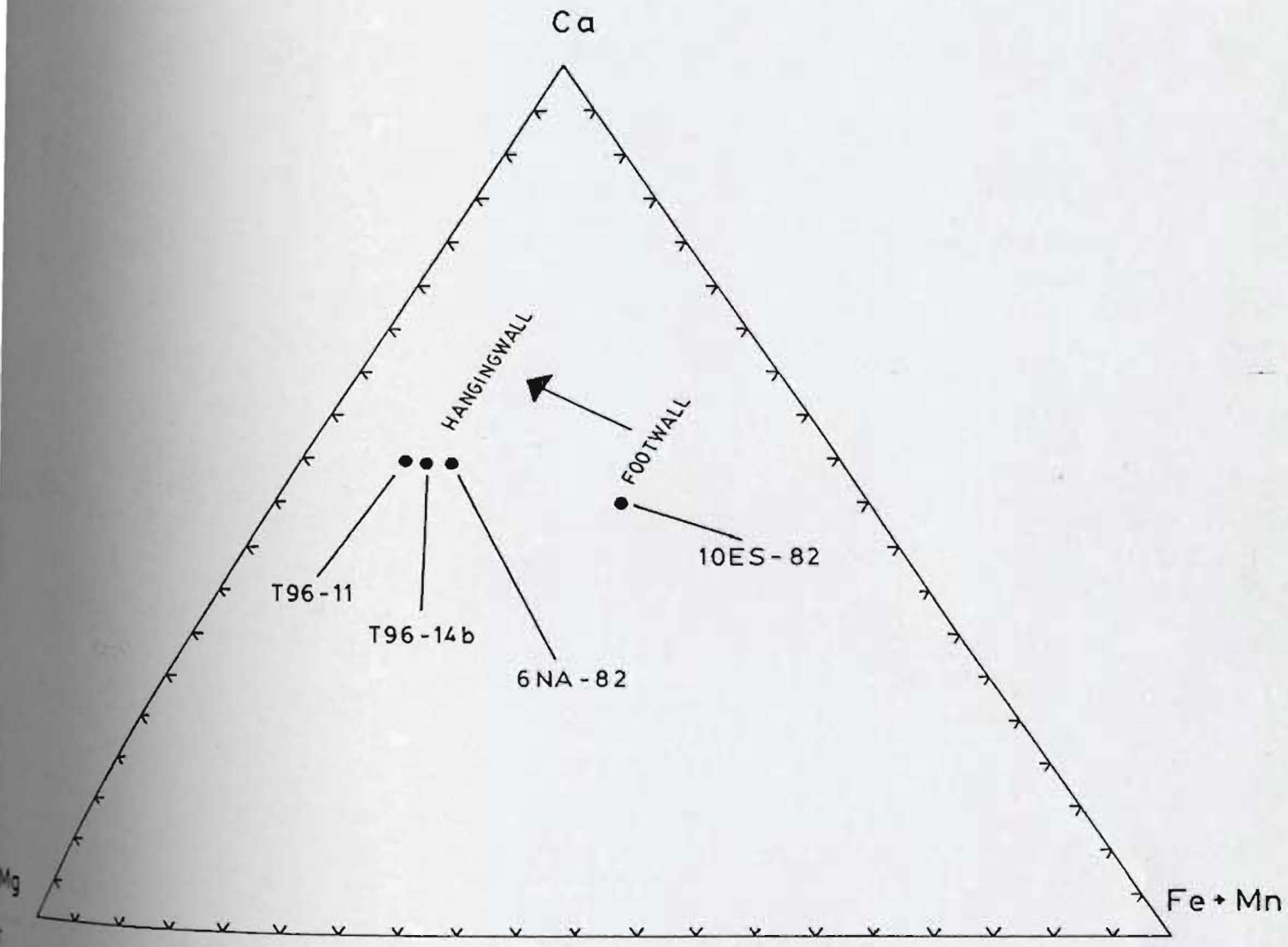

Figure 8.3: Ca : Mg : (Fe+Mn) cation proportion diagram to show the compositional variation of the Tulks Hill carbonates. Dolomitic carbonates tend to occur in the hangingwall.

Of the four cations present, Ca++ is dominant. Three samples from distal (hangingwall) locations (with respect to the mineralisation) have a similar degree of Mg-enrichment. The remaining sample is enriched in Mn and Fe so that the combined wt.% of Mn and Fe exceeds Mg.

Since sulphide mineralisation is common to all samples with carbonate, it is assumed that alkaline conditions prevailed during a part of sulphide deposition, and that the carbonate is hydrothermal. Alkaline conditions could result from mixing with seawater and/or boiling of the fluid to precipitate calcite (Chapter 6).

8.3 SULPHIDES

8.3.1 SPHALERITE

Seventeen analyses are listed in Appendix I. No appreciable content of minor elements (Cd, Sn) was found, but Fe:Zn substitution produces a variation in the mole % FeS.

Figure 8.4 is a histogram of the mole % FeS within the sphalerite:; sphalerites in the footwall samples have the highest mole % FeS (5.9) whereas sphalerites in the samples taken from the hangingwall have a lower mole % FeS (2.71). This is attributed to a reduction in the FeS activity (Vaughan and Craig, 1978; Barton and Skinner, 1979) either by precipitation of the associated sulphides, principally pyrite, or by a decrease in the sulphur fugacity (Fig. 8.5). The mole % FeS of sphalerites from Kuroko deposits

Figure 8.4: Histogram of the mole % FeS in the Tulks Hill sphalerites. The two groups correspond roughly to footwall and hangingwall sphalerite compositions.

Figure 8.5: Sphalerite composition in equilibrium with iron sulphides in the FeS-ZnS system (after Barton and Toulmin, 1966). The figures 0 - 7.5 represent pressures in kbars for sphalerite compositions in equilibrium with pyrrhotite (A) or pyrite (B). The lower temperature relationships (< 250 C) are from Scott and Kissin (1973).

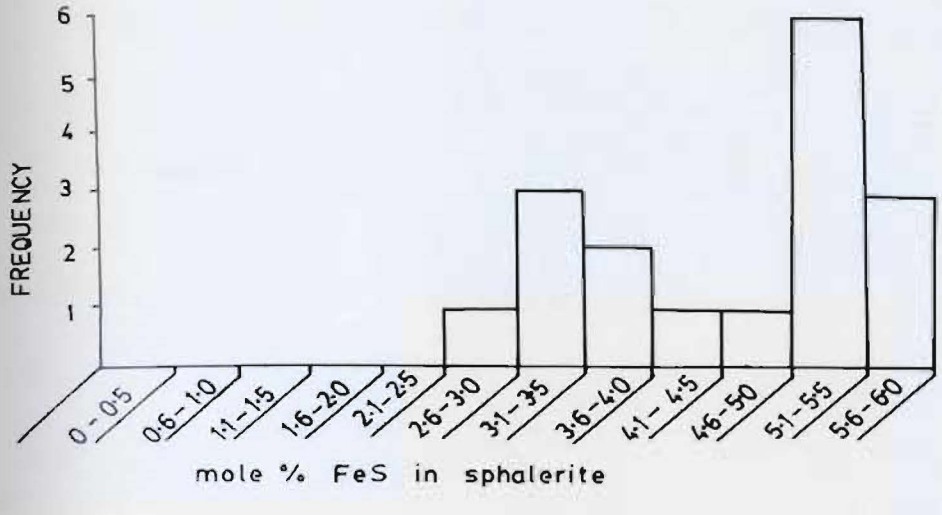
FREQUENCY
6
5
4
3
2
1
0-0·5
0·6-1·0
1·1-1·5
1·6-2·0
2·1-2·5
2·6-3·0
3·1-3·5
3·6-4·0
4·1-4·5
4·6-5·0
5·1-5·5
5·6-6·0
mole % FeS in sphalerite

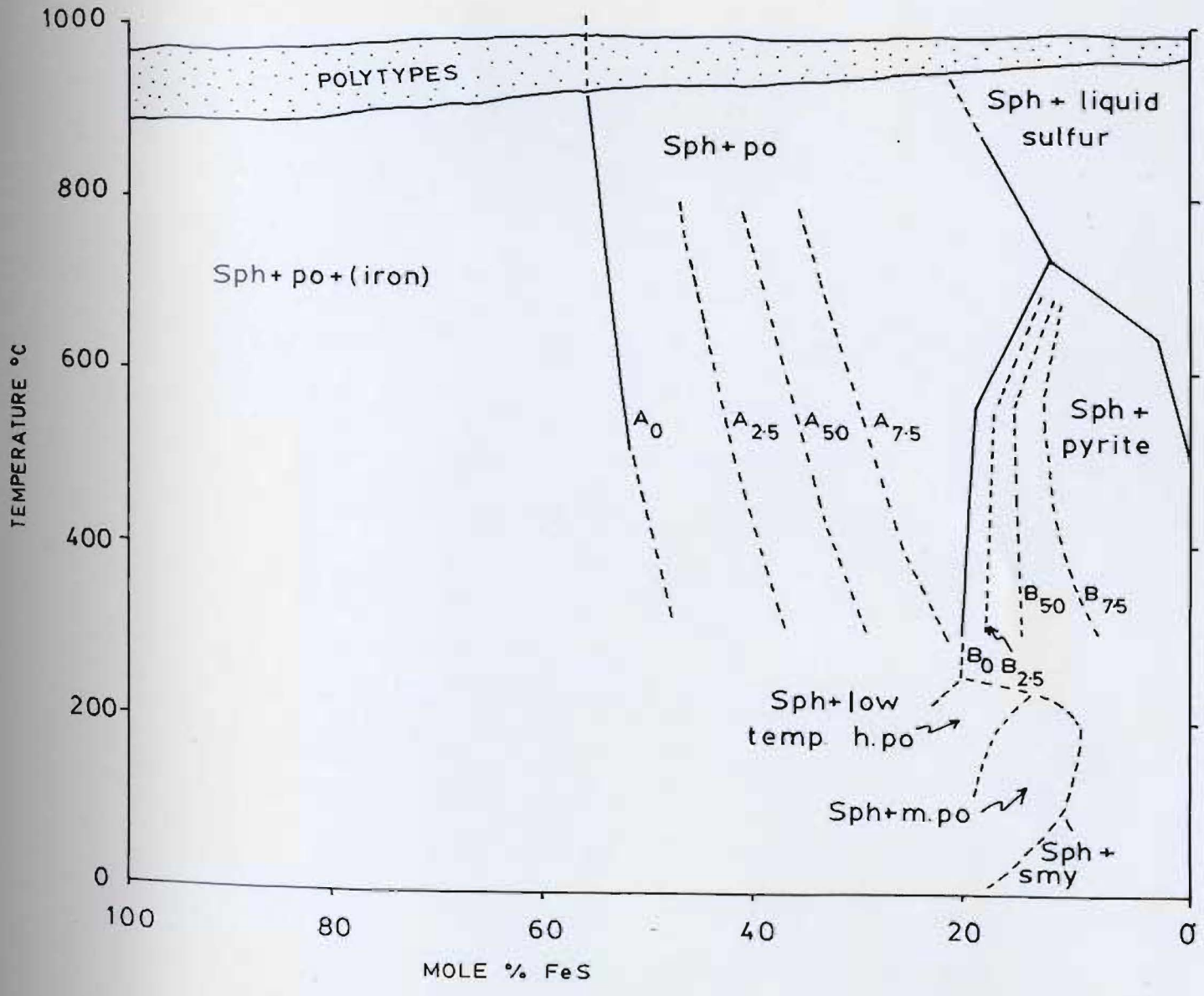
1000
800
600
400
200
0
TEMPERATURE °C
POLYTYPES
Sph + liquid sulfur
Sph + po
Sph + po + (iron)
A0
A2·5
A50
A7·5
Sph + pyrite
B50
B7·5
B0 B2·5
Sph + low temp h.po
Sph + m.po
Sph + smy
100
80
60
40
20
0
MOLE % FeS

exhibit a similar trend (Kajiwara, 1970; Urabe, 1974).

Sphalerite in equilibrium with pyrrhotite typically has at least 20 mole % FeS (Scott and Barnes, 1971). At Tulks Hill, the sphalerite has a maximum mole % FeS of 5.9 suggesting equilibration with pyrite rather than pyrrhotite (Fig 8.5); whether this equilibration is primary (depositional) or secondary (metamorphic) is not known. However, the apparent systematic decrease in mole % FeS of sphalerites with increasing proximity to the hangingwall suggests that it is primary, and that the effects of metamorphic re-equilibration may have been negligible, or at least are not evidenc. It is interesting to note that sphalerites sampled from the Atlantis II Deep had the lowest mole % FeS if they precipitated last whereas the highest mole % FeS occurs in the earliest precipitated sphalerites (Pottorf and Barnes, 1983). This compositional trend with time is apparent in the sphalerites of the Tulks Hill deposit (assuming the stratigraphy is correct) and it strengthens the suggestion that the variation in mole % FeS at Tulks Hill is primary.

8.3.2 TENNANTITE

This mineral is an end-member of the solid solution series known as the Fahlore Group. A complex mineralogy is suggested by the presence of Cu, As, Fe, Sb, Zn, and Ag (in decreasing order of abundance), the latter five elements substituting for copper (Ramdohr, 1969).

Assay data for the mineralised horizons show 1.5 % Ag in T3 lens (unpublished information, ASARCO and Abitibi-Price Mineral Resources). These data prove that some of the silver is contained within the tennantite. This is different to the Casapalca (Wu and Petersen, 1977) and Buchans (Strong, 1981) deposits where the silver is found in tetrahedrite.

8.3.3 GALENA

Bismuth and silver are common minor elements in galena, although their contents rarely exceed 0.8% and 0.26% respectively. A single galena from the chlorite schist however, has exceptional values of 2.68% Bi and 1.02% Ag, suggesting that significant silver may be contained within the galena as well as tennantite.

8.3.4 CHALCOPYRITE

Zinc substitution for Cu in the chalcopyrite lattice produces a slight variation in the ZnS content.

8.3.5 PYRITE AND ARSENOPYRITE

Pyrite and arsenopyrite were analysed for the minor elements Co, Ni, Cu, Zn, Cd, and Sn; both minerals are pure FeS_2 and FeAsS respectively.

CHAPTER 9

STRUCTURE

9.1 INTRODUCTION

All rock types at Tulks Hill are variably deformed, the effects ranging from microscopic grain boundary recrystallisation to megascopic fault displacement. Three deformation phases (D1, D2, D3) are identified at Tulks Hill, one of which (D1) is concordant with the regional structural grain of the CVB. For this reason, it is referred to as the "regional fabric". The remaining 2 deformation phases appear to be locally developed phenomena.

9.2 CLEAVAGES

Cleavages (S1 to S3) are taken as indirect evidence of folding (F1 to F3) because fold closures are rarely identified. Their dip and direction, measured to the nearest 5 degrees, are plotted as poles to cleavage planes and contoured on stereographic projections (Figs. 9.1, 9.3 and 9.4).

9.2.1 FIRST DEFORMATION (D1; REGIONAL FABRIC)

A penetrative schistose fabric is best developed in the pyroclastic rocks. It has an average dip of 78/NNW (Fig. 9.1) and is defined by sericite, chlorite and, locally, quartz stringers. Where quartz phenocrysts were

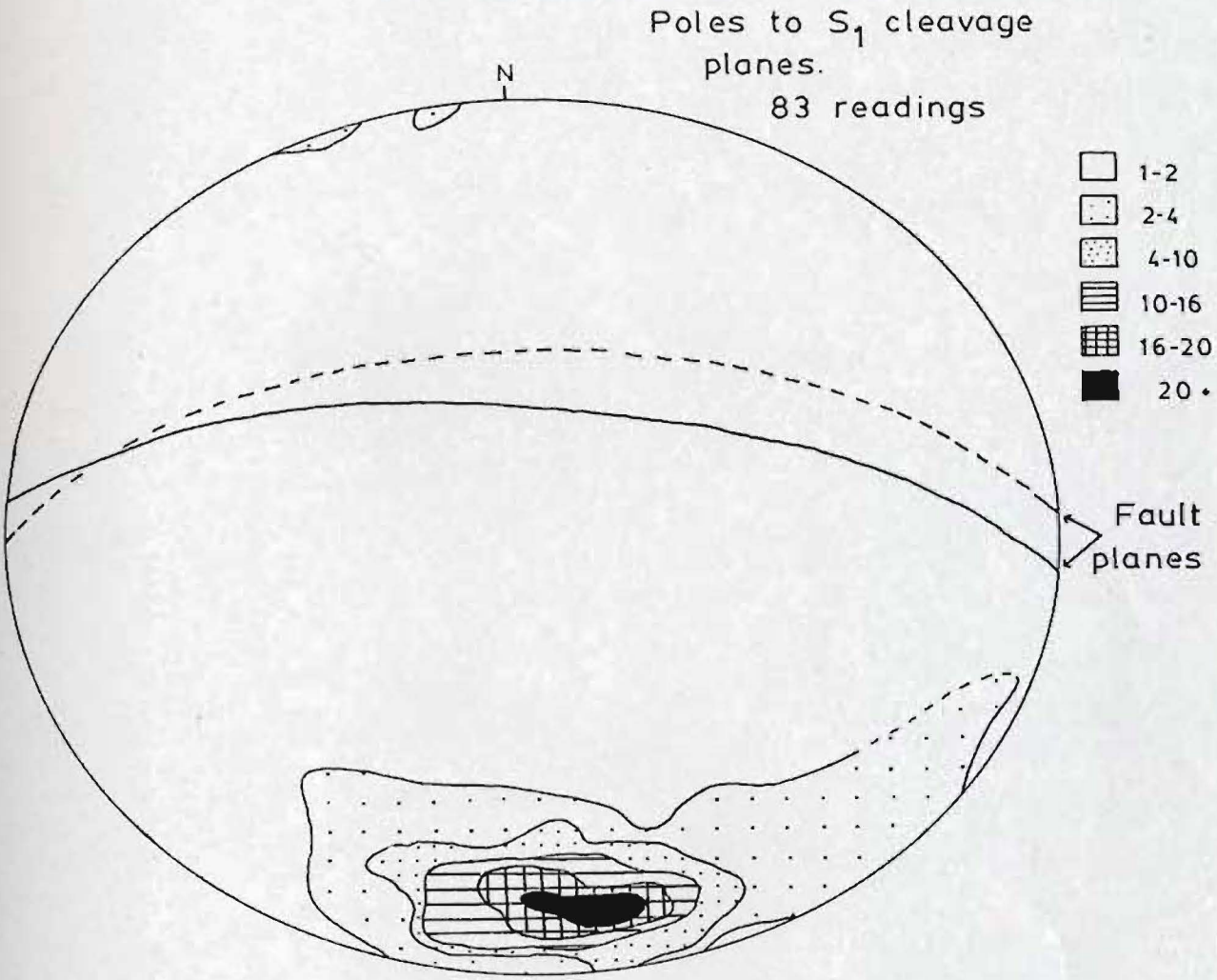

Figure 9.1: Contoured stereographic projection for the poles to S1 cleavage planes. Most planes dip steeply to the north. D1 age fault planes are also marked.

abundant the fabric is disrupted by quartz augen. Volcanic breccia fragments have undergone moderate flattening within the S1 cleavage (Plate 9.1).

Quartz-sericite alternations that characterise the siliceous stockwork and the chemical sediments also trend subparallel to the S1 fabric. The rhyolites lack abundant micaceous minerals and consequently have a massive appearance.

9.2.1.1 D1 related structures

Boudinage structures within the S1 cleavage, as well as locally-developed zones of pyrite granulation and recrystallisation, are attributed to D1.

(a) Boudins: Boudins are developed on every scale from a thin-section to an outcrop. Two modes of occurrence however, are more common: 1) milky-coloured vein quartz boudins, usually containing chalcopyrite, covellite, bornite and/or sphalerite, occurring as isolated "pods" or semi-continuous veins within the S1 cleavage (Plate 9.2), and 2) large-scale "chocolate-block" boudins (Wegmann, 1932) of massive pyrite and/or siliceous stockwork; the latter are approximately 2m.x 2m. x ?m. and are only identified in the East Adit (Map 2).

Boudins develop where there is a competence contrast between rock types in zones of extension (Hobbs et al., 1976). In this instance, the contrast is between either

Plate 9.1: Isolated volcanic breccia fragment is oriented subparallel to the S1 cleavage.

Plate 9.2: Quartz-vein boudins within the S1 cleavage containing chalcopyrite (yellow). Two boudins on either side of the pen cap are separated by a piece of country rock (siliceous stockwork). S1 cleavage planes are perpendicular to the the plane of the photograph.

quartz and the host rock, or siliceous stockwork / massive pyritite and the enveloping chlorite-sericite horizons. The vein quartz boudins are thought to develop by progressive rotation of quartz-filled fractures to orient them subparallel to the S1 cleavage through solution, mobilisation and re-deposition, as shown in Figure 9.2 and Plate 9.3. So-called "chocolate block" boudins are locally developed and are evidence of equal extension in two directions, subparallel to the fold axis, during folding (Hobbs et al., 1976). Their orientation and vertical nature in the East Adit suggests that they represent the limbs of a fold that has an axial plane trending roughly east-west (Map 2).

(b) Pyrite granulation: Mm-size granulation zones occur within the massive pyrite typically oriented subparallel to S1. For this reason they are thought to be features of D1. Locally, remobilised chalcopyrite or second generation covellite fill these zones, the latter producing mineral banding (Plate 9.4).

9.2.2 SECOND DEFORMATION (D2)

A weaker, conjugate cleavage, slightly oblique to S1, strikes approximately WNW-ESE (ig. 9.3). Two average dip directions are identified: approximately 72/SSW and 42/NNE, with a strong development of the latter. In outcrop, this cleavage appears as a spaced fracture

Figure 9.2: Three stage development of a quartz-vein boudin. A fracture, originally oriented perpendicular to a weak fabric, is progressively deformed into subparallel orientation with the cleavage by a process of solution and re-deposition of quartz during shearing along the developing cleavage. The intermediate stage corresponds to that seen in Plate 9.3 although the photograph is reversed so that the sense of shear is different to that shown in this figure.

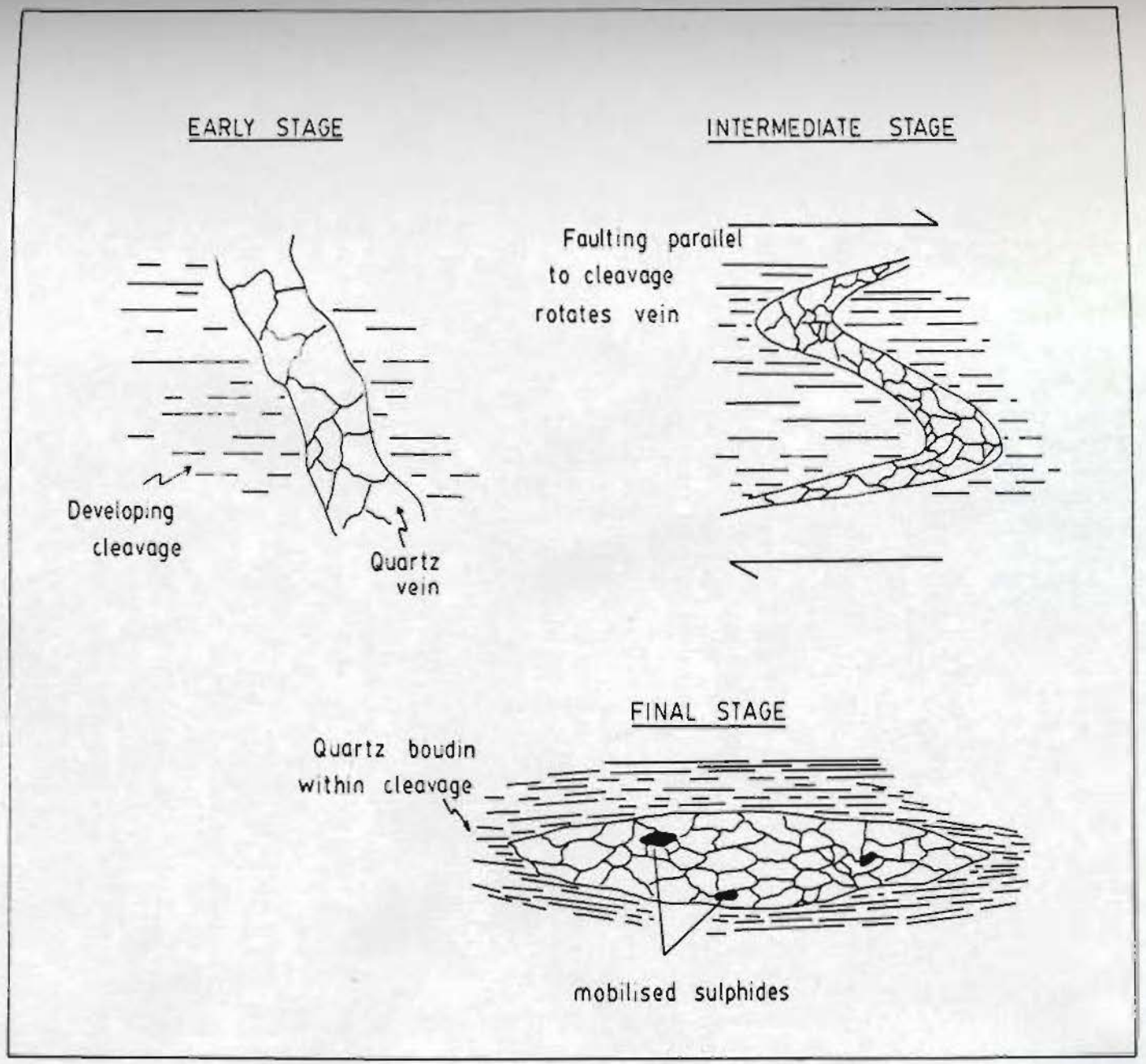
EARLY STAGE
INTERMEDIATE STAGE
Faulting parallel
to cleavage
rotates vein
Developing
cleavage
Quartz
vein
FINAL STAGE
Quartz boudin
within cleavage
mobilised sulphides

Plate 9.3: Quartz vein undergoing progressive rotation towards a parallel orientation with the cleavage. This stage corresponds to the intermediate stage of Figure 9.4.

Plate 9.4: Millimetre-size zones of granulation within the massive pyrite are oriented subparallel to the S1 schistosity and act as channels for supergene/weathering fluids, the latter depositing secondary covellite to produce a mineral banding. Pencil is approx. 12 cm. long.

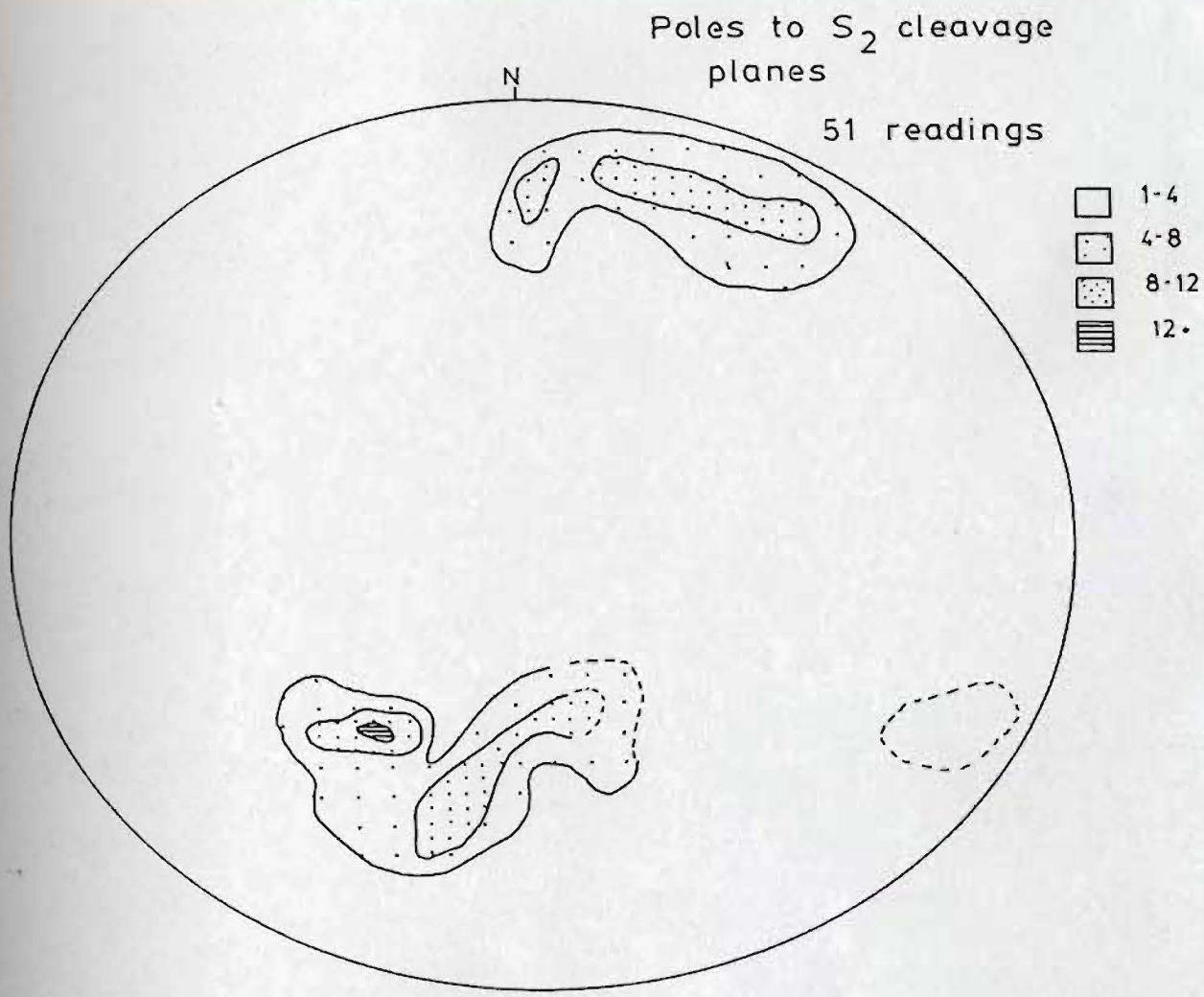

Figure 9.3: Contoured stereographic projection for the poles to S2 cleavage planes. A conjugate pair is developed with moderate to steep dips to the NNE and SSW, respectively

Plate 9.5: The S2 cleavage at Tulks Hill is a spaced fracture cleavage. It is parallel to the arrow on the compass. The S1 cleavage lies parallel to the leather handle of the compass. The compass is approx. 5 cm. square.

cleavage with no mineralogical definition (Plate 9.5). This cleavage clearly cross cuts S1, but its relationship with S3 was not observed.

9.2.2.1 D2 related structures

A diamond-shaped rodding effect and a mineral lineation are characteristic features of S2/S1 intersections.

9.2.3 THIRD DEFORMATION (D3)

Kink bands, a form of asymmetric fold, define the final observable deformation phase (Plate 9.6 and Fig. 9.4). Locally, conjugate sets are developed. Only rarely is an S3 cleavage developed, invariably as a pressure solution feature. An axial plane trace for the asymmetric folds is defined by the intersection of the short and long (S1) limbs; an average plunge of the hinge line of the folds is 80/175 although the plunge may vary between steeply dipping to the north and steeply dipping to the south.

At Tulks Hill en echelon shear zones, formed by the reorientation of the S1 cleavage, trend subparallel to the S3 kink bands and are interpreted to be evidence of ductility during either D3 or D1 (Ramsay, 1980). This structure is shown in Plate 9.7.

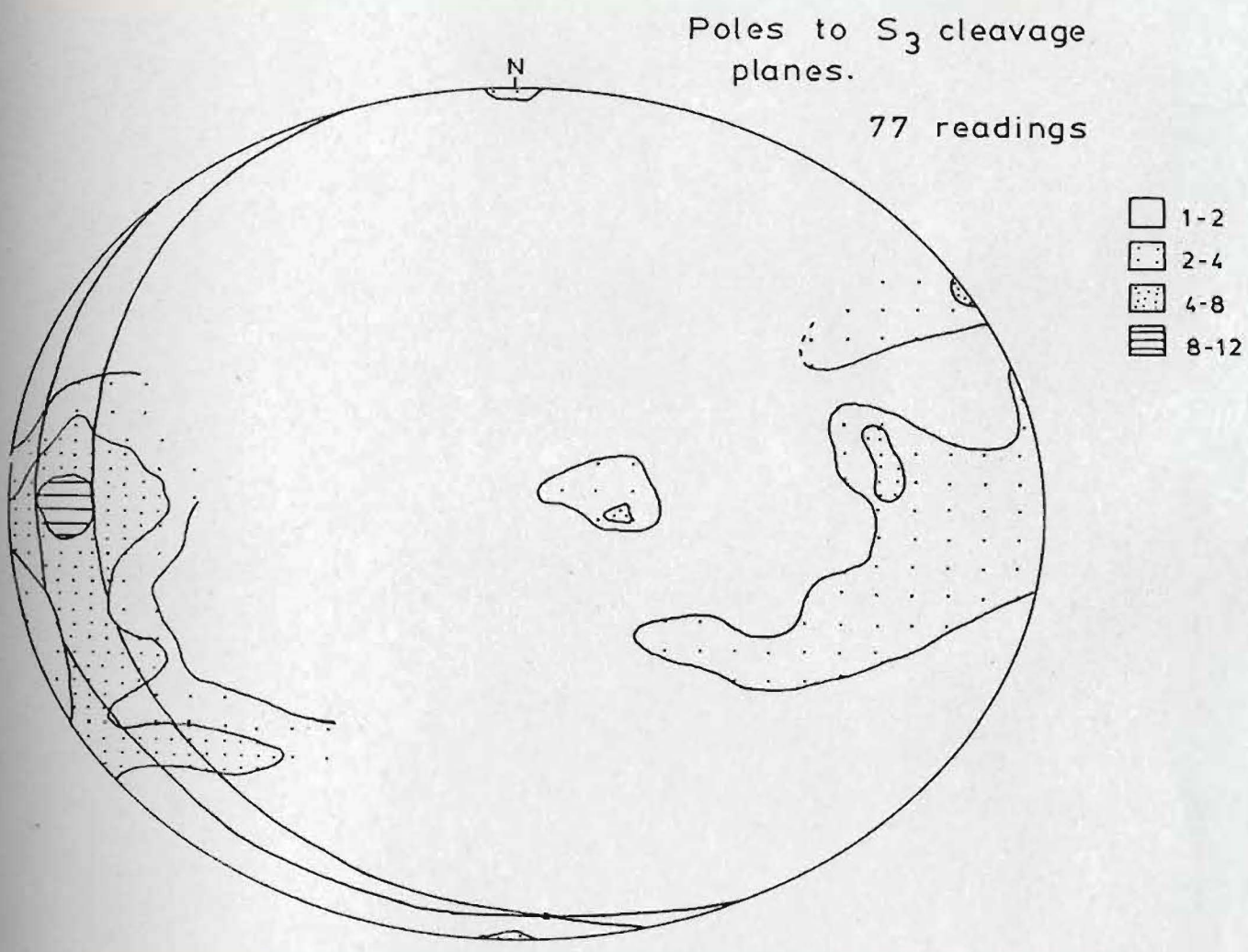

Figure 9.4: Contoured stereographic projection for the poles to S3 cleavage planes. Two dip directions are identified, the east dipping cleavage tending to be the stronger.

Plate 9.6: Reverse kinks in iron-stained quartz-sericite crystal tuff. Pencil is approx. 12 cm. long.

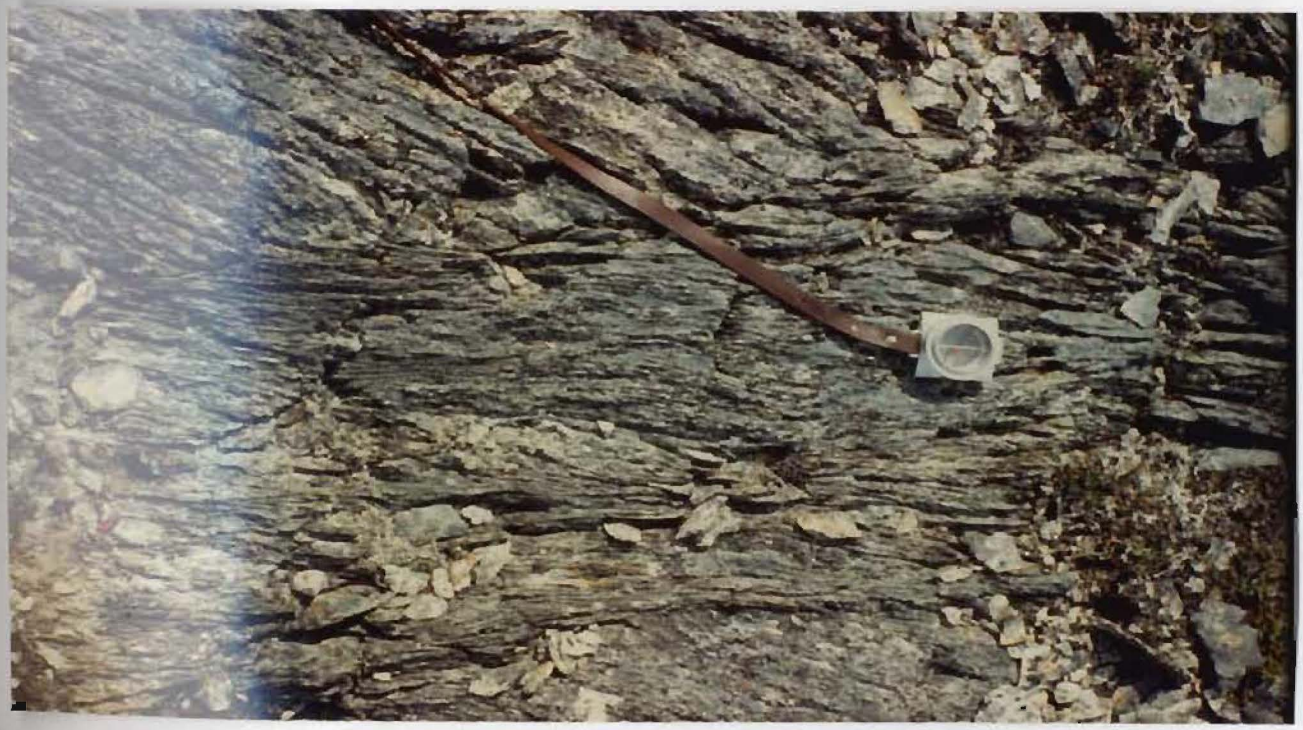

Plate 9.7: D3 (?) ductile shear zone reorients the S1 cleavage. S1 cleavage lies parallel to the leather handle of the compass whereas the shear zone is parallel to the arrow on the compass. Compass is approx. 5 cm. square.

9.3 FAULTS AND JOINTS

9.3.1 FAULTING

Discrete faults associated with D1 and D3 are relatively abundant, although the amount and direction of displacement on these faults is difficult to document, as are displacements on faults within the Victoria Lake Group in general (Kean, 1977). The estimated lengths of the fault planes vary from a few microns to several tens of metres and in all cases their attitude is subparallel to the fabric associated with either D1 or D3. D2 faults are not recognised.

9.3.1.1 D1 faults

Underground outcrop provides the best exposure of these faults. They can be found in every lithology, including the mineralisation, although they are less well developed in the massive portions of the rhyolite.

Displacement of the limbs of mm-size chlorite veinlets, which are isoclinally folded and have axial planes subparallel to the regional fabric (S1 cleavage), is taken as evidence of faulting parallel to S1 (Plate 9.8). Consequently, this faulting is interpreted to be D1 in age (although it is possible that the movement along these faults post-dated D1). Any faults with a similar attitude are termed D1 faults; thus, zones of recrystallisation within the massive pyrite that trend subparallel to S1 are

Plate 9.8: Faulted limbs of tight to isoclinally folded chlorite veinlets within the silca-sericite stockwork alteration of the South Adit. Pencil is approximately 6 cm. long.

Plate 9.9: Tight to isoclinally folded quartz veinlets within the chlorite-sericite alteration zone of the siliceous stockwork. Pen is approx. 1 cm. wide.

D1 faults that destroy pre-deformational(?) jointing (Plate 5.3). Similarly, the numerous faults in the Main Hall, identified by profuse quartz veins, have an S1 trend and are therefore probably D1 in age (Map 2).

9.3.1.2 D3 faults

D3 age faults are inferred from surface topographic depressions that cross-cut the S1 foliation but trend subparallel to the D3 kink band cleavage. Locally, displacements of ~ 50m on these faults can be inferred (see southern portion of Map 1).

9.3.2 JOINTING

Absence of slickensides, quartz veins and large-scale displacement characterises joints. In the surface outcrops, most major joints trend subparallel to the D3 cleavage and faults and are therefore interpreted to be D3 in age. Joints are not marked on Map 1.

9.4 MICROSTRUCTURES

No primary structures (eg. perlitic cracks in volcanic rocks) are identified and all microstructures are thought to be deformation-induced.

9.4.1 GRAIN POLYGONISATION

Domains of varying grain size and subgrain formation

in quartz phenocrysts represent strain removal through grain polygonisation (Bell and Etheridge, 1973). Some phenocrysts within the same thin section either show no grain polygonisation or undulose extinction, suggesting that high strain occurred in discrete zones.

9.4.2 ANNEALING

Euhedral pyrite crystals overgrow the penetrative S1 fabric in some rock types, particularly the tuffaceous chert. Within the massive pyrite, 120 degree triple junctions are relatively common and are also thought to have formed during annealing (Plate 5.10). Similarly, pyrite porhyroblasts within the S1 foliation probably reflect high temperature annealing. In most thin sections a later stage of brittle deformation is suggested by granulation of the annealed pyrite edges.

9.4.3 PRESSURE SHADOWS

Well-developed pressure fringes, elongated subparallel to the S1 cleavage, form in the lower strain areas of pyrite crystals and quartz phenocrysts (Plate 5.4). They consist of chlorite, sericite and/or quartz fibres, and locally have a sinuous shape.

9.4.4 CATACLASIS

Pyrite and arsenopyrite crystals within the massive mineralisation are fractured, suggesting a period of

brittle deformation (D1?). The fractures often act as a host to the mobilised, plastically deformed sulphides such as chalcopyrite, galena and sphalerite (Plate 5.8).

9.5 INTERPRETATION AND DISCUSSION

9.5.1 FIRST DEFORMATION

Tight to isoclinally folded chlorite veinlets within the siliceous stockwork have an axial plane cleavage that is subparallel to the S1 cleavage at Tulks Hill, suggesting that these veinlets were folded during D1 and that D1 was a phase of tight to isoclinal folding (Plate 9.8). Numerous other examples of isoclinal folds, all of which have their axial planes subparallel to S1, occur in most of the Tulks Hill rocks: the carbonate-chert stringers in the iron formation are tightly folded, as are quartz veinlets within the siliceous stockwork (Plate 9.9). In these cases the limbs are so compressed that there is little inter-limb material visible. Tight folding of sericite-quartz-sulphide horizons within the tuffaceous chert is also common (Plate 9.10) and a cross-section of the mineralised horizon (T 3) (Fig 9.5) shows that both the mineralised horizon and the chlorite stockwork are repeated as limbs of a large-scale tight to isoclinal fold.

D1 folds are non-cylindrical since both upright and lateral closing is observed, that is, the fold axes are both vertical and horizontal (eg. Plate 9.11). Both of these fold types have axial planes subparallel to S1. In

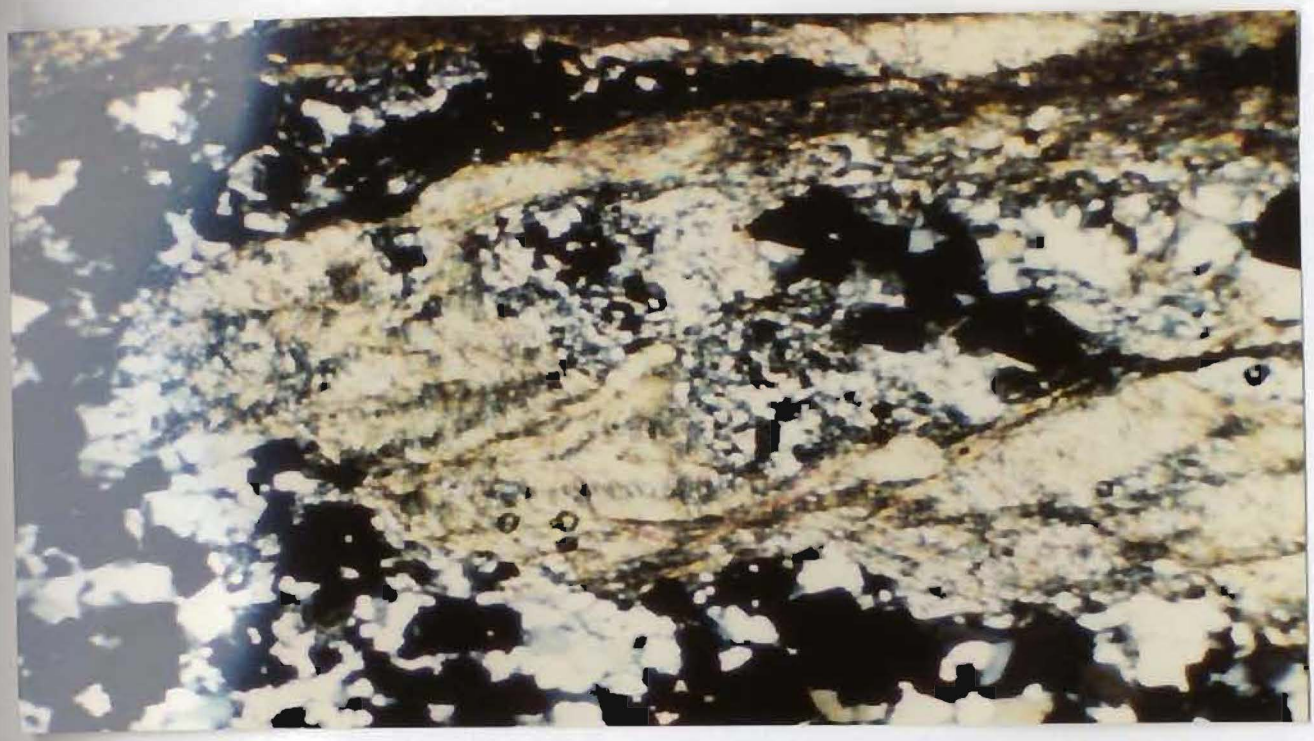

Plate 9.10: Tight to isoclinally folded tuffaceous beds within the tuffaceous chert. A weak crenulation cleavage is developed subparallel to the axial plane of the fold. Note that the chert horizon hosts the pyrite mineralisation. Field of view 0.1mm x 0.07mm (25x magnification).

Figure 9.5: Diagrammatic cross-section of the T3 (a+b) sulphide lens at Tulks Hill. An earlier stage of recumbent folding (D0) is deformed by later tight to isoclinal folding (D1). D0 inverted the stratigraphy but D1 produced the dominant cleavage. The mineralised horizon outcrops at deeper levels towards the south (see section 9.5.4 for a further explanation). S0 and S1 represent the cleavages associated with the recumbent folds (inferred) and the tight to isoclinal folds respectively.

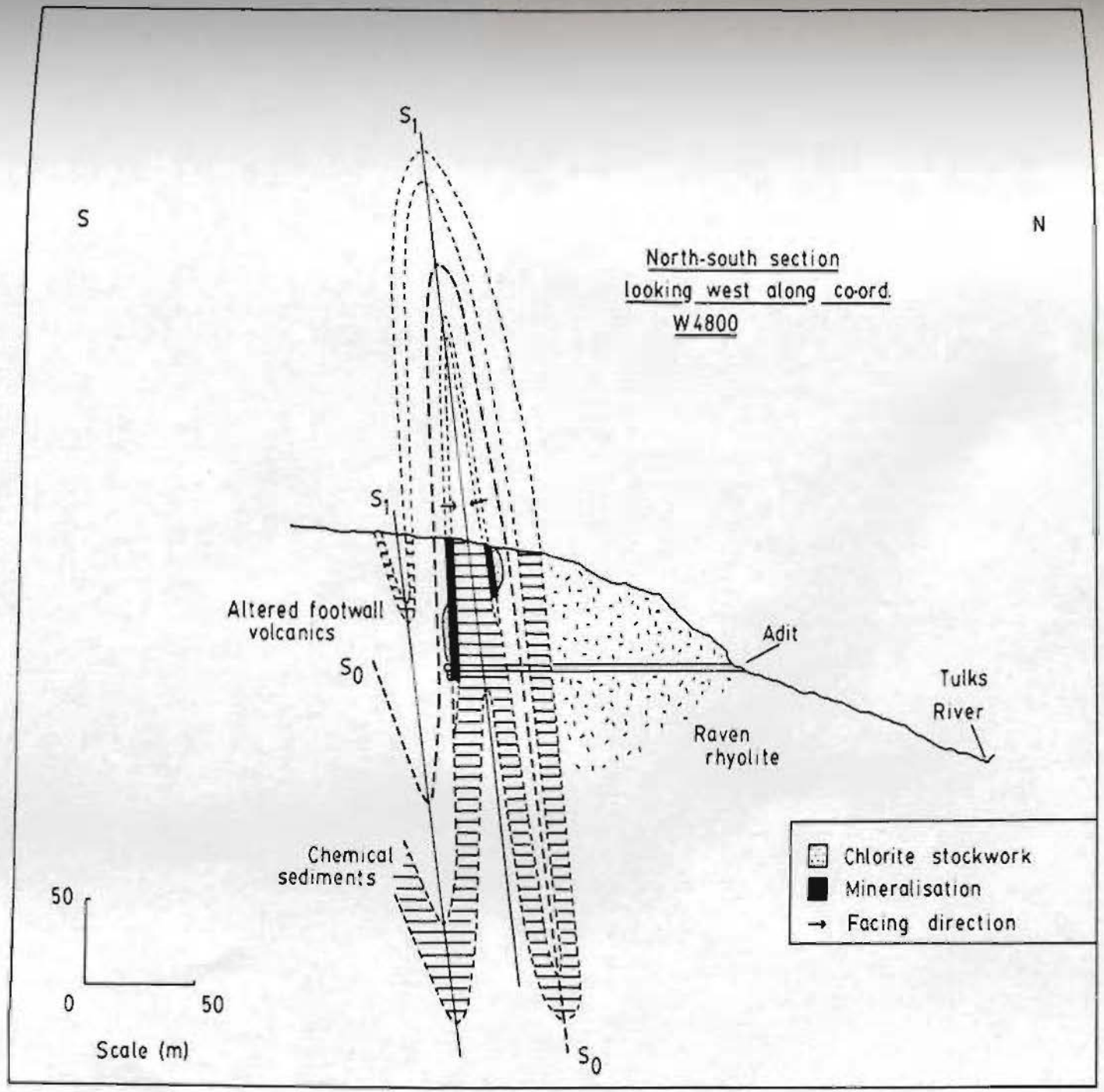
S
N
S_1
North-south section
looking west along co-ord.
W4800
S_1
Altered footwall
volcanics
S_0
Adit
Tulks
River
Raven
rhyolite
Chemical
sediments
50
0
50
Scale (m)
S_0
Chlorite stockwork
Mineralisation
Facing direction

Plate 9.11: Folded pyrite bed closes to the west. The axial plane is vertical. This pyrite bed is exposed in the roof of the East Adit. Pencil is approx. 7 cm. long.

the West Adit the siliceous stockwork contains multiple folds with axial planes oriented East-West. These folds are probably minor folds associated with major folds. If this is true, then the major folds must have their fold axes oriented East-West (as suggested by the chocolate block boudinage effect in the East Adit; Fig. 9.6).

Annealed massive pyrite, as well as individual euhedral pyrite crystals that overgrow the S1 fabric, suggest that higher temperatures post-dated the development of S1 (Stanton, 1964); these features are visible on the scale of a thin section and in hand sample. Such static annealing could have been associated with either of the three deformation phases but the preferential alignment of the euhedral pyrite crystals within the S1 fabric, as well as discrete zones of granulated pyrite trending subparallel to S1, strongly suggests that annealing occurred either during the final stages or shortly after D1. A period of brittle deformation must therefore have post-dated the annealing in order to account for the granulated pyrite. Again it is possible that the brittle deformation could have occurred during any of the three deformation phases --- since the plane of displacement is subparallel to S1 it is thought that the granulation occurred shortly after D1.

It is apparent that the structural events accompanying D1 were complex; that this is the case is indicated by the close association of brittle (faulting, recrystallised quartz) and ductile (pressure shadows) deformation within

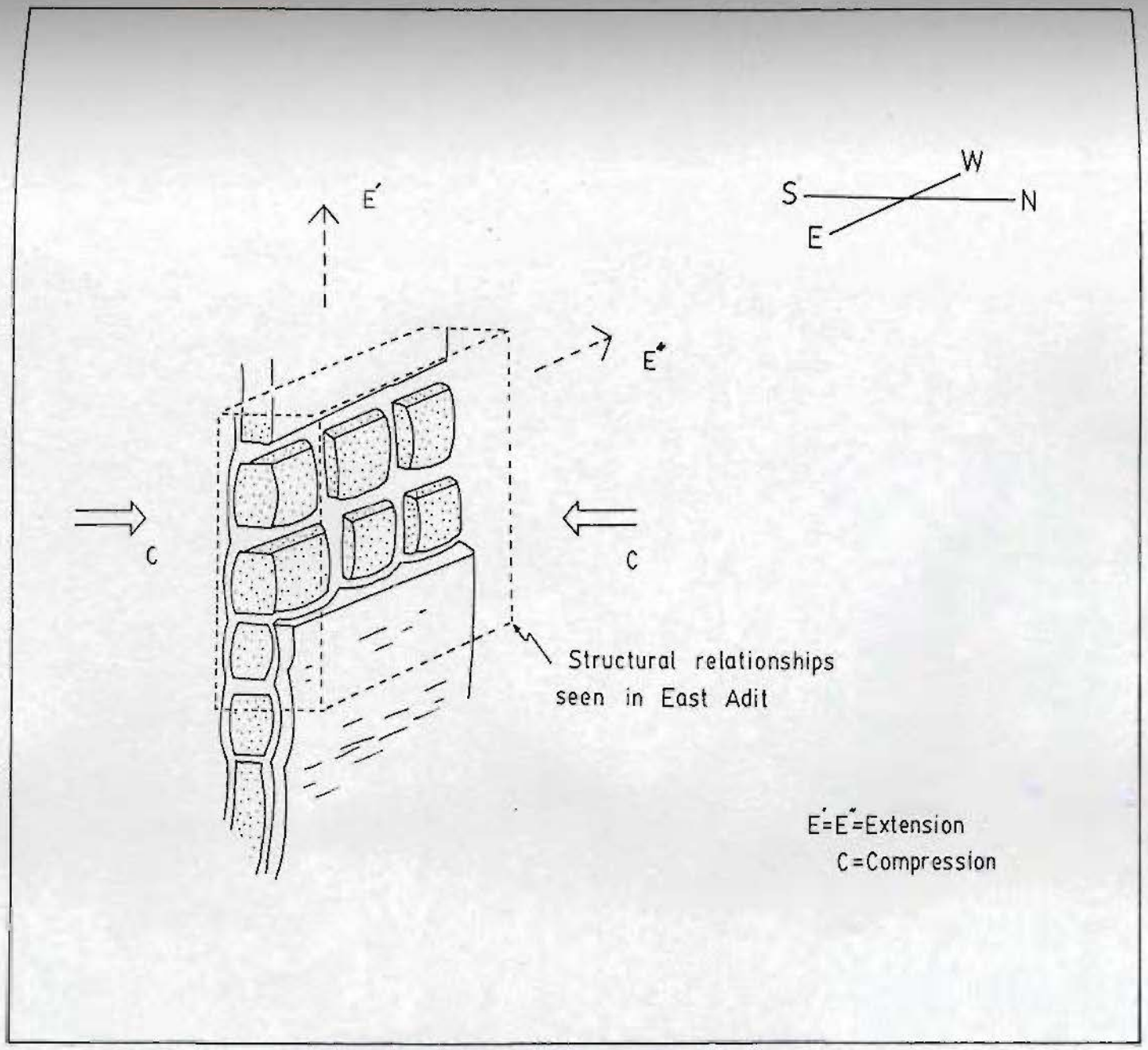

Figure 9.6 : Diagrammatic view of the "chocolate-block" boudinage effect seen in the East Adit. Such a relationship suggests a fold axis trending east-west.

the same thin section. Such an association suggests inhomogenous deformation at low temperatures and low strain rates (Kerrich and Allison, 1978).

9.5.2 SECOND DEFORMATION

F2 fold closures are not abundant at Tulks Hill (see Plate 9.12) which, according to Hobbs et al. (1976), is usually the case with conjugate cleavages. A spaced fracture cleavage often post-dates tight to isoclinal folding (Hobbs et al., 1976) which is further evidence, albeit indirect, that the first phase of folding was isoclinal. Since the S2 cleavage trends subparallel to S1 it is possible that it did not form by a separate deformation event but represents the last stages of D1. Indeed it is possible that all of the phases of deformation are part of one period of continuous deformation.

9.5.3 THIRD DEFORMATION

Experimental evidence suggests that kinking develops in layered rocks that have contrasting mechanical properties (Paterson and Weiss, 1966). At Tulks Hill, the alternations of quartz and sericite within the quartz crystal tuff could produce this contrast; these alternations could be primary bedding differences or a mineral banding formed by mineral segregation during D1 folding, in a manner similar to that described by Cosgrove (1976). Asymmetric folding during D3 probably developed in

Plate 9.12: Possible F2 fold closure with an axial plane trending subparallel to the leather handle of the compass.

response to 5 - 10 % shortening parallel to the S1 foliation (Hobbs et al., 1976).

9.5.4 WAS THERE AN EARLIER DEFORMATION AT TULKS HILL?

Various lines of reasoning suggest that recumbent folding (D0) may have preceeded isoclinal folding (D1) at Tulks Hill:

1. The repetition of the distal portion of the T3 sulphide lens (as T3b which is richer in galena - sphalerite - tennantite) suggests that the sulphide lens has been isoclinally folded

2. Stockwork alteration, which marks the stratigraphic base of the mineralisation, outcrops to the south of the T3 lens but to the north of T3b. This suggests that the two lenses structurally face towards each other.

3. The geometry of both sulphide lenses suggests that they close upwards. If this is so then the tuffaceous chert, which is younger than the mineralisation, lies structurally beneath the mineralisation. One of three mechanisms could invert the stratigraphy: 1) recumbent folding post-dating a period of isoclinal folding, or 2) recumbent folding followed by isoclinal folding, or 3) repetition by thrust faulting followed by isoclinal folding.

Of the three mechanisms option (1) is thought to be the least likely. Evidence for thrust faulting prior to isoclinal folding is not observed but it cannot be

discounted. Perhaps the simplest method of stratigraphy inversion and the generation of a strong schistosity is option (2), that is, isoclinal folding post-dating recumbent folding. It is interesting to note that recumbent and isoclinal folding have been proposed for the deformation in those groups that are stratigraphically equivalent to the Victoria Lake Group, although the relative timing of the fold styles has yet to be resolved: Swinden (Baie D'Espoir Group; 1982) prefers isoclinal folding followed by recumbent folding, whereas Chorlton (La Poile Group; 1980) prefers the reverse. The latter is in keeping with the author's preference for Tulks Hill.

A structural cross-section (Fig. 9.5) of the Tulks Hill deposit (T3 lens) shows the relationship between recumbent folds (F0) and later isoclinal folds (F1). This diagram is a sketch and is not meant to portray exact structural relationships: it is an attempt to explain the stratigraphic facing of the mineralised horizon. It appears that the sulphide horizon is repeated about an antiformal syncline of D1 age. The iron formation that outcrops on the surface at Tulks Hill is thought to be a distal equivalent (relatively speaking) of the iron formation identified in the adit and hence is pinched out at this location. Also it is assumed that the iron formation is either younger than, or is a lateral equivalent of, the tuffaceous chert and they are shown as interdigitated units of "chemical sediment".

It appears that the complex structural relationships at Tulks Hill can be reconciled, in a generalised way, by suggesting an initial phase of recumbent folding to invert the stratigraphy (D0), followed by superimposed tight to isoclinal folding (D1); the latter would account for the overthickening and repetition of many of the rock types at Tulks Hill (eg. the tuffaceous chert). This fold geometry may also explain the localised occurrence of siliceous stockwork in the footwall, minor bedded pyrite horizons within the quartz crystal tuff and the local development of Mg-rich chloritic alteration in areas distant from the mineralisation (note that the trace of the mineralised horizon in this "model" would have a shallow sub-surface outcrop to the south of the mineralisation).

If the large scale aspects of this model are true, it suggests that the mineralised horizon progresses to deeper levels with increasing distance to the south. Thus, if any further sulphide accumulations exist (assuming their deposition on a single stratigraphic horizon) they would be found at depth.

It should be noted however, that this model does not solve all of the stratigraphic problems at Tulks Hill: the spatial geometry of the Raven rhyolite with respect to the D0 and/or D1 folds (and the footwall volcanics) is difficult to evaluate (see Fig. 9.5).

9.6 SUMMARY

Although detailed microstructural and other studies could still be done, three phases of deformation (D1-D3), with associated faulting (F1-F3), can be recognised at Tulka Hill. D1 is the most important deformation event and is characterised by tight to isoclinal folding. Mineral relationships suggests that regional(?) metamorphism, which is thought to have produced annealed textures, probably occurred after or during the later stages of D1:

Fold style	Isoclinal	Conjugate	Kink
Deformation	D1	D2	D3
Metamorphism	----------?		

The effects of D2 and D3 are minimal, the former being characterised by a spaced conjugate cleavage and the latter by kink bands.

Discrete fault zones associated with D1 are thought to have produced recrystallised pyrite. Recrystallised quartz phenocrysts, as well as pressure shadow development subparallel to S1, are also thought to be D1 effects.

The three cleavages at Tulka Hill suggest two distinct directions of compression during deformation: one direction, oriented roughly north-south, was associated with D1 and D2, whereas the second direction, oriented parallel to the S1 and S2 foliations, produced the kink band cleavages associated with D3.

Structural studies in southwest Newfoundland have defined three tectonic events (Wilton, 1983). D1 produced a dominant northeast striking planar fabric that is axial planar to isoclinal folds. This fold style is similar to D1 identified at Tulks Hill. If this similarity is real then the earliest deformation at Tulks Hill (excluding the inferred recumbent folding) must be younger than Middle Devonian, as suggested by radiometric dates of deformed plutons in southwest Newfoundland (Wilton, 1983).

CHAPTER 10

GENETIC MODEL

10.1 INTRODUCTION

This chapter synthesises, and in part summarises, the preceeding six chapters to produce a genetic model: it will attempt to explain the significance of the geology, the alteration mineralogy, their inter-relationship with mineralisation and the effects of later deformation.

10.2 FOOTWALL ROCKS

The footwall rocks to the Tulks Hill deposit are composed of three lithofacies of quartz crystal tuff, coarse volcanic breccias and minor lava flows. Hydrothermal alteration is extensive and primary textures and mineralogies are usually absent. However, a rhyolite-dacite composition is suggested by both trace element data (Zr, Y, TiO2) and petrographic studies.

Microscopic graded beds of albite and crystal-rich rip-up clasts are locally-developed within the quartz crystal tuffs, as are interbeds of black shale. Both features indicate that the tuffs, and therefore the footwall rocks, were deposited in a submarine environment. A lack of internal stratification within the crystal tuffs, their wide areal extent (Map 1) and the presence of isolated, large volcanic blocks within finer-grained tuffs (Plate 4.12), are taken as evidence for their deposition as

submarine ash flows. Welded textures, typical of subaerial ash flows, are absent, although wisp-like sericite horizons may be altered, felsic volcanic glass. It is probable that the interbedded volcanic breccias, which are comparable to the "mill rock" of Sangster (1972), had a similar mode of deposition, representing coarser fractions of the ash flow.

A sub-volcanic intrusion in the northern part of Tulks Hill, called the Raven rhyolite, has an identical trace element chemistry to the footwall volcanics and therefore is thought to be co-magmatic with them. Unfortunately, no contact relationships with the footwall rocks are exposed and it can only be inferred that the rhyolite intrudes the tuffaceous rocks. Assuming this to be the case, then the Raven rhyolite would be equivalent to the "white rhyolite lava domes" of Kuroko deposits (Hashiguchi, 1983; Sato, 1977) or the sub-volcanic intrusions associated with many Archaean Cu-Zn deposits (Franklin et al., 1981). Bleaching and mineralisation of parts of the Raven rhyolite suggest that it did play an integral part in the mineralising process. No penecontemporaneous brecciation of either the host rock or the ore can be attributed to rhyolite intrusion, unlike the rhyolite dome associated with the Uchinotai deposit in Japan (Hashiguchi, 1983), suggesting a passive role for the Raven rhyolite during mineralisation.

Thus, prior to mineralisation and hydrothermal alteration, Tulks Hill was blanketed by submarine ash flows and intruded by the Raven rhyolite, either as a dome or as

a sill.

10.3 ALTERATION

A hydrothermal system developed after the deposition of the ash-flow tuffs. Two styles and intensities of alteration are recognised, both of which appear to relate to alkali dominance in the hydrothermal fluid(s).

Chequerboard albite, with calcite and/or epidote inclusions, is common in the footwall rocks and suggests replacement of preexisting (probably magmatic) feldspar (Battey, 1955). In the absence of a regional geochemical survey, which might highlight Na metasomatism as being typical for the Victoria Lake Group, it is suggested that the albite is hydrothermal (as opposed to metamorphic). If this is true then migration of the hydrothermal fluid(s) through the volcanic pile would either "reconstitute" magmatic albite and remove Ca, or exchange K for Na during albitisation of magmatic K-feldspar. This would produce a chemically pure albite and release K, and some Ca, to the fluid.

The alteration assemblage sericite-albite is common in the footwall rocks, either as discrete minerals or as a slight sericite dusting of albite. The coexistence of the two minerals reflects the variation in K^+, Na^+ and H^+ ion activity in the solution, as shown in Figure 4.2. Perhaps the simplest way to vary the K^+, Na^+ and H^+ ion content in the fluid is through alteration. For example, albitisation

of magmatic K-feldspar would release and concentrate K+ ions in the solution and so increase the chances of sericite formation. It seems reasonable to suggest that the chemical evolution of the fluid with time is an adequate way to explain the coexistence of Na (albite) and K (sericite) minerals.

Other alteration effects within the footwall rocks include the development of scaly sericite mats, Fe-Mg chlorite, as well as quartz overgrowths on primary quartz phenocrysts.

For a hydrothermal fluid to flow through a rock at least two requirements must be satisfied: 1) the rock should be permeable, and 2) a geothermal gradient is needed to provide the impetus for fluid movement. At Tulks Hill, the tuffaceous rocks in the footwall would be an adequate permeable medium. Recent theoretical modelling of fossil hydrothermal systems associated with Kuroko-type deposits has shown that the heat generated during cooling of a lava dome is not sufficient to support the relatively long-lived hydrothermal systems necessary for sulphide deposits (Cathles, 1977; Ohmoto, 1978; Ohmoto et al., 1983). Therefore, the Raven rhyolite is excluded as a possible localised heat source. Most workers prefer a heat source generated by the cooling of a sub-volcanic intrusion, the latter typically at a depth of 2-4 kms. below the fossil seawater-rock interface. It probably is not a coincidence that such intrusions are common in the footwall of

volcanogenic massive sulphide deposits (Franklin et al., 1981). At Tulks Hill, the Costigan Lake Intrusion (informal), located approx. 6 kms. to the south of the mineralisation, is a likely candidate as a localised heat source. It is possible that this intrusion was the source of the ash-flow tuffs that outcrop at Tulks Hill, their eruption caused by a process akin to caldera collapse. Such a process would have created a fractured, and therefore permeable, environment which should have enabled easier migration of hydrothermal fluids.

An intensely altered rock, known as stockwork alteration, reflects a concentration of hydrothermal fluid flow immediately beneath the sulphide deposit. The two lithofacies that are identified (siliceous and chloritic stockwork) are genetically linked with the mineralisation because of 1) gradational contacts of the siliceous stockwork with a bed of massive pyrite in the East Adit (Map 2); 2) Mg chlorites in the chlorite stockwork and as a gangue mineral to the sulphide mineralisation; and 3) high background counts for base metals in stockwork alteration samples. For these reasons, and because the rock outcrops only at the stratigraphic base of the sulphide horizon, it is interpreted to mark the fossil feeder for the hydrothermal fluids.

Similar phenocryst textures and trace element chemistry, as well as gradational contacts with the less

altered footwall rocks, suggest that the stockwork alteration had a rhyolitic tuff as a protolith.

Both Na2O and CaO are depleted within the stockwork which is in marked contrast to the enrichment of these oxides in the footwall volcanics and Raven rhyolite, respectively. Conversely, K2O and MgO are enriched in the stockwork. As a consequence of the enrichment / depletion of these oxides sericite and chlorite are dominant but albite is absent. Quartz pseudomorphs after feldspar suggest its destruction, possibly by the following reaction:

$$2NaAlSi_3O_8 + 5FeS_2 + 2H^+ + 13H_2O \rightleftharpoons$$

$$(Fe_5Al)Si_3AlO_{10}(OH)_8 + 2Na^+ + 10H_2S + 3SiO_2 + 5/2\ O_2$$

(Froese, 1981)

Pyrite is preserved in the stockwork suggesting that it was in excess during albite destruction (see reaction above). Pyrite, sphalerite and/or chalcopyrite veinlets in the stockwork are relics of fluid channelways in a fossil feeder pipe (now deformed).

10.4 SULPHIDE DEPOSITION

Massive beds of pyrite and sphalerite mineralisation overlie the stockwork alteration zone, ie. they overlie the feeder "pipe". Their massive nature suggests that the seawater depth was great enough to prevent premature fluid boiling and consequent formation of vein-type deposits in the subsurface (Ridge, 1973). Caldera collapse may have

rapidly depressed the palaeo- seawater-rock interface to a great enough depth to prevent such boiling, an hypothesis offered by Ohmoto et al. (1983) to explain the sinking of the Hokuroko district immediately prior to mineralisation.

A reduced environment surrounding the hydrothermal fluid vent is suggested by the absence of barite and oxide minerals (eg. magnetite). Sulphide precipitation probably ocurred through a combination of a simple temperature drop and a pH increase upon mixing with seawater. Ce-depletion in some samples and Mg-rich chlorites in the gangue suggest seawater interaction. Fluid boiling may have aided destabilisation of the metal-chloride complexes in favour of metal-sulphide complexes since Mn-rich carbonate, which precipitates when the fluid boils (Holland and Malinin, 1979), is found within some samples of siliceous stockwork alteration.

A paragenetic sequence of sulphide deposition cannot be determined at Tulks Hill because of remobilisation and/or annealing during later periods of deformation. However, a crude, megascopic, zonation of the deposit, from a Cu-rich footwall through a zinc horizon (T3 lens) into a galena-rich (T3b only) hangingwall, can be identified, the sequential precipitation probably reflecting the decreasing temperature and/or pH gradient away from the feeder. A decrease in the mole % FeS in sphalerite with increasing proximity to the hangingwall mirrors the mineral zonation, suggesting a decrease in fS_2 with increasing distance from

the discharge site (Scott and Barnes, 1971).

Precipitation of the sulphides during a hiatus in explosive volcanic activity is suggested by the lack of coarse volcanic detritus. Also, there is no evidence of mechanical reworking of the sulphides which not only suggests that the environment of deposition was relatively stable (cf. Buchans), but that the present location of the sulphides is primary. This implies sulphide precipitation immediately above the feeder, and it is speculated that the hydrothermal fluid was similar to the Type 2b fluids described by Sato (1972), as illustrated in Figure 10.1. Type 2b fluids are initially less dense than seawater and initially plume upwards, mix with seawater and increase their density to eventually collapse back onto the discharge zone. This results in a relative abundance of sulphides close to the feeder. The limited lateral extent of the chemical sediments, overlying the mineralisation, may reflect ponding of the sulphides into a depression (Point A) rather than exhalation from a seafloor "high" (as suggested by Sato; see Fig. 10.1).

Gangue minerals are similar to those in the footwall rocks: sericite, chlorite and quartz are dominant, although albite and carbonate are locally developed.

10.5 CHEMICAL SEDIMENTS

Renewed volcanic activity coincided with the deposition of the tuffaceous chert and iron formation,

Figure 10.1: A) TOP The four types of hydrothermal solution and their probable behaviour upon discharge into a submarine environment, defined according to their initial temperature and salinity relationships (see B below). After Sato (1972). Type 1: density of the hydrothermal solution is always greater than seawater and the solution will flow downslope to collect in a stratified brine pool. Type 2a: hydrothermal solution is initially denser than seawater (point b in Fig. 10.1B) and becomes even more dense upon mixing with seawater so that solution initially plumes upwards but eventually moves downslope. Type 2b: see text. Type 3: hydrothermal solution is always less dense than seawater and plumes upwards so that sulphides are dispersed.

B) BOTTOM The four patterns of density change due to the mixing of a hydrothermal solution and seawater. The Tulks Hill fluid is thought to have been similar to a Type IIb fluid.

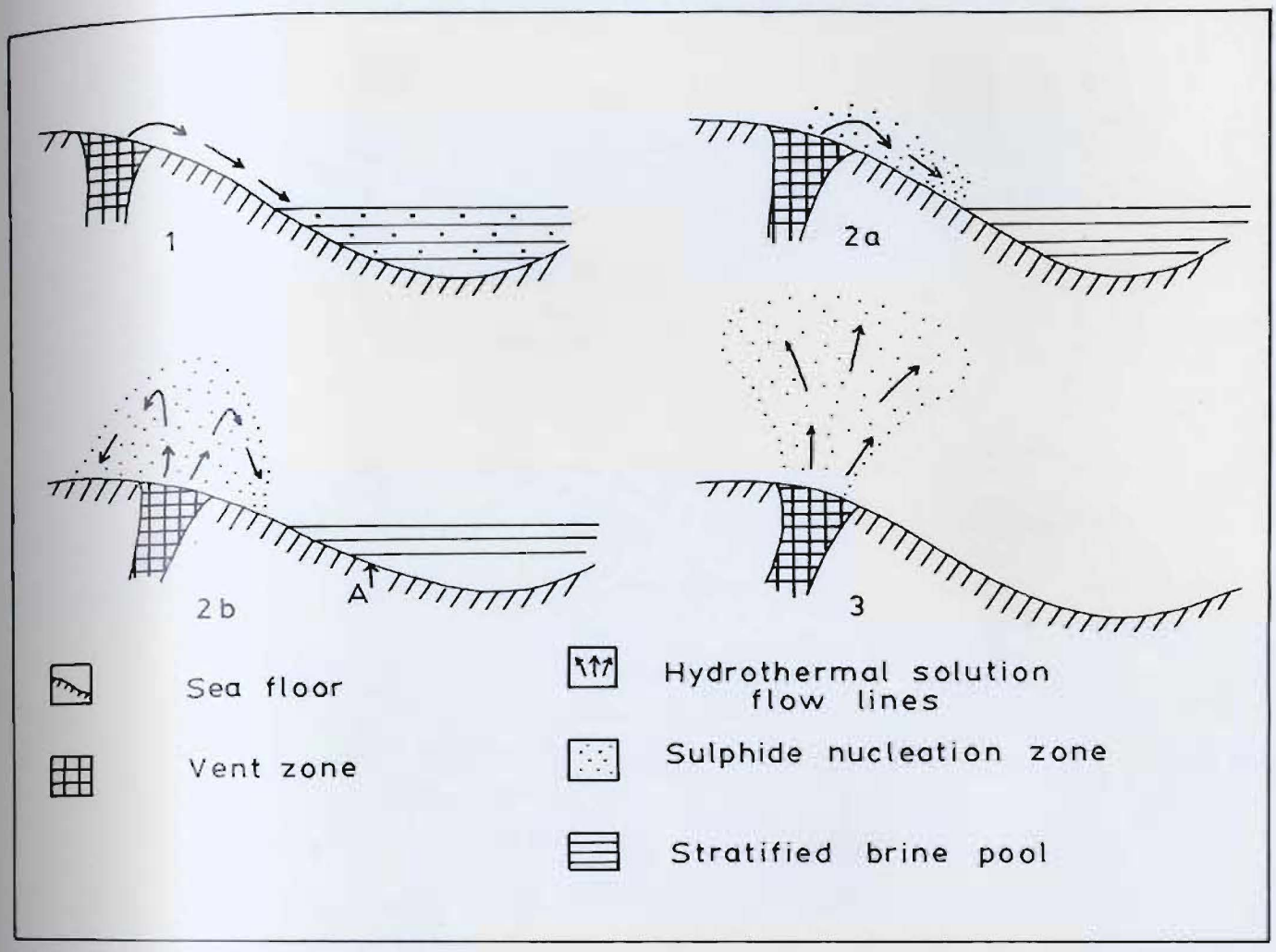
1
2a
2b
A
3
Sea floor
Vent zone
Hydrothermal solution flow lines
Sulphide nucleation zone
Stratified brine pool

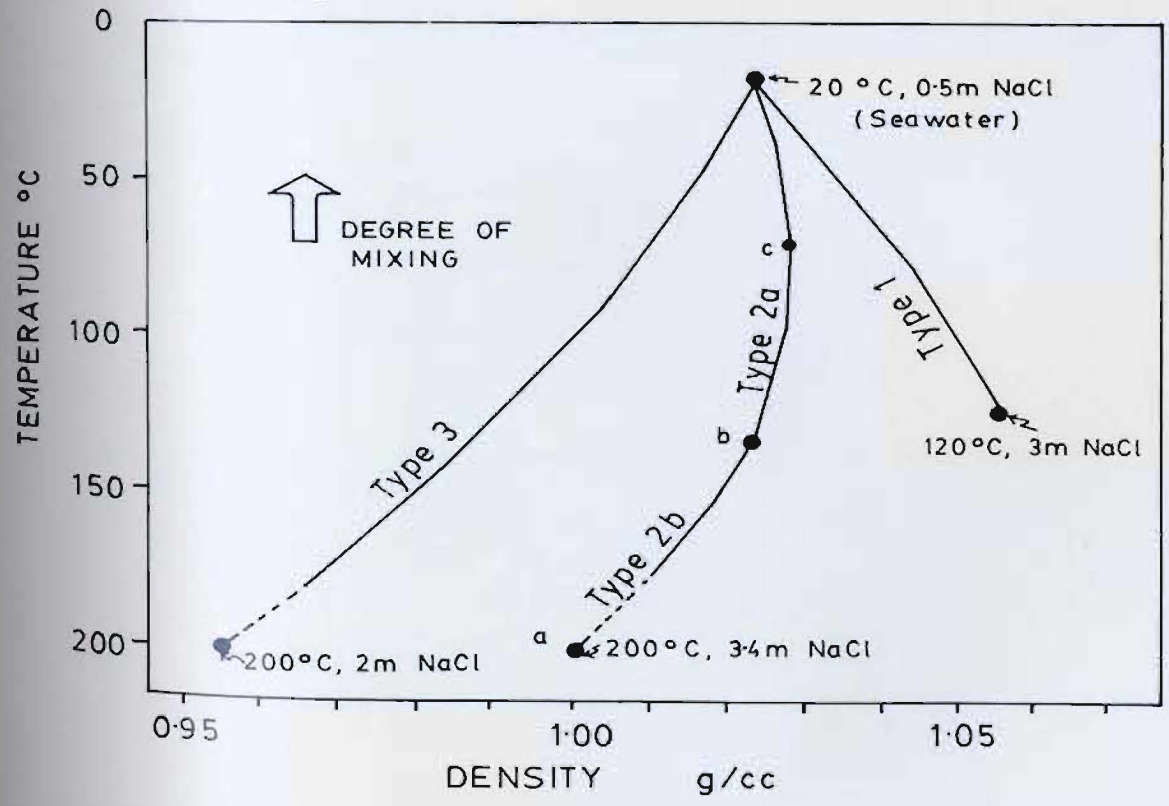
0
50
100
150
200
TEMPERATURE °C
0·95
1·00
1·05
DENSITY g/cc
DEGREE OF MIXING
20 °C, 0·5m NaCl (Seawater)
Type 1
Type 2a
Type 2b
Type 3
a
b
c
200°C, 2m NaCl
200°C, 3·4m NaCl
120°C, 3m NaCl

which overlie the mineralisation, as suggested by the thin (< 2 cm.) beds of tuff (now sericite and/or chlorite). Pyrite is the only sulphide identified which implies either that the bulk of the metal in the fluid was precipitated at the mineralised horizon or, the physico-chemical conditions during depostion of the chemical sediments were not conducive to sphalerite, galena and/or chalcopyrite precipitation. Since both chemical sediments have an abundance of quartz the hydrothermal fluid was probably silica saturated. Simple cooling of the solution, upon mixing with seawater, would precipitate amorphous silica (Alexander et al., 1954; Rimstidt and Barnes, 1980) and increase the pH to allow carbonate deposition.

A Mn-enrichment characterises the dolomitic carbonate of the chemical sediments at Tulks Hill. Manganosiderite is common in the chert capping of the mineralisation of the Atlantis II Deep (Backer, 1975). This indirectly suggests hydrothermal precipitation of carbonate at Tulks Hill. Such precipitation could occur at the same time as the chert, or more likely, by a process of "hydrothermal diagenesis". The latter would be equivalent to the fluid-leakage mechanism proposed by Japanese geologists to explain the hangingwall alteration in some Kuroko deposits. These same fluids probably altered K-rich volcanic detritus within the chert to produce the sericite.

The iron formation is thought to be the youngest rock type identified at Tulks Hill. Its wider outcrop, compared

to the tuffaceous chert, suggests a spatial and temporal widening of the area of quartz deposition as the hydrothermal fluid characteristics expanded into the seawater.

10.6 CHEMICAL CONDITIONS DURING SULPHIDE DEPOSITION

10.6.1 INTRODUCTION

Mineral stability diagrams are used to estimate some of the solution parameters during sulphide deposition. The mineral relationships on these diagrams will reflect both the accuracy of the thermodynamic data and the physico-chemical conditions chosen for their construction. For example, temperature, sulphur fugacity and/or the activity of certain components (eg. K+ ions) can be specified (or assumed) to show how the stability of certain minerals varies as a function of fO_2 and pH (see Fig. 10.5, for example). Since a hydrothermal system is dynamic, the physico-chemical conditions are continuously changing during alteration and sulphide deposition so that the mineral stability diagrams reflect only one instance in time when the chosen physico-chemical conditions were coincident. Also, when using these diagrams to interpret the mode of deposition one must assume that post-depositional changes, such as diagenesis and metamorphism, have not significantly altered the primary mineral assemblage. Considering these approximations and assumptions it is obvious that the solution parameters can

be only a rough approximation.

10.6.2 TEMPERATURE AND SULPHUR FUGACITY DURING SULPHIDE DEPOSITON

The required mineral assemblages needed for certain geothermometric techniques are absent so that the method of Kajiwara (1970), which uses the Ag content of electrum and the mole % FeS of sphalerite, is used to estimate both the temperature and the sulphur fugacity at the time of sulphide deposition.

At Tulks Hill, the mole % FeS of sphalerite varies from 5.9 to 2.71 and an average value for the Ag content of electrum is 32 % (Jambohr, 1983). Using these data (Fig. 10.2) the results are as follows:

Mole % FeS	5.9	2.71
Sulphur fugacity:	10(-8) to	10(-10)
Temperature:	355 C. to	280 C

Using Figure 10.3 the activity (or fugacity) of S2, at an average temperature of 300 degrees centigrade and within the range of sphalerite compositions at Tulks Hill, varies between 10 (-9.5) and 10 (-8.5) which is in good agreement with the fugacity of S2 determined by the method of Kajiwara (1970). Figure 10.3 also shows that the range in sulphur fugacity at 300 degrees centigrade is within the pyrite field only, and since the mole % FeS in the

Figure 10.2: Temperature-fS2 diagram of selected components of Kuroko ores used to establish the temperature of sulphide precipitation at Tulks Hill. Solid lines = mineral phase boundaries; dashed lines = iso-activity curves of FeS in sphalerite: 1 = ~4 mole % FeS; 2 = ~2.5 mole % FeS; 3 = ~0.4 mole % FeS; 4 = ~0.15 mole % FeS. Dotted lines = electrum tarnish curves: a = ~55 wt.% Ag; b = ~35 wt.% Ag; c = ~22 wt.% Ag. (From Kajiwara, 1970).

Figure 10.3: Temperature-aS2-composition diagram for the system Fe-Zn-S, showing the composition of sphalerite in equilibrium with an iron bearing phase. Sphalerite isopleths within the pyrrhotite and pyrite fields are from Scott and Barnes (1971) and Barton and Toulmin (1966) respectively. Redrawn from Barton and Skinner (1979).

The range in aS2 is shown by the light shading; at 300 C (the average temperature of sulphide deposition at Tulks Hill) the aS2 is shown by the heavy shading. Line 1 = ~2.71 mole % FeS in sphalerite; line 2 = ~5.9 mole % FeS in sphalerite.

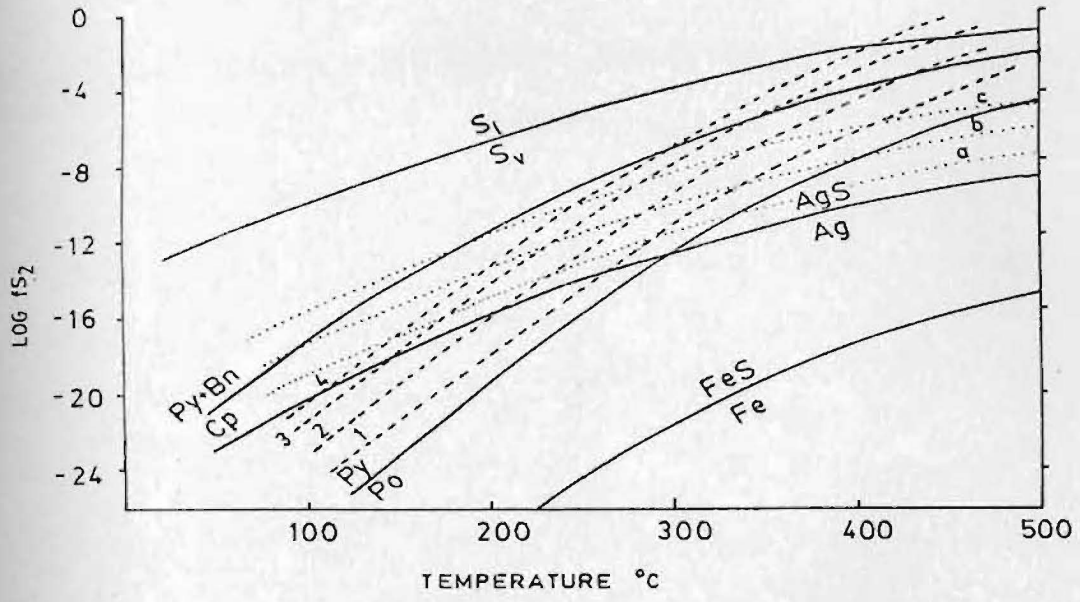
0
-4
-8
-12
-16
-20
-24
LOG fS_2
100
200
300
400
500
TEMPERATURE °C
S_l
S_v
Py·Bn
CP
Py
Po
AgS
Ag
FeS
Fe
a
b
c
1
2
3
4

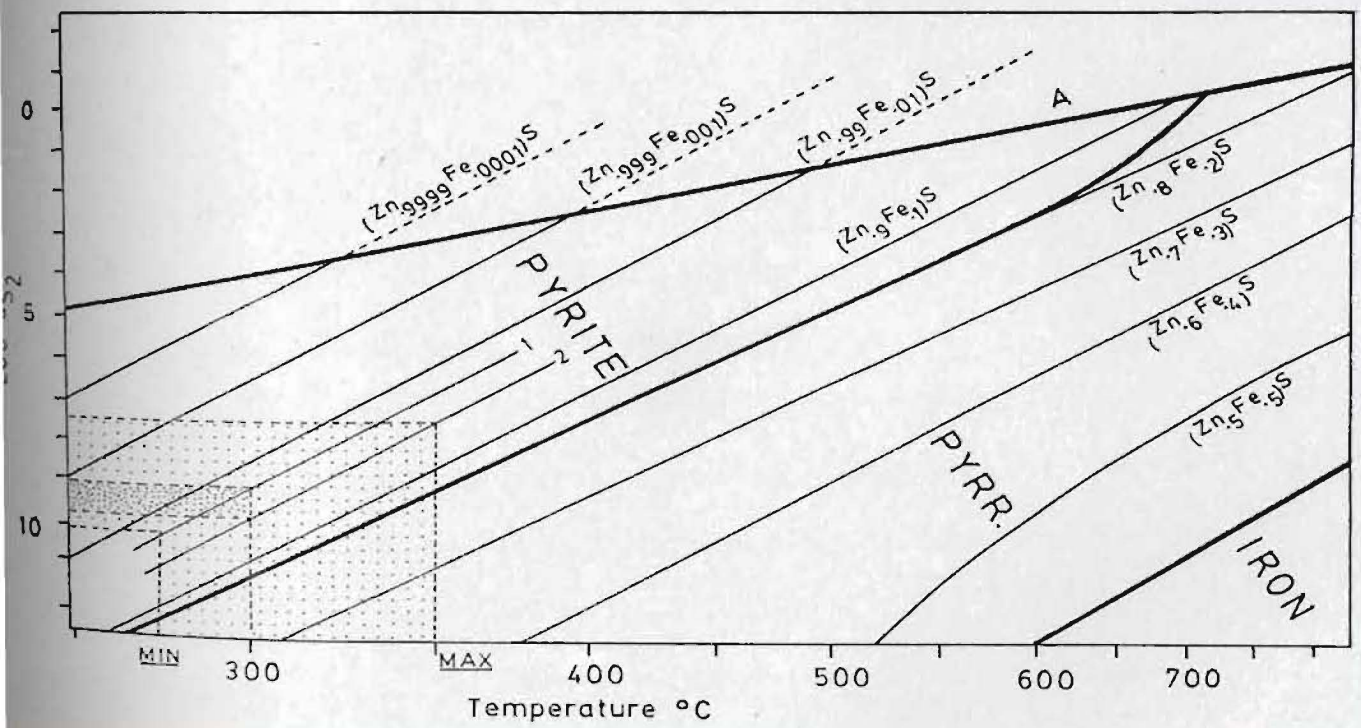
0
5
10
fS_2
$(Zn_{.9999}Fe_{.0001})S$
$(Zn_{.999}Fe_{.001})S$
$(Zn_{.99}Fe_{.01})S$
A
$(Zn_{.9}Fe_{.1})S$
$(Zn_{.8}Fe_{.2})S$
$(Zn_{.7}Fe_{.3})S$
$(Zn_{.6}Fe_{.4})S$
$(Zn_{.5}Fe_{.5})S$
PYRITE
1
2
PYRR.
IRON
MIN
MAX
300
400
500
600
700
Temperature °C

sphalerite is interpreted to be primary, it strengthens the suggestion that primary pyrrhotite was not precipitated at Tulks Hill.

Urabe and Scott (1983), using paragonite, carbonate and sulphur isotope geothermometers, estimated the temperature of ore deposition at the South Bay Mine, Ontario to be 300 degrees centigrade. Since this temperature is approximately the temperature of ore formation at Tulks Hill their log aO2 - log aS2 can be used to independently confirm the estimate of the sulphur activity at Tulks Hill (Fig. 10.4). Based on the absence of pyrrhotite and the local development of the assemblage bornite-pyrite (Chapter 5) the fS2 probably ranged from a minimum of 10 (-11) to a maximum of 10 (-7). This range agrees well with the fS2 values determined using Figures 10.2 and 10.3 and implies that 300 degrees centigrade is a reasonably accurate temperature for deposition of mineralisation at Tulks Hill.

The reduction in temperature (50 degrees), sulphur fugacity and mole % FeS of sphalerite at Tulks Hill, corresponds to an increased proximity of the hangingwall. It is likely that this reduction was caused by cooling of the reduced, acidic mineralising solution by mixing (and/or boiling) with seawater. This would precipitate the metals, oxygenate the solution (and thereby reduce the sulphur activity), permit carbonate precipitation and lower the FeS content of sphalerite; such a process is compatible with

Figure 10.4: Log aO2 - log aS2 diagram for 300° C and CO2 activity of 0.001. Redrawn from Urabe and Scott (1983) with data from Robie *et al.* (1978). Estimated conditions of deposition of the Tulks Hill sulphides ("ore") and the iron formation (IF) are shown.

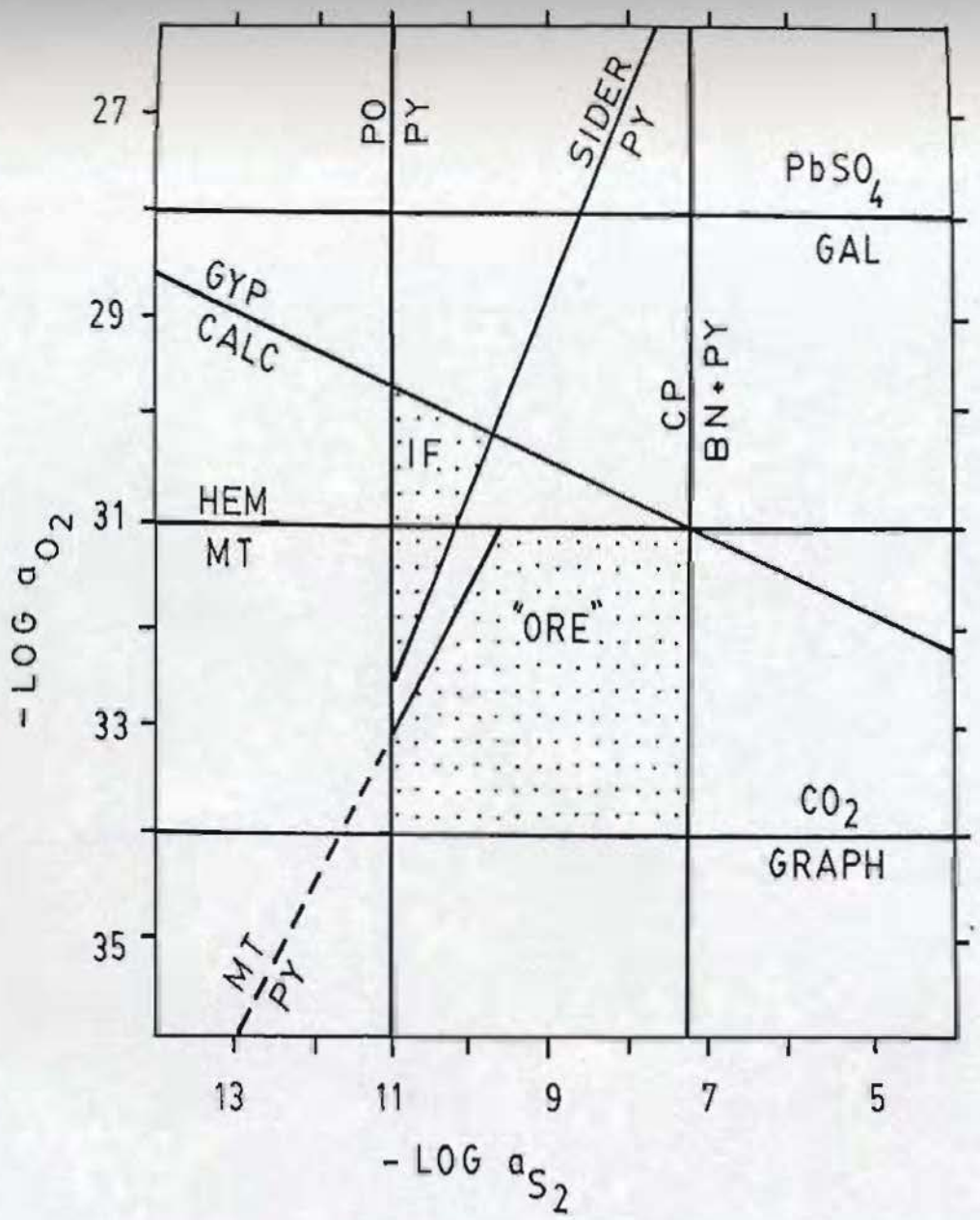
27
29
31
33
35
PO
PY
SIDER
PY
PbSO4
GAL
GYP
CALC
CP
BN + PY
IF
HEM
MT
"ORE"
CO2
GRAPH
MT
PY
13
11
9
7
5
- LOG aO2
- LOG aS2

the current models of sulphide genesis (eg. Hutchinson, 1982).

10.6.3 OXYGEN FUGACITY

At 300 degrees centigrade, and when the log fS2 varies between 10 (-11) and 10 (-7), the upper limit of the oxygen fugacity is marked by the absence of anglesite (approx. 10 (-28); Fig. 10.4) while its lower limit is marked by the absence of pyrrhotite (approx. 10 (-34)). The absence of gypsum at Tulks Hill further constrains the upper limit of the oxygen fugacity to between approx. 10 (-30) when the fS2 = 10 (-11) and approx. 10 (-31) when fS2 = 10 (-7).

10.6.4 ACIDITY-ALKALINITY

Figure 10.5 (Froese, 1981) shows the stability fields of sphalerite and chalcopyrite and some silicate minerals (under specific conditions) in pH - log fO2 space. Also shown is the maximum pH limit of sericite stability under these conditions. The temperature decrease that causes sulphide precipitation (Skinner, 1979) will be accompanied by an increase in the fluid pH and fO2, either through fluid boiling (loss of volatile component), wall rock reaction and/or mixing with alkaline seawater. With this in mind a line of increasing pH-fO2 (X-Y) is drawn on Figure 10.5, its location reflecting both the mineralogy of the deposit and the estimated fO2. Experimental studies show that chalcopyrite precipitates at lower fO2 and pH

Figure 10.5: Log f02 - pH diagram showing the stability of various silicates and sulphides at 300 C, activity of sulphur = 10 (-2) and mNaCl = 3.0. Superimposed (line A) is the stability of sericite, by the hydrolysis of K-feldspar, when the activity of K+ = 0.5 (Froese, 1981).

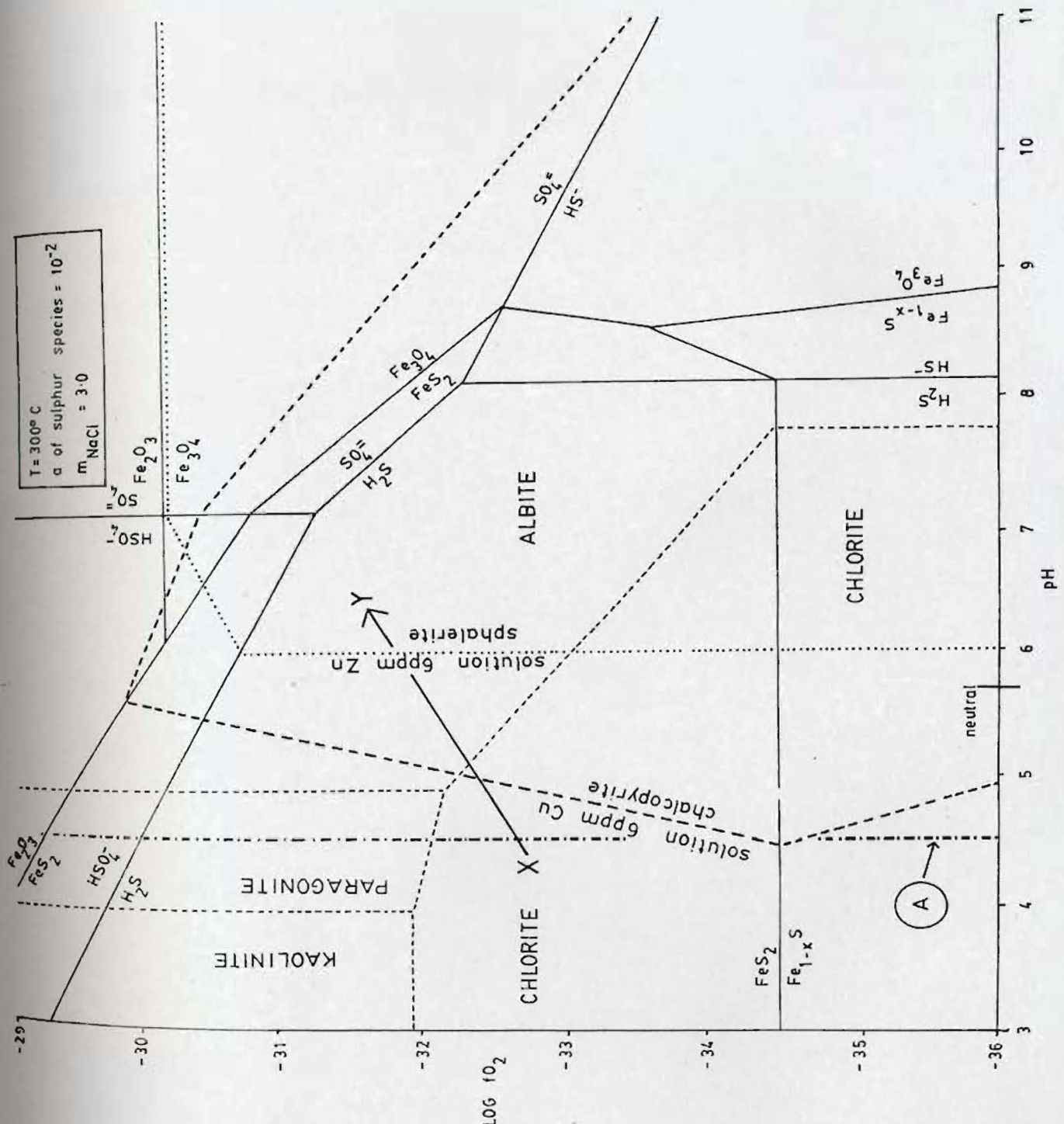
T = 300° C
a of sulphur species = 10⁻²
m NaCl = 3·0
Fe2O3
Fe3O4
SO4=
HSO4-
Fe3O4
FeS2
SO4=
H2S
SO4=
HS-
Fe3O4
Fe1-xS
H2S
HS-
ALBITE
CHLORITE
solution 6ppm Zn
sphalerite
Y
X
solution 6ppm Cu
chalcopyrite
neutral
A
Fe2O3
FeS2
HSO4-
H2S
PARAGONITE
KAOLINITE
CHLORITE
FeS2
Fe1-xS
-29
-30
-31
-32
-33
-34
-35
-36
LOG fO2
3
4
5
6
7
8
9
10
11
pH

values than sphalerite (under the conditions specified) when Cu and Zn are dissolved in equal concentrations in the solution (Barnes, 1975; see Fig. 10.5). Since sphalerite mineralisation overlies chalcopyrite mineralisation at Tulks Hill it suggests that the zonation of minerals reflects the zonation in pH-fO2 shown by the line X-Y.

It should be noted that the line X-Y reflects a spatial zonation only: recent work concerning the Kuroko-type deposits (Eldridge et al., 1983) suggests that chalcopyrite precipitates after sphalerite. Rapid cooling of the solution at the seawater-rock interface causes immediate precipitation and deposition of the lower temperature sulphides (galena-sphalerite) to form a "sulphide blanket" which produces an insulating effect. The result is that higher temperatures predominate beneath the earlier precipitated sulphides which permits only chalcopyrite deposition.

In Figure 10.5 the field for chlorite stability overlaps the fields of stability for chalcopyrite and sphalerite. Since sphalerite is absent from the Mg-chlorite stockwork at Tulks Hill it can be assumed that their stability fields did not overlap. A possible explanation is that either the high Mg content of the chlorites restricted the stability of chlorite to lower pH-fO2 values (Froese, 1981) or, the solution contained lower Zn concentrations so that the sphalerite field was restricted to higher pH values (under the conditions

specified). Since a Zn concentration of 6 ppm is thought to be the minimum required for sulphide precipitation (Barnes, 1979), and the fact that some present-day hydrothermal systems have a much greater abundance of Zn (eg. 540 ppm Zn in the Salton Sea brines; Weissberg et al., 1979) the former explanation is preferred. Thus, the chlorite stability field probably lies to the lower pH side of the Cu solution-chalcopyrite boundary. This suggests that a low pH prevailed during the formation of the chlorite schist and chalcopyrite deposition (even at a minimum solution concentration of 6 ppm) whereas sphalerite precipitation probably occured at near neutral or only slightly acidic conditions.

The upper limit to the pH is marked by the virtual absence of hydrothermal albite within the stockwork alteration and the mineralisation. At the lowest possible fO2 (10 (-34.5)), under the conditions specified, albite would be stable only at a pH > 7.8 suggesting that a fluid pH > 7.8 was rarely attained.

Froese (1981) determined that sericite formation at 300 degrees centigrade, typically from the hydrolysis of K-feldspar, occurs when the fluid pH is higher than 4.41 and the K+ ion concentration in the solution is 0.5 (Fig. 10.5). The assemblage sphalerite-sericite is stable in the siliceous stockwork suggesting their coeval formation. According to Figure 10.5 however, sphalerite precipitation is restricted to higher pH values than that of sericite,

which suggests that either, 1) the physico-chemical conditions at Tulks Hill differed from those assumed by Froese (1981) to calculate the stability of muscovite (eg. different activity K+) so that it actually forms over a much wider range, or at least at higher pH values, or 2) the Zn concentration in the solution was much higher than 6 ppm, which may have induced earlier sphalerite precipitation.

A combination of the two mechanisms is probable, not only because most present-day hydrothermal solutions contain > 6 ppm Zn (see above), but because the assemblage sericite-chalcopyrite is only locally developed implying a higher pH for the formation of sericite (approx. 5.0?)

10.6.5 SUMMARY OF THE CHEMICAL CONDITIONS DURING ALTERATION AND SULPHIDE DEPOSITION

Mineral stability diagrams, constructed from thermodynamic data, have been used to estimate the solution characteristics during sulphide precipitation. Although these diagrams simplify conditions somewhat, to reduce the number of variables to a manageable quantity, they do provide one means of qualitively evaluating the significance of the sulphides and silicates with respect to the chemical and physical environment. Table 10.1 is a summary of the conditions for the Tulks Hill deposit.

Table 10.1: Summary of the physico-chemical conditions during hydrothermal alteration and sulphide deposition. In all cases the upper and lower limits represent the maximums determined by the various methods described in the text.

S fugacity	O fugacity	Temp. (°C)	pH	mole % FeS	
Max 10 (-11)	Max 10 (-30)	280	Max ~7.8 ~5.5	2.71	H.W.
10 (-7)	10 (-34.5)	355	~4.0	5.90	F.W.

10.7 FLUID FLOW AND COMPOSITION

10.7.1 FLUID:ROCK RATIO

According to Mottl (1983) the assemblage chlorite+quartz develops at seawater:rock ratios > 50 whereas chlorite+quartz+albite occurs between 35 and 50 the implication being that albite will only form at lower SW/R ratios. Since albite is absent from the chlorite stockwork this rock type probably represents an area of high fluid flow, which is compatible with its interpretation as being a fossil feeder vent, whereas albite in the remainder of the footwall rocks suggests a lower fluid:rock ratio (deeper areas of the system?).

10.7.2 FLUID COMPOSITION

It is generally accepted that seawater is the dominant component of the hydrothermal solution during massive sulphide deposition (Hutchinson, 1982; Ohmoto and Skinner, 1983; Spooner and Bray, 1977) although arguments for a magmatic component have recently been proposed (Urabe et al., 1983; Bryndzia et al., 1983). It is probable that seawater was a dominant component of the hydrothermal fluid at Tulks Hill since Mg-chlorite, Mg-carbonate and Ce-depletion anomalies all suggest seawater interaction (Heming and Rankin, 1979; Mottl, 1983).

From the alteration mineralogy in the footwall volcanics it is evident that K^+, Na^+ and Mg^{++} were prominent components of the fluid, the latter two ions

probably being derived from seawater (Mottl 1983; Rosenbauer et al., 1983) The K content would probably reflect Na^+:K^+ ion exchange during albitisation of magmatic feldspar. Rhodocrosite-rich carbonate within the siliceous stockwork alteration and iron formation not only suggests the presence of Mn^{++} but also a high CO_3^{--} ion activity near the seawater-rock interface.

REE abundances for samples from the Raven rhyolite and the siliceous stockwork can be explained by Cl^- ion complexing and leaching of LREE, and possibly CO_3^{--} complexing and stabilisation of HREE during alteration (Taylor and Fryer, 1982, 1980, 1983); these ions must have been prominent in the fluid, the Cl^- possibly complexing with, and therefore transporting, the metals (Barnes, 1979).

Since the sulphides are precipitates from the hydrothermal fluid their mineralogy is a direct consequence of the fluid composition: Fe, Cu, Zn, Pb, As, Sb, Ag and Au must have been carried in solution, predominantly as Cl^- complexes, but probably also as aqueous species of Te, Se, etc. (Barnes, 1979).

10.7.3 METAL SOURCE

A source for the metals within the solution is difficult to determine: current theories are divided between a magmatic source (eg. Sawkins and Kowalik, 1981; Urabe et al., 1983) and a leaching process as the fluid

traverses the footwall volcanic pile (Hutchinson, 1982; Stephens et al., 1983). In the absence of any definitive evidence (eg. isotope data) a combination of the two mechanisms is proposed for the source of the metals at Tulks Hill. Perhaps the Costigan Lake Intrusion (informal) was the source of the magmatic component. Within the footwall volcanics Cu and Zn could be released to the solution by alteration of intermediate-mafic rocks, through the destruction of pyroxenes and amphiboles, whereas Pb could be leached from felsic rocks through the breakdown of K-feldspar and mica. During the leaching process therefore mafic-intermediate rocks must have acted as the metal source since Cu and Zn minerals occur at Tulks Hill. Such rock types are absent from the study area but occur in other parts of the Victoria Lake Group. This would suggest that either the hydrothermal system had a large capture area for the metals, much larger than the study area at present, or there was a significant input of metals from a magmatic source.

10.8 DEFORMATION

Both volcanic and hydrothermal activity ceased with the deposition of the iron formation. The next recognisable geological event is large-scale recumbent folding (D0; inferred) followed by isoclinal folding (D1) and the development of a prominent schistosity (S1). Faulting associated with the recumbent folding cannot be

identified presumably because of the intensity of the later deformation (unlike in the Bathurst area, Van Staal and Williams (in press)). Faults associated with D1 however, are extensive although their relative motion is unknown. The age of D1 at Tulks Hill is thought to be Taconic, primarily because the overlying Buchans Group (Ordovician-Silurian age) is relatively undeformed which implies a pre-Acadian (pre-Ordovician-Silurian) time of deformation for the Victoria Lake Group. It is possible that the two periods of later deformation (D2 and D3) are Acadian deformation features since they are weakly developed (ie. similar to the Buchans Group). Indeed, if the Tulks River Fault to the north of Tulks Hill (thought to be of D1 age) is a splay of the Cape Ray fault, as is suggested by its trend and spatial relationship to known splays (eg. Lloyds River Fault), later movements on the Taconic-age fault are possible since movement on the Cape Ray Fault is thought to be Acadian (Wilton, 1983).

10.9: SUMMARY AND CONCLUSIONS FOR THE GENESIS OF THE TULKS HILL MASSIVE SULPHIDE DEPOSIT

The following is a summary of the more important geological, geochemical and structural features of the Tulks Hill sulphide deposit (T3 lens), and the conclusions inferred from these features.

1) The footwall rocks are predominantly volcanic,

consisting of rhyodacitic (s.l.) submarine ash-flow tuffs, with interbedded rhyolites (s.l.) and black shale (minor). A sub-volcanic intrusion in the northern part of Tulks Hill, known as the Raven rhyolite, is co-magmatic with the volcanic rocks and is thought to be a sill or a dome feature. Caldera collapse, with subsequent emptying of a crystal-rich portion of a magma chamber, is thought to be the most likely mechanism for the generation of both the crystal tuffs and the Raven rhyolite, the latter probably as a resurgent dome.

2) Two styles and intensities of hydrothermal alteration obliterate the primary mineralogy and textures of the footwall volcanic rocks. Chequerboard albite, and consequent enrichment of Na_2O, is a distinguishing feature of all footwall rocks, excluding the stockwork alteration and the Raven rhyolite. The latter two rock types have high K_2O values because of the development of sericite and secondary microcline, respectively. Sulphide veinlets and K enrichment in the Raven rhyolite suggest that its alteration was synchronous with the mineralising episode(s).

A stockwork alteration at the stratigraphic base of the sulphide deposit marks a fossil feeder zone for the hydrothermal fluids. Loss of Na_2O and CaO in favour of K_2O (as sericite) and MgO (as chlorite), as well as a ramifying network of pyrite-sphalerite veinlets, are characteristic.

A facies of the same intense alteration, known as the chlorite stockwork, consists of Mg chlorite with chalcopyrite and pyrite mineralisation. This mineralogy is compatible with the stockwork forming in a region of high fluid flow, close to the seawater-rock interface.

3) Massive pyrite and sphalerite were precipitated at the site of hydrothermal fluid expulsion, probably within a depression on the seafloor, in a relatively stable environment (brecciated sulphides are absent). A temperature of 300 degrees centigrade is probable for the hydrothermal fluid during alteration and sulphide deposition.

Seawater is thought to have destabilised the metal chloride complexes in favour of metal sulphide complexes but it is not known if seawater comprised the bulk of the hydrothermal fluid in general.

A crude mineralogical zoning is evident, from a chalcopyrite base through a sphalerite horizon into a galena-tennantite rich peripheral zone. A systematic decrease in the mole % FeS of sphalerite mirrors this crude zoning implying that it is primary. However, a detailed paragenetic sequence of sulphide deposition is difficult to establish because of post-mineralisation deformation and metamorphism.

4) A tuffaceous chert and an iron formation overlie the

sulphides, their chert-rich nature suggesting both silica saturation and metal depletion of the fluid. Both rocks contain pyrite and fine-grained volcanic detritus (tuff), the mineralisation tending to be restricted to the cherty beds. Alkaline conditions are suggested by the abundance of dolomitic carbonate in both rocks. Siderite and iron chlorite are distinctive minerals in the iron formation, the carbonate occurring in chert-rich stringers in a chlorite matrix.

5) Deposition of the iron formation marked the end of hydrothermal and volcanic activity. Recumbent folding (inferred), which inverted the stratigraphy, is the next recognisable geological event. This period of deformation is thought to predate tight to isoclinal folding at Tulks Hill, although both periods of deformation are thought to be Taconic in age. A strong schistosity developed during tight to isoclinal folding, and the mineralised horizon was repeated towards the north (as lens T3b). Faults subparallel to this schistosity are recognised in both the host rocks and the mineralisation, ranging from measurable displacements in the surface outcrops to microscopic granulation of pyrite. Pressure shadows and granulated pyrite are interpreted as D1 features, their coexistence suggesting that deformation was transitional between a brittle and a ductile regime; en echelon shear zones may be either D1 or D3 in age

Two episodes of weaker deformation (both Acadian?) may control the disposition of the other sulphide lenses at Tulks Hill.

6) The Tulks Hill Cu-Zn (-Pb) volcanogenic massive sulphide deposit shows many similarities to both Archaen and Phanerozoic (Kuroko-type) deposits. These similarities include a siliceous/chloritic stockwork, mineralogical zoning of the sulphides, overlying chemical sediments and a possible rhyolite dome / sill in the footwall. However, certain features differentiate the Tulks Hill deposit from both the Achaean and the Kuroko types: albite, with consequent enrichment in Na_2O, in most of the footwall rocks is notable, as is the absence of thick barite / gypsum deposits (Kuroko type) and the relative abundance of galena when compared to the Archaen deposits. It seems reasonable to suggest that the Tulks Hill deposit is transitional between these two "end-members", at least as far as the similarities and contrasts discussed above are concerned.

REFERENCES

ALEXANDER, G.B., HESTON, W.M. and ILER, R.K., 1954: The solubility of amorphous silica in water: Jour. of Phys. Chem., v.58, pp.453-455

ANDERSON, C.A. and NASH, J.J., 1972: Geology of the massive sulfide deposits at Jerome, Arizona --- a reinterpretation: Econ. Geol., v.67, pp.845-863

ARNOTT, R.J., 1983: Sedimentology of Upper Ordovician-Silurian sequences of New World Island, Newfoundland: separate fault controlled basins?: Can. Jour. of Earth Sci., v.20, pp.345-355

ATKINSON, B.K., 1975: Experimental deformation of polycrystalline pyrite: effects of temperature, confining pressure, strain rate and porosity: Econ. Geol., v.70, pp.473-487

BACHINSKI, D.J., 1976: Metamorphism of cupriferous iron sulfide deposits, Notre Dame Bay, Newfoundland: Econ. Geol., v.71, pp.443-452

BACKER, H., 1975: Exploration of the Red Sea and Gulf of Aden during the M.S.Valdivia cruises "Erzschlamme A" and "Erzschlamme B": Geol. Jahrb., v.D13, pp.3-78

BARNES, H.L., 1975: Zoning of ore deposits: Types and causes: Trans. Roy. Soc. Edinburgh, v.69, pp.295-311

----------, 1979: Solubilities of ore minerals: In Barnes, H.L., (ed.), Geochemistry of Hydrothermal Ore deposits, 2nd edition, pp.404-460, John Wiley and Sons Inc.

---------- and CZAMANSKE, G.K., 1967: Solubilities and transport of ore minerals: In Barnes, H.L., (ed.), Geochemistry of Hydrothermal Ore deposits, pp.336-381, Holt, Rinehart and Winston Inc.

BARTON, P.B., Jr., 1978: Some ore textures involving sphalerite from the Furotobe Mine, Akita Prefecture, Japan: Min. Geol., v.28, pp.293-300

---------- and SKINNER, B.J., 1979: Sulfide mineral stabilities: In Barnes, H.L., (ed.), Geochemistry of Hydrothermal Ore deposits, 2nd edition, pp.278-403, John Wiley and Sons Inc.

---------- and TOULMIN, P., 1966: Phase relations involving sphalerite in the Fe-Zn-S system: Econ. Geol., v.61, pp.815-849

BATTEY, M.L., 1965: Alkali metasomatism and the petrology of

some keratophyres: Geol. Mag., v.92, pp.104-126

BEANE, R.E., 1974: Biotite stability in the porphyry copper environment: Econ. Geol., v.69, pp.241-256

BELL, K. and BLENKINSOP, J., 1981: A geochronological study of the Buchans area, Newfoundland: In Swanson, E.A., Strong, D.F. and Thurlow, J.G. (eds.) The Buchans Orebodies: Fifty years of Geology and Mining, Geol. Assoc. Can., Spec. Paper 22, pp.91-112

BELL, T.T. and ETHERIDGE, M.A., 1973: Microstructure of mylonites and their descriptive terminology: Lithos, v.6, pp.337-348

BERGE, J.W., 1981: Recent investigations of two quartz-eye porphyroidal rock-volcanogenic massive sulfide occurrences: Econ. Geol., v.76, pp.1211-1215

BISCHOFF, J.L. and DICKSON, F.W., 1975: Seawater-basalt interaction at 200°C and 500 bar: Implications for origin of seafloor heavy metal deposits and regulation of seawater chemistry: Earth and Planet. Sci. Letts., v.25, pp.385-397

----------, RADTKE, A.S. and ROSENBAUER, R.J., 1981: Hydrothermal alteration of graywacke by brine and seawater: roles of alteration and chloride complexing on metal stabilization at 200°C and 350°C: Econ. Geol., v.76, pp.659-676

BOSTOCK, H.H., 1978: Volcanic rocks of the Appalachian Province: Roberts Arm Group, Newfoundland: In Current Research Part A, Geol. Surv. Can., Paper 78-1A, pp.231-233

BROWN, R.L., 1964: Geology of the Tulks Hill area: Unpubl. Map ASARCO, Buchans, Newfoundland

BRYNDZIA, L.T., SCOTT, S.D. and FARR, J.E., 1983: Mineralogy, geochemistry and mineral chemistry of siliceous ore and altered footwall rocks in the Uwamuki 2 and 4 deposits, Kosaka Mine, Hokuroko District, Japan: Econ. Geol. Mon. 5, pp.507-522

CAMPBELL, I.H., FRANKLIN, J.M., GORTON, M.P., HART, T.R. and SCOTT, S.D., 1981: The role of subvolcanic sills in the generation of massive sulfide deposits: Econ. Geol., v.76, pp.2248-2252

----------, GORTON, M.P., SCOTT, S.D., FRANKLIN, J.M. and THURSTON, P.C., 1982: Rare earth elements in volcanic rocks associated with Cu-Zn massive sulphide mineralisation: a preliminary report: Can. Jour. of

Earth Sci., v.19, pp.619-623

CAMERON, K.L. and HANSON, G.N., 1982: Rare earth element evidence concerning the origin of voluminous mid-Tertiary rhyolitic ignimbrites and related volcanic rocks, Sierra Madre Occidental, Chihuahua, Mexico: Geochem. Cosmochim. Acta, v.46, pp.1489-1504

CARMICHAEL, I.S.E., TURNER, F.J. and VERHOOGEN, J., 1974: Igneous Petrology: McGraw-Hill, 739p

CATHLES, L.M., 1977: An analysis of the cooling of intrusives by groundwater convection which includes boiling: Econ. Geol., v.72, pp.804-826

----------, GUBER, A.L., LENAGH, T.C. and DUDAS, F.O., 1983: Kuroko-type massive sulfide deposits of Japan: Products of an aborted island-arc rift: Econ. Geol. Mon. 5, pp.96-114

CHORLTON, L., 1980: Geology of the La Poile River area (110/16), Newfoundland: Nfld. Dept. Mines and Energy, Min. Dev. Div., Rep. 80-3, 86p

CHURCH, W.R. and STEVENS, R.K., 1971: Early Paleozoic ophiolite complexes of the Newfoundland Appalachians as mantle-oceanic crust sequences: Jour. Geophys. Res., v.76, pp.1460-1466

COLLERSON, K.D. and FRYER, B.J., 1978: The role of fluids in the formation and subsequent development of early continental crust: Con. Min. Pet., v.67, pp.151-167

COLMAN-SADD, S.P., 1980: Geology of south-central Newfoundland and evolution of the eastern margin of Iapetus: Am. Jour. Sci., v.280, pp.991-1017

---------- and SWINDEN, H.S., 1982: Geology and mineral potential of south-central Newfoundland: Nfld Dept. Mines and Energy, Min. Dev. Div., Rep. 82-8, 102 p

COOPER, G.E., 1968: Petrology and mineralization of Tulks Hill: Unpubl. MSc thesis, Memorial University of Newfoundland, St. John's, 111p

COSGROVE, J.W., 1976: The formation of crenulation cleavage: Jour. Geol. Soc. Lond., v.132, pp.155-178

COWARD, M.P., 1965: Geology of parts of the Mineral Belt, southeast of Red Indian Lake, Central Newfoundland: Unpubl. 3rd year treatise, Royal School of Mines, London

CRAIG, J.R. and VAUGHAN, P.J., 1981: Ore microscopy and ore

petrography: John Wiley and Sons Inc., 406p

DATE, J. and WATANABE, Y., 1979: Alteration around Fukazawa Kuroko deposits, Akita Prefecture, with special reference to zonal distribution of alteration minerals in the hangingwall rocks: Min. Geol., v.29, pp.351-361

-------, WATANABE, Y. and SAEKI, Y., 1983: Zonal alteration around the Fukazawa Kuroko deposits, Akita Prefecture, Japan: Econ. Geol. Mon. 5, pp.365-386

DAVIES, J.L., 1980: Geology of the Bathurst-Newcastle area: Geol. Assoc. Canada, Ann. Mtg., Halifax, May 1980, Field Trip Guidebook 16, pp.1-16

DEAN, P.L., 1977: A report on the geology and metallogeny of the Notre Dame Bay area to accompany metallogenic maps 12H/1, 8, 9 and 2E/3, 4, 5, 6, 7, 8, 9, 10, 11, and 12: Nfld Dept. of Mines and Energy, Min. Dev. Div., Rep. 77-10, 17p

---------- 1978: The volcanic stratigraphy and metallogeny of Notre Dame Bay, Newfoundland: Memorial University of Newfoundland, Geology Report 7

---------- and MEYER, J. R., 1981: Lithogeochemistry of mid-Ordovician cherts and shales of Central Newfoundland: Nfld. Dept. Mines and Energy, Min. Dev. Div., Open File Nfld (1317)

---------- and ----------, 1982: Metallogenic studies of mid-Ordovician cherts and shales of Central Newfoundland: In Current Research, Nfld. Dept. Mines and Energy, Min. Dev. Div., Rep. 82-1, pp.175-187

---------- and ----------, 1983: Mineral potential in clastic sedimentary basins in Newfoundland: In Current Research, Nfld. Dept. Mines and Energy, Min. Dev. Div., Rep. 83-1, pp.138-149

---------- and ----------, 1984: Mineral potential of clastic sedimentary basins in Newfoundland: In Current Research, Nfld Dept. Mines and Energy, Min. Dev. Div., Rep. 84-1, pp.283-287

---------- and STRONG, D.F., 1975: The volcanic stratigraphy, geochemistry and metallogeny of the central Newfoundland Appalachians: Geol. Assoc. Canada, Program and Abstracts, pp.745-746

DEWEY, J.F. and BIRD, J.M., 1971: Origin and emplacement of the ophiolite suite: Appalachian ophiolites in Newfoundland: Jour. Geophys. Res., v.76, pp.3174-3266

DUDAS, F.O., CAMPBELL, I.H. and GORTON, M.P., 1983: Geochemistry of igneous rocks in the Hokuroko District, Northern Japan: Econ. Geol. Mon. 5, pp.115-133

DUNNING, G.R., 1984: The geology, geochemistry, geochronology and regional setting of the Annieopsquotch Complex and related rocks of southwest Newfoundland: Unpubl. PhD thesis, Memorial University of Newfoundland

---------- and HERD, R.K., 1980: The Annieopsquotch ophiolite complex southwest Newfoundland and its regional relationships: In Current Research, Geol. Survey of Canada, Paper 80-1A, pp.227-234

---------- and KROGH, T.E., 1983: Tightly clustered U/Pb (zircon) ages of ophiolites from the Newfoundland Appalachians: Geol. Soc. Am., Abstracts, Northeastern section

----------, CARTER, P.J. and BEST, M.A., 1982: Geology of Star Lake (west half), southwest Newfoundland: In Current Research, Part B, Geol. Survey Canada, Paper 82-1B, pp.21-26

EBY, G.N., 1972: Determination of rare earth, yttrium and scandium abundances in rocks and minerals by an ion-exchange X-ray fluorescence procedure: Anal. Chem., v.44, pp.2137-2143

ELDRIDGE, C.S., BARTON, P.B., Jr. and OHMOTO, H., 1983: Mineral textures and their bearing on formation of the Kuroko orebodies: Econ. Geol. Mon. 5, pp.241-281

EWART, A., 1979: A review of the mineralogy and chemistry of Tertiary-Recent dacitic, rhyolitic and related salic volcanic rocks: In Barker, F. (ed.) Trondhjemites, dacites and related rocks, pp.13-121, Elsevier, Amsterdam

FLANAGAN, F.J., 1970: Sources of geochemical standards - II: Geochem. Cosmochim. Acta, v.23, pp.121-125

FLYNN, R.T. and BURNHAM, C.W., 1978: An experimental determination of rare earth partition coefficients between a chloride containing vapour phase and silicate melts: In Drake, M.J. and Holloway, J.R. (eds.) Experimental trace element geochemistry, Proceedings of an International Conference, Sedona, AZ, 1977. Pergamon, Oxford, England.

FRANKLIN, J.M. and THORPE, R.I., 1982: Comparitive metallogeny of the Superior, Slave and Churchill provinces: In Hutchinson, R.W., Spence, C.D. and Franklin, J.M., (eds.), Precambrian Sulphide Deposits H.S. Robinson Memorial Volume, Geol. Assoc. Can., Spec. Paper 25, pp.3-90

----------, GIBB, W., POULSEN, K.H. and SEVERIN, P.W.A., 1977: Archean metallogeny and stratigraphy of the South Sturgeon Lake area: - Inst. on Lake Superior Geology, 23rd Ann. Mtg., Thunder Bay, Ontario, Guidebook, 73p.

----------, LYDON, J.W. and SANGSTER, D.F., 1981: Volcanic-associated massive sulfide deposits: In Skinner, B.J., (ed.), Economic Geology 75th Anniversary Volume, pp.485-627

FRATER, K.M., 1983: Effects of metasomatism and development of quartz "eyes" in intrusive and extrusive rocks at Golden Grove Cu-Zn deposit, Western Australia: Trans. Inst. Min. Metall. (Section B) v.92, August, 1983, pp.B121-B131

FROESE, E., 1981: Applications of thermodynamics in the study of mineral deposits: Geol. Survey Canada, Paper 80-28, 38p.

FRYER, B.J., 1977: Rare earth evidence in iron formations for changing Precambrian oxidation states: Geochem. Cosmochim. Acta, v.41, pp.361-368

GALE, G.H. and PEARCE, J.A., 1982: Geochemical patterns in Norwegian greenstones: Can. Jour. of Earth Sci., v.19, pp.385-397

GRAF, J.L., Jr., 1977: Rare earth elements as hydrothermal tracers during the formation of massive sulfide deposits in volcanic rocks: Econ. Geol., v.72, pp.527-548

HAJASH, A., 1975: Hydrothermal processes along mid-ocean ridges: an experimental investigation: Con. Min. Pet., v.53, pp.205-266

HANOR, J.S., 1979: The sedimentary genesis of hydrothermal fluids: In Barnes, H.L., (ed.), Geochemistry of Hydrothermal Ore deposits, 2nd edition, pp.137-172, John Wiley and Sons Inc.

HANSON, G.N., 1978: The application of trace elements to the petrogenesis of igneous rocks of granitic composition: In Allegre, C.J. and Hart, S.R. (eds.) Trace elements in igneous petrology, pp.26-42 Elsevier

----------, 1980: Rare earth elements in petrogenetic studies of igneous systems: In Annual Review of Earth and Planet. Sci. Letts., pp.371-406

HASHIGUCHI, H., 1983: Penecontemporaneous deformation of Kuroko ore at the Kosaka Mine, Akita, Japan: Econ. Geol. Mon. 5, pp.167-183

----------, YAMADA, R. and INOUE, T., 1983: Practical

application of low Na2O anomalies in footwall acid lava for delimiting promising areas around the Kosaka and Fukazawa Kuroko deposits, Akita Prefecture, Japan: Econ. Geol. Mon. 5, pp.387-394

HASKIN, L.A., FREY, F.A., SCHMITT, R.A. and SMITH, R.H., 1966: Meteoritic, solar and terrestrial rare-earth distributions: In Ahrens, L.H., Press, F., Runcorn, S.K. and Urey, H.C. (eds.) Phys. and Chem. of the Earth, v.7, pp.167-322

HELGESON, H.C., DELANY, J.M., NESBITT, H.W. and BIRD, D.K., 1978: Summary and critique of the thermodynamic properties of rock forming minerals: Am. Jour. Sci., v.278A, pp.1-229

HEMING, R.F. and RANKIN, P.C., 1979: Ce-anomalous lavas from Rabaul caldera, Papua, New Guinea: Geochem. Cosmochim. Acta, v.43, pp.1351-1355

HENLEY, R.W. and THORNLEY, P., 1981: Low grade metamorphism and the geothermal environment of massive sulphide ore formation, Buchans, Newfoundland: In Swanson, E.A., Strong, D.F. and Thurlow, J.G., (eds.), The Buchans Orebodies: Fifty Years of Geology and Mining, Geol. Assoc. Can. Spec. Paper 22, pp.205-228

HERD, R.K. and DUNNING, G.R., 1979: Geology of the Puddle Pond map area, southwestern Newfoundland: In Current Research, Part A, Geol. Survey Canada, Paper 79-1A, pp.305-310

HEY, M.H., 1954: A new review of the chlorites: Min. Mag., v.30, p.227

HIBBARD, J.P., 1976: The southwestern extension of the Dunnage melange and its relationships to nearby groups: Unpubl. MSc thesis, Memorial University of Newfoundland

---------- and WILLIAMS, H., 1979: The regional setting of the Dunnage mélange: Am. Jour. Sci., v.279, pp.993-1021

HILL, J.D. and THOMAS, A., 1983: Correlation of two Helikian peralkaline granite-volcanic centres in central Labrador: Can. Jour. of Earth Sci., v.20, pp.753-763

HOBBS, B.E., MEANS, W.D. and WILLIAMS, P.F., 1976: An outline of structural geology: John Wiley and Sons Inc., 571p

HOLLAND, H.D. and MALININ, S.D., 1979: The solubility and occurrence of non-ore minerals: In Barnes, H.L., (ed.), Geochemistry of Hydrothermal Ore deposits, 2nd edition, pp.461-508, John Wiley and Sons Inc.

HOPWOOD, T.P., 1976: "Quartz-eye"-bearing porphyroidal rocks and volcanogenic massive sulfide deposits: Econ. Geol., v.71, pp.589-612

HUGHES, C.J., 1973: Spilites, keratophyres and the igneous spectrum: Geol. Mag., v.109 (6), pp.513-527

HUTCHINSON, R.W., 1980: Massive base metal sulphide deposits as guides to tectonic evolution: In Strangway, D.W. (ed.), The Continental Crust and its Mineral Deposits, Geol. Assoc. Can., Spec. Paper 20, pp.761-791

----------, 1982: Syn-depositional hydrothermal processes and Precambrian sulphide deposits: In Hutchinson, R.W., Spence, C.D. and Franklin, J.M., (eds.), Precambrian Sulphide Deposits H.S. Robinson' Memorial Volume, Geol. Assoc. Can., Spec. Paper 25

IZAWA, E., YOSHIDA, T. and SAITO, R., 1978: Geochemical characteristics of hydrothermal alteration around the Fukazawa, Kuroko deposit, Akita, Japan: Min. Geol., v.28, pp.325-336

JAMBOHR, J.L., 1983: Preliminary report of the mineralogy of the Tulks Hill massive sulfide deposit, Buchans area, Newfoundland: In Preliminary Current Research Reports, 1983, Dept. Mines and Energy, Min. Dev. Div., St. John's

JAYASINGHE, N.R., 1979: Geology of the Noel Paul's Brook area (12A/9), Newfoundland: In Report of Activities for 1978, Nfld. Dept. of Mines and Energy, Min. Dev. Div., Rep. 79-1, pp.25-29

KAJIWARA, J., 1970: Some limitations on the physico-chemical environment of deposition of the Kuroko ore: In Tatsumi, T., (ed.), Volcanism and ore genesis, pp.367-380, Univ. Tokyo Press

KALOGEROPOULAS, S.I. and SCOTT, S.D., 1983: Mineralogy and geochemistry of tuffaceous exhalites (tetsusekiei) of the Fukazawa Mine, Hokuroko District, Japan: Econ. Geol. Mon. 5, pp.412-432

KARLSTROM, K.E., van de PLUIJM, B.A. and WILLIAMS, P.F., 1983: Sedimentology of Upper Ordovician-Silurian sequences on New World Island: separate fault-controlled basins?. Discussion: Can. Jour. of Earth Sci., v.20, p.1757

KAY, E.A., 1982: A geochemical and fluid inclusion study of the arsenopyrite-stibnite-gold mineralisation, Moretons Harbour, Newfoundland: Unpubl. MSc thesis, Memorial University of Newfoundland, 209p

KEAN, B.F., 1973: Stratigraphy, petrology and geochemistry of volcanic rocks of Long Island, Newfoundland: Unpubl. MSc thesis, Memorial University of Newfoundland, 155p

----------, 1976: Geology of the Victoria Lake area: In Report of Activities for 1975, Nfld. Dept. Mines and Energy, Min. Dev. Div., Rep. 76-1, pp.31-37

----------, 1977a: Geology of the Victoria Lake map area (12A/6), Newfoundland: Nfld Dept. Mines and Energy, Min. Dev. Div., Rep. 77-4, 11p.

----------, 1977b: Geology of the Lake Ambrose sheet, west half: In Report of Activities for 1976, Nfld. Dept. Mines and Energy, Min. Dev. Div., Rep. 77-1, pp.21-26

----------, 1978: Geology of the Star Lake east half sheet (12A/11E), Newfoundland: In Report of activities for 1977, Nfld. Dept. Mines and Energy, Min. Dev. Div., Rep. 78-1, pp.129-134

----------, 1979: Buchans map area (12A/15), Newfoundland: In Report of Activities for 1978, Nfld. Dept. Mines and Energy, Min. Dev. Div., Rep. 79-1, pp.18-24

----------, 1983: Geology of the King George IV Lake map area (12A/4): Nfld. Dept. Mines and Energy, Min. Dev. Div., Rep. 83-4, 67p

---------- and JAYASINGHE, N.R., 1980: Geology of the Lake Ambrose (12A/16) - Noel Paul's Brook (12A/9) map areas, central Newfoundland: Nfld Dept. Mines and Energy, Min. Dev. Div., Rep. 80-2, 29p

---------- and ----------, 1981: Geology of the King George IV Lake map area (12A/4) Newfoundland: In Current Research, Nfld Dept. Mines and Energy, Min. Dev. Div., Rep. 81-1, pp.32-39

---------- and MERCER, N.L., 1978: Geology of the Grand Falls map area, west half (2D/13W), Newfoundland: In Report of Activities for 1977, Nfld. Dept. Mines and Energy, Min. Dev. Div., Rep. 78-1, pp.135-139

---------- and STRONG, D.F., 1975: Geochemical evolution of an island arc of the central Newfoundland Appalachians: Am. Jour. Sci., v.275, pp.97-118

----------, DEAN, P.L. and STRONG, D.F., 1981: Regional geology of the Central Volcanic Belt of Newfoundland: In Swanson, E.A., Strong, D.F. and Thurlow, J.G. (eds.), The Buchans Orebodies: Fifty Years of Geology and Mining, Geol. Assoc. Can. Spec. Paper 22, pp.65-78

KELLY, W.C. and CLARKE, B.R., 1975: Sulfide deformation studies: III. Experimental deformation of chalcopyrite to 2000 bars and 500°C: Econ. Geol., v.70, pp.431-453

KERRICH, R. and ALLISON, I., 1978: Flow mechanisms in rocks: Geosci. Can., 5 No. 3, Sept. 1978, pp.109-118

KOO, J. and MOSSMAN, J., 1975: Origin and metamorphism of the Flin-Flon stratabound Cu-Zn sulfide deposit, Saskatchewan and Manitoba: Econ. Geol., v.70, pp.48-62

LANGMYR, F.J. and PAUS, P.E., 1968: The analysis of inorganic siliceous materials by atomic absorption spectrophotometry and the hydrofluoric acid decomposition technique, Part I: The analysis of silicate rocks: Anal. Chem. Acta, v.43, pp.397-408

LARGE, R.R., 1977: Chemical evolution and zonation of massive sulfide deposits in volcanic terrains: Econ. Geol., v.72, pp.549-572

LE MAITRE, R.W., 1976: The chemical variability of some common igneous rocks: Jour. Pet., v.17, pp.589-637

LUDDEN, J.N. and THOMPSON, G., 1978: Behaviour of rare earth elements during submarine weathering of tholeiitic basalt: Nature, 274, pp.147-149

MACGEEHAN, P.J. and MACLEAN, W.H., 1980: Tholeiitic basalt-rhyolite magmatism and massive sulphide deposits at Mattagami, Quebec: Nature, v.286, pp.767-771

MALPAS, J. and STRONG, D.F., 1974: A comparison of chrome spinels in ophiolites and mantle diapirs of Newfoundland: Geochem. Cosmochim. Acta, v.39, pp.1045-1060

MARTEN, B.E., 1971: Stratigraphy of volcanic rocks in the Western Arm area of the central Newfoundland Appalachians: Geol. Assoc. Canada Proc., v.24, pp.73-84

MASUDA, A. and NAGASAWA, S., 1976: Rocks with negative Ce anomalies dredged from Shatsky Rise: Geochem. Cosmochim. Acta, v.9, pp.227-233

McKERROW, W.S. and COCKS, L.R.M., 1977: The location of the Iapetus suture in Newfoundland: Can. Jour. of Earth Sci., v.14, pp.488-495

---------- and ZIEGLER, A.M., 1972: Silurian palaeogeographic development of the Proto-Atlantic Ocean: 24th Internat. Geol. Cong. Montreal, 6, pp.4-10

MENZIES, M., BLANCHARD, D. and JACOBS, J., 1977: Rare earth element geochemistry of metabasalts from the Point Sol

ophiolite, California: Earth and Planet. Sci. Letts., v.37, pp.203-215

MERCER, N.L., 1978: Geology of the Lake Ambrose map area, east half (12A/10E), Newfoundland: In Report of Activities for 1977, Nfld. Dept. Mines and Energy, Min. Dev. Div., Rep. 78-1, pp.151-155

MEYER, C. and HEMLEY, J.J., 1967: Wall rock alteration: In Barnes, H.L., (ed.), Geochemistry of Hydrothermal Ore deposits, pp.166-235, Holt, Rinehart and Winston Inc.

MOTTL, M.J., 1983: Metabasalts, axial hot springs and the structure of hydrothermal systems at mid-ocean ridges: Geol. Soc. Am. Bull., v.94, pp.161-186

---------- and HOLLAND, H.D., 1978: Chemical exchange during hydrothermal alteration of basalt by seawater - I. Experimental results for major and minor components of seawater: Geochem. Cosmochim. Acta, v.42, pp.1103-1115

MUKAIYAMA, H., MONONOBE, S. and YOSHIDA, T., 1974: Genesis of the ore deposits of the Iwami Mine, Shimane Prefecture, Japan: In Ishihara (ed.) Soc. Mining Geologists Japan, Special Issue, No. 6, pp.221-234

OHMOTO,H., 1978: Submarine calderas: A key to the formation of volcanogenic massive sulfide deposits?: Min. Geol., v.28, pp.219-231

---------- and LASAGA, A.C., 1982: Kinetics of reaction between aqueous sulfates and sulfides in hydrothermal systems: Geochem. Cosmochim. Acta, v.46, pp.1727-1746

---------- and SKINNER, B.J., 1983: The Kuroko and related volcanogenic massive sulfide deposits: Introduction and summary of new findings: Econ. Geol. Mon. 5, pp.1-8

---------- and TAKAHASHI, T., 1983: Submarine calderas and Kuroko genesis: Econ. Geol. Mon. 5, pp.39-54

PAJARI, G.E. and CURRIE, K.L., 1978: The Gander Lake and Davidsville Groups of northeastern Newfoundland: a re-examination: Can. Jour. of Earth Sci., v.15, pp.708-714

PATTERSON, M.S. and WEISS, L.E., 1966: Experimental deformation and folding in phyllite: Geol. Soc. Am. Bull., v.77, pp.343-374

PAYNE, J.G. and STRONG, D.F., 1979: Origin of the Twillingate trondhjemite, north-central Newfoundland: partial melting in the roots of an island arc: In Barker, F. (ed.), Trondhjemites, dacites and related rocks,

pp.489-516, Elsevier, Netherlands

PEARCE, J.A., 1980: Geochemical evidence for genesis and eruptive setting of lavas from Tethyan ophiolites: In Panayiotou, A. (ed.) Proc. Internat. Ophiolite Symp., Nicosia, Cyprus, pp.261-272

---------- and CANN, J.R., 1973: Tectonic setting of basic volcanic rocks determined using trace element analyses: Earth and Planet. Sci. Letts., v.19, pp.290-300

PETERSEN, M.D. and LAMBERT, I.B., 1979: Mineralogical and chemical zonation around the Woodlawn Cu-Pb-Zn ore deposit, southeastern New South Wales: Jour. Geol. Soc. Australia, v.26, pp.169-186

POTTORF, R.J. and BARNES, H.L., 1983: Mineralogy, geochemistry and ore genesis of hydrothermal sediments from the Atlantis II Deep, Red Sea: Econ. Geol. Mon. 5, pp.198-223

RAMDOHR, P., 1969: The Ore Minerals and their Intergrowths: Pergamon Press, 1174p

RAMSEY, J.G., 1980: Shear zone geometry: a review: Jour. Struc. Geol., v.2, pp.83-99

RIDGE, J.D., 1973: Volcanic exhalations and ore deposition in the vicinity of the seafloor: Min. Dep., v.8, pp.332-348

RILEY, G.C., 1957: Preliminary map, Red Indian Lake (west half), (Map with marginal notes): Geol. Survey Canada, Map 8-1957

RIVERIN, G., 1977: Wall rock alteration at the Millenbach mine, Noranda area, Quebec: Unpubl. Ph.D thesis, Queen's Univ., Kingston, Ont., 255p.

---------- and HODGSON, C.J., 1980: Wall rock alteration at the Millenbach Cu-Zn mine, Noranda, Quebec: Econ. Geol., v.75, pp.424-444

RIMSTIDT, J.D. and BARNES, H.L., 1980: The kinetics of silica-water reactions: Geochem. Cosmochim. Acta, v.44, pp.1683-1700

ROBERTS, R.G., 1975: The geological setting of the Mattagami Lake mine, Quebec: A volcanogenic massive sulfide deposit: Econ. Geol., v.70, pp.115-129

---------- and REARDON, E.J., 1978: Alteration and ore-forming processes at Mattagami Lake mine, Quebec: Can. Jour. of Earth Sci., v.15, pp.1-21

ROBIE, R.A., HEMMINGWAY, B.S. and FISHER, J.R., 1978: Thermodynamic properties of minerals and related substances at 298.15K and 1 bar (10 (5) pascals) pressure and at higher temperatures: U.S. Geol. Surv., Bull. 1452, 456p

RONOV, A.N., BALASHOV, YU.A. and MIGDNOV, A.A., 1977: Geochemistry of the rare earths in the sedimentary cycle: Geochem. Int., v.44, pp.1-17

ROSE, A.W. and BURT, D.M., 1979: Hydrothermal alteration: In Barnes, H.L., (ed.), Geochemistry of Hydrothermal Ore deposits, 2nd edition, pp.173-235, John Wiley and Sons Inc.

ROSENBAUER, R.J., BISCHOFF, J.L. and RADTKE, A.S., 1983: Hydrothermal alteration of graywacke and basalt by 4 molal NaCl: Econ. Geol., v.78, pp.1701-1710

SAIF, S.I., 1983: Petrographic and geochemical characteristics of iron-rich rocks and their significance in exploration for massive sulfide deposits, Bathurst, New Brunswick, Canada: Jour. Geochem. Expln., v.19 (1-3), pp.705-723

SANGSTER, D.F., 1972: Precambrian volcanogenic massive sulphide deposits in Canada: A review: Geol. Survey Canada, Paper 72-22, 44p

---------- and SCOTT, S.D., 1976: Precambrian stratabound, massive Cu-Zn-Pb sulfide ores of North America: In Wolf, K.H., (ed.), Handbook of stratabound and stratiform ore deposits, pp.129-222, Elsevier, Amsterdam

SATO, T., 1972: Behaviours of ore-forming solutions in seawater: Min. Geol., v.22, pp.31-42

--------, 1977: Kuroko deposits: their geology, geochemistry and origin: In Volcanic processes in ore genesis, Inst. Min. Met. Special Pub. 7, Geol. Soc. London, pp.153-161

SAWKINS, F.J. and KOWALIK, J., 1981: The source of ore metals at Buchans: magmatic versus leaching models: In Swanson, E.A., Strong, D.F. and Thurlow, J.G. (eds.) The Buchans Orebodies: Fifty Years of Geology and Mining, Geol. Assoc. Can. Spec. Paper 22, pp.229-254

SCHERMERHORN, L.J.G., 1970: The deposition of volcanics and pyritite in the Iberian Pyrite Belt: Min. Dep., v.5, pp.273-279

----------, 1973: What is a keratophyre?: Lithos, v.6, pp.1-11

SCOTT, S.D., 1978: Structural control of the Kuroko deposits

of the Hokuroku district, Japan: Min. Geol., v.28, pp.301-311

---------- and BARNES, H.L., 1971: Sphalerite geothermometry and geobarometry: Econ. Geol., v.66, pp.653-667

---------- and KISSIN, S.A., 1973: Sphalerite composition in the Zn-Fe-S system below 300°C: Econ. Geol., v.68, pp.475-479

SHIROZU, H., 1974: Clay minerals in altered wall rocks of the Kuroko-type deposits: Soc. Mining Geologists Japan, Special Issue 6, pp.303-311

----------, 1978a: Chlorite minerals: In Sudo, T. and Shimoda, S., (eds.), Clays and clay minerals of Japan, pp.243-264, Elsevier

----------, 1978b: Wall rock alteration of Kuroko deposits: In Sudo, T. and Shimoda, S., (eds.), Clays and clay minerals of Japan, pp.127-145, Elsevier

SKINNER, B.J., 1979: The many origins of hydrothermal mineral deposits: In Barnes, H.L., (ed.), Geochemistry of Hydrothermal Ore deposits, 2nd edition, pp.1-21, John Wiley and Sons Inc.

SMITH, T.E. and JACKSON, T.A., 1974: Tertiary spilites and quartz keratophyres of the Wagwater Belt, Jamaica, West Indies: Bull. Volc., v.38, pp.870-890

SOLOMON, M. and WALSHE, J.L., 1979: The formation of massive sulfide deposits on the sea floor: Econ. Geol., v.74, pp.797-813

SPITZ, G. and DARLING, R., 1975: The petrochemistry of altered volcanic rocks surrounding the Louvem copper deposit, Val d'Or, Quebec: Can. Jour. of Earth Sci., v.12, pp.1820-1849

SPOONER, E.T.C. and BRAY, C.J., 1977: Hydrothermal fluids of seawater salinity in ophiolitic sulphide ore deposits in Cyprus: Nature, v.266, pp.808-812

STANTON, R.L., 1964: Mineral interfaces in stratiform ores: Inst. Min. Met., pp.45-79

----------, 1972: Ore petrology: McGraw Hill Inc., 713p

STEPHENS, M.B., 1982: Spilitization, volcanite composition and magmatic evolution --- their bearing on massive sulphide composition and siting in some volcanic terrains: Trans. Inst. Min. Met. (Section B), pp.B200-B213

----------, SLACK, J.F. and SWINDEN, H.S., (in press): Correlation of massive sulphide deposits in the Caledonian-Appalachian orogen on the basis of palaeotectonic setting

STRONG, D.F., 1973: Lushs Bight and Roberts Arm Groups of central Newfoundland: possible juxtaposed oceanic and island arc volcanic suites: Geol. Soc. Am. Bull., v.84, pp.3917-3928

----------, 1977: Volcanic regimes of the Newfoundland Appalachians: In Barager, W.R.A., Coleman, L.C. and Halls, J.M. (eds.), Volcanic regimes in Canada, Geol. Assoc. Can. Spec. Paper 16, pp.61-90

----------, 1981: Notes on ore mineralogy of the Buchans district: In Swanson, E.A., Strong, D.F. and Thurlow, J.G. (eds.) The Buchans Orebodies: Fifty Years of Geology and Mining, Geol. Assoc. Can. Spec. Paper 22, pp.143-160

SWINDEN, H.S., (1982): Metallogenesis in the Bay d'Espoir area, southern Newfoundland: C.I.M. Bull., v.75, pp.172-183

---------- and THORPE, R.I., (in press): Variations in the style of volcanism and massive sulfide deposition in early-middle Ordovician island arc sequences of the Newfoundland Central Mobile Belt

TAYLOR, R.P. and FRYER, B.J., 1980: Multiple stage hydrothermal alteration in porphyry copper systems in Northern Turkey: the temporal interplay of potassic, propylitic and phyllic fluids: Can. Jour. of Earth Sci., v.17, pp.901-926

---------- and ----------, 1982: Rare earth element geochemistry as an aid to interpreting hydrothermal ore deposits: In Metallization associated with acid magmatism, v.6, pp.357-365 Wiley, London

----------, STRONG, D.F. and FRYER, B.J., 1981: Control of contrasting trace element distributions in peralkaline granitic and volcanic rocks: Con. Min. Pet., v.77, pp.267-271

TAYLOR, S.R. and GORTON, M.P., 1977: Geochemical application of spark source mass spectrography III. Element sensitivity, precision and accuracy: Geochem. Cosmochim. Acta, v.41, pp.1375-1380

THURLOW, J.G., 1981a: Geology, ore deposits and applied rock geochemistry of the Buchans Group, Newfoundland: Unpubl. PhD thesis, Memorial University of Newfoundland, 305p

----------, 1981b: The Buchans Group: its stratigraphic and structural setting: In Swanson, E.A., Strong, D.F. and Thurlow, J.G. (eds.), The Buchans Orebodies: Fifty Years of Geology and Mining, Geol. Assoc. Can. Spec. Paper 22, pp.79-89

----------, SWANSON, E.A. and STRONG, D.F., 1975: Geology and lithogeochemistry of the Buchans polymetallic sulphide deposits, Newfoundland: Econ. Geol., v.70, pp.130-144

TUACH, J., 1976: Structural and stratigraphic setting of the Ming and other sulphide deposits in the Rambler area, Newfoundland: Unpubl. MSc thesis, Memorial University of Newfoundland, 128p

UPADHYAY, H.D., 1973: The Betts Cove ophiolite and related rocks of the Snooks Arm Group, Newfoundland: Unpubl. PhD thesis, Memorial University of Newfoundland, 224p

----------, DEWEY, J.F. and NEALE, E.R.W., 1971: The Betts Cove ophiolite complex, Newfoundland: Appalachian oceanic crust and mantle: Geol. Assoc. Canada, Proc., v.24, pp.27-34

URABE, T., 1974: Mineralogical aspects of the Kuroko deposits in Japan and their implications: Min. Dep., v.9, pp.309-324

---------, 1978: Quartz simultaneously precipitated with Kuroko ores in the Uwamuki No. 4 deposit, Kosaka Mine: Min. Geol., v.28, pp.337-348

--------- and SCOTT, S.D., 1983: Geology and footwall alteration of the South Bay massive sulphide deposit, northwestern Ontario, Canada: Can. Jour. of Earth Sci., v.20, pp.1862-1879

---------, ---------- and HATTORI, K., 1983: A comparison of footwall-rock alteration and geothermal systems beneath some Japanese and Canadian volcanogenic massive sulfide deposits: Econ. Geol. Mon. 5, pp.345-364

van STAAL, C. and WILLIAMS, P.F., (in press): Structure, origin and concentration of the Brunswick No. 12 and No. 6 orebodies: Econ. Geol.

VAUGHAN, D.J. and CRAIG, J.R., 1978: Mineral chemistry of metal sulphides: Cambridge University Press, Cambridge, England, 439p

VOKES, F.M., 1970: Comments on Professor A.K. Mikkola's paper. Aspects of the wallrock alteration associated with some Finnish sulfide deposits: A review: Trans. Inst. Min. Met., (Section B), v.79, p.99

WALFORD, P.C. and FRANKLIN, J.M., 1982: The Anderson Lake mine, Snow Lake Manitoba: In Hutchinson, R.W., Spence, C.D. and Franklin, J.M. (eds.), Precambrian Sulphide Deposits H.S. Robinson Memorial Volume, pp.481-524, Geol. Assoc. Can. Spec. Paper, 25, pp.481-524

WEGMANN, C.E., 1932: Note sur le Boudinage: Soc. Geol. de France Bull., pp.471-491

WEISSBERG, B.G., BROWNE, P.R.L. and SEWARD, T.M., 1979: Ore metals in active geothermal systems: In Barnes, H.L., (ed.), Geochemistry of Hydrothermal Ore deposits, 2nd edition pp.738-780, John Wiley and Sons Inc.

WHITEHEAD, R.E.S. and GOODFELLOW, W.D., 1978: Geochemistry of volcanic rocks from the Tetagouche Group, Bathurst, New Brunswick, Canada: Can. Jour. of Earth Sci., v.15, pp.207-219

WIGGINS, L.B. and CRAIG, J.R., 1980: Reconnaissance of the Cu-Fe-Zn-S system: sphalerite phase relationships: Econ. Geol., v.75, pp.742-752

WINCHESTER, J.A. and FLOYD, P.A. 1977: Geochemical discrimination of different magma series and their differentiation products using immobile elements: Chem. Geol., v.20, pp.325-343

WILLIAMS, H., 1979: Appalachian orogen in Canada: Can. Jour. of Earth Sci., v.16, pp.792-807

WILTON, D.H.C., 1983: The geology and structural history of the Cape Ray Fault Zone in southwestern Newfoundland: Can. Jour. of Earth Sci., v.20, pp.1119-1133

WU, I. and PETERSEN, U., 1977: Geochemistry of tetrahedrite and mineral zoning at Casapalca, Peru: Econ. Geol., v.72, pp.993-1017

WYNNE, P.J., 1983: A lithogeochemical study of the Strickland showing: Unpubl. MSc thesis, Memorial University of Newfoundland

APPENDIX I

WHOLE ROCK AND MINERAL CHEMISTRY DATA

TABLE A1 : Major and trace element results

TABLE A1

	ALKALI-ENRICHED RHYOLITE							
	82-2	14NA-82	16NA-82	19NA-82	21NA-82	24NA-82	26NA-82	31NA-82
SiO2	81.00	67.80	81.30	78.70	71.60	72.90	75.00	73.40
TiO2	.10	.23	.17	.15	.10	.08	.04	.04
Al2O3	10.40	15.50	9.95	9.73	9.67	13.40	10.70	12.00
Fe2O3	.95	1.43	.78	1.06	1.28	1.73	1.18	1.89
FeO	0.00	0.00	0.00	0.00	0.00	0.00	0.00	.10
MnO	.01	.06	.02	.02	.16	.02	.06	.06
MgO	.30	1.87	1.00	.58	.59	.71	.56	.74
CaO	.10	1.49	.49	2.55	6.25	.40	1.70	1.25
Na2O	4.44	.32	.07	.09	.34	.75	.97	.58
K2O	.95	5.70	3.66	3.49	3.34	6.97	5.64	6.09
P2O5	0.00	.03	.03	.01	0.00	.01	.01	.05
LOI	.76	4.29	2.28	3.24	7.19	1.64	2.63	2.52
TOTAL	99.01	98.52	99.75	99.68	100.52	98.61	98.35	98.92
Pb	3.00	3.00	0.00	7.00	11.00	4.00	9.00	5.00
Th	0.00	10.00	6.00	8.00	8.00	10.00	5.00	3.00
U	3.00	7.00	3.00	6.00	8.00	4.00	0.00	2.00
Rb	9.00	93.00	42.00	34.00	53.00	52.00	37.00	44.00
Sr	62.00	29.00	13.00	34.00	118.00	14.00	39.00	29.00
Y	43.00	68.00	51.00	57.00	85.00	72.00	72.00	81.00
Zr	118.00	233.00	149.00	120.00	115.00	162.00	125.00	144.00
Nb	2.00	7.00	5.00	4.00	7.00	9.00	6.00	8.00
Zn	48.00	28.00	21.00	31.00	21.00	32.00	22.00	38.00
Cu	13.00	16.00	16.00	15.00	10.00	13.00	13.00	14.00
Ni	0.00	0.00	0.00	0.00	1.00	0.00	0.00	.10
La	0.00	10.00	0.00	4.00	12.00	8.00	7.00	6.00
Ba	241.00	1110.00	791.00	847.00	564.00	564.00	559.00	740.00
V	2.00	8.00	3.00	0.00	1.00	0.00	.10	.10
Ce	22.00	18.00	10.00	9.00	26.00	23.00	15.00	18.00
Cr	0.00	0.00	0.00	0.00	0.00	0.00	0.00	.10
Ga	9.00	13.00	8.00	8.00	10.00	9.00	7.00	12.00

TABLE A1 (contd)

	ALTERED RHYOLITE						TABLE A1			
	10NA-82	11NA-82	12NA-82	17NA-82	18NA-82	20NA-82	22NA-82	23NA-82	81-74	82-31
SiO2	73.60	67.30	44.00	75.90	70.10	64.00	70.50	79.20	84.20	78.90
TiO2	.13	.27	.07	.06	.11	.25	.15	.10	.06	.10
Al2O3	10.10	16.00	17.30	10.80	10.80	16.80	12.40	11.50	9.26	10.80
Fe2O3	1.85	3.25	15.82	2.11	1.79	4.32	2.80	1.54	.81	2.16
FeO	0.00	0.00	0.00	0.00	0.00	0.00	0.00	0.00	0.00	0.00
MnO	.12	.02	.04	.02	.13	.04	.05	.01	0.00	.10
MgO	1.76	3.40	14.25	3.41	1.34	5.03	2.05	1.28	.20	.80
CaO	2.82	.31	.05	.38	3.64	.68	1.79	.11	.10	.12
Na2O	.12	.15	.91	3.99	2.00	.09	.50	3.69	4.51	5.58
K2O	3.11	4.60	.35	.57	2.54	5.19	4.14	1.53	.01	.10
P2O5	.10	.12	.01	.01	.02	.10	.02	0.00	0.00	.10
LOI	4.67	3.21	6.98	1.64	6.01	4.11	4.54	1.60	.84	1.94
TOTAL	98.38	98.63	98.78	98.89	98.88	100.61	98.94	100.56	100.57	99.80
Pb	5.00	0.00	5.00	0.00	12.00	0.00	12.00	0.00	3.00	0.00
Th	7.00	6.00	2.00	0.00	2.00	3.00	12.00	4.00	1.00	0.00
U	11.00	0.00	4.00	0.00	1.00	4.00	7.00	2.00	4.00	3.00
Rb	44.00	58.00	7.00	6.00	29.00	50.00	44.00	18.00	12.00	0.00
Sr	44.00	19.00	15.00	34.00	70.00	19.00	44.00	54.00	38.00	47.00
Y	38.00	48.00	17.00	65.00	61.00	39.00	78.00	62.00	38.00	36.00
Zr	129.00	202.00	38.00	126.00	126.00	173.00	149.00	137.00	118.00	88.00
Nb	4.00	6.00	2.00	5.00	6.00	5.00	8.00	4.00	4.00	1.00
Zn	15.00	28.00	366.00	84.00	20.00	91.00	41.00	12.00	0.00	36.00
Cu	16.00	16.00	19.00	15.00	16.00	13.00	14.00	12.00	14.00	17.00
Ni	0.00	0.00	0.00	0.00	0.00	5.00	0.00	0.00	0.00	0.00
La	6.00	4.00	7.00	7.00	0.00	5.00	5.00	10.00	12.00	1.00
Ba	3290.00	5201.00	75.00	153.00	606.00	1176.00	559.00	204.00	232.00	27.00
V	12.00	39.00	123.00	1.00	0.00	109.00	3.00	0.00	4.00	3.00
Ce	11.00	3.00	3.00	18.00	10.00	6.00	25.00	21.00	41.00	18.00
Cr	0.00	0.00	0.00	0.00	0.00	0.00	0.00	0.00	0.00	0.00
Ga	9.00	13.00	20.00	10.00	10.00	20.00	10.00	9.00	7.00	12.00

TABLE A1 (contd)

	PYROCLASTICS					TABLE A1		
	81-64	82-6	82-32	82-30	82-1	82-12A	82-12B	82-12C
SiO2	73.00	77.60	77.80	73.30	79.60	74.80	79.50	73.00
TiO2	.14	.08	.06	.06	.10	.10	.10	.15
Al2O3	12.50	11.30	10.30	12.00	9.85	13.30	10.50	14.20
Fe2O3	4.63	1.97	3.08	3.95	2.04	1.95	1.68	2.25
FeO	0.00	0.00	0.00	0.00	0.00	0.00	0.00	0.00
MnO	.05	.03	.02	.10	.10	.02	.04	.03
MgO	1.06	1.32	1.79	2.11	.57	1.22	.66	.70
CaO	.15	.12	.20	.23	.64	.13	.08	.05
Na2O	4.86	4.81	4.13	4.19	3.46	3.57	3.83	4.74
K2O	.76	.92	.01	.34	1.28	2.10	1.79	2.62
P2O5	0.00	0.00	.02	0.00	0.00	.01	0.00	0.00
LOI	1.63	1.34	1.68	2.13	1.94	1.26	.90	1.32
TOTAL	98.78	99.70	99.09	98.41	99.58	98.96	99.08	99.06
Pb	6.00	2.00	0.00	3.00	0.00	6.00	0.00	2.00
Th	0.00	0.00	0.00	0.00	1.00	3.00	3.00	8.00
U	3.00	0.00	0.00	4.00	0.00	0.00	0.00	3.00
Rb	10.00	13.00	0.00	6.00	17.00	30.00	24.00	55.00
Sr	39.00	88.00	36.00	52.00	61.00	50.00	38.00	44.00
Y	48.00	52.00	55.00	27.00	40.00	64.00	59.00	85.00
Zr	91.00	130.00	140.00	46.00	127.00	162.00	128.00	193.00
Nb	4.00	4.00	4.00	1.00	3.00	5.00	3.00	6.00
Zn	213.00	119.00	13.00	64.00	12.00	50.00	43.00	56.00
Cu	13.00	16.00	12.00	12.00	17.00	13.00	14.00	12.00
Ni	0.00	0.00	0.00	0.00	0.00	0.00	0.00	1.00
La	15.00	9.00	8.00	0.00	8.00	4.00	8.00	12.00
Ba	223.00	185.00	10.00	168.00	266.00	444.00	390.00	512.00
V	0.00	6.00	12.00	46.00	192.00	0.00	2.00	6.00
Ce	21.00	24.00	29.00	12.00	21.00	19.00	19.00	47.00
Cr	0.00	0.00	0.00	0.00	0.00	0.00	0.00	0.00
Ga	16.00	9.00	10.00	13.00	10.00	16.00	11.00	17.00

TABLE A1 (contd)

	SILICEOUS STOCKWORK					TABLE A1		
	1SES-82	2SA-82	3SA-82	5SA-82	3WA-82	9MH-82	T63-81	4NA-82
SiO2	74.00	73.20	66.90	80.90	45.90	36.90	62.10	76.40
TiO2	.03	.08	0.00	.04	.20	.20	0.00	.17
Al2O3	13.40	13.00	16.10	11.50	16.60	23.30	7.10	13.10
Fe2O3	3.36	3.92	5.56	1.18	19.82	16.06	15.42	2.04
FeO	0.00	0.00	0.00	0.00	0.00	0.00	0.00	0.00
MnO	0.00	.01	.02	.01	.03	.02	.05	.01
MgO	.31	.42	.60	.45	.89	.82	5.18	.54
CaO	.08	.02	.20	.14	.14	.04	.11	.02
Na2O	.38	.31	.19	.38	.17	.24	.04	.20
K2O	3.70	3.75	4.62	3.09	4.62	6.87	.77	3.81
P2O5	0.00	0.00	.11	.05	.06	0.00	.04	.04
LOI	3.41	3.71	4.89	1.80	11.65	11.64	8.88	2.20
TOTAL	98.67	98.42	99.19	98.56	100.08	96.09	99.69	98.53
Pb	526.00	73.00	79.00	3.00	2188.00	1289.00	81.00	2.00
Th	10.00	7.00	6.00	4.00	19.00	22.00	8.00	3.00
U	.10	4.00	4.00	5.00	3.00	24.00	7.00	5.00
Rb	73.00	77.00	95.00	68.00	111.00	157.00	18.00	71.00
Sr	32.00	29.00	36.00	29.00	43.00	74.00	7.00	23.00
Y	24.00	16.00	37.00	27.00	29.00	71.00	12.00	24.00
Zr	150.00	168.00	203.00	142.00	232.00	350.00	88.00	152.00
Nb	6.00	7.00	8.00	4.00	8.00	15.00	6.00	4.00
Zn	173.00	43.00	67.00	7.00	913.00	17030.00	1598.00	22.00
Cu	488.00	725.00	1285.00	17.00	1041.00	481.00	164.00	30.00
Ni	0.00	0.00	0.00	0.00	0.00	2.00	0.00	0.00
La	3.00	6.00	8.00	2.00	3.00	15.00	9.00	8.00
Ba	771.00	929.00	1176.00	1044.00	1259.00	2646.00	207.00	6391.00
V	13.00	6.00	20.00	8.00	18.00	54.00	13.00	18.00
Ce	11.00	14.00	6.00	6.00	8.00	13.00	8.00	10.00
Cr	0.00	0.00	0.00	0.00	0.00	0.00	77.00	0.00
Ga	17.00	16.00	20.00	12.00	35.00	48.00	12.00	15.00

TABLE A1 (contd)

	SILICEOUS STOCKWORK					TABLE A1	
	82-8	82-B1a	82-B1b	82-C17	82-A1b	14EN-82	13ES-82
SiO2	84.50	86.20	77.10	77.50	50.20	69.80	53.50
TiO2	.08	0.00	.10	.09	.33	.14	.17
Al2O3	6.60	7.28	11.60	11.00	27.40	16.30	22.40
Fe2O3	3.44	.67	3.96	3.44	4.20	2.26	6.11
FeO	0.00	0.00	0.00	0.00	.10	0.00	0.00
MnO	.04	0.00	0.00	.02	.02	.01	.01
MgO	1.56	.33	.40	1.56	2.60	.49	.49
CaO	.03	.08	.08	.01	.10	.04	.03
Na2O	.15	2.27	.33	.68	.19	.39	.25
K2O	1.40	1.21	3.32	3.09	9.88	4.70	6.33
P2O5	0.00	0.00	.07	.09	.10	.05	C.[illegible]
LOI	2.02	1.08	2.93	3.02	4.61	3.44	6.25
TOTAL	99.69	99.12	99.89	100.50	99.7[illegible]	97.62	95.5A
Pb	0.00	3.00	24.00	2.00	3.00	689.00	16[illegible]
Th	2.00	3.00	0.00	4.00	15.00	10.00	[illegible]
U	0.00	0.00	0.00	4.00	2.00	4.00	[illegible]
Rb	23.00	15.00	70.00	48.00	125.00	97.[illegible]	128.00
Sr	8.00	32.00	43.00	19.00	22.00	37.00	[illegible]
Y	52.00	47.00	19.00	33.00	133.00	31.00	28.00
Zr	118.00	115.00	108.00	125.00	391.00	194.00	276.00
Nb	4.00	2.00	6.00	2.00	13.00	6.00	1 .00
Zn	55.00	11.00	3.00	19.00	88.00	3023.00	8189.00
Cu	33.00	11.00	16.00	12.00	5.00	244.00	1252.00
Ni	0.00	0.00	0.00	1.00	4.00	0.00	0.00
La	8.00	9.00	11.00	8.00	21.00	10.00	14.00
Ba	1186.00	241.00	1343.00	1211.00	1207.00	1199.00	1152.00
V	1.00	0.00	87.00	104.00	.10	31.00	220.00
Ce	22.00	28.00	0.00	28.00	20.00	22.00	13.00
Cr	0.00	0.00	0.00	0.00	.10	0.00	0.00
Ga	10.00	7.00	18.00	12.00	40.00	32.00	43.00

TABLE A1 (contd)

	MINERALIZED HORIZONS			TABLE A1
	5ES-82	10ES-82	2WA-82	10WA-82
SiO_2	12.40	12.60	54.30	11.60
TiO_2	0.10	0.10	0.10	-
Al_2O_3	4.38	9.99	8.88	1.71
Fe_2O_3	32.06	45.80	19.38	17.49
FeO	-	-	-	-
MnO	0.26	0.35	0.02	0.05
MgO	2.82	8.89	0.46	0.90
CaO	0.79	0.11	0.09	0.07
Na_2O	0.04	-	0.09	0.02
K_2O	0.42	-	2.33	0.29
P_2O_5	0.03	0.04	0.10	0.03
LOI	22.88	20.86	10.88	17.62
TOTAL	76.18	98.74	96.63	49.78
Pb	3.08*	4084.00	1.09*	27.85*
Th	149.00	29.00	48.00	1170.00
U	7.00	4.00	4.00	-
Rb	45.00	7.00	72.00	192.00
Sr	5.00	-	26.00	-
Y	1.00	4.00	27.00	2.00
Zr	94.00	127.00	137.00	317.00
Nb	-	7.00	2.00	-
Zn	20.37*	6295.00	2.94*	43.82*
Cu	9114.00	5552.00	2440.00	8752.00
Ni	-	-	-	-
La	41.00	8.00	7.00	21.00
Ba	236.00	51.00	649.00	115.00
V	32.00	19.00	31.00	72.00
Ce	16.00	5.00	9.00	11.00
Cr	-	-	-	-
Ga	312.00	29.00	100.00	2267.00

*Weight Percent

TABLE A1 (contd)

CHEMICAL SEDIMENTS — TABLE A1

	22EN-82	11MH-82	19MH-82	20MH-82	1NA-82	2NA-82	82-C16	82-A1	82-13	82-14	82-35
SiO2	51.10	60.10	49.60	50.60	70.00	72.70	82.90	71.80	71.10	53.80	62.90
TiO2	.23	.33	.15	.28	.27	.18	.07	.30	.27	.73	.20
Al2O3	25.00	19.50	19.40	21.40	16.40	13.30	5.95	12.00	12.40	13.90	13.30
Fe2O3	5.82	4.88	5.87	6.90	2.52	3.37	3.23	6.29	6.78	11.40	8.49
FeO	0.00	0.00	0.00	0.00	0.00	0.00	0.00	0.00	0.00	0.00	0.00
MnO	.01	.11	.09	.06	.01	.02	.07	.10	.09	.29	.05
MgO	1.41	1.54	10.75	5.42	1.33	.86	2.16	1.32	1.93	6.05	5.62
CaO	.05	.76	.18	.21	.23	.24	.08	.47	.15	2.74	.29
Na2O	.20	.16	6.05	4.33	.09	.19	1.65	4.71	4.03	3.19	3.73
K2O	7.51	5.83	.05	3.33	5.00	4.21	.13	.13	1.09	.41	.02
P2O5	.06	.09	.07	.03	.06	.03	0.01	.09	.20	.03	.09
LOI	6.20	5.85	5.28	5.80	3.89	2.97	2.12	2.14	1.87	5.87	3.48
TOTAL	97.59	99.12	97.49	98.36	99.80	98.07	98.36	99.35	100.24	98.79	98.17
Pb	90.00	33.00	6.00	115.00	136.00	138.00	22.00	0.00	0.00	1.	0.
Th	15.00	17.00	18.00	14.00	11.00	10.00	0.00	2.00	0.00	.00	0.00
U	7.00	12.00	4.00	8.00	8.00	3.00	4.00	0.00	3.00	3.	2.00
Rb	163.00	129.00	0.00	74.00	115.00	90.00	4.00	2.00	12.00	11.00	0.00
Sr	54.00	49.00	85.00	89.00	34.00	29.00	17.00	45.00	48.00	117.00	43.00
Y	96.00	58.00	48.00	54.00	45.00	44.00	32.00	23.00	30.00	24.00	21.00
Zr	296.00	227.00	192.00	249.00	190.00	184.00	92.00	54.00	57.00	47.	42.00
Nb	11.00	8.00	7.00	9.00	7.00	5.00	3.00	3.00	3.00	2.00	1.00
Zn	53.00	82.00	181.00	91.00	303.00	144.00	93.00	88.00	110.00	139.00	99.00
Cu	28.00	22.00	14.00	32.00	32.00	24.00	22.00	8.00	9.00	37.00	8.00
Ni	0.00	0.00	0.00	6.00	0.00	0.00	0.00	0.00	0.00	6.00	0.00
La	16.00	7.00	2.00	11.00	9.00	6.00	14.00	4.00	8.00	10.00	6.00
Ba	2812.00	2537.00	64.00	3402.00	11299.00	5009.00	558.00	57.00	264.00	284.00	61.00
V	20.00	17.00	16.00	23.00	9.00	25.00	38.00	0.00	3.00	583.00	71.00
Ce	30.00	14.00	8.00	25.00	1.00	10.00	32.00	21.00	13.00	19.00	15.00
Cr	0.00	0.00	0.00	0.00	0.00	0.00	0.00	0.00	0.00	0.00	0.00
Ga	28.00	20.00	16.00	25.00	16.00	14.00	7.00	10.00	12.00	15.00	16.00

TABLE A2 : Rare earth element concentrations

ALKALI-ENRICHED RHYOLITE TABLE A2

Sample	16NA-82		19NA-82	
	PPM	CHONDRITE*	PPM	CHONDRITE*
La	24.90	79.05	21.70	68.89
Ce	54.94	67.57	50.10	61.62
Nd	29.26	49.02	30.06	50.36
Sm	7.28	36.95	8.29	42.10
Eu	0.48	6.62	1.80	24.98
Gd	6.25	24.13	8.20	31.64
Dy	4.34	13.34	5.92	18.22
Er	2.78	13.04	4.47	21.01
Yb	3.81	18.29	5.54	26.63
Tm yield:	0.47		0.43	

Sample	24NA-82		26NA-82	
	PPM	CHONDRITE*	PPM	CHONDRITE*
La	14.05	44.62	16.54	52.51
Ce	33.11	40.72	38.29	47.10
Nd	23.39	39.18	26.01	43.56
Sm	6.58	33.40	8.56	43.46
Eu	1.25	17.31	1.06	14.71
Gd	7.49	28.92	7.97	30.76
Dy	6.39	19.65	7.99	24.58
Er	5.24	24.58	5.14	24.14
Yb	6.60	31.75	4.24	20.40
Tm yield:	0.41		0.48	

*Normalised to the values of Taylor and Gorten (1977)

TABLE A2 (contd)

ALTERED RHYOLITE — TABLE A2

Sample	11NA-82		17NA-82		18NA-82	
	PPM	CHONDRITE*	PPM	CHONDRITE*	PPM	CHONDRITE*
La	4.36	13.84	16.81	53.37	25.90	82.24
Ce	14.60	17.96	39.29	47.10	59.61	73.32
Nd	13.03	21.82	22.94	38.42	35.68	59.76
Sm	3.88	19.69	6.64	33.70	8.85	44.92
Eu	1.01	13.98	1.42	19.73	1.12	15.57
Gd	4.27	16.48	7.64	29.49	9.68	37.36
Dy	4.05	12.46	6.83	21.03	9.61	29.58
Er	3.37	15.84	4.61	21.63	5.94	27.87
Yb	4.73	22.75	5.71	27.47	6.66	31.75
Tm yield	0.40		0.39		0.43	

Sample	20NA-82		23NA-82	
	PPM	CHONDRITE*	PPM	CHONDRITE*
La	3.39	10.78	22.09	70.12
Ce	9.05	11.13	47.90	58.92
Nd	6.73	11.27	28.88	48.37
Sm	3.05	15.48	7.72	39.20
Eu	0.91	12.62	1.10	15.23
Gd	2.84	10.98	7.75	29.93
Dy	3.51	10.78	5.76	17.71
Er	2.87	13.49	4.27	20.05
Yb	4.55	21.86	5.86	28.15
Tm yield	0.41		0.60	

*Normalised to the values of Taylor and Gorten (1977)

TABLE A2 (contd)

SILICEOUS STOCKWORK

TABLE A2

Sample	14EN-82 PPM	14EN-82 CHONDRITE*	15ES-82 PPM	15ES-82 CHONDRITE*	5SA-82 PPM	5SA-82 CHONDRITE*
La	22.91	72.73	15.83	50.27	12.64	40.14
Ce	46.30	56.95	33.26	40.91	24.99	30.74
Nd	26.99	45.21	18.69	31.31	15.62	26.17
Sm	6.88	34.93	5.05	25.65	4.07	20.68
Eu	0.78	10.84	0.66	9.18	0.68	9.45
Gd	6.01	23.20	3.75	14.47	4.04	15.61
Dy	3.96	12.20	2.62	8.06	3.12	9.60
Er	2.55	11.96	1.48	6.94	2.02	9.50
Yb	4.02	19.32	2.14	10.30	3.60	17.29
Tm yield:	0.45		0.68		0.70	

Sample	2SA-82 PPM	2SA-82 CHONDRITE*	3SA-82 PPM	3SA-82 CHONDRITE*	4NA-82 PPM	4NA-82 CHONDRITE*
La	11.04	35.06	1.54	4.90	6.74	21.41
Ce	17.74	21.82	0.19	0.23	19.85	24.42
Nd	9.94	16.65	2.43	4.09	16.42	27.50
Sm	2.58	13.07	1.64	8.32	5.09	25.84
Eu	1.33	18.39	0.82	11.42	1.25	17.29
Gd	2.82	10.88	2.12	8.19	5.14	19.86
Dy	2.39	7.37	2.68	8.24	3.15	9.69
Er	2.68	12.56	3.46	16.26	2.47	11.57
Yb	3.96	19.02	5.29	25.41	3.73	17.94
Tm yield:	0.43		0.46		0.47	

*Normalised to the values of Taylor and Gorten (1977)

TABLE A2 (contd)

MINERALISED HORIZON — TABLE A2

Sample	2WA-82 PPM	2WA-82 CHONDRITE*	5ES-82 PPM	5ES-82 CHONDRITE*	10WA-82 PPM	10WA-82 CHONDRITE*
La	14.60	46.35	4.53	14.39	1.93	6.14
Ce	27.49	33.81	7.70	9.47	2.88	3.55
Nd	13.85	23.19	3.37	5.65	2.10	3.52
Sm	3.73	18.96	1.01	5.12	0.72	3.67
Eu	1.44	19.90	0.39	5.42	0.51	7.13
Gd	3.46	13.38	1.47	5.69	1.02	3.93
Dy	2.75	8.45	1.46	4.49	1.00	3.07
Er	1.99	9.35	1.26	5.94	0.86	4.02
Yb	2.99	14.37	1.33	6.38	1.31	6.30
Tm yield	0.51		0.42		0.42	

TUFFACEOUS CHERT

Sample	19MH-82 PPM	19MH-82 CHONDRITE*
La	6.21	19.71
Ce	12.70	15.62
Nd	7.31	12.24
Sm	2.66	13.51
Eu	0.77	10.66
Gd	3.22	12.44
Dy	3.31	10.71
Er	2.83	13.27
Yb	3.59	17.28
Tm yield	0.42	

BIOTITE TUFF

Sample	25NA-82 PPM	25NA-82 CHONDRITE*
La	12.77	40.53
Ce	31.70	39.00
Nd	22.37	37.47
Sm	7.32	37.17
Eu	1.12	15.55
Gd	7.68	29.65
Dy	6.34	19.52
Er	4.72	22.14
Yb	5.86	28.13
Tm yield	0.49	

*Normalised to the values of Taylor and Gorten (1977)

TABLE A3 : Chlorite microprobe analyses

CHLORITE — TABLE A3

Sample		Na	Mg	Al	Si	K	Ca	Ti	Cr	Mn	Fe	Ni	Total
Large Quartz Crystal Tuff													
82-30	wt. %	0.02	19.39	22.22	26.87	0.02	-	-	0.01	0.53	18.45	0.01	87.52
	form.	-	5.656	5.404	5.348	-	-	-	-	0.112	3.36	-	19.85
82-30	wt. %	0.04	19.11	22.38	27.05	-	0.05	-	-	0.59	18.93	-	88.13
	form.	-	5.74	5.32	5.46	-	-	-	-	0.084	3.192	-	19.79
82-30	wt. %	0.01	18.80	22.73	27.36	-	0.02	-	-	0.50	18.36	0.01	87.80
	form.	-	5.656	5.404	5.516	-	-	-	-	0.084	3.08	-	19.74
Quartz Crystal Tuff													
82-C5	wt. %	-	19.21	21.61	26.12	-	-	-	-	0.25	17.90	0.01	85.10
	form.	-	5.964	5.292	5.432	-	-	-	-	0.028	3.108	-	19.85
82-C5	wt. %	-	20.62	21.42	27.16	-	0.01	-	-	0.21	17.91	-	87.34
	form.	-	6.216	5.124	5.488	-	-	-	-	0.028	3.024	-	19.88
82-C5	wt. %	0.04	21.21	22.22	26.05	0.01	-	-	-	0.20	17.80	-	87.53
	form.	-	6.412	5.292	5.264	-	-	-	-	-	2.996	-	19.99
82-C5	wt. %	0.01	21.69	21.89	27.81	0.02	0.01	-	0.02	0.25	17.82	-	89.50
	form.	-	6.384	5.096	5.488	-	-	-	-	-	2.912	-	19.88
82-C5	wt. %	0.01	20.35	21.86	26.12	0.01	0.02	-	-	0.25	17.70	-	86.32
	form.	-	6.216	5.292	5.348	-	-	-	-	-	3.024	-	19.94
82-C16	wt. %	0.13	11.41	22.71	32.28	2.83	0.02	0.01	-	0.25	11.44	0.04	81.13
	form.	-	3.556	5.6	6.776	0.756	-	-	-	-	1.988	-	18.76
82-C16	wt. %	-	20.18	21.63	26.89	0.01	-	-	0.02	0.16	18.90	-	87.80
	form.	-	6.104	5.18	5.432	-	-	-	-	-	3.192	-	19.91
82-C16	wt. %	0.03	20.34	21.57	27.87	0.03	0.02	-	0.02	0.32	17.91	0.03	88.15
	form.	-	6.076	5.096	5.60	-	-	-	-	-	2.996	-	19.91

TABLE A3 (contd)

TABLE A3

Mineralised Horizon

Sample		Na	Mg	Al	Si	K	Ca	Ti	Cr	Mn	Fe	Ni	Total
T48-81	wt. %	0.02	17.57	21.59	25.54	0.01	-	0.02	0.02	0.74	22.49	0.03	88.02
	form.	-	5.432	5.264	5.296	-	-	-	-	0.112	3.892	-	20.02
T48-81	wt. %	-	17.78	21.87	25.29	-	-	0.05	-	0.78	21.73	-	87.50
	form.	-	5.488	5.348	5.264	-	-	-	-	0.112	3.78	-	19.99
T48-81	wt. %	0.02	17.31	22.37	25.51	0.04	0.01	0.04	0.02	0.78	22.07	0.03	88.19
	form.	-	5.32	5.432	5.264	-	-	-	-	0.112	3.808	-	19.94
T48-81	wt. %	0.05	17.48	21.77	26.29	-	0.01	0.04	-	0.84	21.81	0.04	88.31
	form.	-	5.348	5.264	5.404	-	-	-	-	0.14	3.752	-	19.91
5ES-82	wt. %	-	21.9	21.8	25.71	0.01	0.01	0.02	-	0.52	17.88	0.09	87.93
	form.	-	6.606	5.208	5.208	-	-	-	-	0.084	3.024	-	20.13
5ES-82	wt. %	-	22.14	21.52	25.58	-	-	0.03	-	0.55	16.82	-	86.64
	form.	-	6.748	5.18	5.236	-	-	-	-	0.084	2.884	-	20.13
5ES-82	wt. %	-	21.45	21.77	26.89	0.02	0.01	-	-	0.6	16.66	-	87.4
	form.	-	6.44	5.18	5.432	-	-	-	-	0.084	2.80	-	19.94
5ES-82	wt. %	0.03	21.15	21.39	26.66	-	-	0.05	-	0.53	16.16	-	85.97
	form.	-	6.44	5.152	5.432	-	-	-	-	-	2.772	-	19.88
10ES-82	wt. %	-	19.43	20.41	26.45	-	0.01	0.02	-	0.77	20.87	0.02	87.98
	form.	-	5.936	4.928	5.432	-	-	-	-	0.112	3.564	-	20.02
10ES-82	wt. %	0.01	18.89	20.73	26.80	-	0.01	0.05	-	0.79	20.48	0.01	87.78
	form.	-	5.768	5.012	5.488	-	-	-	-	0.112	3.50	-	19.88
10ES-82	wt. %	0.01	19.91	21.89	27.21	-	0.01	-	-	0.82	20.51	0.03	90.39
	form.	-	5.88	5.124	5.404	-	-	-	-	0.112	3.416	-	19.94
10ES-82	wt. %	0.02	18.63	21.30	25.49	-	-	0.05	0.02	0.83	21.31	0.01	87.65
	form.	-	5.74	5.208	5.264	-	-	-	-	0.14	3.696	-	20.1
10ES-82	wt. %	-	19.58	20.49	25.85	0.02	0.01	0.03	-	0.64	20.14	0.03	86.79
	form.	-	6.048	5.012	5.376	-	-	-	-	0.112	3.50	-	20.1
10ES-82	wt. %	-	17.85	21.20	25.66	-	-	0.03	-	0.70	22.09	0.05	87.59
	form.	-	5.516	5.208	5.32	-	-	-	-	0.112	3.836	-	19.99

TABLE A3

Mineralised Horizons (cont'd)

Sample		Na	Mg	Al	Si	K	Ca	Ti	Cr	Mn	Fe	Ni	Total
T74-81	wt. %	-	20.22	22.10	25.69	0.01	0.02	0.01	0.02	0.99	16.65	-	85.70
	form.	-	6.216	5.376	5.292	-	-	-	-	0.168	2.884	-	19.94
T74-81	wt. %	-	23.41	20.85	27.45	0.01	-	0.03	-	0.20	10.65	-	82.60
	form.	-	7.196	5.068	5.656	-	-	-	-	0.028	1.82	-	19.77
T74-81	wt. %	-	23.73	21.86	27.60	-	-	0.02	0.01	0.67	14.38	-	88.26
	form.	-	6.972	5.096	5.432	-	-	-	-	0.112	2.352	-	19.96
6NA-82	wt. %	0.01	24.48	20.80	28.34	-	0.02	-	-	0.23	13.07	0.01	86.95
	form.	-	7.224	4.844	5.628	-	-	-	-	0.028	2.156	-	19.88
6NA-82	wt. %	-	24.82	20.44	27.60	0.01	0.02	0.02	0.02	0.20	12.46	0.05	85.63
	form.	-	7.448	4.844	5.544	-	-	-	-	0.028	2.10	-	19.94
6NA-82	wt. %	0.04	24.63	20.71	26.79	-	0.01	0.02	0.01	0.18	13.23	-	85.61
	form.	-	7.42	4.928	5.404	-	-	-	-	0.028	2.24	-	20.02
6NA-82	wt. %	-	23.8	21.17	26.56	-	-	0.02	-	0.12	12.86	-	84.56
	form.	-	7.252	5.096	5.432	-	-	-	-	-	2.184	-	19.96
6NA-82	wt. %	-	25.23	20.52	28.34	-	-	0.01	-	0.14	12.82	-	87.07
	form.	-	7.448	4.788	5.6	-	-	-	-	-	2.128	-	19.96
6NA-82	wt. %	-	24.27	20.00	27.10	0.01	-	0.03	-	0.17	12.67	0.01	84.26
	form.	-	7.42	4.816	5.54	-	-	-	-	-	2.156	-	19.96
						Chemical Sediments							
82-13	wt. %	-	11.70	21.39	25.94	0.02	-	0.01	-	0.14	30.33	0.04	89.57
	form.	-	3.668	5.32	5.46	-	-	-	-	-	5.348	-	19.82
82-13	wt. %	-	11.65	21.40	26.30	0.01	-	-	-	0.16	30.13	-	89.66
	form.	-	3.64	5.292	5.516	-	-	-	-	-	5.292	-	19.77

TABLE A3 (contd)

Chemical Sediments (cont'd) TABLE A3

Sample		Na	Mg	Al	Si	K	Ca	Ti	Cr	Mn	Fe	Ni	Total
82-13	wt. %	0.03	11.26	20.61	25.64	0.04	0.02	-	-	0.14	30.58	-	88.32
	form.	-	3.584	5.208	5.488	-	-	-	-	-	5.488	-	19.79
T110-82	wt. %	0.01	19.84	19.00	26.65	0.02	-	0.02	0.01	0.11	20.98	0.02	86.71
	form.	-	6.181	4.669	5.557	0.06	-	-	-	0.018	3.66	-	20.1
T110-82	wt. %	0.04	23.3	24.85	39.52	0.07	0.01	0.11	-	0.09	25.45	0.05	113.49
	form.	0.009	5.417	4.570	6.168	0.014	-	0.009	-	0.009	3.320	0.004	19.52
T110-82	wt. %	0.03	18.64	19.93	27.55	0.01	-	0.03	0.02	0.06	21.8	0.08	88.12
	form.	-	5.697	4.813	5.649	-	-	-	-	0.006	3.736	0.012	19.913
T110-82	wt. %	0.09	19.93	17.50	29.61	0.02	-	0.04	-	0.02	21.67	0.05	88.93
	form.	0.029	6.015	4.178	5.997	-	-	-	-	-	3.667	-	19.892

TABLE A4 : Sericite microprobe analyses

SERICITE — TABLE A4

Sample		Na	Mg	Al	Si	K	Ca	Ti	Cr	Mn	Fe	Ni	Total
Quartz Crystal Tuff													
82-1	wt.%	0.22	1.61	30.53	46.13	8.91	-	0.07	0.01	0.02	2.69	-	90.18
	Form.	0.048	0.36	5.448	6.984	1.704	-	-	-	-	0.336	-	14.88
82-1	wt.%	0.17	1.10	32.28	47.29	9.75	-	0.03	0.01	0.09	2.22	-	92.94
	Form.	0.043	0.218	5.147	6.402	1.680	-	0.008	-	0.008	0.250	-	13.757
82-1	wt.%	0.25	1.71	30.42	46.88	9.24	-	0.06	0.04	0.04	3.27	-	91.90
	Form.	0.064	0.345	4.898	6.911	1.608	-	0.016	0.004	0.004	0.373	-	13.72
82-1	wt.%	0.16	1.57	25.64	43.47	8.88	-	0.05	-	-	2.66	0.01	82.45
	Form.	0.044	0.353	4.596	6.615	1.724	-	0.013	-	-	0.335	-	13.681
82-1	wt.%	0.17	1.93	29.49	48.48	9.28	-	0.07	0.02	0.06	2.55	-	92.07
	Form.	0.043	0.390	4.717	6.582	1.605	-	0.016	-	0.004	0.287	-	13.644
Large Quartz Crystal Tuff													
82-30	wt.%	0.86	0.56	36.03	50.10	7.01	-	0.02	-	-	0.99	0.03	95.61
	Form.	0.216	0.096	5.928	7.008	1.488	-	-	-	-	0.096	-	14.59
82-30	wt.%	1.25	0.40	36.02	46.52	8.02	-	0.03	-	-	0.99	0.05	93.29
	Form.	0.336	0.072	6.144	6.744	1.488	-	-	-	-	0.12	-	14.90
82-30	wt.%	0.86	0.53	36.18	49.43	7.69	-	0.01	0.02	0.03	1.10	0.02	95.86
	Form.	0.216	0.096	6.00	6.96	1.368	-	-	-	-	0.12	-	14.78
Biotite Tuff													
82-12c	wt.%	0.05	1.87	27.88	47.76	9.55	0.02	0.05	-	0.27	6.48	0.05	93.97
	Form.	-	0.408	4.872	7.104	1.8	-	-	-	0.024	0.792	-	15.024

TABLE A4 (contd)

SERICITE (cont'd)

TABLE A4

Biotite Tuff (cont'd)

Sample		Na	Mg	Al	Si	K	Ca	Ti	Cr	Mn	Fe	Ni	Total
82-12c	wt.%	0.04	1.84	29.57	50.70	9.04	-	0.05	0.03	0.02	5.02	0.06	96.37
	Form.	-	0.384	4.968	7.224	1.632	-	-	-	-	0.6	-	14.81
82-12c	wt.%	0.06	2.02	28.29	50.20	9.40	-	0.04	-	0.02	4.90	0.02	94.97
	Form.	-	0.432	4.824	7.272	1.728	-	-	-	-	0.576	-	14.88
82-12c	wt.%	0.25	2.98	27.08	44.86	9.30	-	0.09	0.03	0.04	9.03	-	93.67
	Form.	0.072	0.672	4.824	6.792	1.8	-	0.024	-	-	1.128	-	15.31
82-12c	wt.%	0.09	1.79	27.75	48.79	9.50	0.02	0.05	-	0.01	5.07	-	93.07
	Form.	-	0.384	4.848	7.248	1.8	-	-	-	-	0.624	-	14.92
					Quartz Crystal Tuff								
82-c16	wt.%	0.25	1.52	31.41	46.49	7.87	-	0.05	-	0.04	2.44	0.06	90.12
	Form.	0.072	0.336	5.544	6.96	1.512	-	-	-	-	0.288	-	14.71
81-74	wt.%	2.71	0.97	29.26	48.51	6.67	0.04	0.02	-	0.03	0.95	0.02	89.18
	Form.	0.723	0.199	4.772	6.713	1.178	0.004	-	-	-	0.109	-	13.701
81-74	wt.%	0.38	1.32	33.13	51.07	8.94	-	0.02	-	-	0.93	0.05	95.84
	Form.	0.091	0.253	5.039	6.587	1.469	-	0.003	-	-	0.098	0.003	13.544
82-B1(a)	wt.%	0.20	1.75	31.13	48.64	9.12	-	0.07	0.02	-	1.95	-	92.87
	Form.	0.051	0.378	5.325	7.059	1.686	-	0.021	-	-	0.234	-	14.75
82-B1(a)	wt.%	0.31	1.75	31.41	50.42	9.51	-	0.07	-	0.04	1.68	-	95.2
	Form.	0.084	0.372	5.265	7.173	1.725	-	0.015	-	0.003	0.195	-	14.82

TABLE A4 (contd)

SERICITE (cont'd)

TABLE A4

Quartz Crystal Tuff (cont'd)

Sample		Na	Mg	Al	Si	K	Ca	Ti	Cr	Mn	Fe	Ni	Total
82-B1(a)	wt.%	0.29	2.09	30.04	49.70	10.18	-	0.05	0.02	0.04	2.26	0.05	94.72
	Form.	0.078	0.447	5.109	7.179	1.872	-	0.015	-	0.003	0.27	0.003	14.979
					Mineralised Horizon								
T48-81	wt.%	0.99	0.82	32.78	45.02	9.22	-	0.23	-	0.01	2.02	-	91.09
	Form.	0.288	0.168	5.856	6.84	1.776	-	-	-	-	0.24	-	15.19
T48-81	wt.%	0.86	0.78	32.24	43.44	9.54	-	0.28	0.01	0.01	2.17	-	89.32
	Form.	0.24	0.168	5.904	6.744	1.896	-	0.024	-	-	0.264	-	15.26
T48-81 (adj.ch1)	wt.%	0.60	0.94	32.92	46.35	9.22	-	0.28	-	0.04	1.56	0.05	91.95
	Form.	0.168	0.192	5.784	6.912	1.752	-	0.024	-	-	0.192	-	15.024
5ES-82	wt.%	0.80	1.13	32.36	43.24	9.49	-	0.11	-	0.06	1.60	-	88.80
	Form.	0.24	0.264	5.952	6.744	1.872	-	-	-	-	0.192	-	15.24
5ES-82	wt.%	0.81	1.09	31.88	46.36	9.05	-	0.41	0.02	0.04	1.66	0.04	91.36
	Form.	0.216	0.24	5.64	6.984	1.728	-	0.024	-	-	0.192	-	15.048
10WA-82	wt.%	0.56	0.88	32.31	47.28	8.76	-	0.24	0.04	0.01	0.67	0.01	90.76
	Form.	0.144	0.192	5.712	6.888	1.8	-	-	-	-	0.096	-	15.048
10WA-82	wt.%	0.51	0.96	33.00	45.53	9.39	-	0.15	-	0.01	0.88	0.03	90.46
	Form.	0.144	0.216	5.88	6.888	1.8	-	-	-	-	0.096	-	15.048
10WA-82	wt.%	0.44	1.20	31.52	45.40	8.84	-	0.21	-	-	0.73	0.01	89.30
	Form.	0.12	0.264	5.736	7.008	1.72	-	-	-	-	0.072	-	14.90

SERICITE (cont'd) TABLE A4

Mineralised Horizon (cont'd)

Sample		Na	Mg	Al	Si	K	Ca	Ti	Cr	Mn	Fe	Ni	Total
13WA-82	wt%	0.66	0.67	33.86	47.61	9.78	-	0.16	-	0.03	1.03	-	93.80
	Form.	0.148	0.144	5.832	6.96	1.824	-	-	-	-	0.12	-	15.048
13WA-82	wt.%	0.78	0.77	34.27	47.40	9.25	-	0.33	-	0.05	1.30	-	94.16
	Form.	0.216	0.168	5.88	6.888	1.704	-	-	-	-	0.144	-	15.024
13WA-82	wt.%	0.70	0.66	33.47	48.05	9.70	-	0.10	-	0.01	1.68	-	94.38
	Form.	0.192	0.144	5.736	7.008	1.8	-	-	-	-	0.192	-	15.048
13WA-82	wt.%	0.99	0.54	34.56	46.90	9.04	-	0.18	-	0.02	1.61	-	93.85
	Form.	0.264	0.096	5.952	6.864	1.68	-	-	-	-	0.192	-	15.048
13WA-82	wt.%	0.85	0.64	34.48	47.85	8.91	-	0.17	-	-	1.39	-	94.29
	Form.	0.24	0.12	5.88	6.936	1.632	-	-	-	-	0.168	-	15.000
T60-21-82	wt.%	0.28	1.79	30.69	48.15	8.50	0.01	0.20	0.09	0.03	0.82	-	90.56
	Form.	0.072	0.384	5.424	7.224	1.608	-	-	-	-	0.096	-	14.808
T60-21-82	wt.%	0.28	1.78	29.74	48.32	8.70	-	0.35	0.07	-	0.71	-	89.94
	Form.	0.072	0.408	5.28	7.296	1.656	-	-	-	-	0.072	-	14.83
T60-21-82	wt.%	0.42	1.46	31.85	44.54	8.66	0.02	0.18	0.13	0.02	1.10	-	88.38
	Form.	0.12	0.336	5.808	6.912	1.704	-	-	-	-	0.144	-	15.024
T60-21-82	wt.%	0.29	1.96	30.29	47.46	9.17	0.01	0.10	0.04	0.06	0.80	0.01	90.19
	Form.	0.072	0.432	6.12	7.176	1.752	-	-	-	-	0.096	-	14.95

TABLE A5 : Biotite microprobe analyses

BIOTITE

TABLE A5

Biotite Tuff

Sample		Na	Mg	Al	Si	K	Ca	Ti	Cr	Mn	Fe	Ni	Total
82-12c	wt.%	0.02	8.51	16.78	35.58	4.30	0.14	0.30	-	0.16	23.71	0.03	89.54
	Form.	-	1.932	1.62	2.916	0.44	-	0.048	-	-	1.62	-	7.704
82-12c	wt.%	0.01	8.12	15.40	33.50	7.62	0.05	0.31	0.01	0.13	24.62	-	89.82
	Form.	-	1.02	1.524	2.832	0.816	-	0.048	-	-	1.74	-	7.992
82-12c	wt.%	-	8.27	15.42	35.73	8.01	0.07	0.29	-	0.18	24.82	-	92.81
	Form.	-	0.996	1.476	2.916	0.828	-	0.048	-	-	1.692	-	7.968

TABLE A6 : Feldspar microprobe analyses

FELDSPAR

Biotite Tuff

TABLE A6

Sample		Na	Mg	Al	Si	K	Ca	Ti	Cr	Mn	Fe	Ni	Total
82-12b (core)	wt.%	11.41	-	19.88	67.55	0.05	0.08	-	-	-	-	0.04	99.04
	Form.	0.976	-	1.012	2.976	-	-	-	-	-	-	-	4.984
82-12b (halfway)	wt.%	11.60	-	17.83	69.15	0.02	-	-	-	-	0.05	-	98.66
	Form.	0.992	-	0.927	3.053	-	-	-	-	-	-	-	4.97
82-12b (rim)	wt.%	12.16	-	18.94	69.00	0.05	0.06	-	-	0.01	0.04	0.04	100.3
	Form.	1.027	-	0.972	3.01	0.002	-	-	-	-	-	-	5.01
82-12b (d.c)-	wt.%	10.80	-	18.39	68.20	0.06	0.09	-	-	0.02	-	0.05	97.41
	Form.	0.932	-	0.965	3.038	-	-	-	-	-	-	-	4.93
82-12b (d.c)	wt.%	12.37	-	18.50	70.13	0.08	0.07	-	0.02	0.03	0.02	-	101.22
	Form.	1.036	-	0.942	3.030	0.003	0.002	-	-	-	-	-	5.016
82-12b (rim)	wt.%	10.38	-	18.35	66.85	0.03	0.04	-	0.01	0.01	0.03	-	95.72
	Form.	0.913	-	0.981	3.033	0.002	0.001	-	-	-	-	-	4.930
82-12b (core)	wt.%	11.55	0.02	19.03	67.67	0.06	0.14	-	0.02	-	0.03	-	98.52
	Form.	0.993	-	0.994	3.002	0.002	0.005	-	-	-	-	-	4.997
82-12b (d.c)	wt.%	11.44	-	19.04	69.19	0.07	0.10	-	0.01	0.07	0.04	-	99.93
	Form.	0.966	-	0.977	3.018	0.003	0.003	-	-	0.001	0.001	-	4.970
82-12b (rim)	wt.%	11.80	0.02	18.79	68.04	0.17	0.18	-	-	0.03	-	-	99.03
	Form.	1.010	-	0.977	3.006	0.009	0.007	-	-	-	-	-	5.009
82-12c (core)	wt.%	11.23	0.02	18.39	69.27	0.10	0.14	0.01	-	0.03	0.08	-	99.27
	Form.	0.956	-	0.951	3.042	0.005	0.05	-	-	-	0.002	-	4.96
82-12c (rim)	wt.%	12.27	-	18.68	70.87	0.07	0.04	-	-	0.01	0.04	0.01	101.98
	Form.	1.018	-	0.942	3.034	0.002	0.001	-	-	-	-	-	4.998
82-12c (core)	wt.%	11.41	0.05	18.90	68.39	0.32	0.11	-	-	0.02	0.10	-	99.30
	Form.	0.972	0.002	0.980	3.009	0.017	0.003	-	-	-	0.002	-	4.986
82-12c (rim)	wt.%	11.62	-	18.63	66.95	8.05	0.05	-	-	-	-	0.03	97.34
	Form.	1.010	-	0.985	3.006	0.002	0.001	-	-	-	-	-	5.004
82-12c (core)	wt.%	11.09	0.02	18.90	70.21	0.04	0.03	-	0.02	-	-	-	100.3
	Form.	0.930	-	0.964	3.041	0.001	-	-	-	-	-	-	4.937
82-12c (rim)	wt.%	11.84	-	19.13	68.74	0.05	0.13	-	-	0.02	-	-	99.92
	Form.	1.003	-	0.985	3.005	0.002	0.005	-	-	-	-	-	5.000
82-12c (d.)	wt.%	11.74	0.02	18.15	67.35	0.21	0.04	0.1	-	0.01	-	0.01	97.73
	Form.	1.01	-	0.93	3.02	0.12	0.02	-	-	-	-		5.038

TABLE A6 : (contd)

FELDSPAR (contd.)

TABLE A6

		Na	Mg	Al	Si	K	Ca	Ti	Cr	Mn	Fe	Ni	
82-12c	wt.%	10.52	0.09	19.61	70.02	0.78	0.27	-	-	-	0.36	-	101.67
(m)	Form.	0.876	0.005	0.992	3.009	0.042	0.011	-	-	-	0.012	-	4.948
82-12c	wt.%	11.94	-	19.39	71.69	0.05	0.22	-	-	0.01	0.04	-	103.33
	Form.	0.976	-	0.963	3.025	0.002	0.088	-	-	-	0.001	-	4.976
82-12c	wt.%	10.24	-	19.99	70.08	0.08	0.04	-	-	-	0.06	0.04	100.52
	Form.	0.848	-	1.008	3.016	-	-	-	-	-	-	-	4.88
82-12c	wt.%	6.42	0.82	24.52	61.77	4.48	0.05	-	-	0.01	1.24	0.01	100.34
(e)	Form.	9.552	0.048	1.288	2.76	0.256	-	-	-	-	-	-	4.912
82-12c	wt.%	9.98	-	20.14	73.61	0.09	0.03	-	-	-	0.04	0.01	103.91
	Form.	0.800	-	0.984	3.056	-	-	-	-	-	-	-	4.84
82-12c	wt.%	9.02	-	20.13	74.35	0.07	-	-	-	-	0.02	-	103.61
	Form.	0.72	-	0.984	3.056	-	-	-	-	-	-	-	4.784
82-12c	wt.%	10.86	0.02	20.34	74.08	0.07	0.08	-	-	0.01	0.03	0.05	105.55
	Form.	0.856	-	0.984	3.04	-	-	-	-	-	-	-	4.88
82-12c	wt.%	10.99	-	20.24	71.77	0.05	0.06	-	-	-	0.04	-	103.15
	Form.	0.896	-	1.00	3.016	-	-	-	-	-	-	-	4.912
82-12c	wt.%	10.92	-	20.29	72.91	0.06	0.06	-	-	-	0.04	-	104.29
	Form.	0.88	-	0.992	3.024	-	-	-	-	-	-	-	4.896
				Large Quartz Crystal Tuff									
82-30	wt.%	12.81	0.01	20.04	74.27	0.01	0.14	0.02	-	0.02	0.13	0.04	107.48
	Form.	1.009	-	0.960	3.019	-	0.006	-	-	-	0.003	-	4.997
82-30	wt.%	10.68	0.02	19.68	69.53	0.05	0.17	-	-	0.04	0.01	-	99.99
(R.V.C.)	Form.	0.898	0.001	0.997	3.021	0.002	0.007	-	-	0.001	-	-	4.927
82-30	wt.%	11.26	-	20.18	74.68	0.02	0.16	-	-	-	0.07	-	106.31
	Form.	0.888	-	0.968	3.04	-	-	-	-	-	-	-	4.904
82-30	wt.%	10.67	-	20.13	74.20	0.01	0.05	-	0.02	0.03	-	-	105.12
	Form.	0.848	-	0.976	3.048	-		-	-	-	-	-	4.872
82-30	wt.%	10.85	0.13	20.52	72.89	0.25	0.25	-	0.01	-	0.12	0.01	105.02
	Form.	0.864	-	1.00	3.016	0.008	0.008	-	-	-	-	-	4.904
82-30	wt.%	11.27	0.01	19.51	73.02	0.02	0.04	-	-	-	-	-	103.86
	Form.	0.932	-	0.96	3.048	-	-	-	-	-	-	-	4.912
82-30	wt.%	11.72	-	19.61	74.39	0.04	0.13	-	-	-	0.06	0.02	105.75
(d.c)	Form.	0.933	-	0.939	3.056	0.001	0.004	-	-	-	0.001	-	4.934

TABLE A6 : (contd)

		FELDSPAR (contd.)											TABLE A6
		Na	Mg	Al	Si	K	Ca	Ti	Cr	Nb	Ba	Ni	
82-30	wt.%	10.41	0.07	20.14	75.01	0.03	0.11	-	-	0.01	0.1[illegible]	-	105.93
	Form.	0.824	-	0.968	3.056	-	-			-	-	-	4.848
				Quartz crystal tuff									
82-1	wt.%	11.66	-	19.79	72.96	0.04	0.08	-	-	0.01	-	-	104.54
(a)	Form.	0.936	-	0.968	3.032	-	-	-	-	-	-	-	4.936
82-1	wt.%	10.79	-	19.96	66.09	0.05	0.63	-	-	-	0.04	-	97.57
(a)	Form.	0.936	-	1.048	2.96	-	0.024	-	-	-	-	-	4.968
82-1	wt.%	9.55	-	20.16	68.23	0.05	0.13	-	0.02	0.05	0.06	-	98.26
	Form.	0.816	-	1.04	3.00	-	-	-	-	-	-	-	4.856
82-1	wt.%	10.07	-	20.99	74.61	0.03	0.78	-	0.02	0.06	0.04	0.04	106.63
	Form.	0.792	-	1.00	3.024	-	0.037	-	-	-	-	-	4.86
82-1	wt.%	9.37	-	19.90	73.63	0.05	0.18	-	-	-	0.03	-	103.16
	Form.	0.752	-	0.976	3.072	-	-	-	-	-	-	-	4.808
82-1	wt.%	10.84	-	20.03	71.06	0.04	0.73	-	-	-	0.03	-	102.76
	Form.	0.888	-	1.00	3.008	-	0.026	-	-	-	-	-	4.92
82-1	wt.%	10.76	-	20.02	70.67	0.05	0.24	-	0.01	0.01	-	0.05	101.86
	Form.	0.888	-	1.00	3.008	-	0.08	-	-	-	-	-	4.912
82-1	wt.%	10.00	-	20.05	73.83	0.04	0.63	-	0.02	0.02	0.02	0.03	104.62
	Form.	0.8	-	0.976	3.056	-	0.016	-	-	-	-	-	4.848
82-c3a	wt.%	11.81	-	19.07	72.76	0.03	0.02	-	-	-	0.07	-	103.77
	Form.	0.96	-	0.944	3.048	-	-	-	-	-	-	-	4.952
82-c16	wt.%	11.70	-	20.14	72.40	0.04	0.32	-	-	-	0.06	0.03	104.69
	Form.	0.944	-	0.984	3.008	-	0.08	-	-	-	-	-	4.964
82-c16	wt.%	11.38	-	19.23	73.25	0.03	0.01	-	0.02	0.01	0.04	0.04	103.99
	Form.	0.92	-	0.944	3.056	-	-	-	-	-	-	-	4.91
81-74	wt.%	12.59	-	20.56	77.67	0.03	0.09	-	-	0.02	0.03	-	110.99
	Form.	0.952	-	0.944	3.04	-	-	-	-	-	-	-	4.944
81-74	wt.%	10.79	-	19.34	71.91	0.02	0.08	-	-	0.06	-	0.03	102.33
	Form.	0.888	-	0.968	3.048	-	-	-	-	-	-	-	4.896
81-74	wt.%	11.00	-	20.15	67.07	0.07	0.29	-	-	0.01	0.01	0.05	98.64
	Form.	0.943	-	1.050	2.967	0.002	0.013	-	-	-	-	0.001	4.976
81-74	wt.%	11.18	-	19.26	70.37	0.01	[illegible]	-	[illegible]	[illegible]	-	-	100.98
	Form.	0.933	-	0.976	3.028	0.001	0.002	-	[illegible]	-	-	-	[illegible]
81-74	wt.%	10.15	-	19.37	[illegible]	[illegible]	0.13	-	-	[illegible]	[illegible]	-	102.21
	Form.	0.813	-	0.963	[illegible]	[illegible]	0.007	-	-	-	-	-	4.896

TABLE A6 : (contd)

FELDSPAR (cont'd)

TABLE A6

		Na	Mg	Al	Si	K	Ca	Ti	Cr	Mn	Fe	Ni	
82-B1(a)	wt.%	12.64	-	20.41	71.97	0.04	0.04	-	0.02	-	0.04	-	105.20
	Form.	1.018	-	1.00	2.991	0.001	0.002	-	-	-	-	-	5.012
82-B1(a)	wt.%	11.56	-	19.83	72.27	0.04	0.03	-	-	-	0.05	-	103.79
	Form.	0.938	-	0.979	3.028	0.001	-	-	-	-	-	-	4.945
82-B1(a)	wt.%	10.56	-	19.55	73.66	0.03	0.06	-	-	-	-	-	103.86
	Form.	0.851	-	0.958	3.056	0.001	0.002	-	-	-	-	-	4.878
82-B1(a)	wt.%	9.66	-	19.67	73.85	0.03	0.03	-	-	-	-	-	103.23
	Form.	0.780	-	0.966	3.078	0.001	-	-	-	-	-	-	4.825
				Mineralized Horizon									
T48-81	wt.%	11.94	-	18.73	70.03	0.02	0.19	-	-	-	0.14	0.04	101.09
	Form.	1.00	-	0.952	3.024	-	-	-	-	-	-	-	4.984
T48-81	wt.%	11.24	0.02	19.02	68.34	0.01	0.06	-	-	0.03	0.10	-	98.82
	Form.	0.96	-	0.984	3.008	-	-	-	-	-	-	-	4.952
T48-81	wt.%	12.03	-	18.45	69.23	0.02	0.16	-	-	-	0.11	-	100.01
	Form.	1.016	-	0.952	3.024	-	-	-	-	-	-	-	4.992
SES-82	wt.%	12.00	-	18.98	70.82	0.05	0.29	-	-	0.01	0.21	0.03	102.39
	Form.	0.992	-	0.952	3.016	-	-	-	-	-	-	-	4.976
SES-82	wt.%	11.89	-	19.99	72.17	0.04	0.32	-	-	-	0.13	-	104.55
	Form.	0.96	-	0.984	3.008	-	0.001	-	-	-	-	-	4.968
SES-82	wt.%	11.82	-	19.62	68.19	0.03	0.57	0.03	0.02	-	0.08	-	100.35
	Form.	1.00	-	1.008	2.976	-	0.24	-	-	-	-	-	5.008
T60-21	wt.%	12.08	-	18.48	68.82	0.02	0.10	-	-	-	0.04	-	99.53
	Form.	1.024	-	0.952	3.016	-	-	-	-	-	-	-	5.00
T60-21	wt.%	11.25	-	19.24	71.08	0.04	0.21	-	-	0.02	0.03	-	101.88
	Form.	0.928	-	0.968	3.032	-	-	-	-	-	-	-	4.928
T60-21	wt.%	11.97	-	18.44	68.58	0.03	0.15	-	0.03	0.01	0.05	0.07	99.34
	Form.	1.016	-	0.952	3.016	-	-	-	-	-	-	-	4.992
				Chemical Sediment									
82-13	wt.%	12.01	-	19.78	72.18	0.04	0.06	-	-	-	0.14	-	104.21
	Form.	0.976	-	0.976	3.016	-	-	-	-	-	-	-	4.968
82-13	wt.%	11.59	-	19.54	72.29	0.07	0.04	-	0.02	0.01	0.10	-	103.65
	Form.	0.944	-	0.968	3.032	-	-	-	-	-	-	-	4.944
82-13	wt.%	11.37	0.01	19.62	74.19	0.04	0.02	-	0.01	0.01	0.04	-	105.90
	Form.	0.904	-	0.952	3.059	-	-	-	-	-	-	-	4.912

TABLE A7 : Carbonate microprobe analyses

CARBONATE

Mineralised Horizon

TABLE A7

Sample		Na	Mg	Al	Si	K	Ca	Ti	Cr	Mn	Fe	Ni	Total
10ES-82	wt.%	-	12.16	-	0.04	0.01	30.29	-	-	8.35	9.16	0.05	60.07
	Form.	-	0.828	-	-	-	1.485	-	-	0.321	0.351	-	2.985
10ES-82	wt.%	0.08	12.25	-	-	-	28.14	0.01	0.04	8.69	8.72	-	57.93
	Form.	0.006	0.867	-	-	-	1.431	-	-	0.348	0.345	-	2.996
6NA-82	wt.%	0.01	19.72	0.05	0.05	-	33.00	-	0.02	2.64	5.47	0.03	61.00
	Form.	-	1.227	-	-	-	1.476	-	-	0.093	0.189	-	2.985
6NA-82	wt.%	0.02	20.10	-	-	0.01	33.68	0.01	0.04	2.23	5.59	0.04	61.72
	Form.	-	1.233	-	-	-	1.485	-	-	0.075	0.192	-	2.988
6NA-82	wt.%	-	19.82	-	-	-	33.30	-	-	2.20	5.99	0.03	61.34
	Form.	-	1.227	-	-	-	1.485	-	-	0.075	0.207	-	2.994
6NA-82	wt.%	0.02	19.48	-	0.04	0.01	33.36	-	-	2.36	5.61	-	60.89
	Form.	-	1.215	-	-	-	1.497	-	-	0.084	0.195	-	2.991
T96-11	wt.%	-	21.74	-	0.04	-	35.10	0.01	0.03	3.98	3.57	0.05	64.52
	Form.	-	1.269	-	-	-	1.473	-	-	0.129	0.117	-	2.988
T96-11	wt.%	0.01	22.08	-	0.06	0.01	32.82	-	0.02	2.39	2.28	0.04	59.70
	Form.	-	1.368	-	-	-	1.461	-	-	0.084	0.078	-	2.991
T96-11	wt.%	0.04	22.24	-	0.04	0.02	33.65	-	-	2.94	3.27	0.05	62.35
	Form.	-	1.335	-	-	-	1.443	-	-	0.099	0.111	-	2.988
T96-148	wt.%	0.01	21.01	-	0.16	-	34.32	-	0.02	2.93	3.49	-	62.14
	Form.	-	1.326	-	0.006	-	1.497	-	-	0.099	0.122	-	2.988
T96-148	wt.%	-	22.60	-	-	0.01	34.48	-	-	2.36	4.55	-	64.00
	Form.	-	1.32	-	-	-	1.446	-	-	0.076	0.147	-	2.997
T96-148	wt.%	0.03	19.48	0.57	0.04	-	31.71	-	0.01	1.99	4.31	-	58.19
	Form.	-	1.251	0.027	0.003	-	1.464	-	-	0.072	0.133	-	2.473

TABLE A8 : Arsenopyrite microprobe analyses

TABLE A9 : Pyrite microprobe analyses

ARSENOPYRITE — TABLE A8

Sample		S	Fe	Co	Ni	Cu	Zn	As	Cd	Sn	Total
SES-82	wt%	20.89	37.93	0.03	-	-	0.12	47.07	-	-	106.05
	Form.	0.996	1.039	-	-	-	0.004	0.961	-	-	3.000
SES-82	wt%	21.00	37.64	0.07	0.06	0.03	0.09	47.78	-	0.02	106.69
	Form.	0.996	1.027	-	-	-	-	0.969	-	-	2.992
T60-21	wt%	20.21	37.21	0.08	0.02	-	0.21	46.61	0.01	0.02	104.37
	Form.	0.984	1.039	0.004	-	-	0.004	0.969	-	-	3.000
T60-21	wt%	21.34	36.64	0.02	0.04	0.07	0.33	45.45	-	0.06	103.95
	Form.	1.031	1.016	-	-	-	0.008	0.941	-	-	2.996
T60-21	wt%	21.31	37.57	0.05	-	-	0.03	45.39	0.05	0.03	104.43
	Form.	1.023	1.039	-	-	-	-	0.934	-	-	2.996

PYRITE — TABLE A9

Sample		S	Fe	Co	Ni	Cu	Zn	As	Cd	Sn	Total
SES-82	wt%	51.33	48.68	0.05	-	0.05	0.02	0.03	0.01	0.03	100.21
	Form.	1.961	1.055	-	-	-	-	-	-	-	2.996
SES-82	wt%	51.19	47.91	0.07	-	-	-	0.06	-	0.03	99.27
	Form.	1.949	1.047	-	-	-	-	-	-	-	2.996
SES-82	wt%	51.03	47.38	0.05	0.03	0.01	0.01	0.32	-	-	98.82
	Form.	1.953	1.039	-	-	-	-	0.04	-	-	2.996
10WA-82	wt%	50.69	46.07	0.02	-	0.01	0.09	0.02	-	0.03	96.68
	Form.	1.969	1.031	-	-	-	-	-	-	-	3.000
10WA-82	wt%	51.27	46.27	-	0.07	0.03	-	0.03	0.05	0.02	97.74
	Form.	1.973	1.023	-	-	-	-	-	-	-	2.996
106WA-82	wt%	51.80	48.87	0.04	-	0.02	-	0.07	0.01	-	100.81
	Form.	1.945	1.055	-	-	-	-	-	-	-	3.000
T96-13	wt%	52.11	47.88	0.04	0.01	0.10	0.14	0.03	-	-	100.33
	Form.	1.961	1.035	-	-	-	-	-	-	-	2.996
T96-13	wt%	50.63	48.88	0.07	0.08	0.09	0.16	0.02	0.02	0.01	99.97
	Form.	1.926	1.066	-	-	-	0.04	-	-	-	2.996

TABLE A10 : Sphalerite microprobe analyses

SPHALERITE — TABLE A10

Sample	S	Fe	Co	Ni	Cu	Zn	As	Cd	Sn	Total
SES-82 wt%	32.95	3.51	0.04	0.04	0.11	65.07	0.08	0.29	0.02	102.09
Form.	1.473	0.09	-	-	0.004	1.426	-	0.004	-	2.996
SES-82 wt%	32.52	3.48	-	-	0.05	65.17	0.08	0.27	-	101.57
Form.	1.465	0.09	-	-	-	1.441	-	0.004	-	3.00
SES-82 wt%	31.96	2.50	-	-	0.07	64.69	0.04	0.13	-	99.39
Form.	1.496	0.066	-	-	-	1.461	-	-	-	2.996
SES-82 wt%	30.68	2.80	0.06	-	-	64.77	0.09	0.17	0.05	98.68
Form.	1.434	0.074	-	-	-	1.484	-	0.004	-	2.996
SES-82 wt%	31.03	3.35	0.04	0.05	0.01	62.55	-	0.14	0.02	97.19
Form.	1.465	0.09	-	-	-	1.445	-	-	-	2.996
SES-82 wt%	31.68	3.48	-	0.06	0.04	64.47	0.03	0.18	0.02	99.96
Form.	1.453	0.09	-	-	-	1.449	-	0.004	-	2.996
10WA-82 wt%	32.42	3.48	0.05	0.05	0.09	64.38	0.01	0.14	0.02	100.64
Form.	1.469	0.09	-	-	-	1.434	-	-	-	2.992
10WA-82 wt%	32.72	3.79	0.05	0.04	-	64.21	-	0.12	0.02	100.94
Form.	1.477	0.098	-	-	-	1.422	-	-	-	2.996
10WA-82 wt%	31.62	4.00	-	-	-	63.25	0.02	0.16	0.04	99.09
Form.	1.461	0.105	-	-	-	1.434	-	0.004	-	3.004
10WA-82 wt%	31.61	4.05	0.01	-	0.01	63.45	-	0.16	0.02	98.62
Form.	1.430	0.094	-	-	-	1.473	-	0.004	-	3.000
T60-21 wt%	32.82	2.29	-	0.01	-	66.9	-	0.21	-	100.20
Form.	1.492	0.059	-	-	-	1.445	-	0.004	-	3.000
T60-21 wt%	31.63	1.87	0.10	-	-	66.90	-	0.13	0.06	100.70
Form.	1.445	0.051	0.004	-	-	1.500	-	-	-	3.000
T96-13 wt%	30.30	2.07	0.04	-	0.07	64.21	-	0.08	0.01	96.79
Form.	1.441	0.055	-	-	-	1.500	-	-	-	2.996
T96-13 wt%	30.09	3.30	-	0.04	0.04	63.78	-	0.30	-	97.56
Form.	1.426	0.09	-	-	-	1.480	-	0.004	-	3.000
T96-13 wt%	31.11	2.44	-	0.03	0.03	65.58	0.04	0.17	0.02	99.42
Form.	1.441	0.066	-	-	-	1.488	-	0.004	-	3.000
T96-13 wt%	30.65	2.07	-	-	-	65.45	-	0.28	0.05	98.49
Form.	1.438	0.055	-	-	-	1.504	-	0.004	-	3.000

TABLE A11 : Chalcopyrite microprobe analyses

CHALCOPYRITE — TABLE A11

Sample		S	Fe	Co	Ni	Cu	Zn	As	Cd	Sn	Total
T4A-81	wt%	33.27	30.57	0.05	0.04	33.61	-	0.03	-	0.02	97.61
	Form.	1.961	1.035	-	-	1.000	-	-	-	-	3.996
T4A-81	wt%	31.89	30.41	0.05	0.02	33.06	0.34	0.01	0.01	0.03	95.82
	Form.	1.926	1.055	-	-	1.008	0.012	-	-	-	4.000
5ES-82	wt%	34.06	31.52	0.02	0.05	33.93	0.63	0.03	-	0.07	100.13
	Form.	1.957	1.035	-	-	0.984	0.02	-	-	-	3.996
5FS-82	wt%	32.77	30.68	0.02	-	33.42	0.07	-	-	0.07	97.04
	Form	1.949	1.047	-	-	1.004	0.004	-	-	-	4.004
10WA-82	wt%	31.27	28.02	0.07	-	33.15	0.17	0.08	-	0.06	92.83
	Form.	1.945	1.000	0.004	-	1.043	0.004	-	-	-	4.000
10WA-82	wt%	30.90	28.14	-	-	29.20	2.90	0.02	0.02	0.05	91.24
	Form.	1.953	1.023	-	-	0.934	0.09	-	-	-	4.000
6NA-82	wt%	32.27	30.08	0.02	-	33.05	0.11	0.08	-	0.04	95.66
	Form.	1.945	1.043	-	-	1.004	0.004	-	-	-	4.000
T60-21	wt%	31.98	28.90	0.05	0.04	33.07	0.14	0.07	-	0.10	94.34
	Form.	1.957	1.016	-	-	1.020	0.004	-	-	-	3.996
T60-21	wt%	32.68	30.05	0.02	0.03	33.63	0.23	-	-	0.12	96.75
	Form.	1.949	1.027	-	-	1.012	0.008	-	-	0.004	4.000
T96-13	wt%	31.70	29.38	0.06	-	32.55	1.51	0.02	0.05	0.03	95.31
	Form.	1.926	1.023	-	-	1.000	0.047	-	-	-	3.996
T96-13	wt%	30.82	28.43	0.05	0.04	32.73	0.30	-	-	0.06	92.45
	Form.	1.930	1.023	-	-	1.035	0.008	-	-	-	3.996
T96-13	wt%	32.50	28.35	0.05	0.03	33.42	0.18	-	0.01	0.04	94.58
	Form.	1.977	0.988	-	-	1.027	0.004	-	-	-	3.996

TABLE A12 : Galena microprobe analyses

GALENA — TABLE A12

Sample		S	Pb	Bi	Ag	Sb	Au	Total
T48-81	wt%	14.66	80.68	3.68	1.02	-	0.04	99.08
	Form.	1.051	0.895	0.031	0.023	-	-	2.000
SES-82	wt%	14.63	79.82	0.29	-	0.07	0.08	94.90
	Form.	1.082	0.914	0.004	-	-	-	2.000
SES-82	wt%	14.61	85.10	0.21	0.01	0.05	0.16	100.14
	Form.	1.051	0.945	0.004	-	-	-	2.000
SES-82	wt%	14.64	83.46	0.55	0.11	0.02	-	98.77
	Form.	1.059	0.934	0.008	0.004	-	-	2.004
SES-82	wt%	14.37	86.35	0.53	0.11	0.01	-	101.36
	Form.	1.031	0.961	0.004	0.004	-	-	2.000
IOWA-82	wt%	14.36	89.69	0.06	-	0.05	0.01	104.17
	Form.	1.016	0.980	-	-	-	-	1.996
IOWA-82	wt%	13.35	88.13	0.14	-	0.02	-	102.03
	Form.	0.992	1.000	0.004	-	-	-	1.996
IOWA-82	wt%	14.38	88.70	0.29	-	0.04	0.19	103.59
	Form.	1.020	0.973	0.004	-	-	0.004	2.000
IOWA-82	wt%	13.80	86.65	0.24	0.18	0.07	-	101.03
	Form.	1.012	0.980	0.004	0.004	-	-	2.000
IOWA-82	wt%	14.38	91.55	0.35	-	0.07	0.14	106.50
	Form	1.004	0.988	0.004	-	-	-	1.996
IOWA-82	wt%	14.52	90.77	0.23	0.09	0.04	0.18	105.82
	Form.	1.012	0.980	0.004	-	-	0.004	2.000
T53-81	wt%	14.35	87.64	0.39	0.25	0.06	0.04	103.14
	Form.	1.020	0.965	0.008	0.004	-	-	1.996
T53-81	wt%	14.33	87.33	0.68	0.20	0.04	-	102.98
	Form.	1.020	0.969	0.008	0.004	-	-	2.000
T53-81	wt%	13.70	91.02	0.63	0.14	0.05	-	105.53
	Form.	0.980	1.008	0.008	0.004	-	-	2.000
T53-81	wt%	14.15	84.93	0.56	0.18	0.05	0.13	105.02
	Form.	1.004	0.984	0.008	0.004	-	-	2.000
T60-21	wt%	13.59	87.79	0.49	0.11	0.09	-	102.07
	Form.	0.996	0.996	0.004	0.004	-	-	2.000
T60-21	wt%	14.13	87.45	0.17	0.09	0.06	-	101.90
	Form.	1.020	0.977	-	-	-	-	1.996
T60-21	wt%	13.89	87.39	0.56	0.11	0.03	0.03	101.98
	Form.	1.008	0.980	0.008	0.004	-	-	2.000
T60-21	wt%	14.52	83.42	0.048	0.04	0.06	0.05	98.57
	Form.	1.055	0.938	0.004	-	-	-	1.996
T60-21	wt%	14.16	87.79	0.20	0.02	0.04	-	102.21
	Form.	1.020	0.977	0.004	-	-	-	2.000

TABLE A12 : (contd)

TABLE A13 : Tennantite microprobe analyses

GALENA (cont'd)

Sample		S	Pb	Bi	Ag	Sb	Au	Total
T96-11	wt%	14.16	88.95	0.60	0.12	0.05	-	104.08
	Form.	1.016	0.973	0.008	0.004	-	-	2.000
T96-11	wt%	14.45	86.44	0.48	0.05	0.09	0.09	101.61
	Form.	1.035	0.957	0.004	-	-	-	1.996
T96-11	wt%	14.14	84.64	0.46	0.19	0.04	-	99.66
	Form.	1.039	0.949	0.004	0.004	-	-	1.996
T96-11	wt%	13.98	87.73	0.63	0.16	0.07	0.01	102.58
	Form.	1.008	0.980	0.008	0.004	-	-	2.000
T96-13	wt%	14.91	86.14	0.80	0.25	-	0.05	102.37
	Form.	1.047	0.938	0.008	0.004	-	-	1.996
T96-13	wt%	14.08	87.36	0.71	0.17	0.04	-	102.35
	Form.	1.016	0.973	0.008	0.004	-	-	2.000
T96-13	wt%	14.32	88.20	0.66	0.26	0.03	-	103.48
	Form.	1.016	0.969	0.008	0.004	-	-	1.996
T96-13	wt%	14.30	88.19	0.59	0.24	0.04	0.06	103.63
	Form.	1.016	0.969	0.008	0.004	-	-	1.996
T96-14B	wt%	13.64	85.52	0.02	0.20	0.23	-	99.61
	Form.	1.012	0.980	-	0.004	0.004	-	2.000
T96-14B	wt%	14.59	87.29	0.13	0.09	0.06	-	102.15
	Form.	1.035	0.961	-	-	-	-	1.996
T96-14B	wt%	13.81	87.14	0.12	0.01	0.16	0.16	101.43
	Form.	1.008	0.984	-	-	-	-	1.992

TENNANTITE — TABLE A13

Combination of 2 calibrations: (sample T96-13)

	S	Pb	Bi	Ag	Sb	Au	Total
wt%	24.39	-	-	1.10	6.30	-	31.79

	S	Fe	Co	Ni	Cu	Zn	As	Cd	Sn	Total
wt%	26.48	5.53	-	-	40.09	1.89	17.95	0.05	0.02	92.01

Combination:

S*	Fe	Cu	Zn	Ag	Sb	As	Cd	Sn	Total
25.43	5.53	40.09	1.89	1.10	6.3	17.95	0.05	0.02	98.36

*Average of the 2 calibrations

APPENDIX II

ANALYTICAL TECHNIQUES USED IN THIS STUDY

AII.1: SAMPLE COLLECTION AND PREPARATION

Samples were collected from each rock type that outcrops at Tulks Hill. Those from the adit were relatively fresh and required minimal pre-crushing preparation. Surface rock samples however, needed trimming with a trim saw to remove oxidised portions.

AII.2: MAJOR AND TRACE ELEMENT WHOLE ROCK ANALYSIS

A jaw-crusher was used to reduce the samples to rock chips. These rock chips were pulverised at -200 mesh in a tungsten carbide puck mill for 3 minutes. Between samples the jaw crusher was cleaned with a plastic brush and the finer dust removed using a compressed air hose. The puck mill and rings were thoroughly cleaned with distilled water or ethyl alcohol, and dried with a compressed air hose. Powders were stored in labelled glass jars until use.

MAJOR ELEMENTS: Determinations were made with a digitised Perkin-Elmer (model 370) atomic absorption spectrophotometer, using the flame technique (Analyst: Mrs G.Andrews). The sample preparation followed tha method of Langmhyr and Paus (1968). The limits of precision are listed below in Table AI (from Kay, 1982) using 4 test runs of a granitic rock standard (G-1).

Precision of AAS analysis (n=4)

Element	Published value*	X	S	Range (min-max)
SiO2	69.11	69.70	0.57	68.2-69.96
Al2O3	15.40	15.10	0.24	14.75-15.6
Fe2O3	2.65	2.60	0.02	2.64-2.74
MgO	0.76	0.80	0.05	0.75-0.82
CaO	1.94	2.00	0.10	1.92-2.14
Na2O	4.07	4.30	0.02	4.07-4.21
K2O	4.51	4.56	0.02	4.50-4.57
TiO2	0.50	0.50	0.01	0.47-0.51
MnO	0.03	0.03	0.00	----------

S: standard deviation
X: mean
*: Flanagan 1970

Loss on ignition was determined by weighing an amount of sample in a porcelain crucible, heating to a 1000 degrees centigrade for 2 hours, transfering to a dessicator when cool and re-weighing to determine the percent volatile loss. Gloves were worn during the re-weighing process in order to minimise moisture addition.

TRACE ELEMENTS: The elements Pb, Th, U, Rb, Sr, Y, Zr, Nb, Zn, Cu, Ni, La, Ba, V, Ce, Cr, and Ga were determined by a Philips 1450 fully automated X-ray fluorescence spectrometer equipped with spectrometer/detector, X-ray generator, HP mini-computer, computer controlled input-output and an automatic feeding tray of pressed pellets. The latter are made by weighing out 10g of rock powder and mechanically mixing with 1-1.5g phenyl formaldehyde thermal binding agent (Union Carbide Phenolic Resin, material TR-16933) in a Spex-Mill shaker. The

powder mix is pressed into a disc using a Herzog hydraulic press at a pressure of 300 tons p.s.i., for 60 seconds, followed by baking at 200 degrees centigrade for 7-10 minutes. Sulphide-rich samples tend to blister on baking which may render them useless for analysis. D. Press prepared the analytical calibration programs. USGS standard G-1 was used as a monitor. Analyses are considered accurate to within 10 ppm for most elements, and 10-25 ppm for Ba, Sr and V. Precision is within 10 ppm. Zn, Cu and Pb are less precise at higher abundances in the mineralised samples. Also, secondary Pb peaks interfere with Ga to give erroneously high values for this particular element.

RARE EARTH ELEMENTS: A suite of underground rock samples from the footwall through to the hangingwall were analysed for REE using a thin-film X-ray fluorescence technique after Eby (1972) as modified by Fryer (1977). Analytical errors are given by Fryer (1977). REE plots were normalised to the chondrite values of Taylor and Gorton (1977).

AII.3: ELECTRON MICROPROBE ANALYSIS

Sulphides, silicates and carbonates were analysed using a fully automated JEOL JXA-50A electron probe microanalyser with Kriesel control through a PDP-11 computer. Analyses were performed under the operating

conditions of 15Kv accelerating voltage, a beam current of 0.21-0.23 microamps and a beam diameter of approximately 1 micron. Drift of the beam was checked and corrected periodically. Counts were made for 30 seconds or until 30,000, whichever came first and corrected using the MAGIC correction program (sulphides) or the Alpha Bence-Albee matrix (silicates and carbonates). Calibrations were made using the appropriate standard materials for either the sulphides or the silicates:

1) Clinopyroxene (F-CPX): Na, Mg, Al, Si, K, Ca, Ti, Cr, Mn, Fe, Ni. This calibration was used to analyse feldspar, biotite, sericite, chlorite and carbonate

2) Galena (PBS-CM): Pb, S, Bi, Ag, Sb, Au. This calibration was used to analyse galena

3) Sphalerite (SP20C.2STD): S, Fe, Co, Ni, Cu, Zn, As, Cd, Sn. This calibration was used to analyse sphalerite, chalcopyrite, arsenopyrite, tennantite and pyrite.

Addendum 1

A recent publication by Nowlan and Thurlow (1984) suggests that the Buchans Group and its correlatives are pre-Caradocian in age. Conodonts of latest Arenig - early Llanvirn age were retrieved from a limestone clast within a polylithic breccia unit of the Buchans Group. Although an in-situ source for the limestone clast has not been discovered, a local origin is favoured because the remaining clasts within the breccia are considered to have a local origin. If this age for the Buchans Group is correct the regional model of Dean and Strong (1975) for the evolution of the CVB is in need of revision. Nowlan and Thurlow suggest that the Buchans Group is a correlative of the Victoria Lake Group that now lies structurally above the Victoria Lake Group due southeasterly directed thrusting. This correlation implies that significant mineralisation in the CVB is restricted to the pre-Caradocian phase of volcanism, and the mineralisation at Tulks Hill is of a similar age to the mineralisation at Buchans.

REFERENCE

Nowlan, G.S. and Thurlow, J.G., 1984: Middle Ordovician conodonts from the Buchans Group, central Newfoundland, and their significance for regional stratigraphy of the Central Volcanic Belt: Can. Jour. Earth Sci., vol. 21, pp.284-296

Addendum 2

Iron formation: In this thesis the definition of an iron formation is a rock that has both a cherty matrix and a relative abundance of iron-bearing minerals, for example, iron chlorite (as opposed to magnesium chlorite), iron-rich carbonate and pyrite. These minerals are thought to be the metamorphosed equivalents (greenschist facies) of iron-rich sedimentary/diagenetic minerals (eg. vermiculite). In this respect therefore, the iron formation at Tulks Hill is compatible with the iron formation definition of Bates and Jackson (1980; Glossary of Geology). However, the chemical analyses of this rock do not appear to justify the term iron formation since the iron content of the 3 samples analysed (82-13, -14, -35; Table A1) is less than the "required" 15% (as suggested in the definition of Bates and Jackson, 1980). Because of sampling difficulties many of the thicker orange-coloured lenses of carbonate-chert (the so-called "stringers" in Chapter 4) could not be properly sampled. Therefore the analysis is deficient in the components that comprise these lenses which will bias the chemical analyses towards lower CaO, Fe_2O_3, MgO and SiO_2 values since siderite-rich carbonate and quartz are excluded from the analysis. Since petrographic and chemical studies are dependent upon the sample size (and the quality of sampling) the term iron formation may appear inaccurate based on the chemistry and the mineralogy. In this thesis the term iron formation is based on the

megascopic mineralogy rather than the petrography and the chemistry; the relative abundance of the carbonate-chert lenses suggests that this is a carbonate-silicate facies of an iron formation (although the chemical analysis may not suggest this).

REFERENCE

Bates, R.L. and Jackson, J.A., 1980: Glossary of Geology 2nd edition. Publisher: American Geological Institute, Falls Church, Virginia.

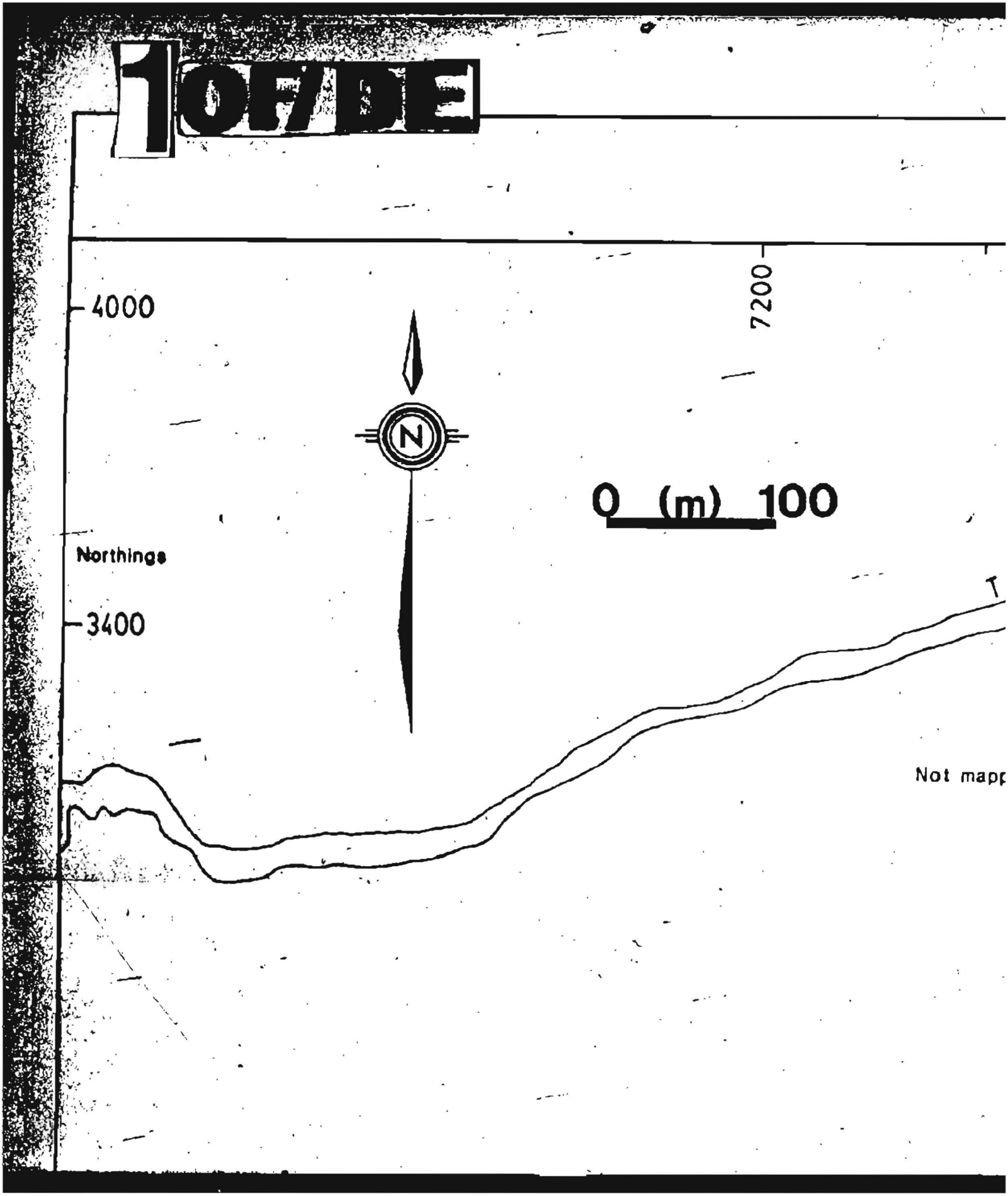
10F/DE
4000
7200
N
0 (m) 100
Northings
3400
Not mapp

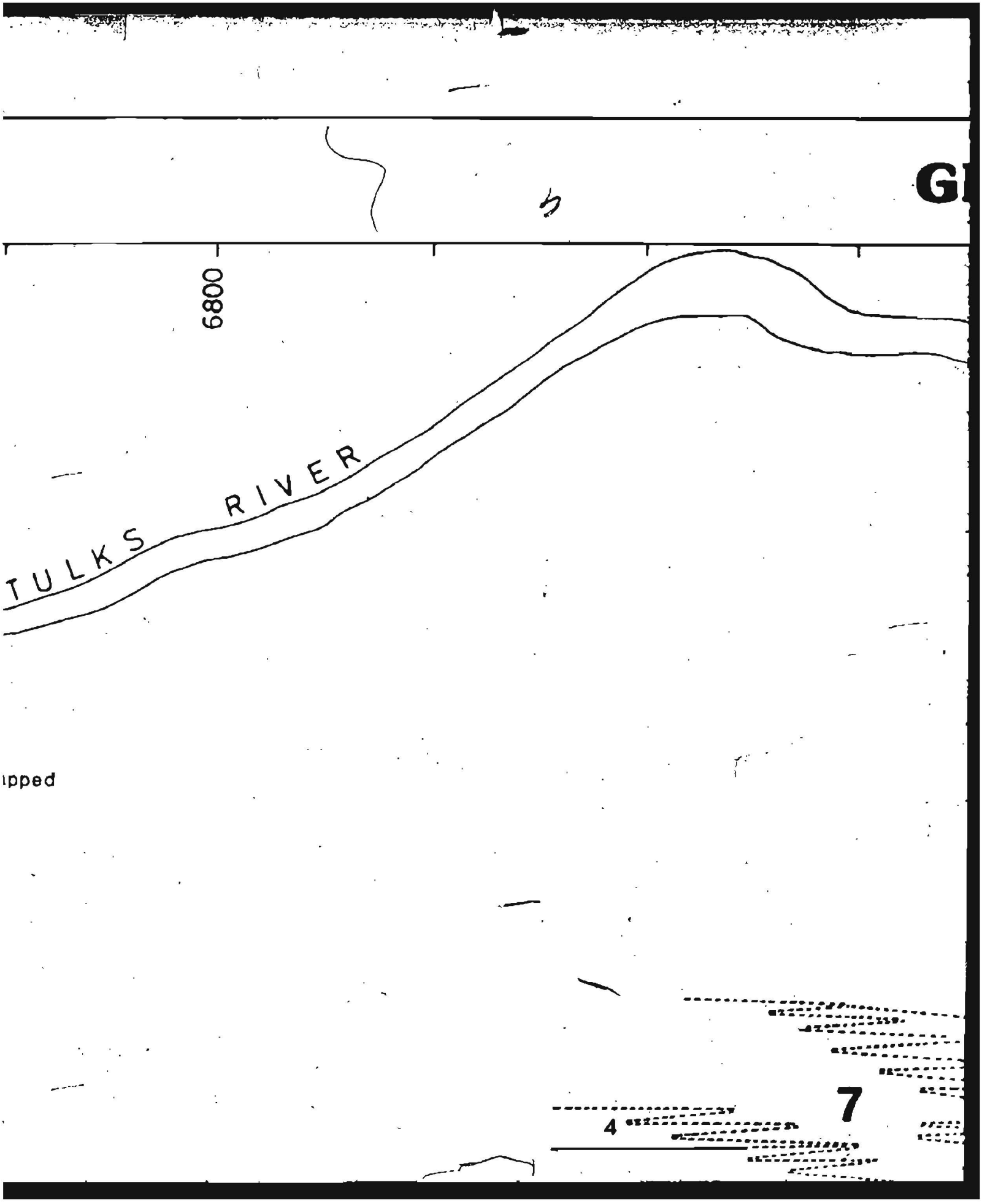
6800
TULKS RIVER
ipped
7
4

2 OF/DE

GEOLOGY OF

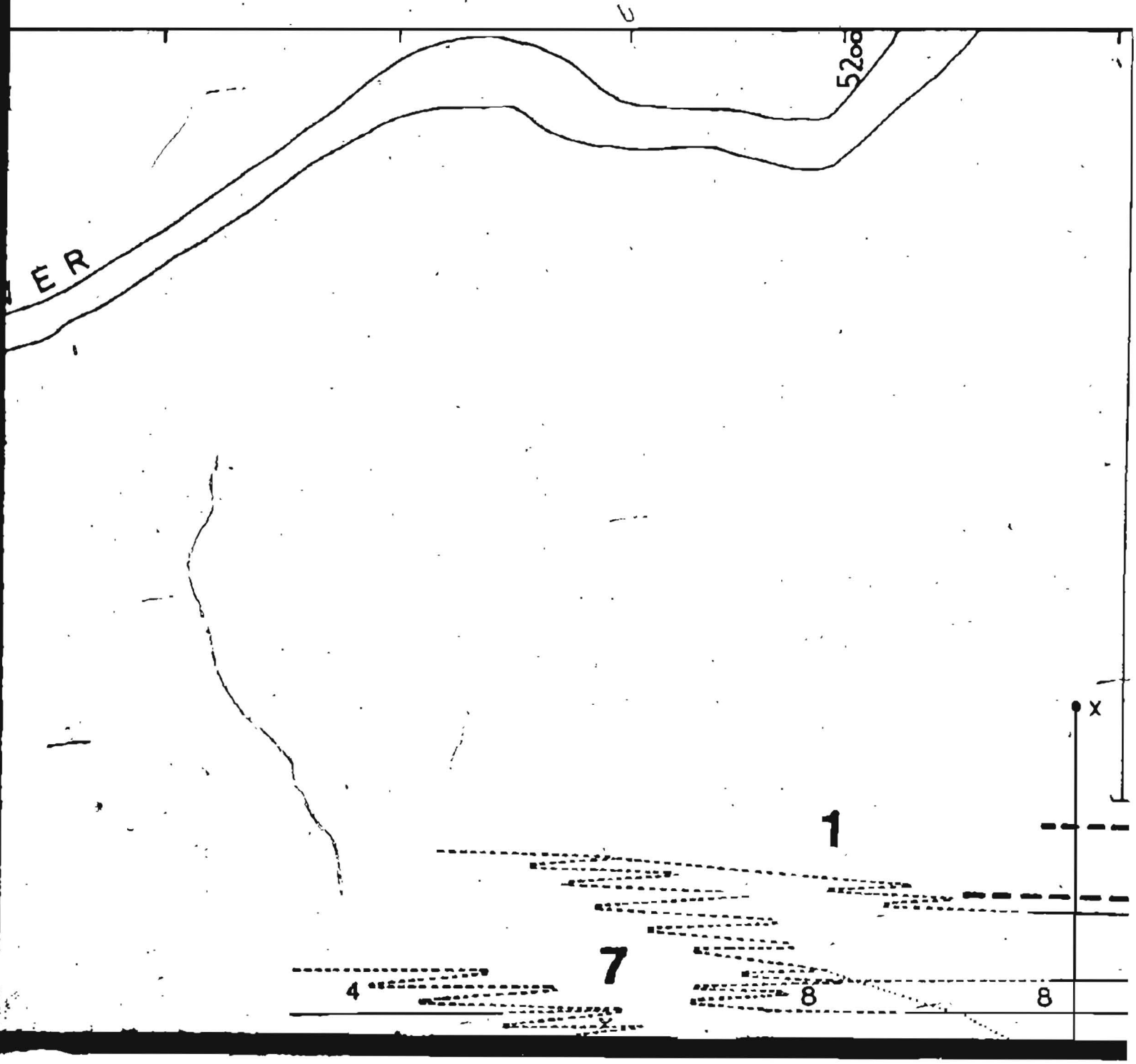

TULKS HILL

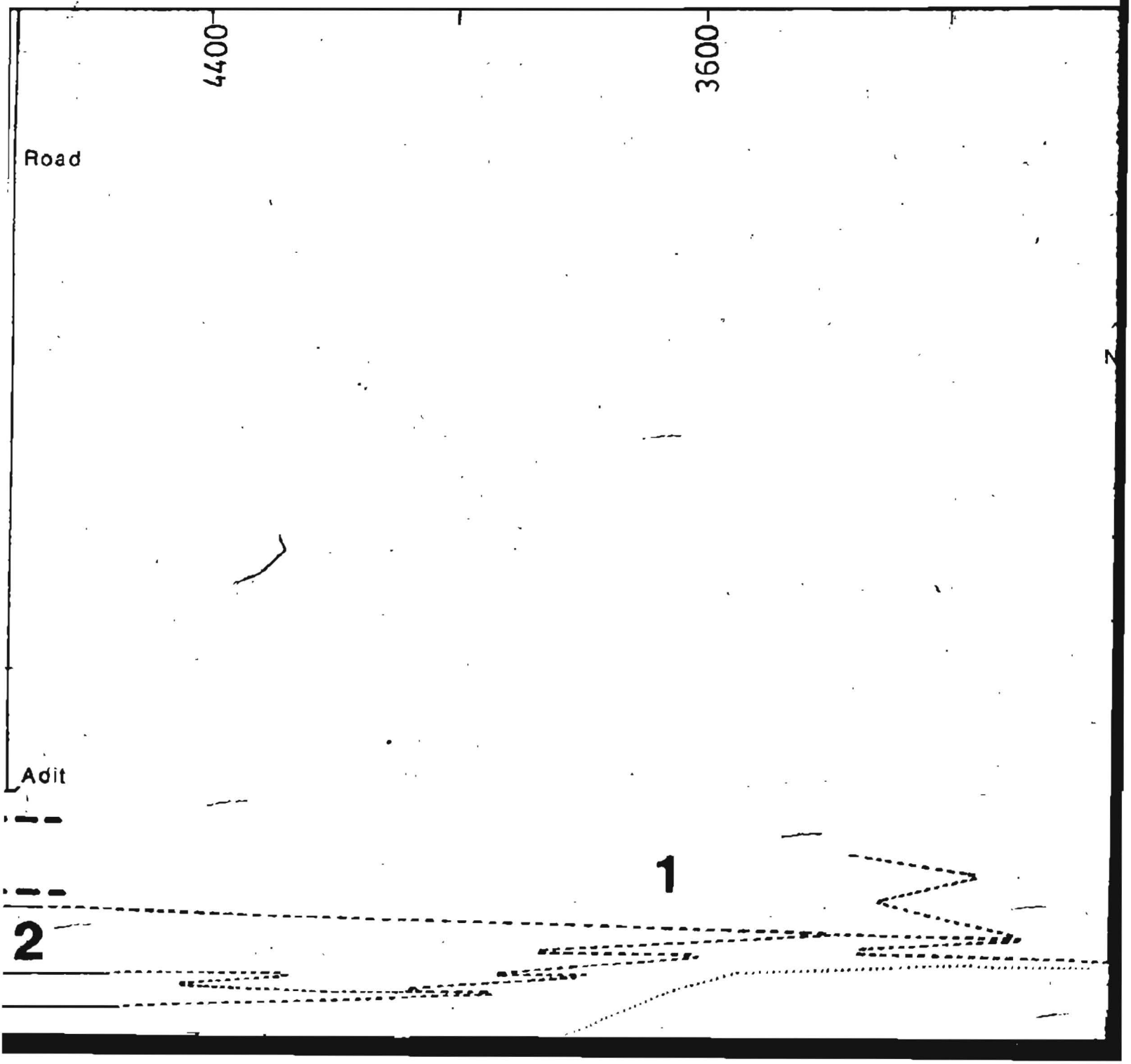

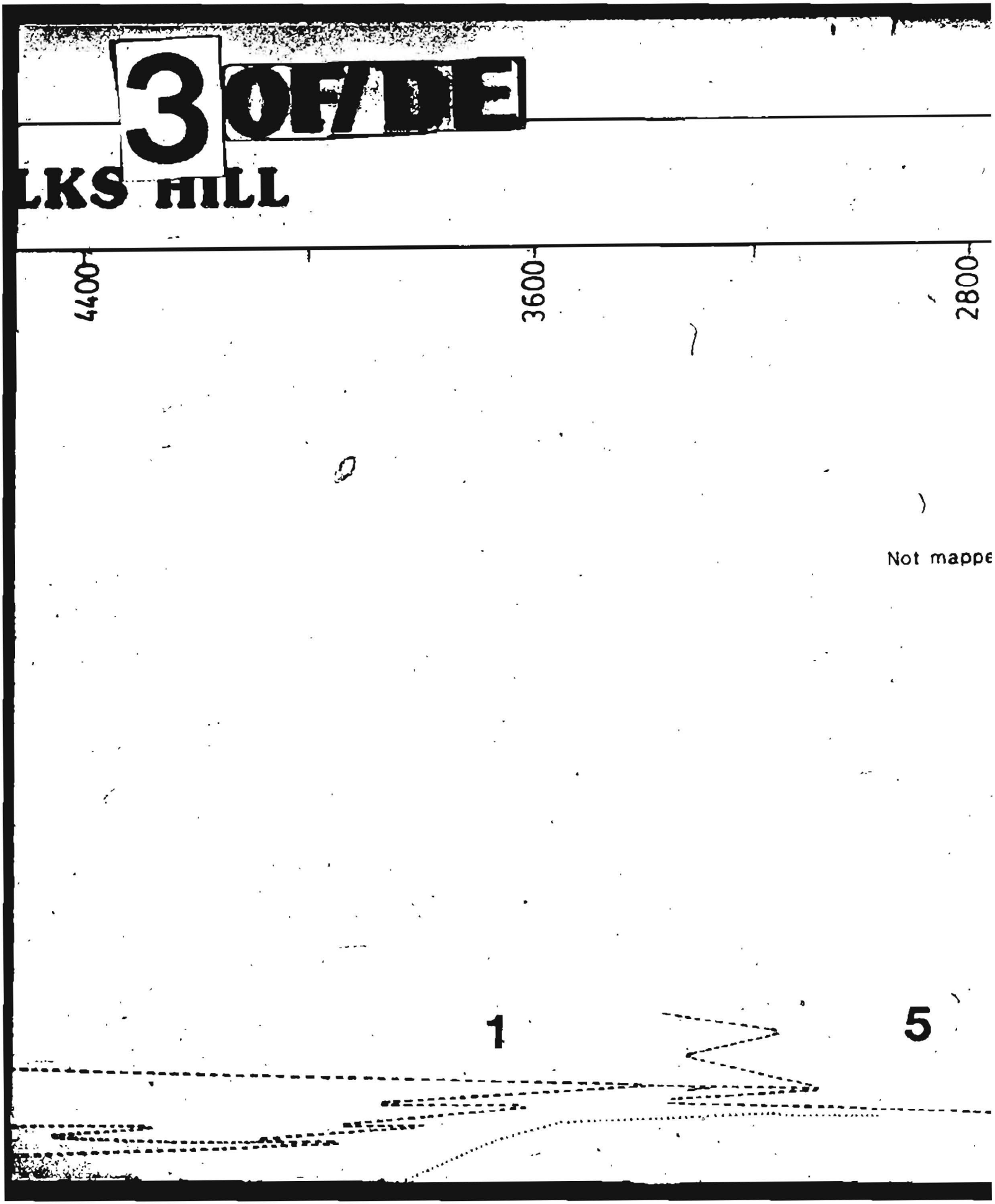
3 OF/DE
LKS HILL
4400
3600
2800
Not mappe
1
5

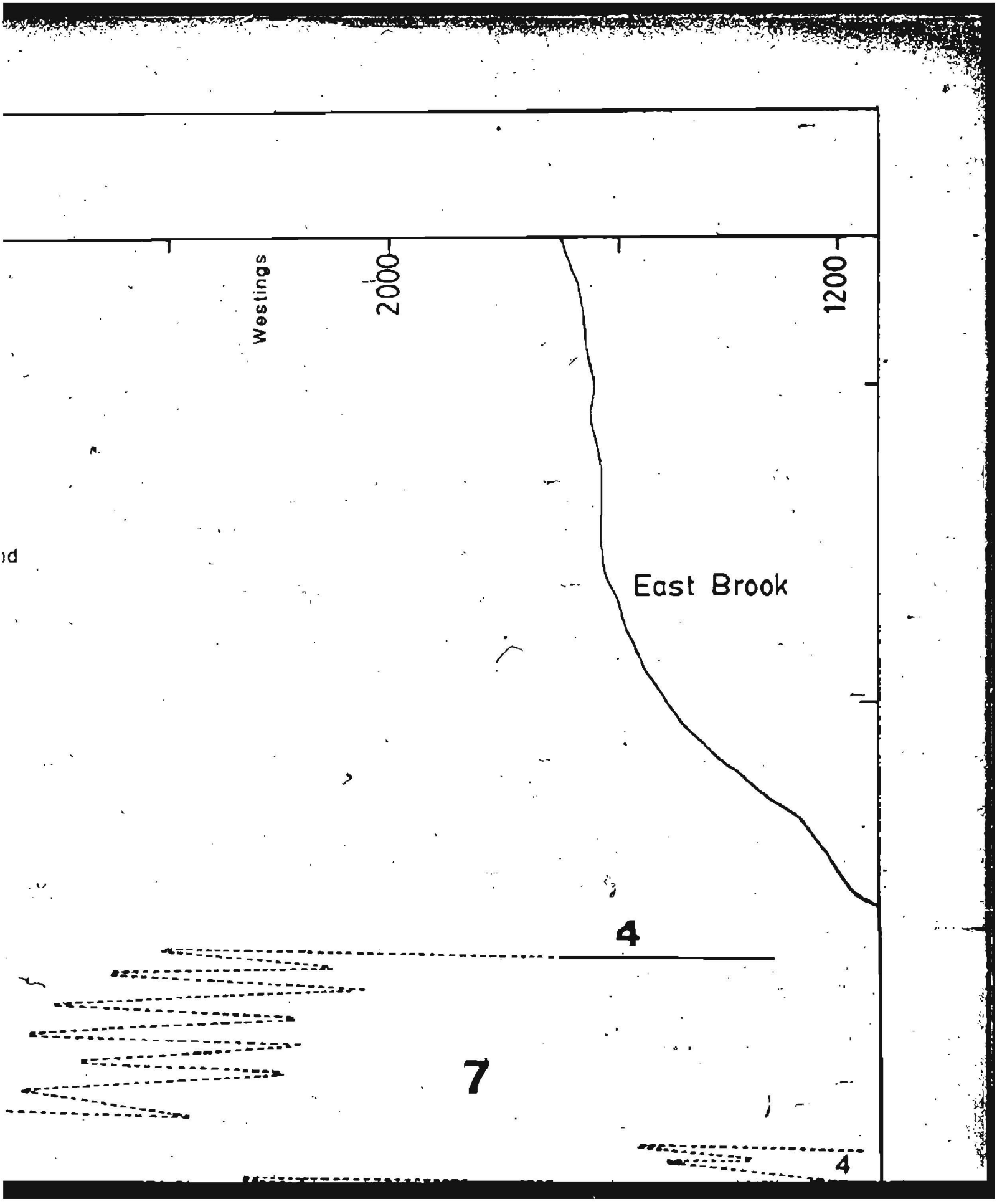
Westings
2000
1200
East Brook
4
7
4

4OF/DE

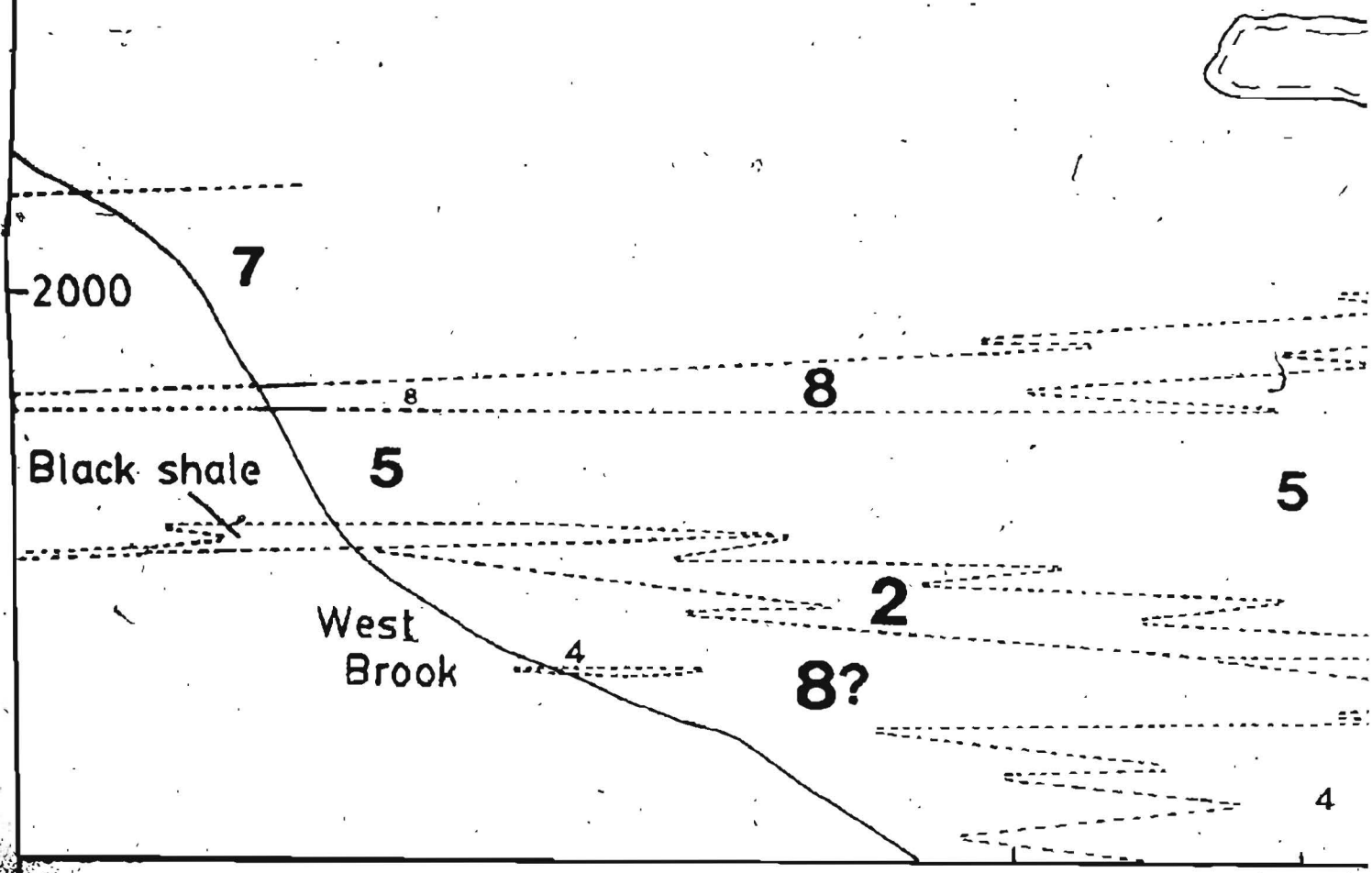

LEGE

1 **RAVEN RHYOLITE**

2 **ALTERED RHYOLITE**

Albitised, chloritised and/or sericitised

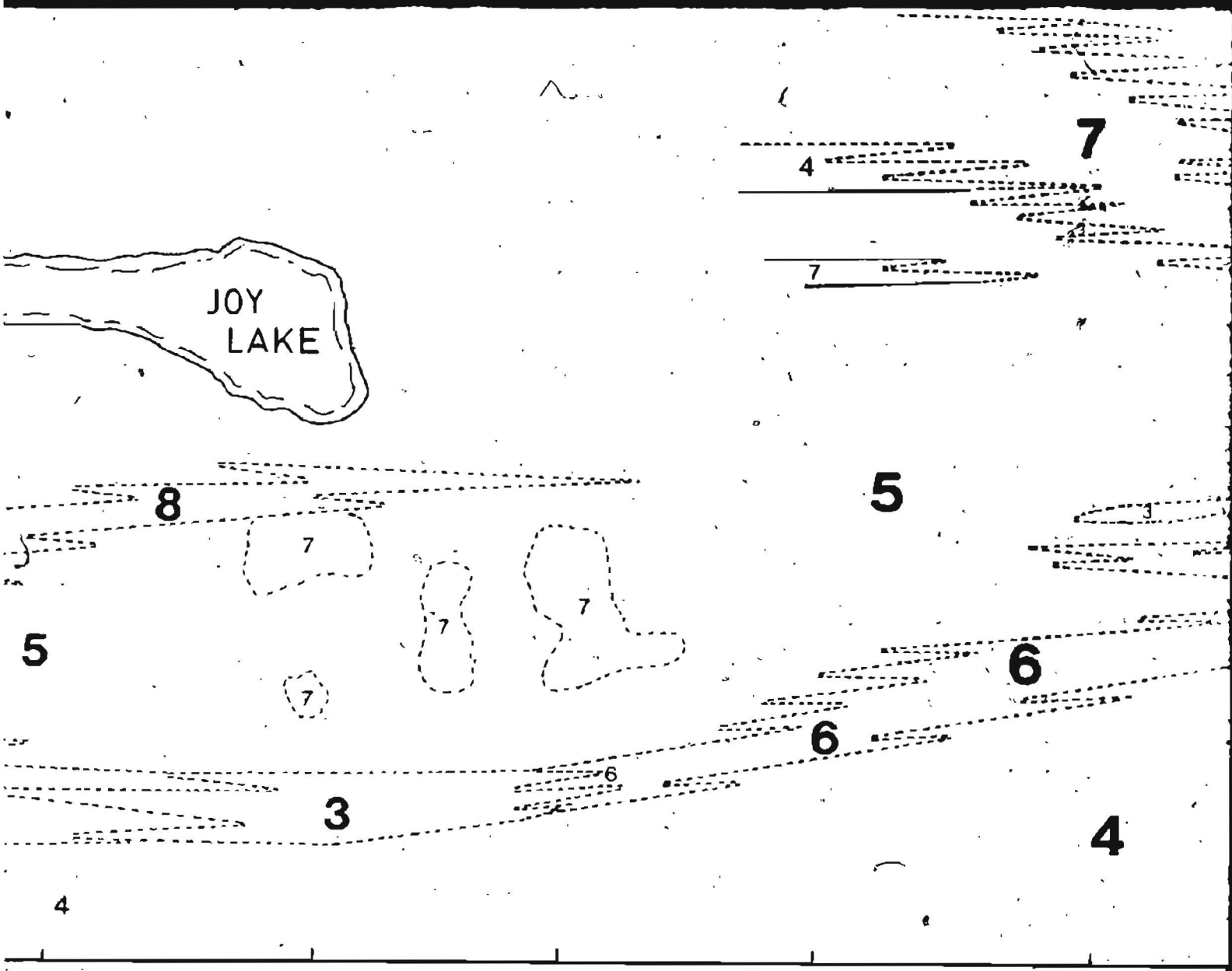

EGEND

5	LARGE QUARTZ CRYS TUFF
6	BIOTITE CRYSTAL TU

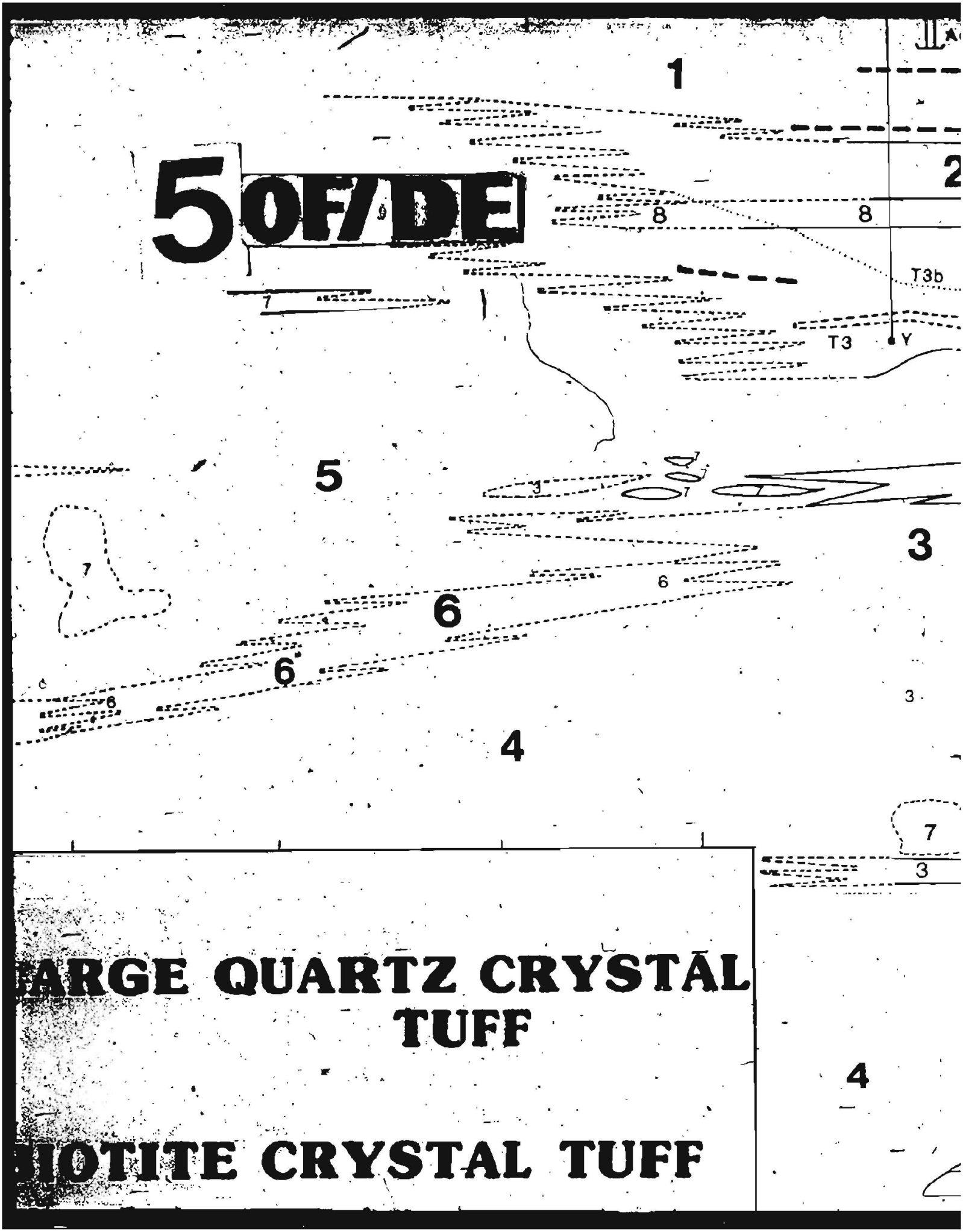
5OF/DE
1
2
8
8
T3b
T3
Y
7
5
3
7
6
6
6
6
4
3
7
3
4
ARGE QUARTZ CRYSTAL
TUFF
IOTITE CRYSTAL TUFF

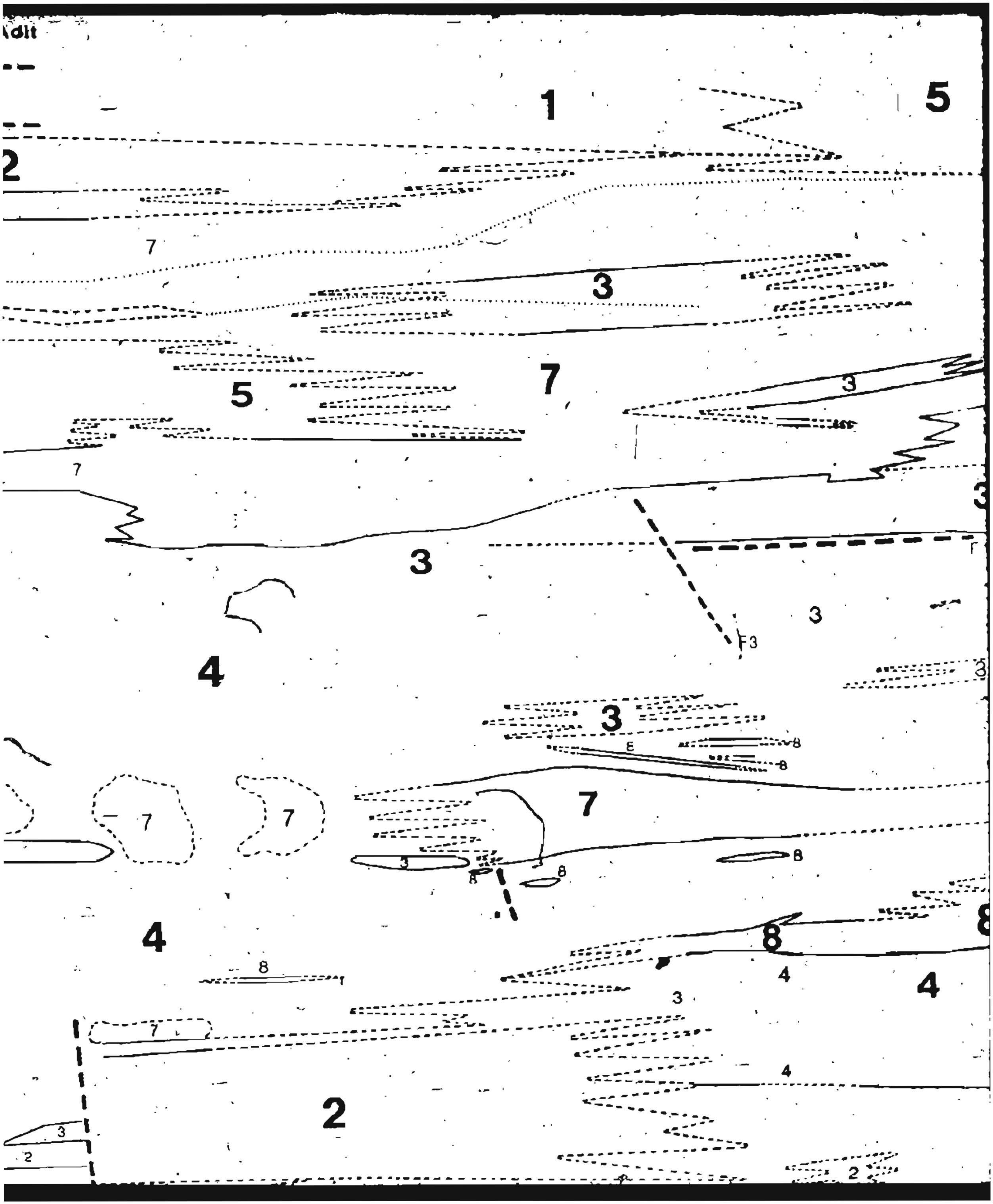
Adit
1
5
2
7
3
7
5
3
3
F3
4
3
8
8
7
7
7
3
8
8
4
8
8
4
4
3
7
4
2
3
2
2

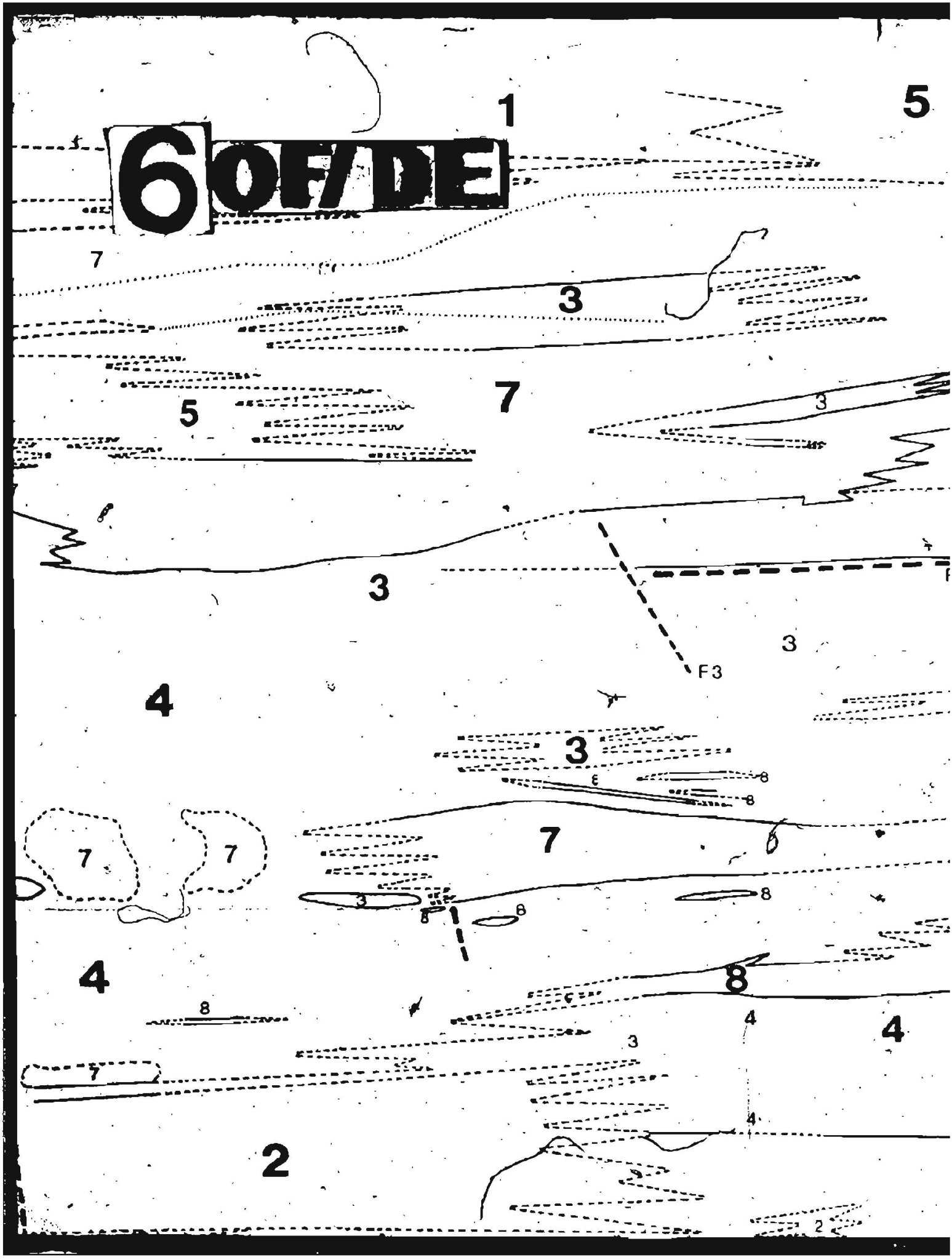
6 OF/DE
1
5
7
3
5
7
3
3
3
F3
4
3
7
7
8
8
4
8
8
4
4
3
7
4
2

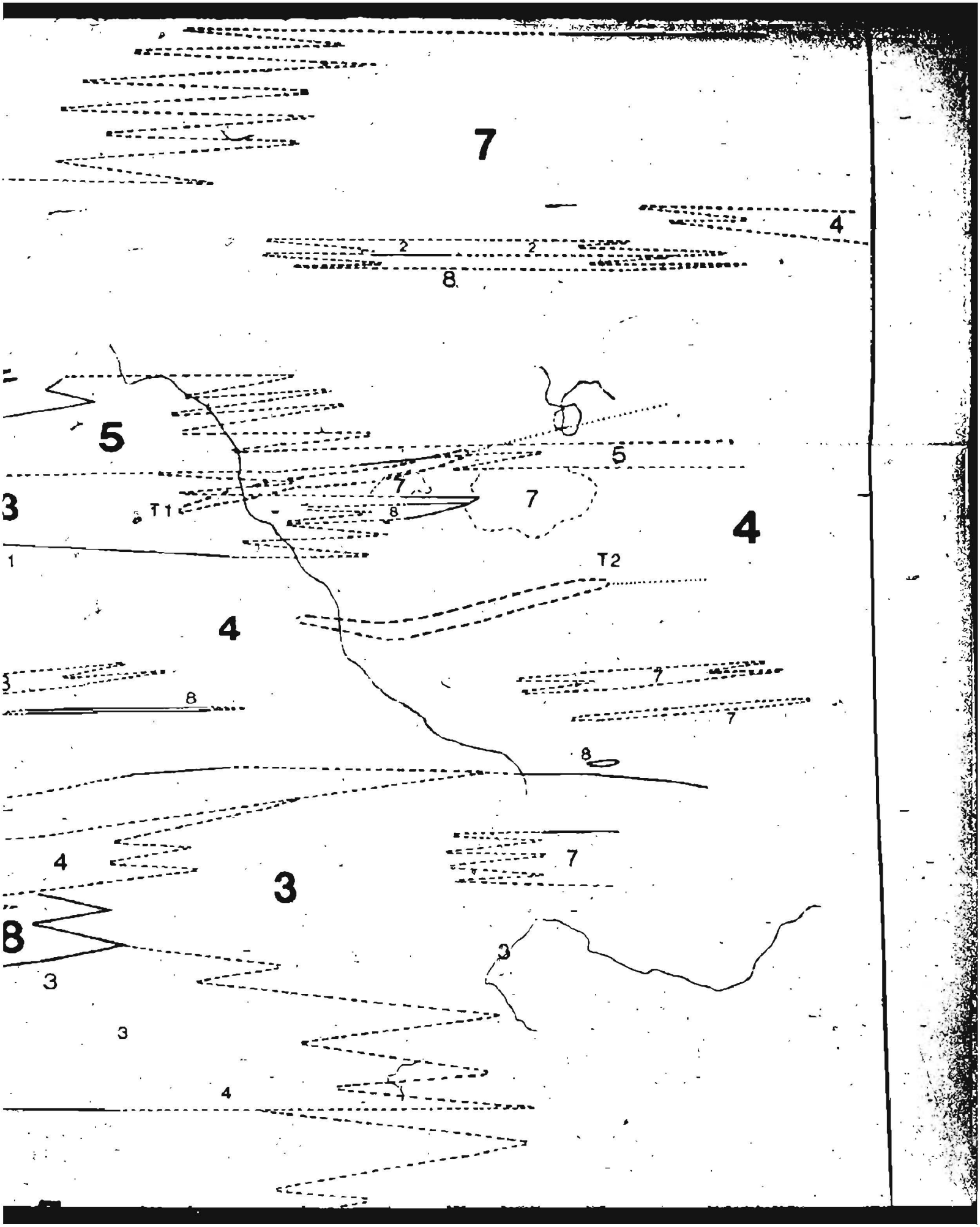
7
4
2
2
8
5
5
3
T1
7
7
8
4
1
T2
4
8
7
7
8
4
7
3
8
3
3
3
4

7 OF/DE

LEGE

1 **RAVEN RHYOLITE**

2 **ALTERED RHYOLITE**

Albitised, chloritised and/or sericitised

3 **VOLCANIC BRECCIA**

4 **QUARTZ CRYSTAL TUFF**

——— Unit contact

- - - - - - Inferred contact

———— Fault

X-Y:Approx. lin

✪ Northings and westings refer to l

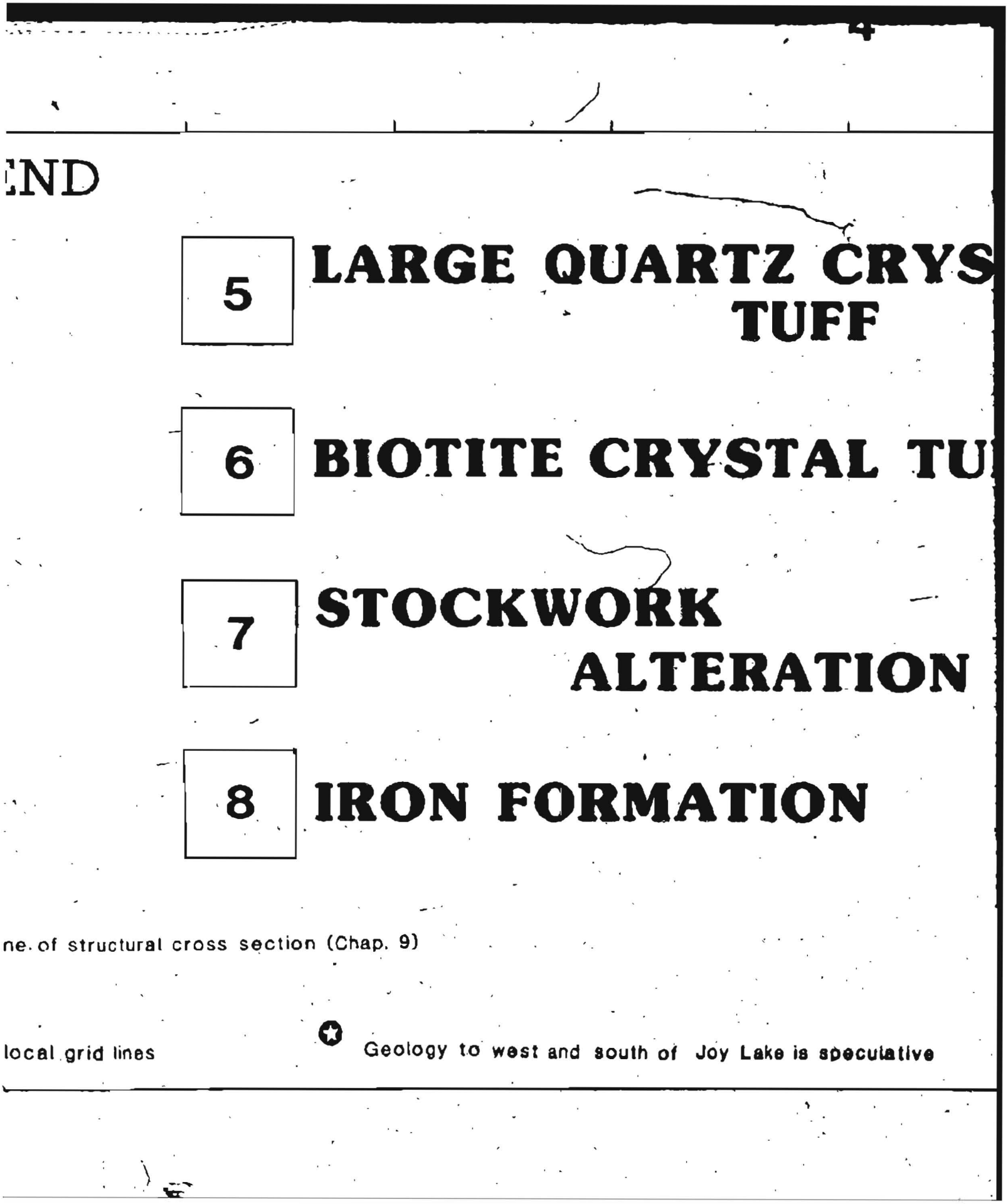
END
5
LARGE QUARTZ CRYS
TUFF
6
BIOTITE CRYSTAL TU
7
STOCKWORK
ALTERATION
8
IRON FORMATION
ne. of structural cross section (Chap. 9)
local grid lines
Geology to west and south of Joy Lake is speculative

ARGE 8 OF/DE YSTAL
TUFF

IOTITE CRYSTAL TUFF

TOCKWORK
ALTERATION

RON FORMATION

nap. 9)

Geology to west and south of Joy Lake is speculative

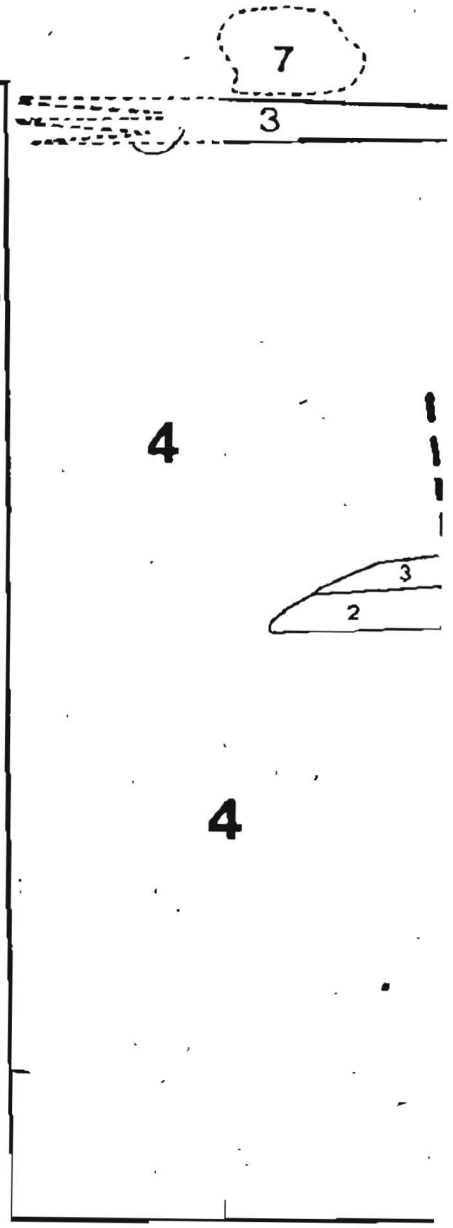

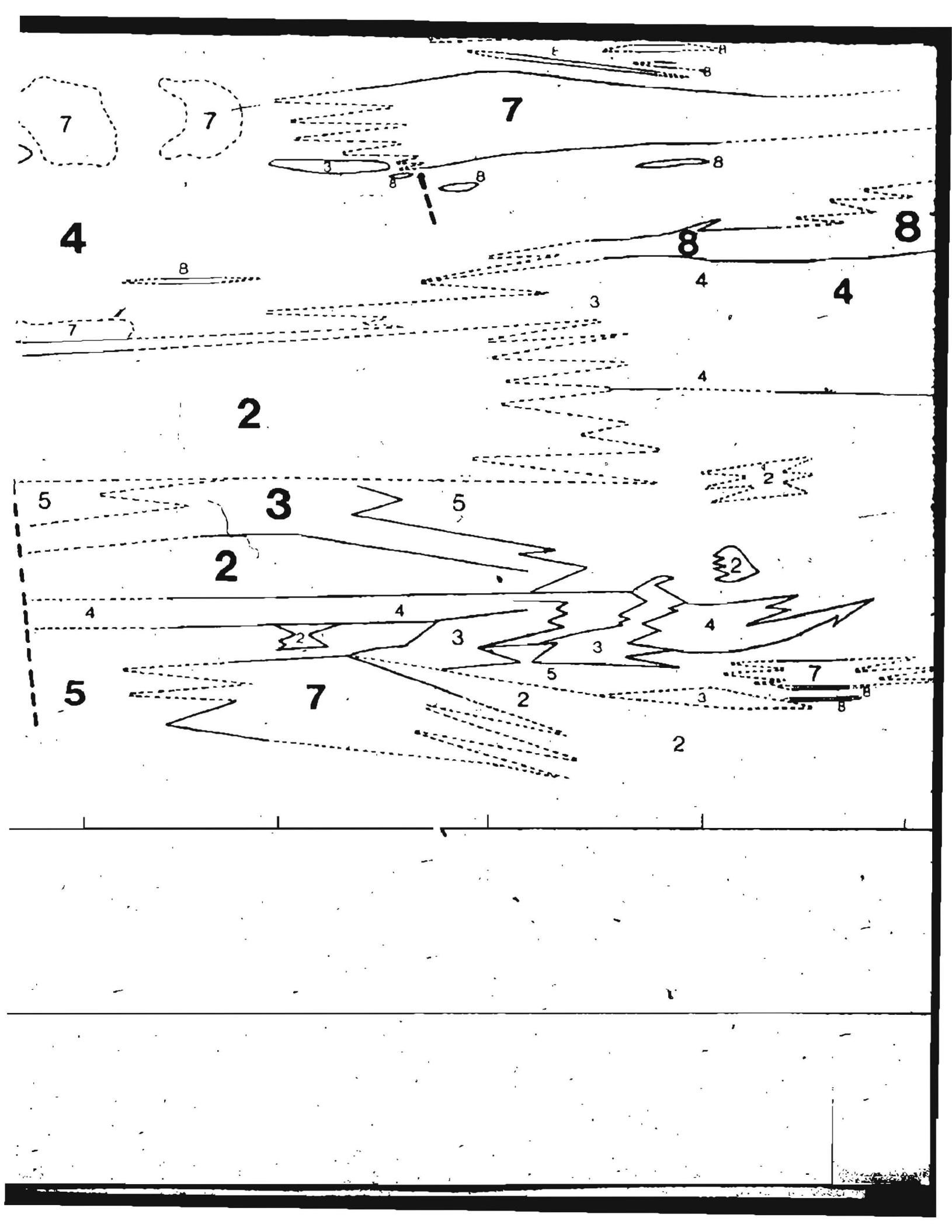

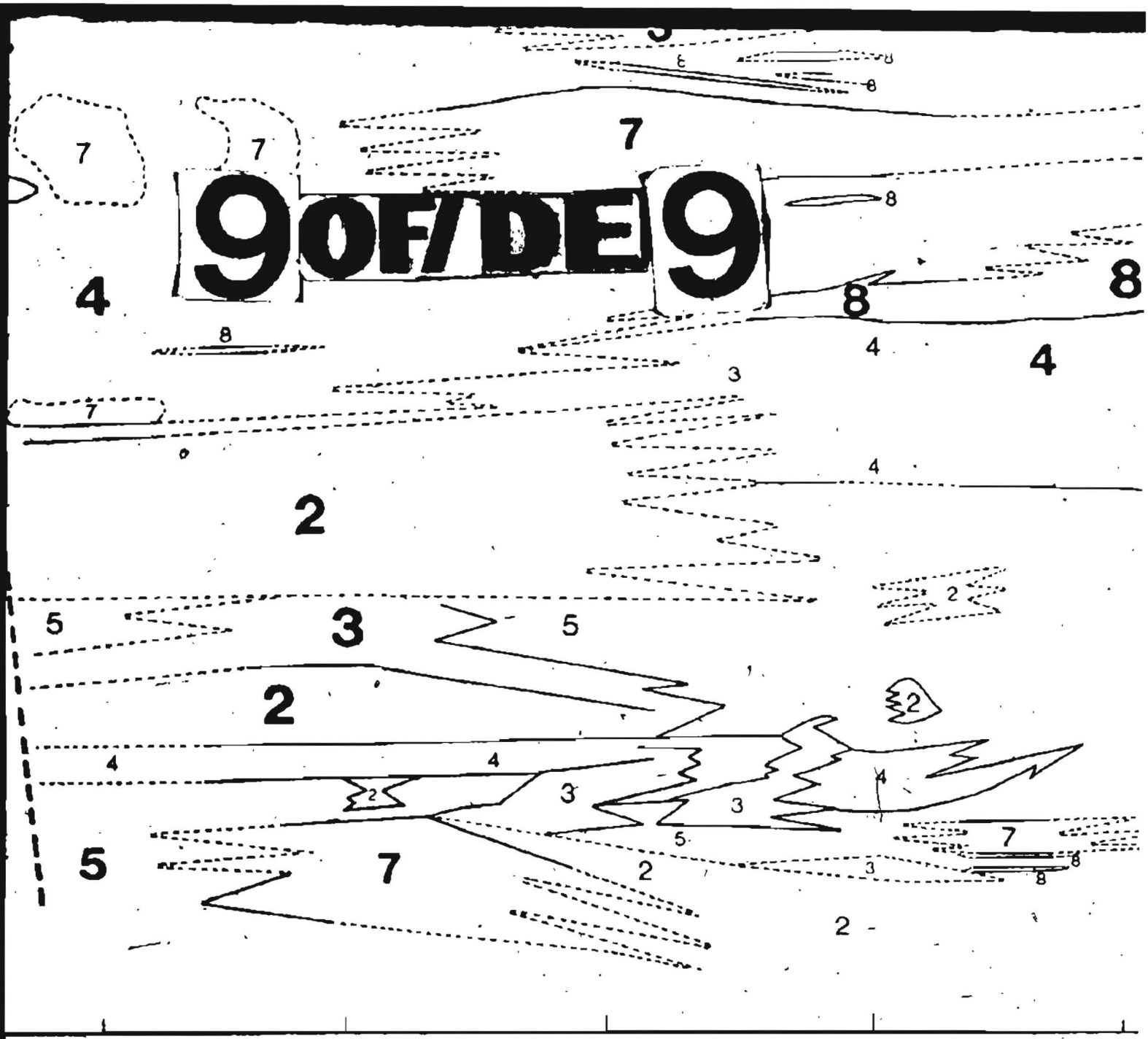
9OF/DE9

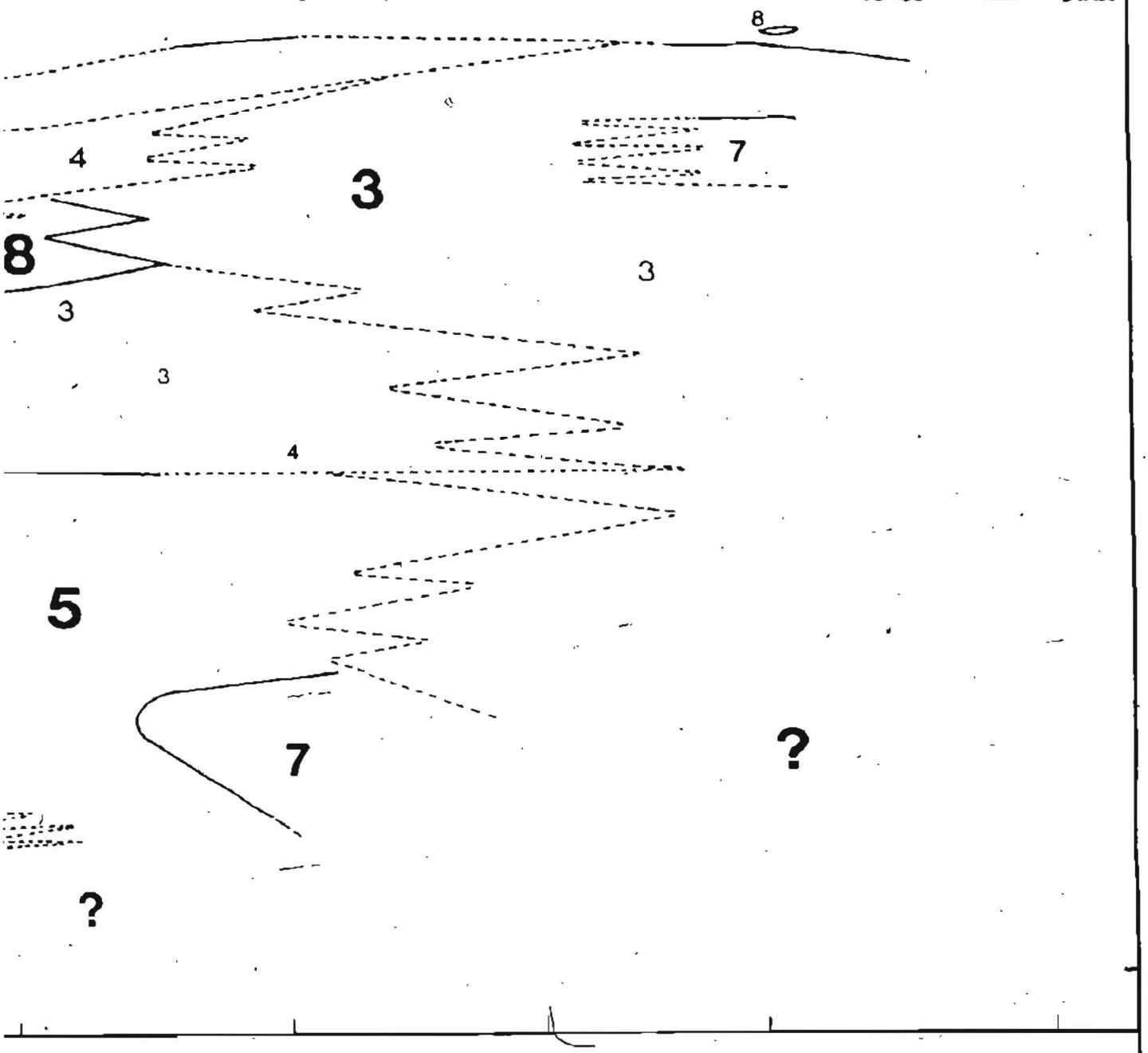

Geology and draughting by C. MORETON 1984


1 OF 1 DE

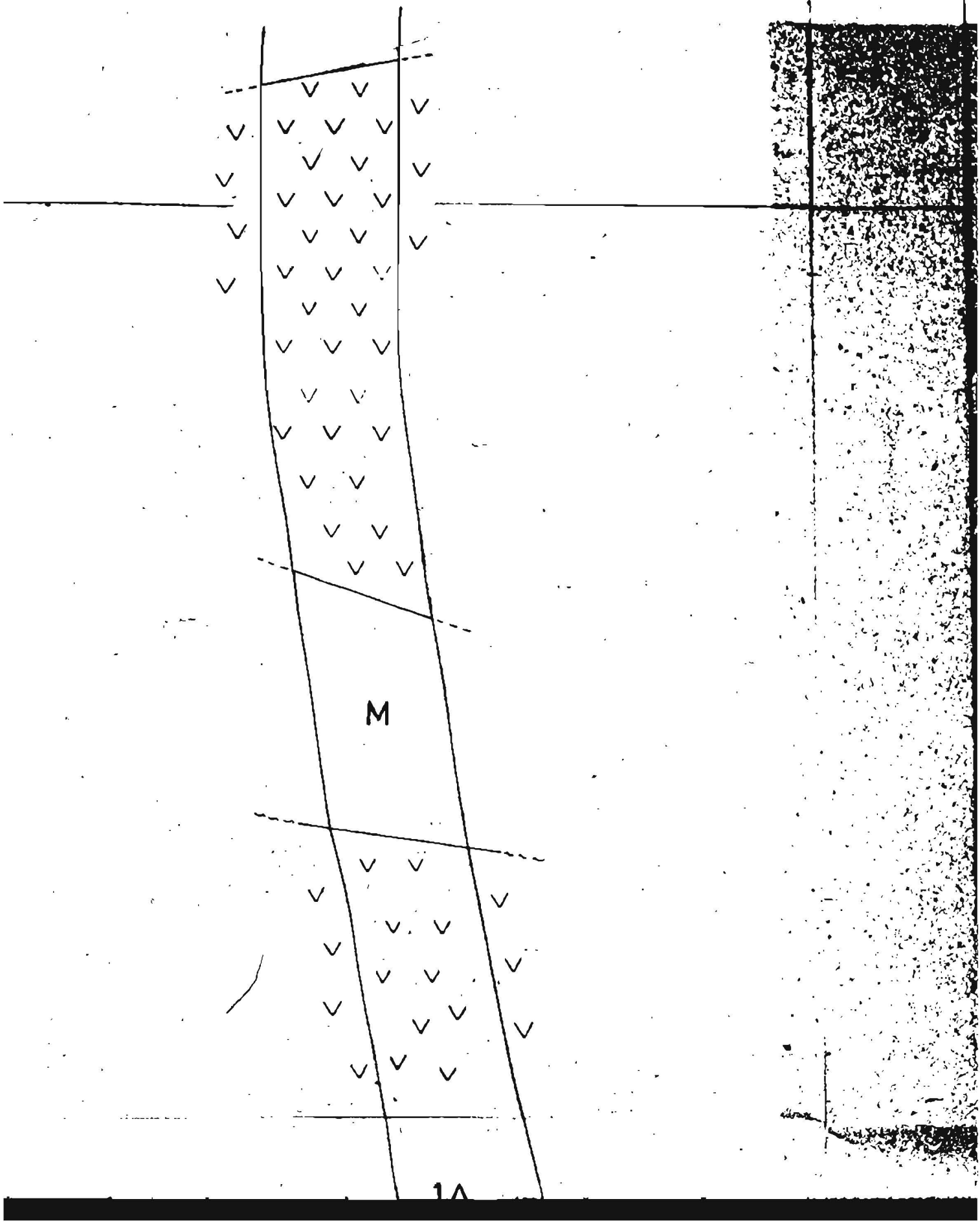
M

2 OF/DE

[redacted]

[redacted] well jointed

[redacted] PYRITE - no jointing

[redacted] WORK

[redacted] OCKWORK

[redacted] E UNIT (CHLORITIC STOCKWORK)

[redacted] ONS

[redacted] ERT UNIT

[redacted] UNIT


3 OF/DE


N

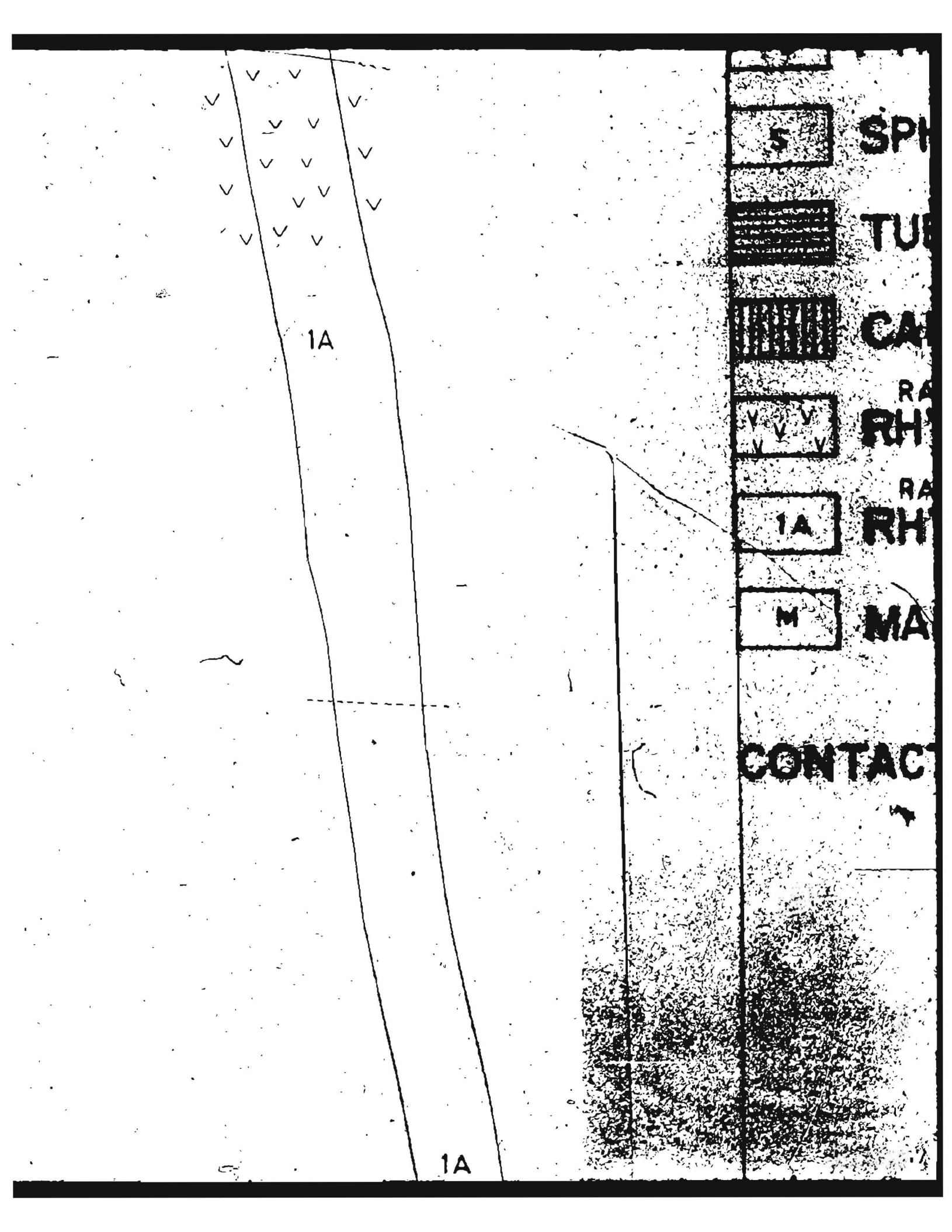
1A
1A
S
SP
TU
CA
RA
RH
RA
RH
1A
M
MA
CONTAC

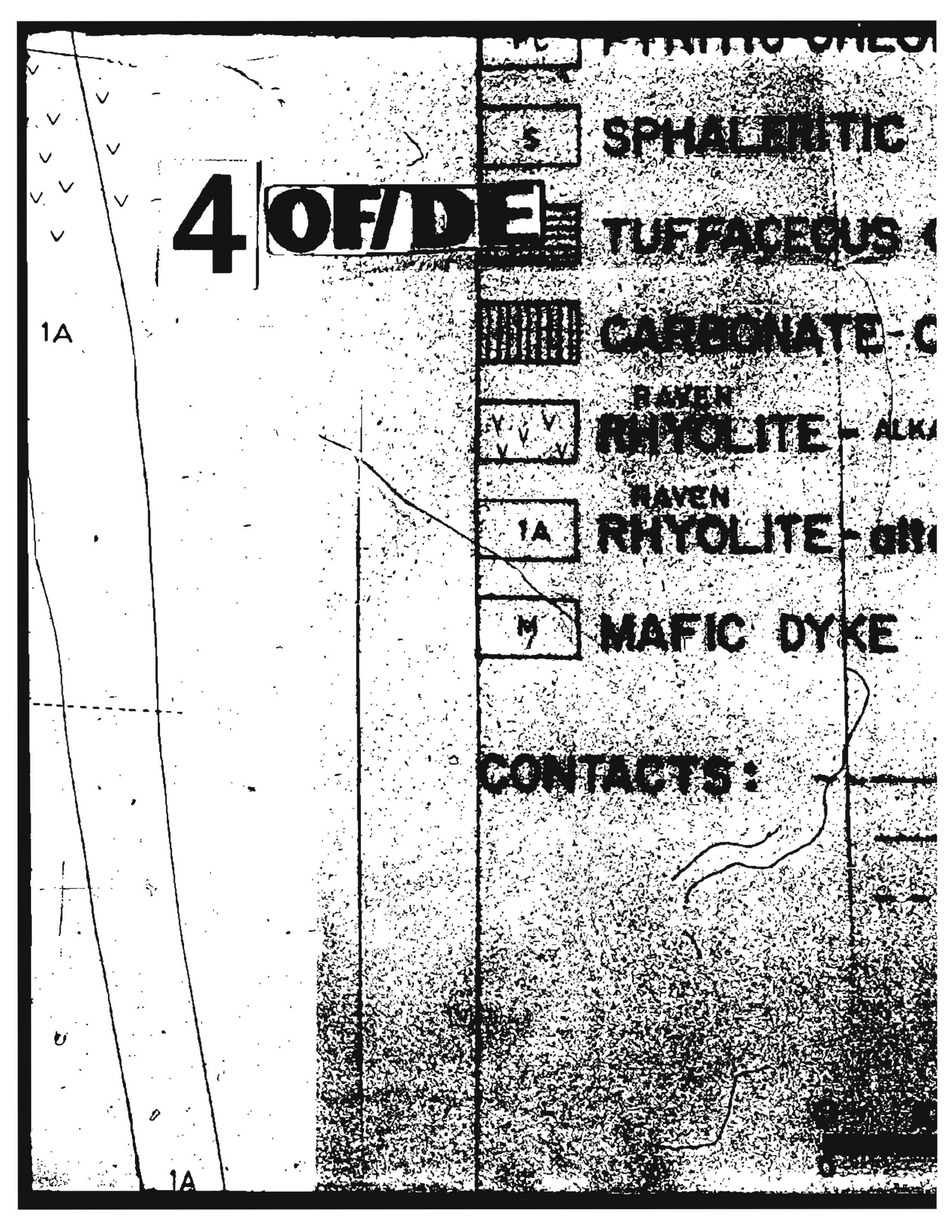
4 OF/DE
1A
SPHALERITIC
TUFFACEOUS
CARBONATE-C
RAVEN
RHYOLITE - ALK
RAVEN
1A
RHYOLITE - GN
MAFIC DYKE
CONTACTS :
1A

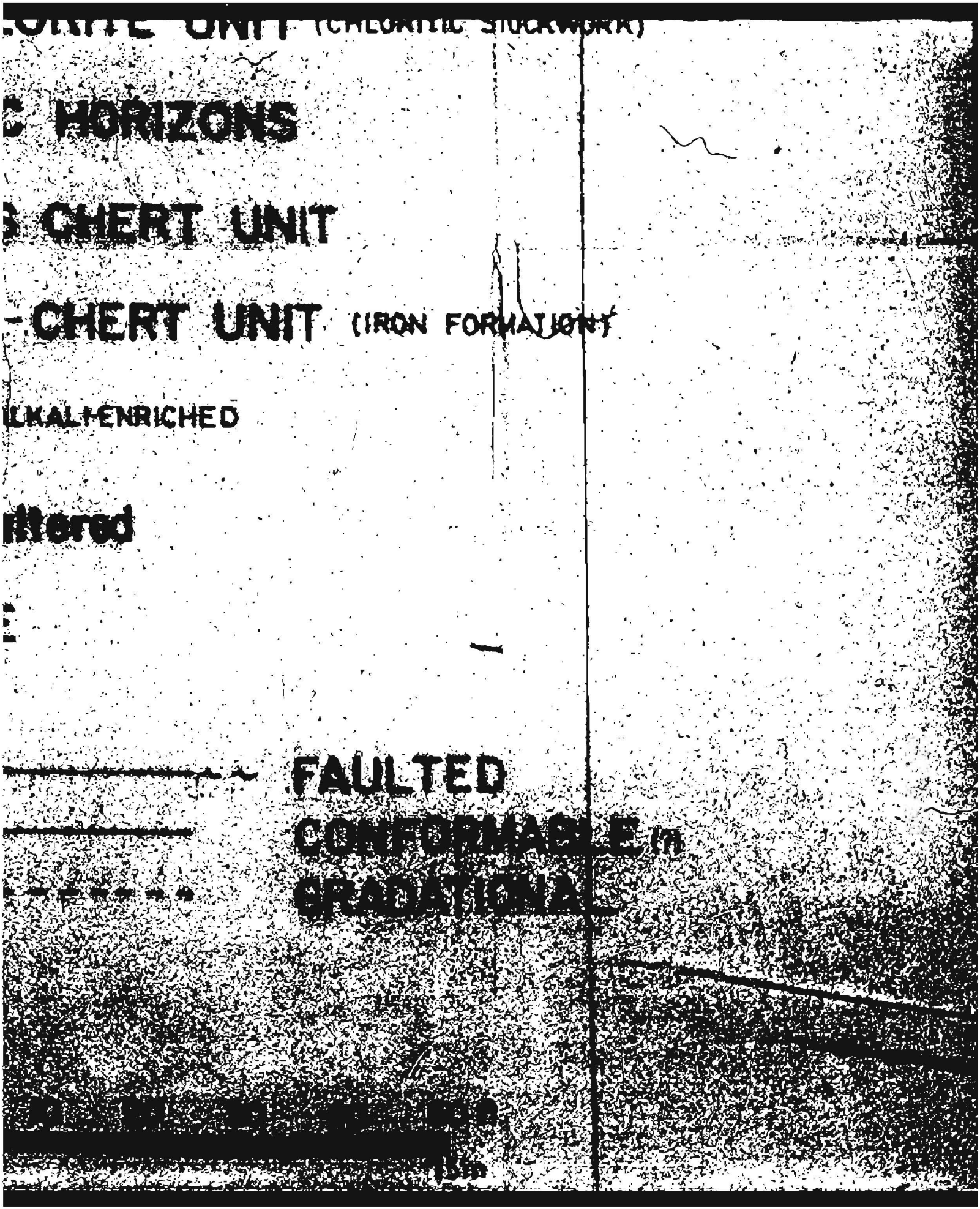
UNIT (CHLORITIC SHOCKWORK)
HORIZONS
CHERT UNIT
-CHERT UNIT (IRON FORMATION)
LKALI-ENRICHED
ltered
FAULTED
CONFORMABLE (?)
GRADATIONAL

5 OF/DE

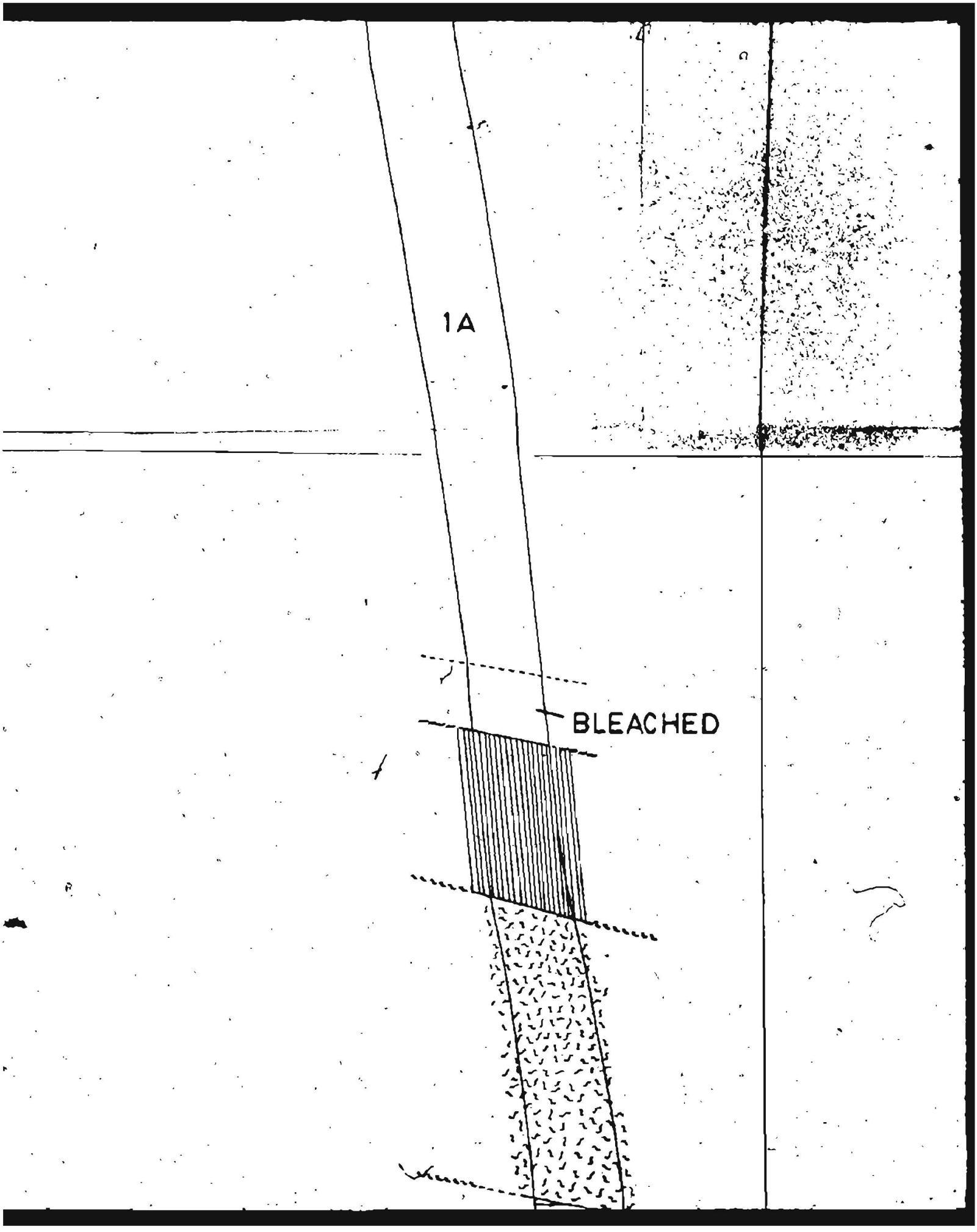
1A
BLEACHED

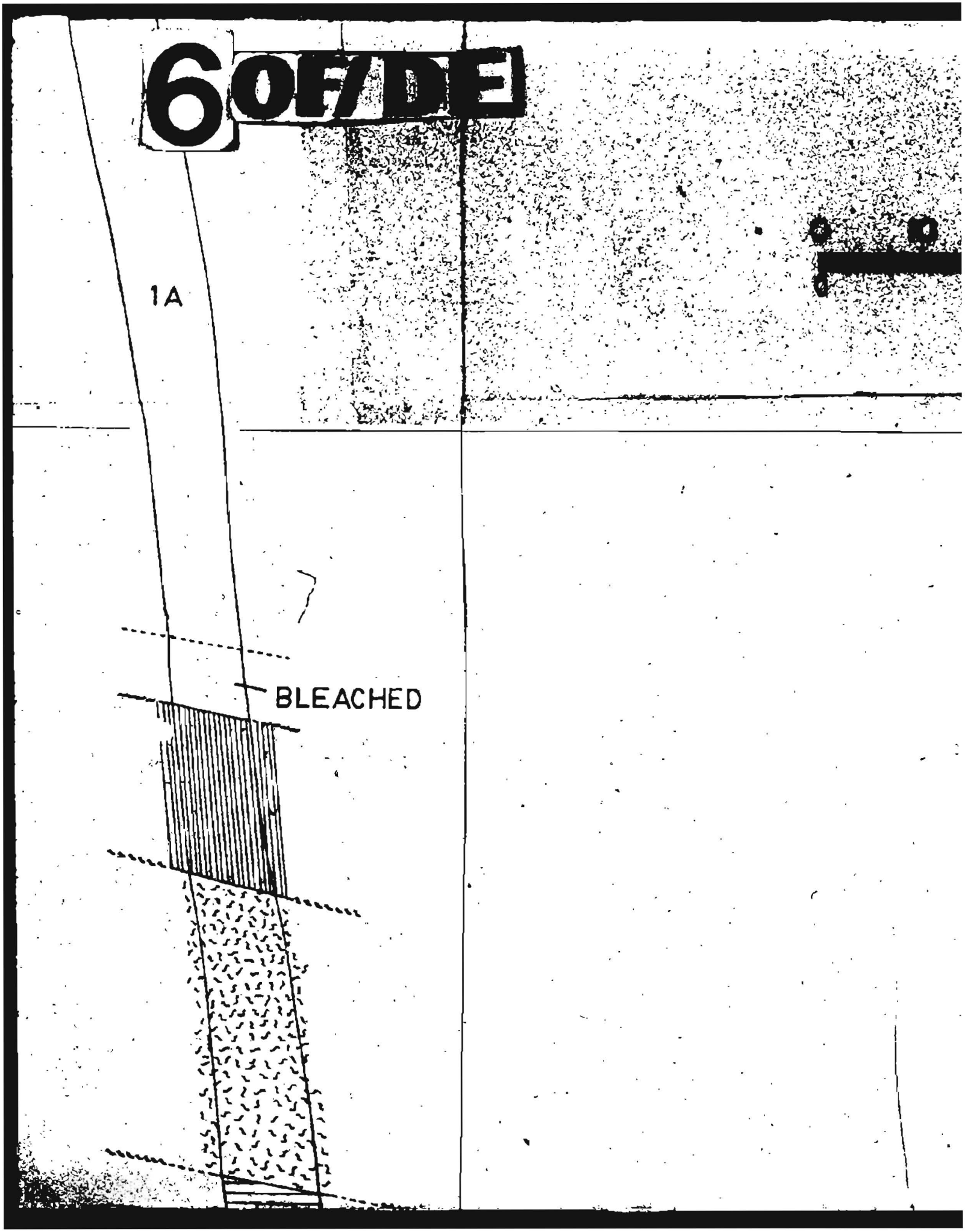
6 OF 7 DE
1A
BLEACHED

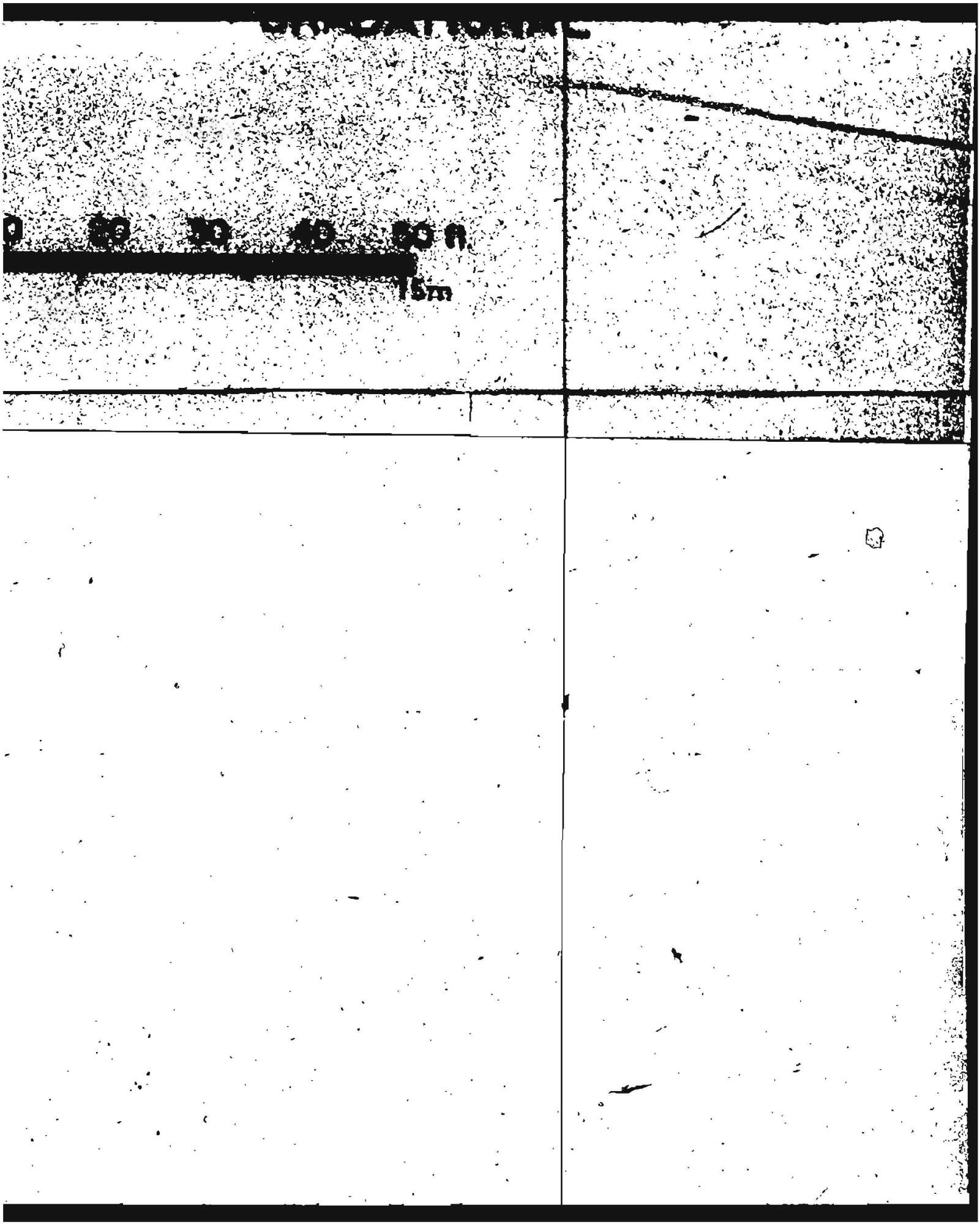

7OF/DE

MAP 2 : UND

WEST

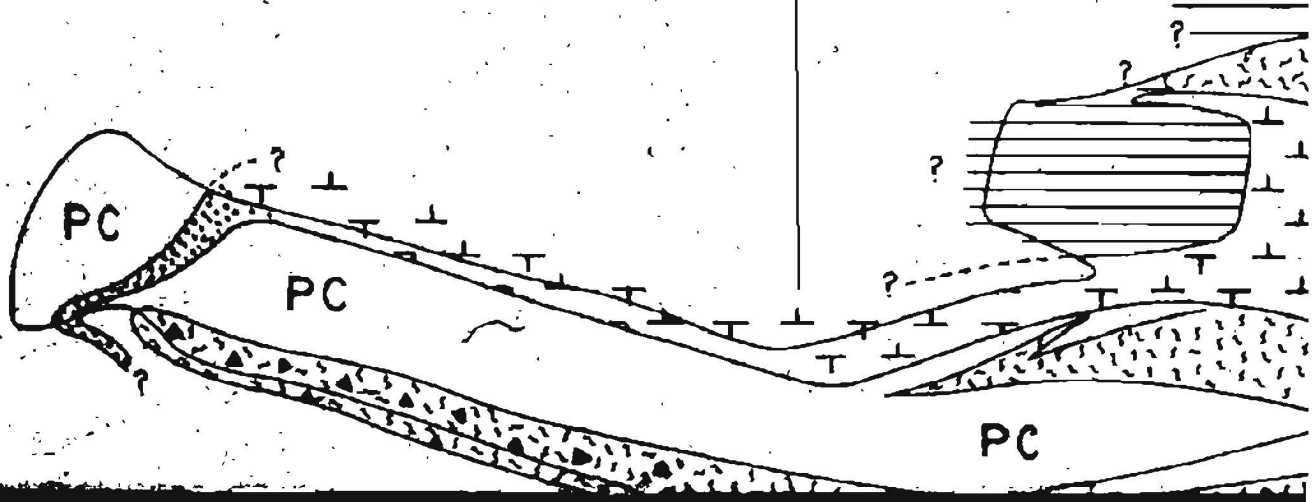

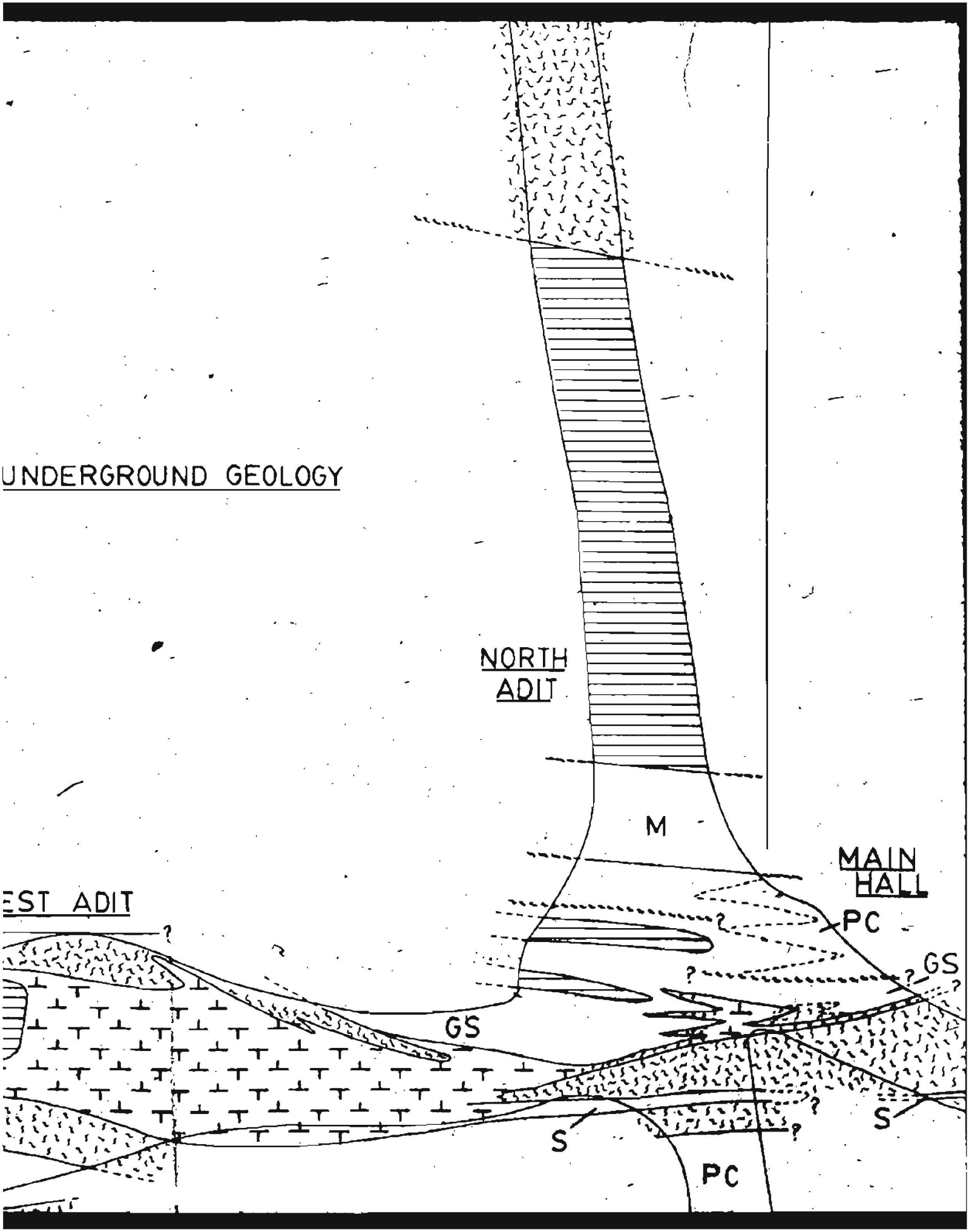
UNDERGROUND GEOLOGY
NORTH ADIT
M
MAIN HALL
EST ADIT
PC
GS
GS
S
S
PC

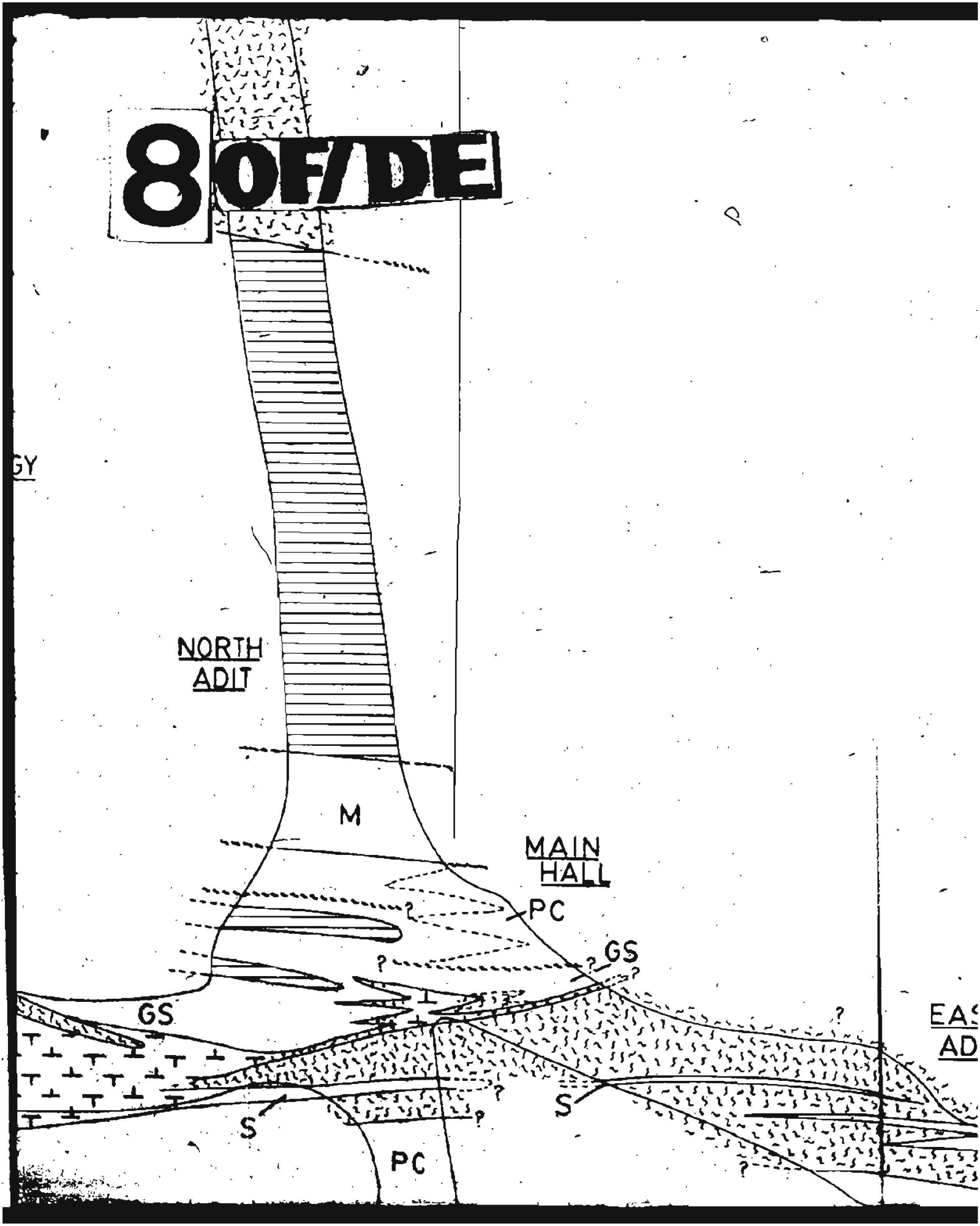
8 OF/DE
GY
NORTH
ADIT
M
MAIN
HALL
PC
GS
GS
S
S
PC
EA
AD

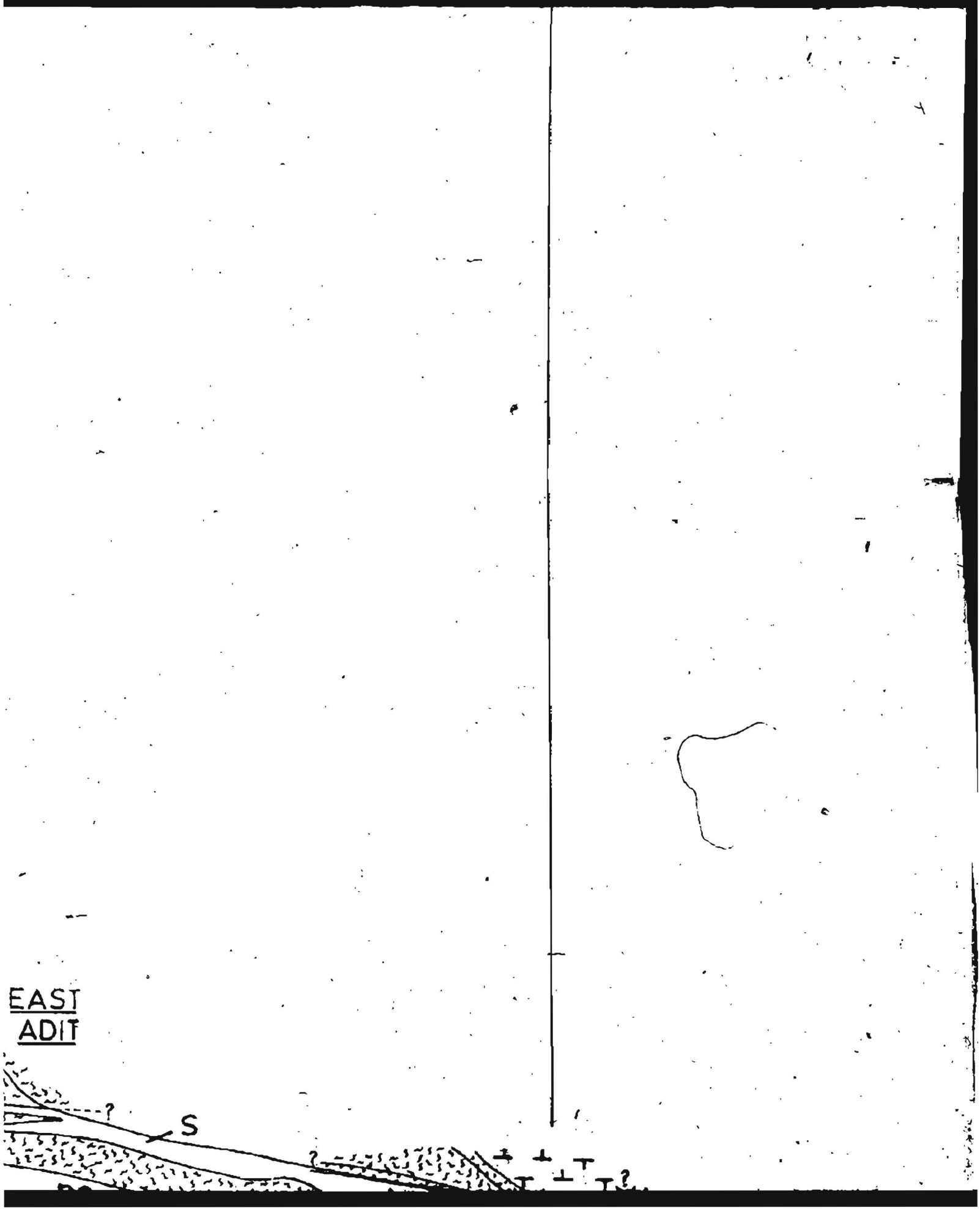
EAST
ADIT
S

9 OF/DE

MAP 2 : UNDE

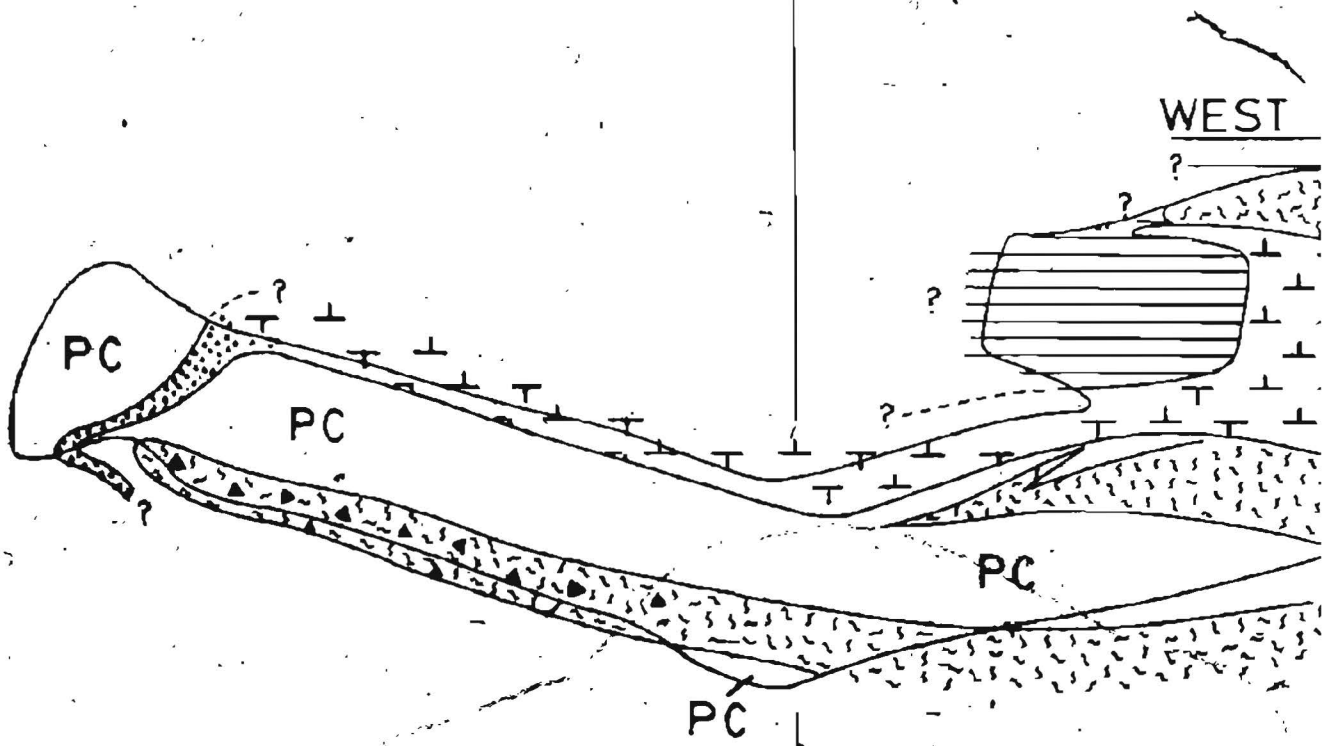

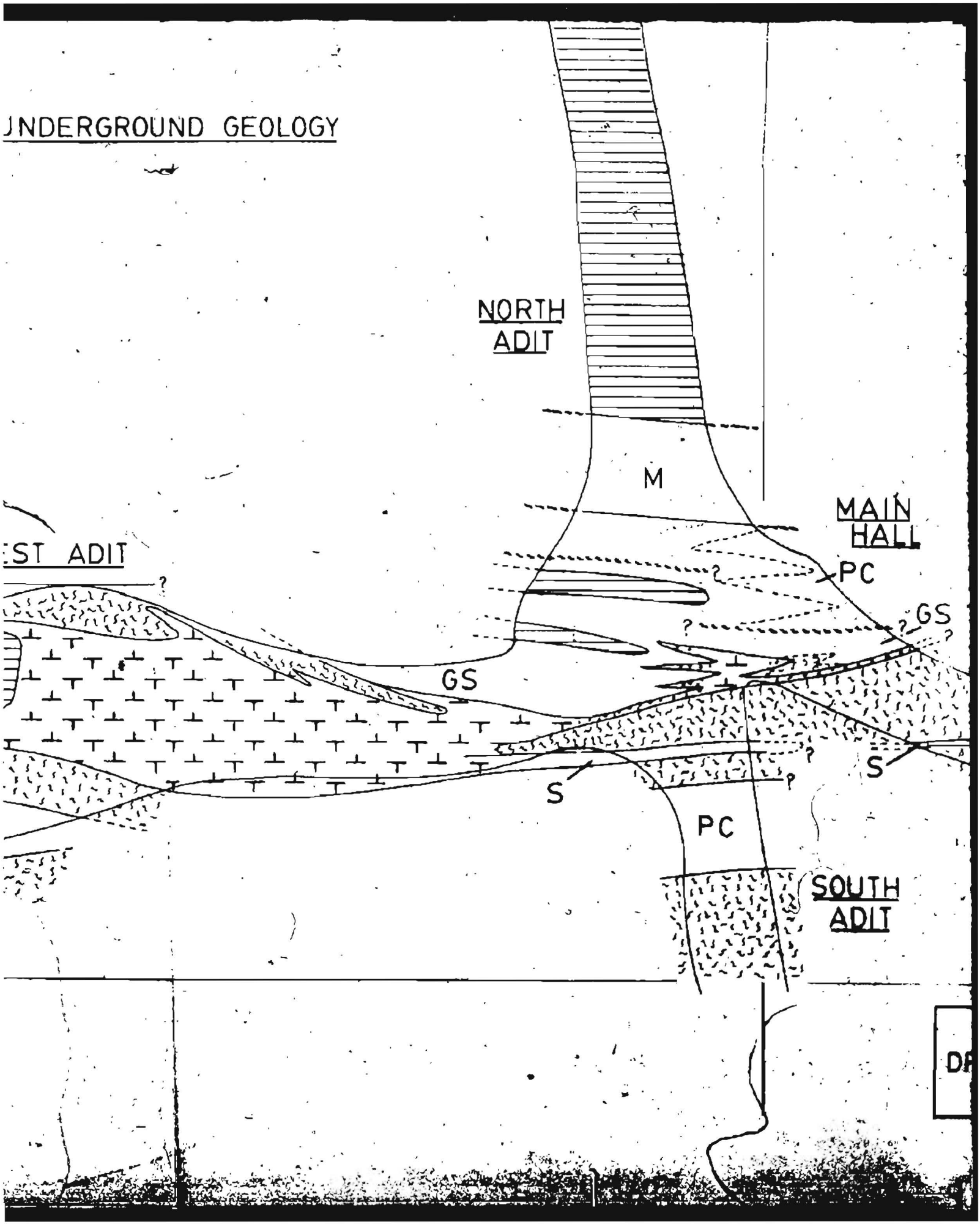
UNDERGROUND GEOLOGY
NORTH ADIT
M
MAIN HALL
EST ADIT
PC
GS
GS
S
S
PC
SOUTH ADIT

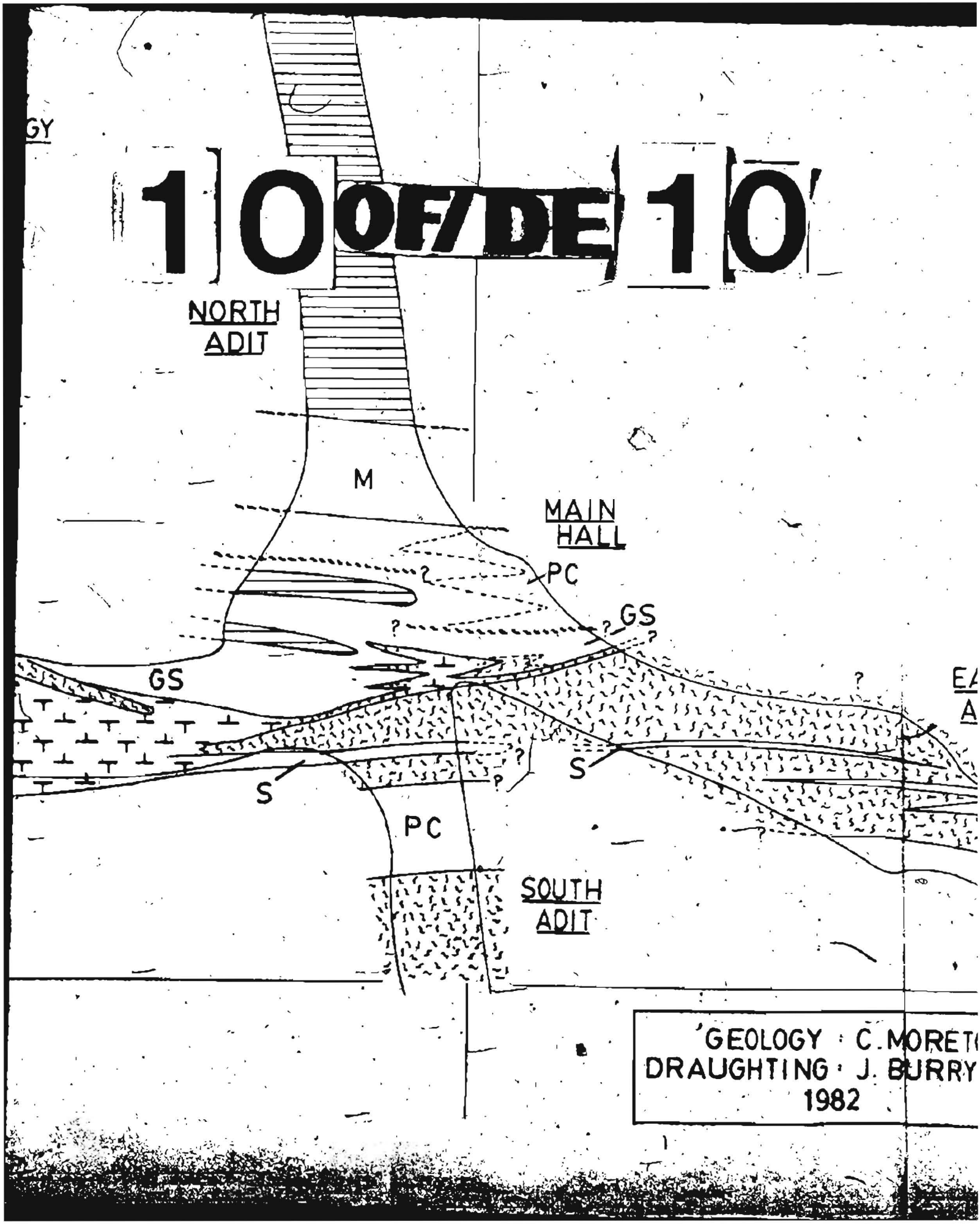
GY
NORTH
ADIT
M
MAIN
HALL
PC
GS
GS
S
S
PC
SOUTH
ADIT
GEOLOGY : C. MORET
DRAUGHTING : J. BURRY
1982

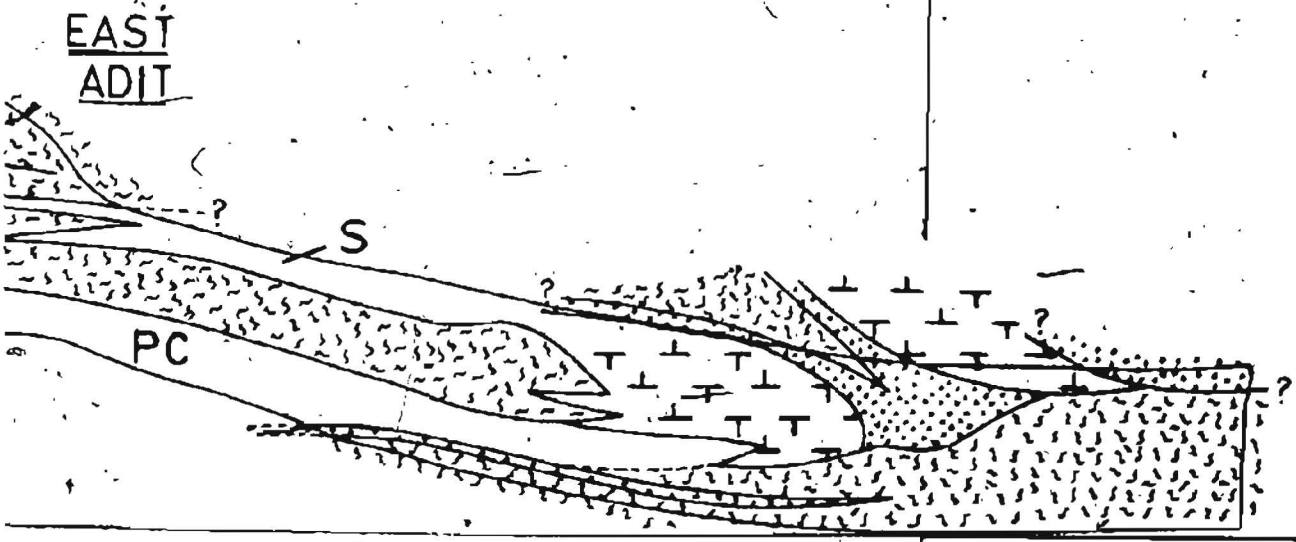

)RETON
URRY/C. MORETON

Generalised
N-S section, looking w
along co-ord W4800

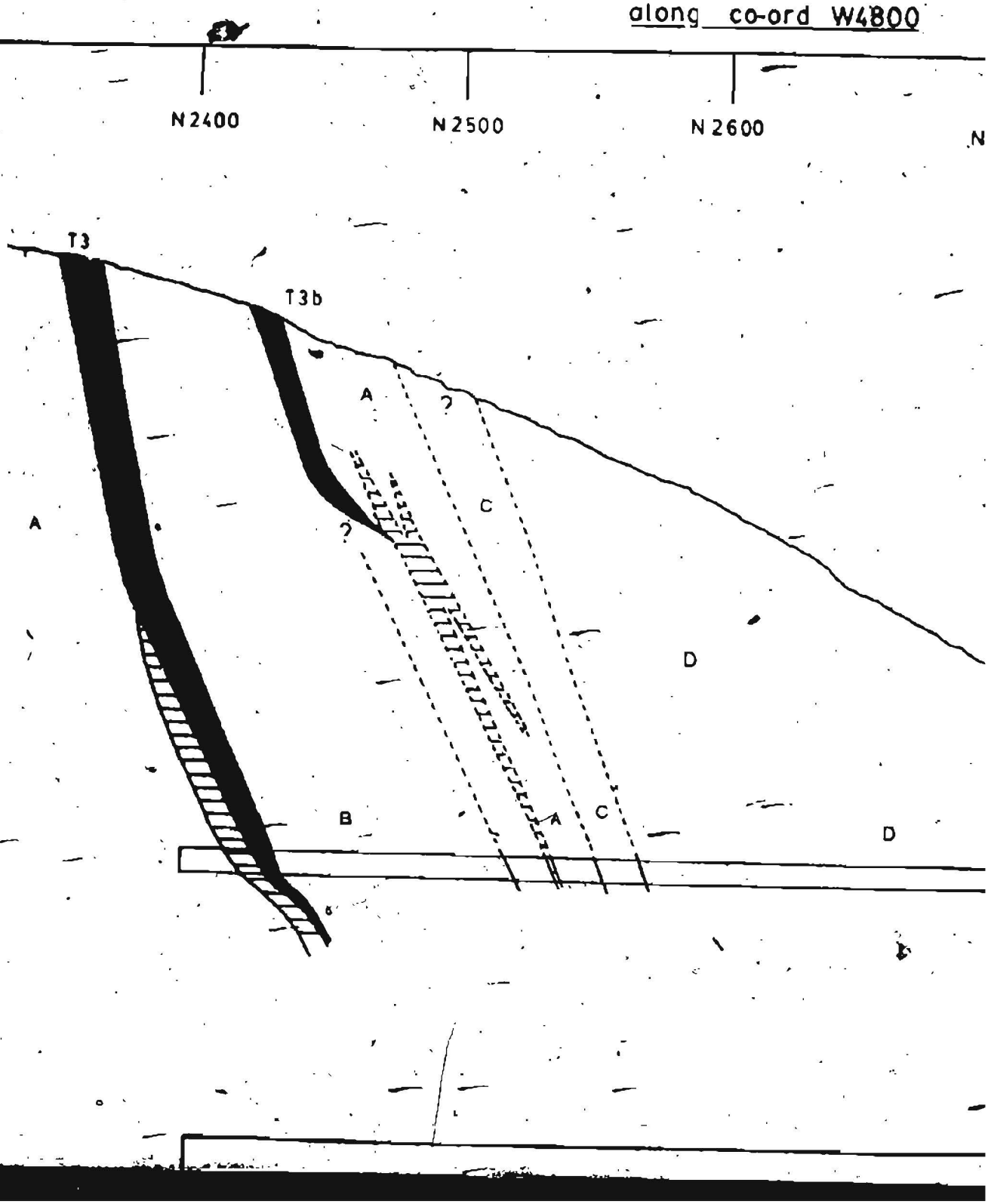

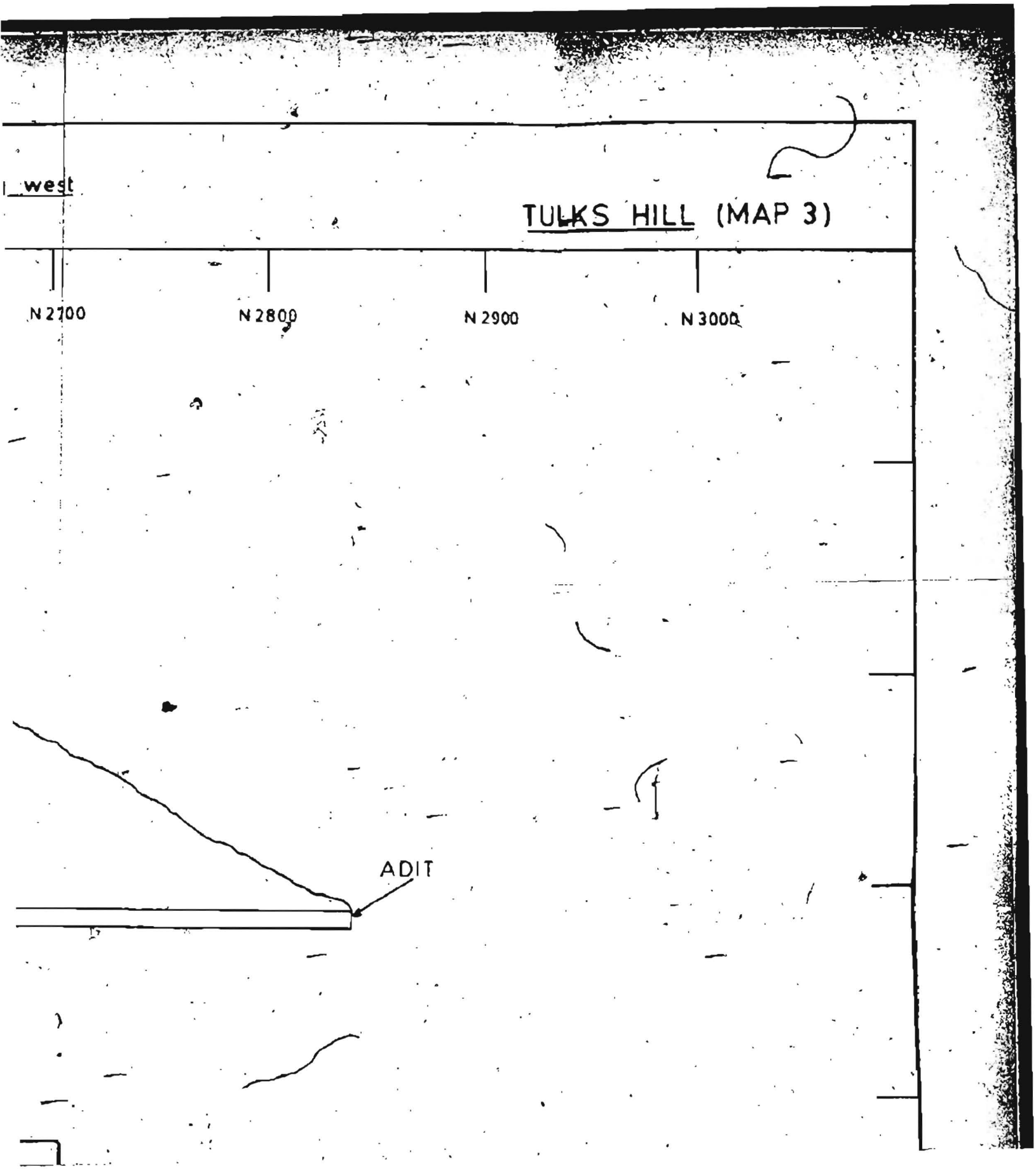
west
TULKS HILL (MAP 3)
N 2700
N 2800
N 2900
N 3000
ADIT

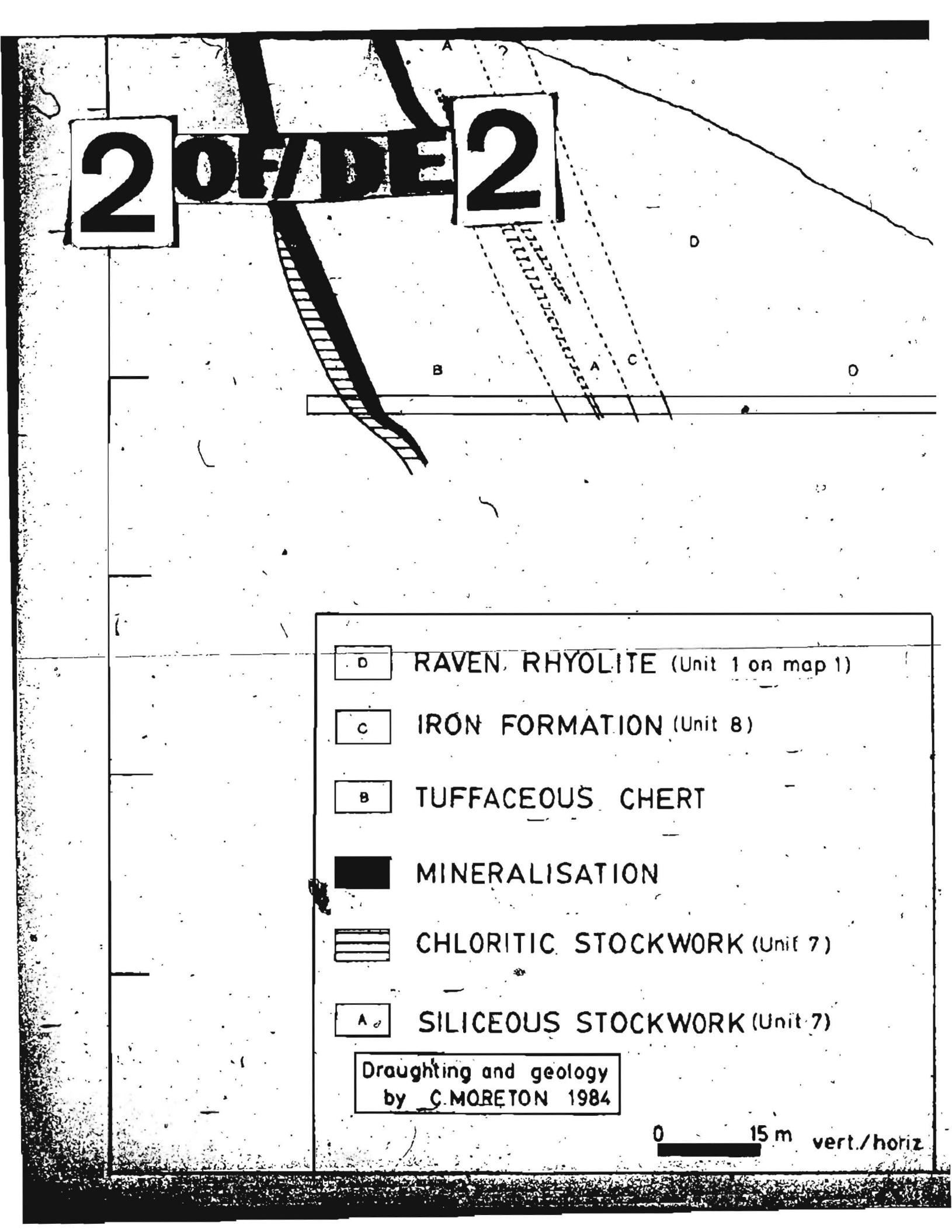
2 OF/DE 2
A
D
B
A
C
D
D
RAVEN RHYOLITE (Unit 1 on map 1)
C
IRON FORMATION (Unit 8)
B
TUFFACEOUS CHERT
MINERALISATION
CHLORITIC STOCKWORK (Unit 7)
A
SILICEOUS STOCKWORK (Unit 7)
Draughting and geology
by C.MORETON 1984
0
15 m
vert./horiz

CENTRE FOR NFLD. STUDIES
MAR 16 1988
MEMORIAL UNIVERSITY
OF NEWFOUNDLAND

CHAPTER 3

VICTORIA LAKE GROUP

CHAPTER 4

THE GEOLOGY AND PETROGRAPHY OF THE TULKS HILL ROCKS